Nanoscale phenomena in lubrication:
from atomistic simulations to their integration into continuous models

N° d'ordre : 2013-ISAL-0112   2013

Thèse

Nanoscale phenomena in lubrication: from atomistic simulations to their integration into continuous models

Présentée devant
L'Institut National des Sciences Appliquées de Lyon
et le
Karlsruher Institut für Technologie

Pour obtenir
Le grade de Docteur

Formation doctorale : Mécanique
Ecole doctorale : Mécanique, Energétique, Génie civil, Acoustique (MEGA)

par

Daniele SAVIO
(Ingénieur INSA de Lyon – Karlsruher Institut für Technologie)

Soutenance le 31 octobre 2013 devant la commission d'examen

Jury

Examinateur	J.L. Barrat	Professeur (Université Joseph Fourier, Grenoble)
Co-Directeur	N. Fillot	Maître de Conférences, HdR (INSA de Lyon)
Rapporteur	G. Galliero	Professeur (Université de Pau et des Pays de l'Adour)
Rapporteur	P. Gumbsch	Professeur, Directeur de Recherche (Fraunhofer IWM)
Co-Directeur	H. Hetzler	Docteur (Karlsruher Institut für Technologie, ITM)
Examinateur	G.E. Morales-Espejel	Principal scientist, HdR (SKF ERC, Pays-Bas)
Directeur	W. Seemann	Professeur (Karlsruher Institut für Technologie, ITM)
Directeur	P. Vergne	Directeur de Recherche (CNRS - INSA de Lyon)

Laboratoire de recherche : Laboratoire de Mécanique des Contacts et des Structures
(LaMCoS, INSA de Lyon, CNRS UMR5259)

INSA Direction de la Recherche - Ecoles Doctorales – Quinquennal 2011-2015

SIGLE	ECOLE DOCTORALE	NOM ET COORDONNEES DU RESPONSABLE
CHIMIE	**CHIMIE DE LYON** **http://www.edchimie-lyon.fr** **Insa : R. GOURDON**	**M. Jean Marc LANCELIN** **Université de Lyon – Collège Doctoral** **Bât ESCPE** **43 bd du 11 novembre 1918** **69622 VILLEURBANNE Cedex** **Tél : 04.72.43 13 95** **directeur@edchimie-lyon.fr**
E.E.A.	**ELECTRONIQUE, ELECTROTECH-NIQUE, AUTOMATIQUE** **http://edeea.ec-lyon.fr** **Secrétariat : M.C. HAVGOUDOU-KIAN** **eea@ec-lyon.fr**	**M. Gérard SCORLETTI** **Ecole Centrale de Lyon** **36 avenue Guy de Collongue** **69134 ECULLY** **Tél : 04.72.18 65 55 Fax : 04 78 43 37 17** **Gerard.scorletti@ec-lyon.fr**
E2M2	**EVOLUTION, ECOSYSTEME, MICRO-BIOLOGIE, MODELISATION** **http://e2m2.universite-lyon.fr** **Insa : H. CHARLES**	**Mme Gudrun BORNETTE** **CNRS UMR 5023 LEHNA** **Université Claude Bernard Lyon 1** **Bât Forel** **43 bd du 11 novembre 1918** **69622 VILLEURBANNE Cédex** **Tél : 06.07.53.89.13** **e2m2@ univ-lyon1.fr**
EDISS	**INTERDISCIPLINAIRE SCIENCES-SANTE** **http://www.ediss-lyon.fr** **Sec : Samia VUILLERMOZ** **Insa : M. LAGARDE**	**M. Didier REVEL** **Hôpital Louis Pradel** **Bâtiment Central** **28 Avenue Doyen Lépine** **69677 BRON** **Tél : 04.72.68.49.09 Fax :04 72 68 49 16** **Didier.revel@creatis.uni-lyon1.fr**
INFOMATHS	**INFORMATIQUE ET MATHEMA-TIQUES** **http://infomaths.univ-lyon1.fr** **Sec :Renée EL MELHEM**	**Mme Sylvie CALABRETTO** **Université Claude Bernard Lyon 1** **INFOMATHS** **Bâtiment Braconnier** **43 bd du 11 novembre 1918** **69622 VILLEURBANNE Cedex** **Tél : 04.72. 44.82.94 Fax 04 72 43 16 87** **infomaths@univ-lyon1.fr**
Matériaux	**MATERIAUX DE LYON** **http://ed34.universite-lyon.fr** **Secrétariat : M. LABOUNE** **PM : 71.70 –Fax : 87.12** **Bat. Saint Exupéry** **Ed.materiaux@insa-lyon.fr**	**M. Jean-Yves BUFFIERE** **INSA de Lyon** **MATEIS** **Bâtiment Saint Exupéry** **7 avenue Jean Capelle** **69621 VILLEURBANNE Cedex** **Tél : 04.72.43 83 18 Fax 04 72 43 85 28** **Jean-yves.buffiere@insa-lyon.fr**
MEGA	**MECANIQUE, ENERGETIQUE, GENIE CIVIL, ACOUSTIQUE** **http://mega.ec-lyon.fr** **Secrétariat : M. LABOUNE** **PM : 71.70 –Fax : 87.12** **Bat. Saint Exupéry** **mega@insa-lyon.fr**	**M. Philippe BOISSE** **INSA de Lyon** **Laboratoire LAMCOS** **Bâtiment Jacquard** **25 bis avenue Jean Capelle** **69621 VILLEURBANNE Cedex** **Tél :04.72 .43.71.70 Fax : 04 72 43 72 37** **Philippe.boisse@insa-lyon.fr**
ScSo	**ScSo*** **http://recherche.univ-lyon2.fr/scso/** **Sec : Viviane POLSINELLI** **Brigitte DUBOIS** **Insa : J.Y. TOUSSAINT**	**M. OBADIA Lionel** **Université Lyon 2** **86 rue Pasteur** **69365 LYON Cedex 07** **Tél : 04.78.77.23.86 Fax : 04.37.28.04.48** **Lionel.Obadia@univ-lyon2.fr**

*ScSo : Histoire, Géographie, Aménagement, Urbanisme, Archéologie, Science politique, Sociologie, Anthropologie

Acknowledgements

In a few lines I wish to thank various people for their contribution to this project and three very pleasant years of work.

First of all I would like to express my gratitude the SKF Company and the French Government, who provided the funding for this thesis.

I am very thankful to all my PhD supervisors at the LaMCoS laboratory: Dr. Philippe Vergne and Dr. Nicolas Fillot have offered a great guidance, outstanding advice and continuous encouragement during the whole research and writing of this thesis. My gratitude goes also to Prof. Wolfgang Seemann and Dr. Hartmut Hetzler at the Institut für Technische Mechanik in Karlsruhe for the interesting discussions, their support and for welcoming me in their research team.

Special appreciation goes to Dr. Guillermo Morales-Espejel from SKF ERC for his kind advice, his interest during the numerous progress meetings, as well as for his participation to the jury of my Ph.D. defense. My gratitude also goes to Dr. Rihard Pasaribu, Dr. Maurizio Zaccheddu at SKF ERC, and Hervé Carrerot and Thierry Hauswald at SKF Aeroengine for several technical and general discussions. I would also like to thank Dr. Hassan Berro for helping me getting acquainted with the subject of my thesis. Moreover, I wish to acknowledge the fruitful exchanges with Dr. Benoit Lorentz and Benedikt Wiegert.

I would like to offer my gratitude to Prof. Guillaume Galliero and Prof. Peter Gumbsch for accepting to review the manuscript and to be present among the jury of my Ph.D. defense. I am also thankful to Prof. Jean-Louis Barrat for his interest in my work and his participation to the jury.

My thanks also go to Isabelle Hornik, Dr. Mathias Heckele, Dr. Arnaud Sandel and Dr. Marie-Hélène Meurisse, without whom the establishment of the franco-german cotuition for my thesis would not have been possible. Moreover I would like to acknowledge the Université Franco-Allemande for the financial support of the co-tuition project.

I also wish to thank all my colleagues for the enjoyable stay, the musical moments and coffee breaks, and notably Vincent, Andrew, David, Lionel, Nathalie, Thomas, Charlotte, Stefan, Michel, Nicolas, Jerôme and Simon.

Finally, words are not strong enough to express my thanks to my family, my Mom, Dad and Brother for their continuous support and for always being there when needed. And last but not least, a big hug and Kuss to my dear Rike, who has been at my side enthusiastically, patiently and lovingly throughout this whole life experience.

Table of Contents

Résumé étendu

i.1 Introduction

Un des principaux objectifs industriels et de recherche dans le contexte tribologique actuel est le développement de mécanismes capables de résister à des puissances transmises, pressions et températures de plus en plus sévères. En particulier, une bonne lubrification des mécanismes est fondamentale pour augmenter leurs performances et durée de vie en réduisant le frottement et l'usure des pièces [1]. En conséquence, la plupart des applications telles que les roulements sont conçues pour opérer avec un film de lubrifiant séparant complètement les surfaces dans la zone de contact. Dans ce cas, un régime de lubrification dit élasto-hydrodynamique (EHD) est atteint. Classiquement, il est décrit par une théorie basée sur le couplage entre l'équation de Reynolds [2] pour la circulation du lubrifiant dans le contact, et l'équation d'élasticité pour la déformation des solides sous des fortes pressions. De nombreuses études ont permis d'appliquer cette théorie pour obtenir une compréhension détaillée des phénomènes dans un contact lubrifié, qui peut être utilisée dans l'optimisation d'applications tribologiques.

Cependant, les tendances actuelles visent à une réduction de la quantité d'huile pour répondre à des contraintes environnementales. De plus, le downsizing mène à s'affranchir de systèmes de lubrifications séparés afin de réduire l'encombrement des mécanismes. Ainsi, des fluides à très faible viscosité, comme par exemple des réfrigérants, doivent assurer la lubrification des pièces.

En conséquence, l'épaisseur de film séparant les surfaces diminue sévèrement et peut atteindre localement l'ordre de grandeur du nanomètre [1], correspondant à la taille des molécules (Figure i-1). Les propriétés de ces films fortement confinés sont influencées par des paramètres à l'échelle atomique, telles que la structure moléculaire du lubrifiant ou des surfaces en contact. Il est donc nécessaire de caractériser ces effets nanométriques, leur présence pouvant impacter fortement le comportement global d'un mécanisme.
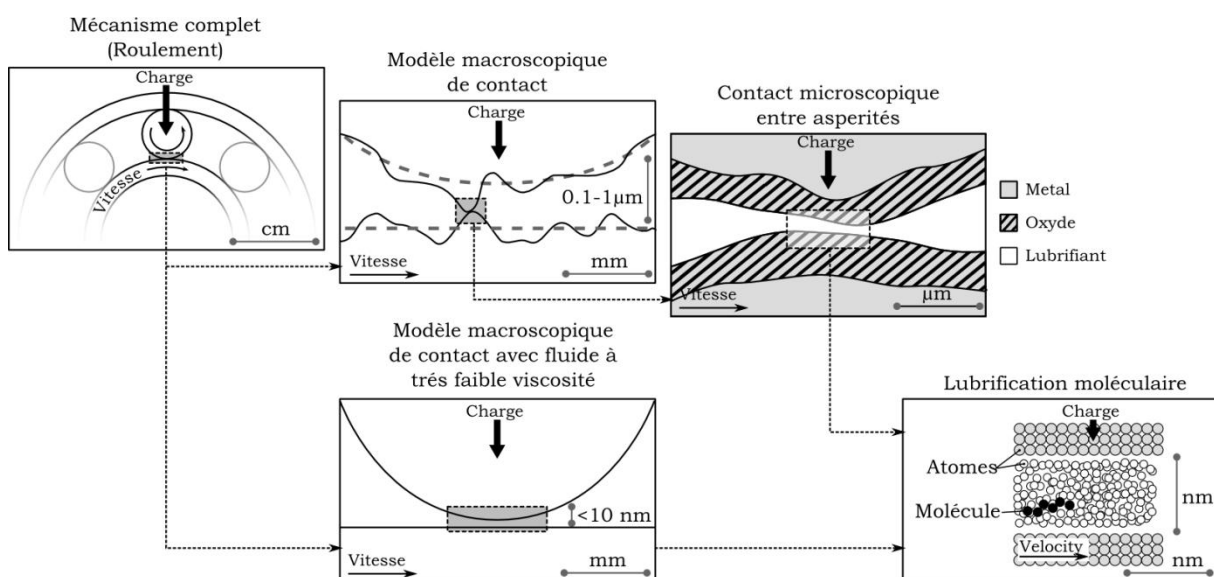
Figure i-1: Problématique multi-échelle d'un contact lubrifié où la quantité de lubrifiant est réduite et l'épaisseur de film est de l'ordre du nanomètre.

i.2   Etat de l'art et objectifs

i.2.1   *Lubrification moléculaire*

La lubrification moléculaire est un régime où seulement quelques molécules de lubrifiant assurent la séparation des surfaces, qui est de l'ordre de quelques nanomètres. En général, les modèles de contact macroscopiques ne sont pas assez détaillés pour le caractériser. Par contre, des nouvelles techniques expérimentales ont été utilisées pour sonder le comportement de films très minces entre deux surfaces : l'Appareil à Force de Surface [3] et le Microscope à Force Atomique [4]. De plus, des méthodes numériques comme la Dynamique Moléculaire [5] permettent de simuler le mouvement de chaque atome dans un lubrifiant confiné, et donc d'analyser en détail la disposition et le comportement dynamique des molécules. Plusieurs études faisant appel à ces outils ont mis en évidence trois principaux phénomènes caractéristiques des films confinés : les effets structuraux, la nano-rhéologie, et les conditions de vitesse à l'interface fluide-solide.

i.2.1.a   *Effets structuraux*

Des études expérimentales ont montré que la force entre deux surfaces en présence de films très minces est oscillatoire, avec une périodicité spatiale égale au diamètre des molécules [3]. Ce phénomène, appelé solvation, est dû à la stratification du fluide en couches parallèles aux parois. En fait, les molécules sont influencées par les potentiels des deux surfaces très rapprochées, et se disposent dans de structures ordonnées à travers l'épaisseur de film. Cette organisation du fluide peut être observée grâce à des profils de densité obtenus par des simulations de Dynamique Moléculaire (Figure i-2) [6]: des pics apparaissent en correspondance de chaque couche.

Les phénomènes structuraux dépendent aussi de la nature du lubrifiant et des surfaces. Des molécules sphériques ou des chaines courtes sont très sensibles aux forces de solvation [7]. De plus, des parois énergétiquement et géométriquement affines avec les fluide (mouillantes) causent une structuration marquée à la fois dans l'épaisseur de film et parallèlement aux surfaces [8]. Par contre, des parois nano-rugueuses [9] ou des molécules ramifiées [10] réduisent l'ordre dans le fluide.
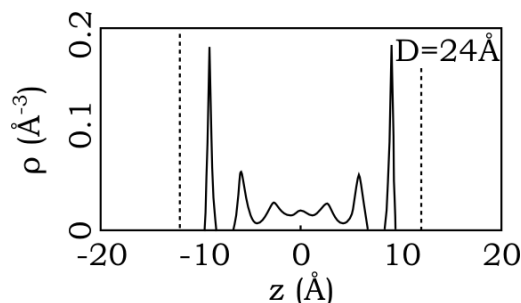
Figure i-2: Pics de densité caractéristiques de la formation de couches dans un film confine. Les traits pointillés représentent les surfaces, séparées ici de 2.4 nm.

i.2.1.b   Nano-rhéologie

Les effets structuraux entrainent une modification des propriétés rhéologiques des films nanométriques sous cisaillement. En particulier, une augmentation de la viscosité de plusieurs ordres de grandeur se manifeste quand l'épaisseur de film devient inférieure à 5-6 couches moléculaires [11]. De plus, une transition réversible vers un état quasi-solide peut être observée si le confinement augmente d'avantage [12]. Cependant, ces effets peuvent être réduits par un comportement rhéo-fluidifiant lorsque le cisaillement augmente, jusqu'à atteindre un plateau [13].

Ainsi que les effets structuraux, la modification de la viscosité sous confinement est plus marquée pour des molécules sphériques ou des chaines courtes [6], alors qu'elle est limitée par la présence de ramifications ou de surfaces rugueuses [9, 14].

i.2.1.c   Conditions dynamiques aux parois

Un troisième effet concerne la dynamique du lubrifiant près des parois. La condition de non-glissement universellement utilisée dans des modèles de lubrification n'est plus valable sous confinement. En fait, un phénomène de glissement, c.à.d. une différence de vitesse, peut se manifester à l'interface solide-fluide [15].

Cet effet est typique des parois non-mouillantes, qui présentent des interactions faibles et peu d'affinité géométrique avec les molécules de lubrifiant [8]; il se manifeste d'avantage en présence de longues chaines ou molécules ramifiés [16]. De plus, le glissement croît avec le cisaillement [17], le confinement ou la pression locale [18]. Cependant, la présence de nano-rugosités sur les surfaces cause une suppression de cet effet [9]. A l'opposé des couches moléculaires peuvent adhérer aux parois : ce phénomène opposé est appelé "locking" [19].

L'état de l'art montre donc que les propriétés des films d'épaisseur nanométrique sont différentes par rapport à l'état "bulk" (non-confiné). Il est donc intéressant de les intégrer dans des modèles macroscopiques pour la caractérisation d'un contact complet.

i.2.2   Intégration des effets moléculaires dans des modèles continus

A cause de limites en puissance de calcul des ordinateurs actuels, les outils numériques pour la caractérisation des effets moléculaires sont souvent restreints à l'échelle du nanomètre. Un contact entier, de quelques millimètres, ne peut donc pas être simulé. Ainsi, un couplage multi-échelle entre les simulations atomistiques et les modèles continus est nécessaire.

La littérature propose des approches basées sur des lois analytiques approximant le comportement des fluides confinés. Par exemple, les effets de solvation ont été décrits par une force oscillatoire entre les surfaces [20]. Comme conséquence, l'épaisseur de film dans la zone centrale d'un contact macroscopique peut atteindre seulement certaines valeurs correspondant à des couches entières de lubrifiant [21].

La modification de la condition d'adhérence aux parois peut aussi impacter le comportement global d'un système. Par exemple, la présence de glissement constant sur toute la longueur du contact entrainait une diminution de l'épaisseur de film sous une charge don-

née [22]. Enfin, des lois caractérisant la dépendance du glissement avec les conditions locales de pression, vitesse et confinement ont été déjà intégrées dans un contact EHD avec un film confiné [18]. Cette étude a permis d'observer la formation d'un dimple (une zone d'épaisseur de film plus importante) au centre du contact, ainsi qu'une réduction du frottement sous des taux de cisaillement élevés.

i.2.3   Objectifs de la thèse

Cette thèse vise à explorer les phénomènes intervenant dans des mécanismes lubrifiés où l'épaisseur de film de lubrifiant est de l'ordre de grandeur du nanomètre. Le travail va porter sur deux principales directions de recherche.

- D'abord, une analyse des films confinés va être effectuée à l'échelle moléculaire, de façon à pouvoir quantifier leur comportement sous des conditions typiques d'applications élasto-hydrodynamiques.
- Le deuxième objectif est de développer une approche multi-échelle pour intégrer les effets moléculaires dans un modèle macroscopique, et ainsi explorer leur impact sur le comportement global d'un contact élasto-hydrodynamique.

Pour aborder ces objectifs, la démarche suivante est appliquée. D'abord des simulations en Dynamique Moléculaire sont développées pour caractériser les films confinés sous cisaillement (i.3). Le modèle numérique est ensuite utilisé pour étudier le glissement aux parois sous différentes configurations typiques de l'interface d'un contact (i.4). En particulier, des lois décrivant l'évolution de ce phénomène avec la nature des surfaces, du lubrifiant et des conditions opératoires locales sont formulées.

En i.5, ces expressions sont couplées à des modèles continus dans une approche multi-échelle ; cette dernière est ensuite exploitée pour étudier l'impact du glissement moléculaire sur l'épaisseur de film et le frottement dans un contact EHD. Enfin, en i.6 la problématique de réduction de la quantité de lubrifiant est poussée à ses limites, jusqu'à atteindre la rupture locale du film de lubrifiant et le contact direct entre solides.

i.3   Le modèle de Dynamique Moléculaire

La construction du modèle nanométrique pour l'étude des films confinés fait recours à la Dynamique Moléculaire. Cette approche numérique se base sur la résolution explicite des équations de mouvement sur tous les atomes qui composent le système.

En particulier, la méthode s'articule en quatre étapes principales [5]. 1) A chaque pas de temps le potentiel agissant sur chaque atome est calculé à partir des interactions avec ses voisins en fonction de leur position ; le gradient du potentiel donne la force atomique. 2) A celle-ci sont ajoutées des contraintes thermodynamiques additionnelles, représentant les conditions aux limites du système. 3) A travers les équations du mouvement, l'accélération de chaque atome peut être déterminée. 4) Enfin une double intégration de cette quantité à travers l'algorithme de Verlet [5] permet de calculer les nouvelles positions atomiques. Ainsi, l'évolution de tous les atomes du système au cours du temps peut être simulée.

Cependant, les simulations par Dynamique Moléculaires sont limitées à des échelles de temps et d'espace, respectivement de la nanoseconde (10^6 pas de temps) et du nanomètre (env. 10000 atomes) à cause de la capacité de calcul des ordinateurs actuels.

i.3.1   Le modèle pour la simulation de fluides confinés

Un nano-spot de la zone de contact, où l'épaisseur de film est nanométrique, est donc considéré : ainsi, le fluide est confiné entre deux surfaces, comme le montre la Figure i-3. Des conditions périodiques en x et y permettent de répéter le système à l'infini dans ces directions.
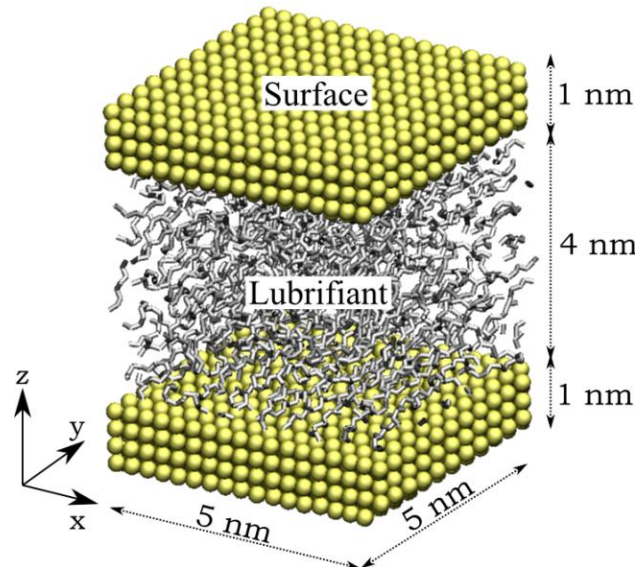
Figure i-3: Vue d'ensemble du système simulé par Dynamique moléculaire, représentant une parcelle de l'aire de contact avec un fluide confiné

Ensuite, chaque élément du modèle (les parois, le fluide et l'interface entre les deux) est paramétrisé de façon réaliste. Les surfaces constituent les dernières couches solides en contact avec le lubrifiant. Des matériaux avec des propriétés représentatives des métaux ou oxydes métalliques sont donc choisis. Ceux-ci sont modélisés par des structures cristallines régulières, qui peuvent être canoniques ou complexes. Les déformations élastiques des réseaux sont simulées à travers des ressorts harmoniques entre les atomes, dont la raideur est réglée pour obtenir des propriétés mécaniques réalistes [23].

Le fluide est composé d'alkanes, représentatifs des huiles de base utilisées en lubrification EHD. Chaque molécule est modélisée par un chaine flexible d'atomes, dont les degrés de liberté en étirement, torsion et rotation sont donnés par des champs de force de la littérature [24]. Les interactions de van-der-Waals entre atomes appartenant à des molécules différentes sont décrites par un potentiel de Lennard-Jones [5].

Enfin, le potentiel entre la surface et le fluide est paramétrisé à partir de deux méthodes. La première permet d'ajuster les interactions pour correspondre à des énergies d'adsorption/desorption obtenues expérimentalement pour des alkanes sur des surfaces métalliques [25] ; la seconde se base sur le lien entre l'énergie de surface macroscopique et les interactions moléculaires [26].

i.3.2 Conditions opératoires

Une fois définis les éléments constitutifs du système, il est nécessaire d'appliquer les conditions opératoires pour simuler le cisaillement du fluide. Celles-ci sont choisies typiques d'un contact en régime élasto-hydrodynamique, et sont appliquées en trois étapes principales. En premier, une phase de minimisation d'énergie permet aux molécules de fluide, initialement disposées de façon aléatoire, d'atteindre une disposition réaliste. Dans une étape de compression (phase 2), la pression extérieure est appliquée aux couches atomiques externes des deux parois jusqu'à atteindre une valeur stable de l'épaisseur de film sous charge. Ensuite, la pression est gardée constante lors du reste de la simulation. De plus, des vitesses opposées sont appliquées aux surfaces, et le fluide est cisaillé (phase 3). Dans ces conditions, la durée simulée est de quelques nanosecondes, ce qui permet d'atteindre un état stationnaire.

La plupart des simulations est effectuée avec des températures de paroi régulées à une valeur constante à l'aide d'un thermostat de Langevin [27] qui dissipe l'énergie générée par le cisaillement du fluide. Une méthode de dissipations avancée [28] est utilisée en i.6 pour simuler les effets thermiques et l'augmentation de température sous confinement extrême.

i.3.3 Grandeurs d'intérêt du modèle

Les sorties du modèle de Dynamique Moléculaire sont les positions et les vitesses des atomes. Ces données sont moyennées en espace et en temps de façon à obtenir les grandeurs tribologiques usuelles, comme par exemple l'épaisseur de film et la densité.

Un échantillonnage spatial des positions et des vitesses atomiques en couches parallèles aux surfaces permet d'obtenir respectivement les profils de densité et de vitesse du fluide à travers l'épaisseur de film. Enfin, les forces tangentielles s'opposant au mouvement des parois sont reliées au frottement et à la viscosité du fluide.

i.4 Etude du glissement aux parois par Dynamique Moléculaire

Un phénomène caractéristique des films nanométriques est la différence de vitesse à l'interface fluide-solide, aussi appelé glissement aux parois (Figure i-4). Cet effet est en contradiction avec l'hypothèse de non-glissement typique des modèles continus. Il est quantifié à travers un paramètre adimensionné s, lié aux taux de cisaillement appliqué au système, ainsi qu'à la réponse effective du fluide confiné. Alternativement la longueur de glissement L_s, représentée en Figure i-4, peut être utilisée.
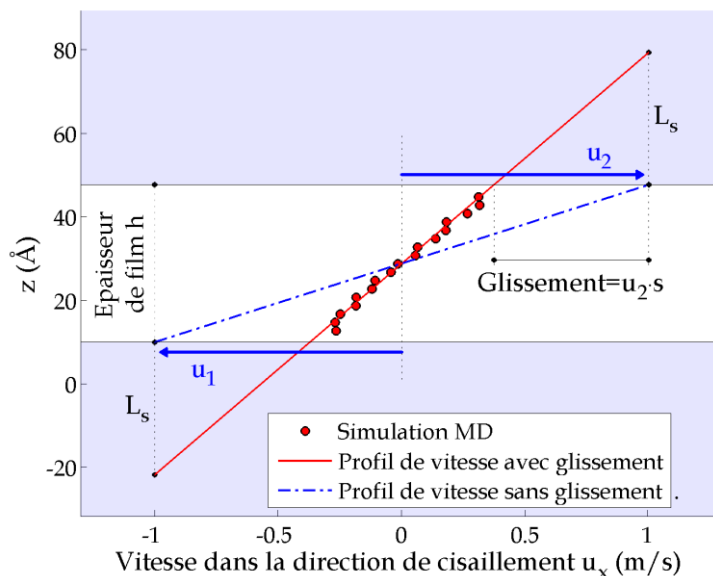
Figure i-4: Phénomène de glissement aux parois pour un fluide sous confinement. Les vitesses des parois u_1 et u_2 selon x sont représentées par les flèches bleues, tandis que la vitesse du fluide obtenues par des simulations MD est montrée par les points rouges.

i.4.1 Influence des surfaces et du lubrifiant : un modèle de prédiction du glissement

Deux facteurs principaux pour l'apparition du glissement aux parois sont la morphologie des surfaces et la nature du lubrifiant. La Figure i-5a montre qu'en changeant la nature des parois, différents sauts de vitesse à l'interface peuvent être obtenus ; de plus, le glissement varie avec la longueur des chaines (Figure i-5b).
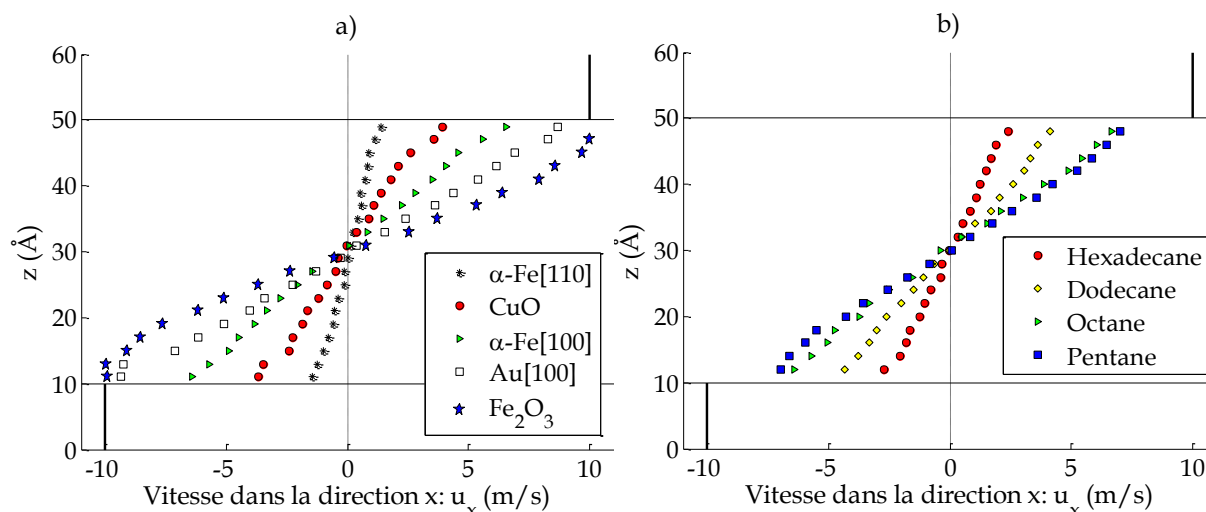
Figure i-5: Dépendance du glissement avec la nature des surfaces et du lubrifiant. Les profils de vitesse dans l'épaisseur de film sont représentés pour : a) de l'hexadecane confiné entre différentes surfaces métalliques ; b) une surface canonique avec différentes alkanes linéaires. La vitesse des parois est imposée à ±10 m/s.

Dans une interface lubrifiée il existe de nombreuses configurations paroi-fluide possibles, à cause des variations de la composition des surfaces : la caractérisation de chacune d'entre elles par Dynamique Moléculaire demanderait des coûts et temps de calculs importants. L'objectif est de donc formuler un modèle de prédiction du glissement, basé sur la compétition entre la nature des surfaces (matériaux métalliques et oxydes) et du lubrifiant (alkanes linéaires représentatives d'huiles de base).

i.4.1.a   Caractérisation des surfaces

Les parois sont caractérisées en premier : ainsi, une technique de scanning est développée, valable à la fois pour des structures canoniques et complexes (Figure i-6). Chaque surface est sondée par un atome dont la taille et les caractéristiques énergétiques sont représentatives d'un groupe hydrocarboné d'alkanes. Pour des coordonnés planaires (x, y) fixées, l'atome évolue vers sa position d'équilibre par rapport à la paroi, correspondant à un minimum de potentiel. En répétant ce processus sur toute la surface, un champ de potentiel (Figure i-6) et une hauteur d'équilibre sont obtenus. Ces quantités sont reliées aux interactions énergétiques paroi-fluide (corrugation) et à l'affinité géométrique entre les molécules et le réseau cristallin (commensurabilité). Ainsi, un paramètre de caractérisation de surface ζ_{surf} est obtenu.
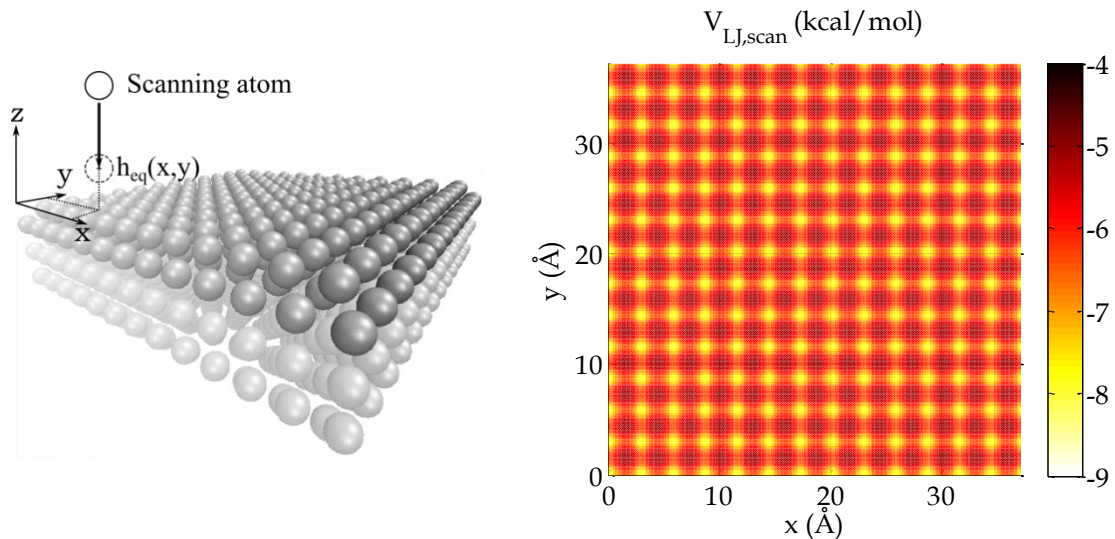
Figure i-6: Méthode de scanning sur une surface de ferrite α-Fe[100], avec le champ de potentiel correspondant.

Cette grandeur, liée au transfert de quantité de mouvement tangentiel à l'interface, permet d'ordonner les surfaces selon leur capacité à entrainer le fluide. La contrainte tangentielle à la paroi τ_{zx} est donc tracée en fonction de ζ_{surf} pour différentes couples surface-alkanes en Figure i-7.

Pour des faibles valeurs de paramètre de caractérisation de surface, la contrainte est limitée par les faibles interactions parois-fluide, et le glissement apparaît. Ensuite, il croit avec jusqu'à atteindre un plateau : dans ce cas, les molécules du lubrifiant adhèrent aux parois et la contrainte est limitée par le cisaillement total du fluide. Les courbes $\tau_{zx}(\zeta_{surf})$ sont enfin décrites par des expressions analytiques, valables pour des alkanes linéaires confinés entre deux surfaces métalliques canoniques ou complexes.
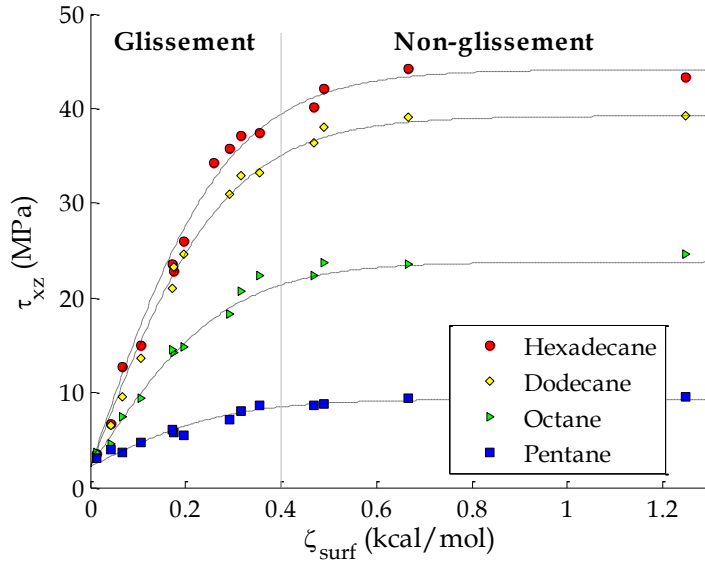
Figure i-7: Contrainte de cisaillement en fonction du paramètre de caractérisation de surface, pour différents alkanes linéaires. Chaque point représente le résultat d'une simulation par Dynamique Moléculaire.

i.4.1.b   Caractérisation du lubrifiant sous confinement

La nano-rhéologie du lubrifiant sous confinement est caractérisée par sa viscosité effective η_{eff}. Des comparaisons avec des simulations de fluides dans leur état non-confiné montrent que η_{eff} peut être approximée par une viscosité "bulk" η_{bulk} lorsque que l'épaisseur de film est supérieure à 2-3 nm et il qu'il n'y a pas de transition vers un état solide dans le lubrifiant. La viscosité $\eta_{bulk}(\tau_{zx}, P, T)$ dépend des conditions opératoires, ainsi que de la contrainte de cisaillement τ_{zx}.

i.4.1.c   Le modèle de prédiction du glissement

Enfin, l'influence de la morphologie des surfaces et de la nature du lubrifiant est intégrée dans un modèle de prédiction du glissement :

$$s = 1 - \dot{\gamma}_{app}^{-1} \frac{\tau_{zx}(\zeta_{surf})}{\eta_{bulk}(\tau_{zx}, P, T)}$$

où $\dot{\gamma}_{app}$ est le taux de cisaillement appliqué au système à travers les conditions opératoires. La contrainte $\tau_{zx}(\zeta_{surf})$ est donnée par les courbes de la Figure i-7 en fonction du paramètre de caractérisation surface, obtenu par la technique de scanning. Enfin, la viscosité η_{bulk} du lubrifiant peut être décrite par des modèles de la littérature. Le modèle de prédiction de glissement ainsi obtenu est valable pour des alkanes linéaires confinés entre des surfaces métalliques simples ou complexes.

i.4.2   Influence des conditions opératoires : une loi analytique de glissement

Le modèle de prédiction du glissement en fonction du couple surface-fluide a été développé pour un seul ensemble de conditions opératoires. Cependant la différence des vitesses des parois Δu, l'épaisseur de film h et la pression P peuvent aussi influencer ce phé-

nomène. Comme ces grandeurs varient sur toute la surface du contact, il est nécessaire de caractériser leur impact sur le glissement.

Des études paramétriques par Dynamique Moléculaire sont donc effectuées en faisant varier Δu, h et P pour un couple surface-fluide présentant des faibles interactions à l'interface. La plage de valeurs choisie est typique des conditions d'un contact élasto-hydrodynamique.

Une augmentation de la vitesse de cisaillement, du degré de confinement du fluide et de la pression locale entraine un glissement plus important (Figure i-8), en cohérence avec les tendances de la littérature [17, 18, 29]. Cette dépendance du paramètre de glissement s ou de la longueur de glissement L_s avec les conditions opératoires est décrite par des loi analytiques à partir des résultats des simulations atomistiques :

$$s = s(\Delta u, h, P)$$

$$L_s = \frac{h}{2} \cdot \left(\frac{1}{1 - s(\Delta u, h, P)} - 1 \right)$$
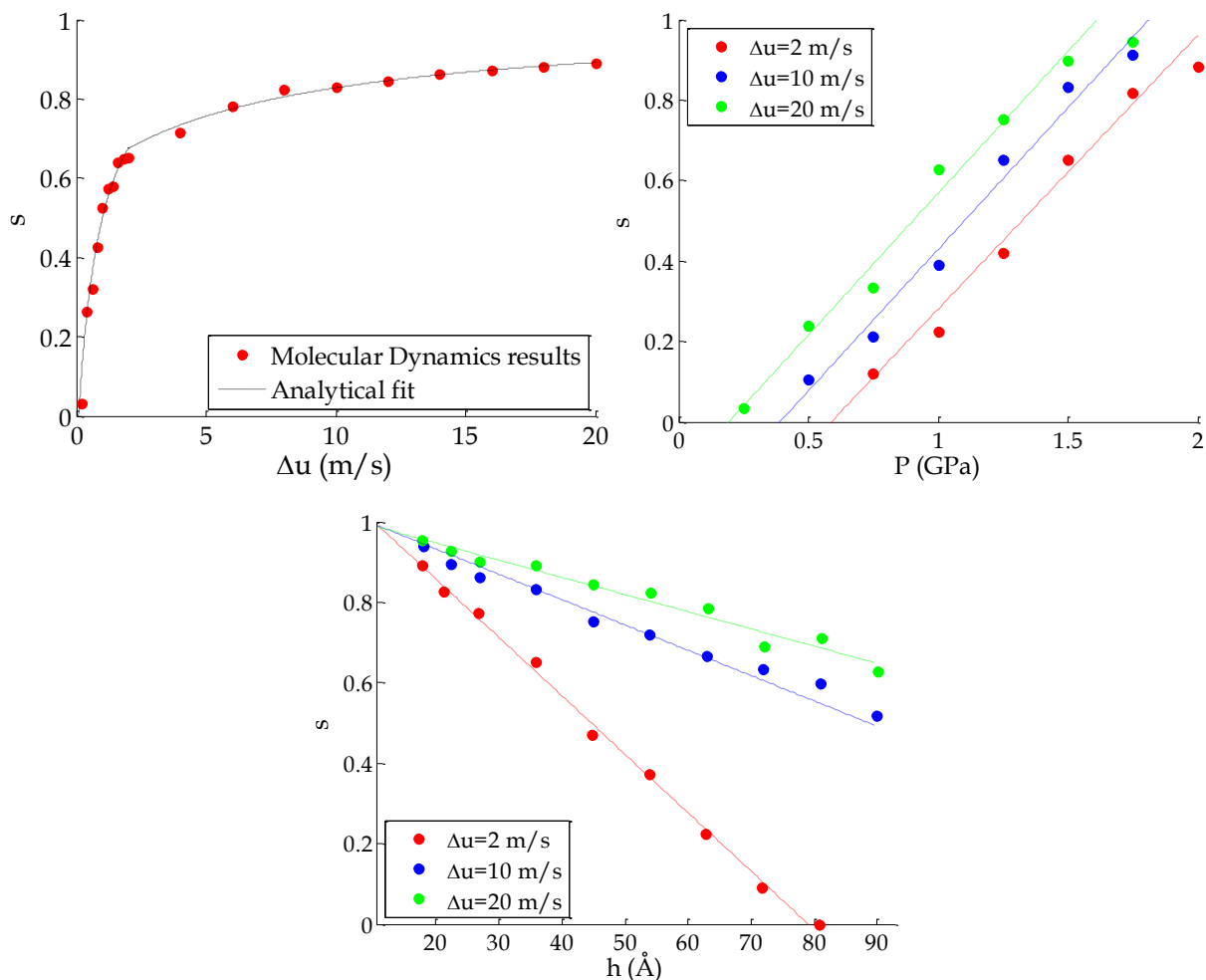
Figure i-8: Dépendance du glissement avec la différence de vitesse des parois, l'épaisseur de film et la pression, pour un couple surface-fluide présentant des faibles interactions à l'interface. Les points sont les résultats issus de la Dynamique Moléculaire, tandis que les pointillés représentent les lois analytiques de glissement.

En conclusion, cette partie s'est focalisée sur la quantification du glissement en fonction des principaux paramètres d'une interface de contact. Des lois analytiques et modèles prédictifs ont été formulés, qui permettent de caractériser son évolution pour une grande variété de couples surface-alkane, ainsi que des conditions typiques du régime EHD. Ces expressions vont permettre une intégration aisée des résultats obtenus à l'échelle nanométrique dans des modèles continus macroscopiques.

i.5 Vers un couplage entre les effets moléculaires et les modèles continus

Le deuxième objectif de cette thèse est d'analyser l'impact des effets moléculaires sur le comportement global des contacts avec des films confinés. Pour cette raison une modélisation multi-échelle, appelée nano-EHL, est mise en place afin de coupler les simulations atomistiques aux modèles continus.

i.5.1 L'approche multi-échelle nano-EHL

L'étude porte principalement sur le phénomène de glissement aux parois. L'équation de Reynolds, utilisée pour décrire la circulation du lubrifiant dans le contact, est modifiée pour prendre en compte cet effet. La condition classique de non-glissement est remplacée par une frontière de Navier [30] sur une seule paroi (la surface inférieure). Ainsi, l'équation de Reynolds avec glissement s'écrit :

$$\frac{\partial}{\partial x}\left(\frac{\rho}{12\eta}\left(h^3\frac{h+4L_s}{h+L_s}\right)\frac{\partial P}{\partial x}\right) = \frac{\partial}{\partial x}\left(\frac{\rho h^2}{2(h+L_s)}u_1 + \frac{\rho h(h+2L_s)}{2(h+L_s)}u_2\right)$$

pour un contact linéique, avec un fluide newtonien et dans des conditions stationnaires et isothermes.

Dans cette expression, la variation de la longueur de glissement L_s en fonction des conditions en pression, vitesse et épaisseur de film dans le contact est quantifiée par les lois formulées en i.4. La résolution couplée de ces deux équations constitue le noyau de l'approche nano-EHL. Le modèle est complété par la théorie d'élasticité pour les déformations des corps solides, les relations pression-viscosité et pression-densité pour le lubrifiant, et les équations d'épaisseur de film et équilibre de la charge. Ce système est résolu par la méthode des Eléments Finis, avec un couplage fort entre les différents phénomènes physiques.

i.5.2 Application à un contact EHD avec film nanométrique

Le modèle nano-EHL est appliqué à un contact linéique sous les conditions typiques du régime EHD. Un fluide de très faible viscosité est employé, générant une épaisseur de film nanométrique au centre du contact. De plus, une des surfaces présente des interactions faibles à l'interface. Par conséquent, un phénomène de glissement apparait près de cette paroi au centre du contact : cet effet modifie radicalement l'épaisseur de film, la circulation du lubrifiant et le frottement par rapport à la théorie classique de la lubrification.

Comme le système présente à la fois une surface glissante et une adhérente, deux configurations sont considérées. Dans le premier cas, la surface avec glissement se déplace plus rapidement que l'autre et entraine le fluide dans le contact. Un dimple, c.à.d. une augmentation locale de l'épaisseur de film, est formé dans la zone centrale (Figure i-9a). Son amplitude croît avec la différence de vitesse imposée aux parois, représentée par le paramètre SRR (Slide-to-Roll-Ratio), qui entraine aussi une augmentation du glissement.
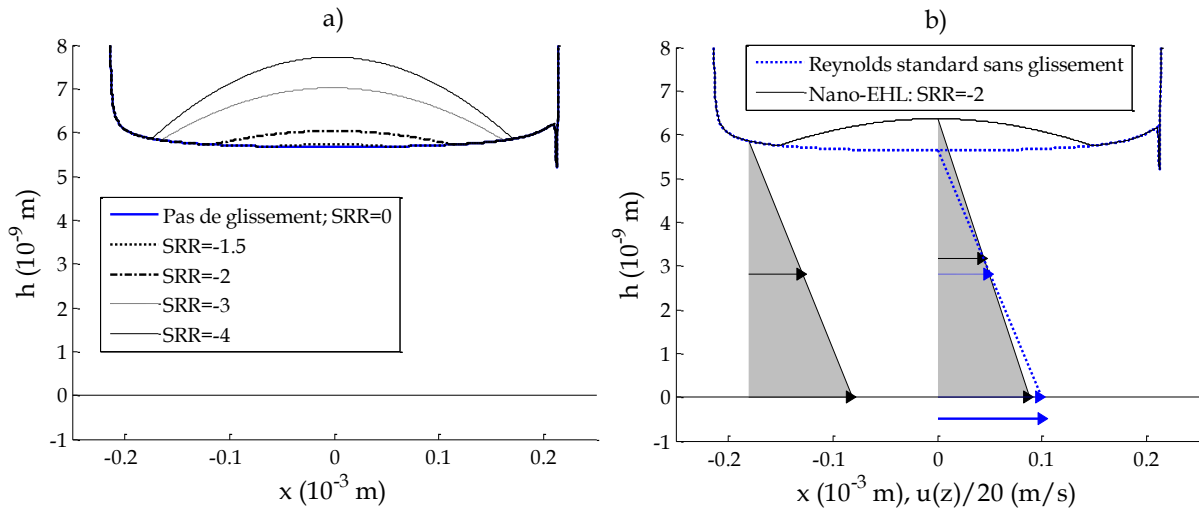
Figure i-9: Résultats du modèle nano-EHL avec une seule surface glissante. Cette dernière entraine principalement le fluide. a) Un dimple se forme au centre du contact, dépendant de la différence de vitesse des parois ; b) Profils de vitesse dans l'épaisseur de film, avec l'aire foncée représentant le débit du fluide

La modification de l'épaisseur de film peut être expliquée en analysant la dynamique du lubrifiant dans le domaine confiné. Figure i-9b montre comment le glissement décélère le fluide dans la zone centrale. En conséquence le débit massique décroit. Cependant, cette quantité doit être conservée tout au long du contact linéique. L'augmentation d'épaisseur de film permet de compenser la décélération du fluide et ainsi avoir un débit constant.

Le phénomène opposé apparaît lorsque la surface adhérente entraine le fluide (Figure i-10). La présence de glissement sur la paroi opposée a pour conséquence d'accélérer le fluide à l'interface et donc dans toute l'épaisseur de film (Figure i-10b). Ainsi, le débit massique augmente : cet effet est balancé par une importante réduction d'épaisseur de film, dont le minimum est déplacé de la zone de sortie au centre du contact.

La présence de glissement influence aussi le frottement dans le système (Figure i-11). Selon la théorie de lubrification classique pour un cas isotherme avec un fluide Newtonien, cette grandeur varie linéairement avec la différence de vitesse imposée aux parois. En présence d'effets moléculaires des déviations sont cependant observées. Lorsque la paroi glissante entraine le fluide, le frottement est réduit à cause de l'augmentation d'épaisseur de film, qui réduit les contraintes de cisaillement dans le fluide. Par contre, quand la surface adhérente emmène le lubrifiant dans le contact et l'épaisseur diminue, la contrainte de cisaillement croît, ainsi que le frottement.

a)

b)
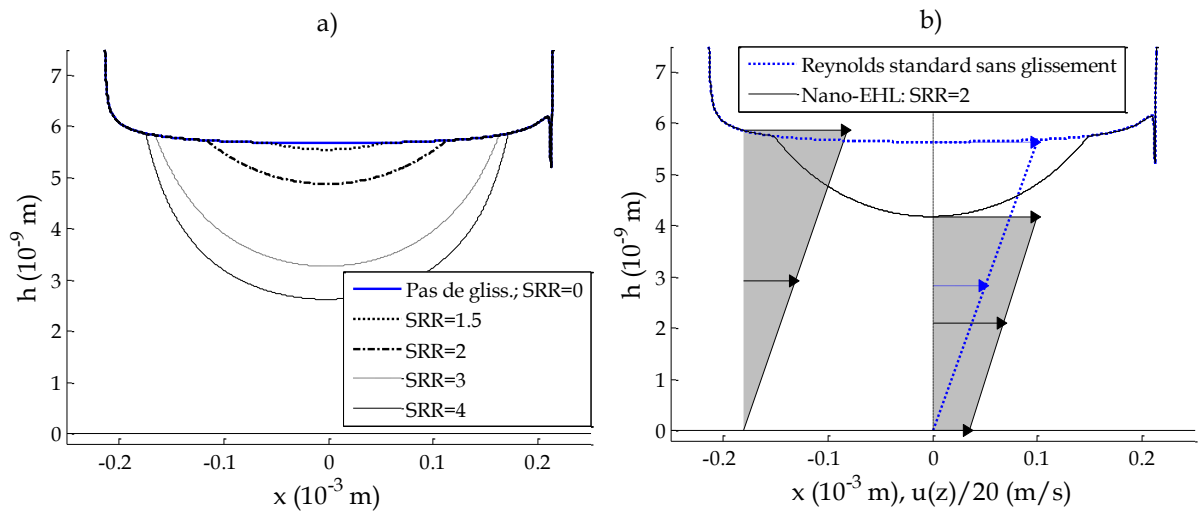
Figure i-10: Résultats du modèle nano-EHL avec une seule surface glissante. Ici la surface mouillante entraine le fluide. a) L'épaisseur de film est réduite dans la zone centrale en fonction de la différence de vitesse des parois ; b) Profils de vitesse dans le fluide, avec l'aire foncée représentant le débit
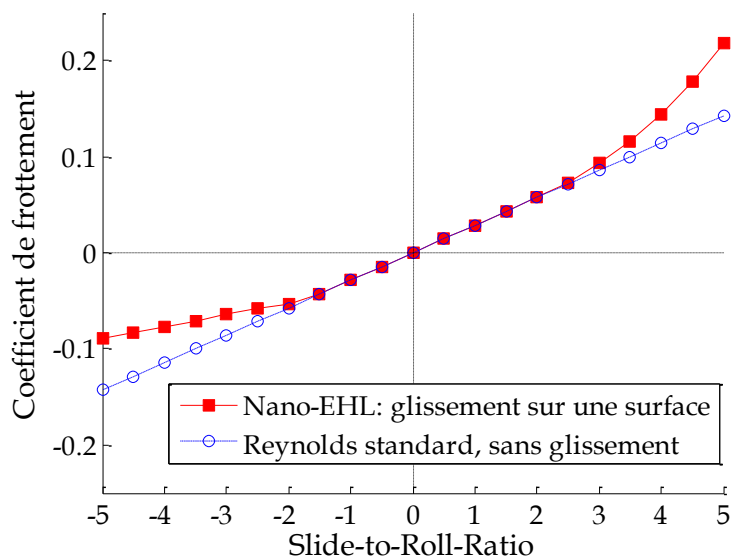
Figure i-11: Coefficient de frottement en fonction de la différence de vitesse des parois

Enfin, une surface dont la composition varie le long du contact est simulée ; chaque grain présente un matériau et des conditions de glissement différents. L'épaisseur de film varie localement en suivant la structure de la surface, avec des sauts brusques aux joints de grain (Figure i-12).
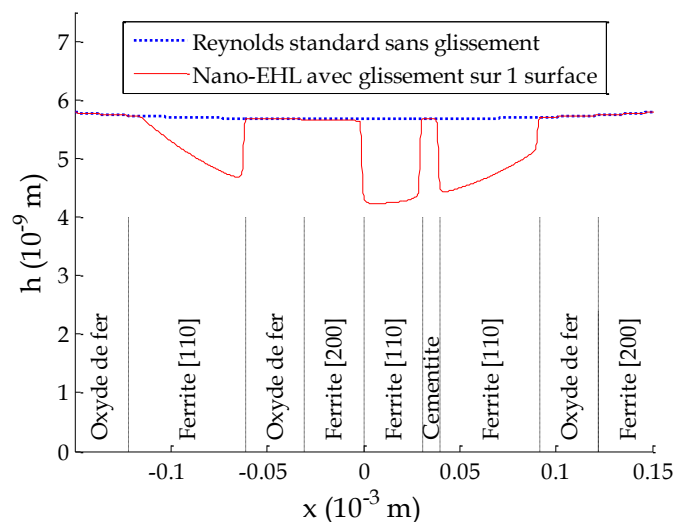
Figure i-12: Résultats du modèle nano-EHL en présence de grains de composition différente sur la surface glissante.

En conclusion, une approche multi-échelle a permis d'observer l'impact profond du phénomène de glissement à l'échelle moléculaire sur l'épaisseur de film et le frottement dans des contacts macroscopiques. D'autres effets peuvent néanmoins être abordés pour améliorer les outils de modélisation en présence de films nanométriques. En particulier, la problématique de la réduction de la quantité de lubrifiant est poussée à ses limites dans la section suivante, jusqu'à atteindre le contact direct entre solides.

i.6 Etude de la rupture du film de lubrifiant par Dynamique Moléculaire

A cause des tendances actuelles qui visent à réduire la quantité d'huile dans les mécanismes, il peut arriver que l'épaisseur du film ne soit plus suffisante pour séparer complètement les surfaces. Ainsi, des zones de contact direct entre solides se forment. Pour modéliser ce régime de lubrification mixte, la rupture du film d'huile doit donc être étudiée.

Une analyse détaillée des phénomènes sous ces conditions de confinement extrême, comme par exemple la transition du lubrifiant vers un état solide, requiert un focus sur l'échelle atomique. Ainsi, des simulations par Dynamique Moléculaire sont à nouveau utilisées. La quantité de lubrifiant confiné dans le nano-patch du contact est réduite jusqu'à atteindre une interaction directe entre les surfaces.

i.6.1 Structuration du fluide et frottement pour deux surfaces lisses

Deux parois lisses et mouillantes, présentant donc de fortes interactions avec le fluide confiné sont choisies en premier ; de l'hexadécane linéaire est utilisé comme lubrifiant. A cause de l'épaisseur de film très mince, ce fluide se structure en un nombre entier de couches parallèles aux surfaces. L'épaisseur de film évolue donc en escalier en fonction du nombre des molécules dans le fluide (Figure i-13).
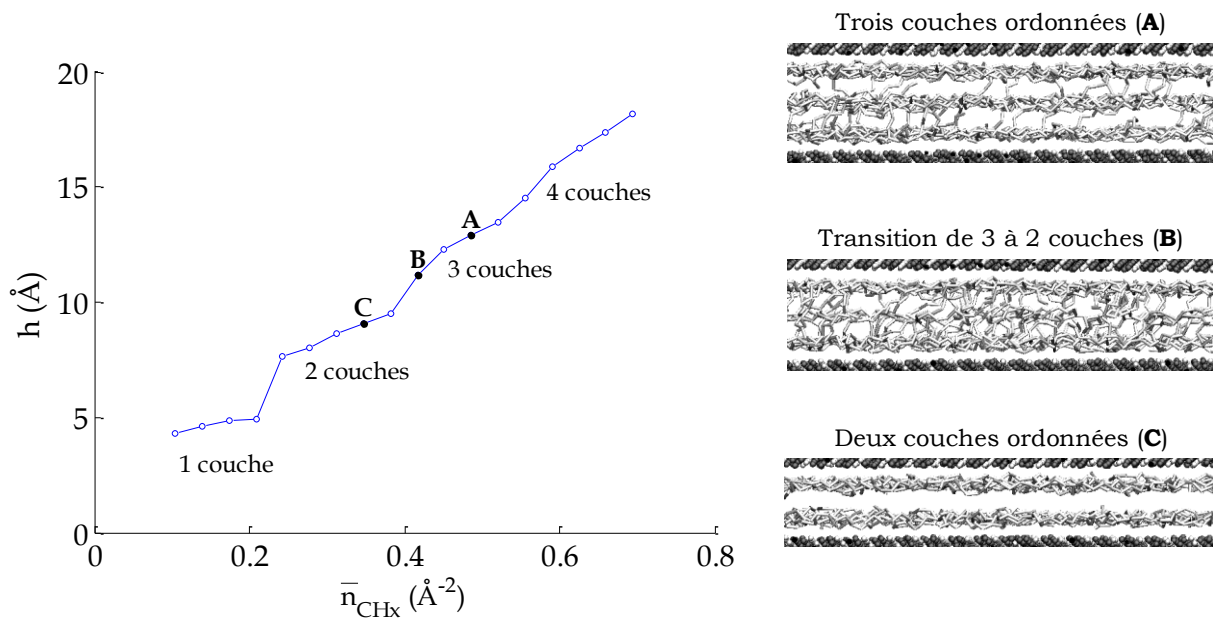
Figure i-13: Epaisseur de film en fonction de la quantité de fluide dans le contact pour deux surfaces lisses. Les configurations A, B et C montrent la transition entre des structures ordonnées en passant par un état désordonné.

De plus, deux types de configurations sont possibles. D'un côté les états **A** et **C** dans la Figure i-13 montrent des structures ordonnées, caractérisées par des couches bien définies sans beaucoup de ponts, i.e. des molécules partagées entre deux couches. De l'autre, des zones de transition (configuration **B**) sont caractérisées par un état désordonné dans lequel les couches centrales fusionnent et les molécules sont entremêlées.

Des profils de vitesse comportant des sauts entre les couches sont observés dans tous les cas. Ainsi, la notion classique de viscosité avec un cisaillement uniforme n'est plus applicable dans le processus de rupture local du film, et le fluide passe à un état quasi-solide. Comme le cisaillement se produit entre les couches, le frottement dans le système est lié au degré d'organisation du lubrifiant (Figure i-14). Des minima apparaissent en correspondance avec les configurations ordonnées, où les couches glissent les unes sur les autres avec peu de résistance. Par contre les états de transition sont caractérisés par des maxima de frottement, car les molécules entremêlées s'opposent au cisaillement. La valeur la plus élevée est atteinte pour une épaisseur de film constituée d'une seule couche. Dans ce cas, un phénomène de glissement aux parois apparait : le cisaillement se produit à l'interface fluide-solide malgré les fortes interactions tangentielles dues aux surfaces mouillantes.

Des taux de cisaillement et un frottement élevés causent une génération importante de chaleur et une augmentation significative de la température du système. Cependant, les effets thermiques sont réduits dans les configurations ordonnées à cause d'un frottement plus faible, et il n'y a pas d'augmentation significative de la température
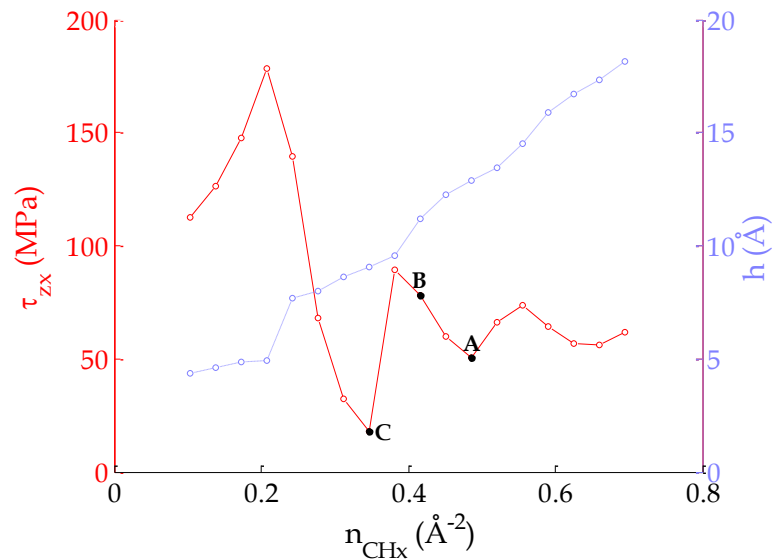
Figure i-14: Contrainte de cisaillement et épaisseur de film en fonction de la quantité de fluide dans le contact, pour deux surfaces lisses.

i.6.2   Influence de la nature des lubrifiants

La nature des lubrifiants peut aussi influencer le comportement local à l'échelle nanométrique. Par exemple des molécules sphériques comme le méthane sont très sensibles au confinement, et les sauts dans l'évolution de l'épaisseur de film sont plus marqués par rapport aux molécules linéaires (Figure i-15a). De plus, il ne peut pas y avoir de ponts entre les couches, ce qui entraine des valeurs très faibles de frottement (Figure i-15b).

D'un autre côté, la présence de ramifications sur les chaines moléculaires favorise la présence de ponts et de configurations entremêlées. Ainsi, les configurations ordonnées caractéristiques des molécules linéaires disparaissent : l'épaisseur de film ne présente presque pas de sauts, et le frottement est généralement élevé avec peu d'oscillations.
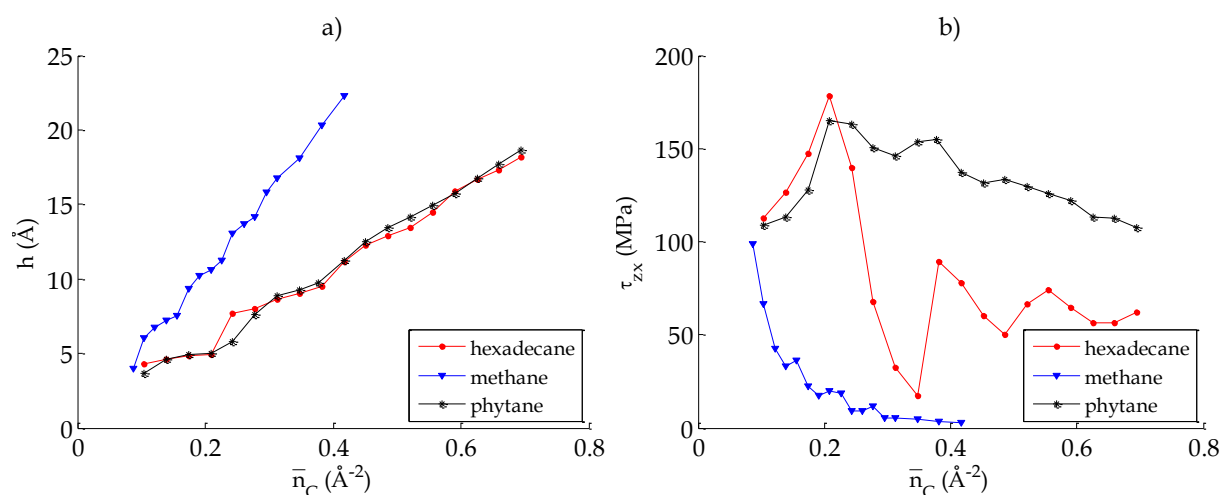
Figure i-15: Epaisseur de film (a) et contrainte de cisaillement (b) pour différents types de molécule (linéaires, sphériques et ramifiées) en fonction de la quantité de fluide, pour deux surfaces lisses.

i.6.3   Influence des nano-rugosités et de la mouillabilité des surfaces

Similairement aux molécules ramifiées, la présence de nano-rugosités sur les parois entraine un état désordonnée du fluide confiné (Figure i-16, configuration D): le frottement est donc toujours élevé. De plus, lorsque la réduction de la quantité de lubrifiant est poussée à l'extrême, les dernières molécules se disposent dans les vallées de la rugosité. Les pics peuvent donc interagir directement avec l'autre surface (configuration E). Un comportement tribologie typique d'un contact direct solide-solide est atteint, avec la présence de forces d'adhésion et des contraintes de cisaillement importantes, ainsi que la déformation des aspérités. Dans cette configuration le maximum absolu de frottement est localement atteint.

Etat désordonné en présence de nano-rugosités (**D**)

Contact direct solide-solide et deformation des asperités (**E**)

Légende:
- 2 surfaces lisses et mouillantes
- Surf. rugueuese mouillante - lisse mouillante: **Etat desordonné**
- 2 surfaces lisses et non mouillantes: **Glissement aux parois**
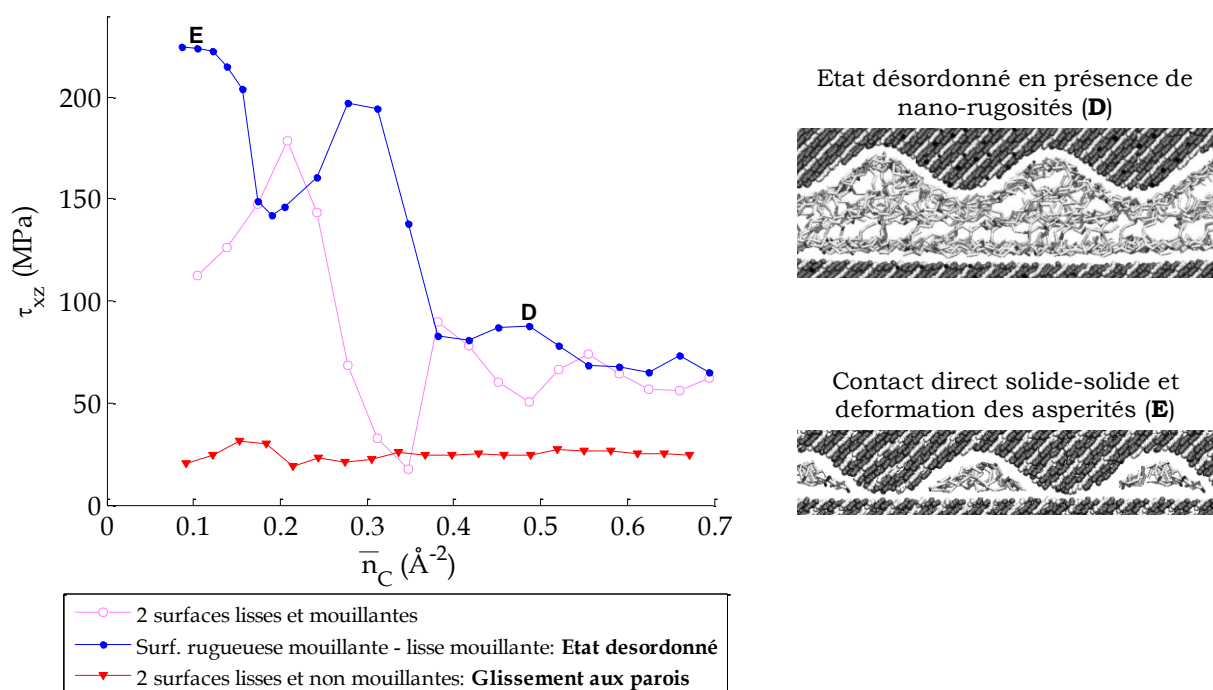
Figure i-16: Contrainte de cisaillement pour différentes morphologies et nano-rugosités sur les surfaces

En réduisant la mouillabilité des surfaces, et donc les interactions moléculaires avec le lubrifiant, le cisaillement du système se produit à l'interface fluide-solide. Un phénomène de glissement aux parois apparaît, limitant le frottement à une valeur faible et constante (Figure i-16). Par contre ce phénomène est entravé par la présence de nano-rugosités sur les parois mouillantes, et des frottements élevés sont à nouveau observés.

En conclusion, cette dernière section porte sur le cas d'une réduction extrême de la quantité de lubrifiant, qui entraine la rupture locale du film et le contact direct entre solides. Des simulations par Dynamique Moléculaire ont permis d'analyser en détail ce phénomène, et de faire le lien entre la structuration des molécules du fluide et le frottement local. De plus, l'impact de différentes natures des lubrifiants ou de la géométrie et de la morphologie des surfaces a été exploré.

i.7   Conclusion générale et perspectives

Les tendances modernes en lubrification visent à créer des mécanismes où la quantité d'huile est de plus en plus réduite. Ceci entraine une diminution de l'épaisseur de film, qui peut atteindre quelques nanomètres. Les propriétés de ces films hautement confinés peuvent dévier fortement par rapport à l'état "bulk" : des phénomènes typiques sont la structuration du lubrifiant, une augmentation de viscosité, ou la modification de la vitesse à l'interface paroi-fluide par rapport à une condition de non-glissement.

L'objectif de cette thèse était donc de caractériser les phénomènes moléculaires dans des films nanométriques, ainsi que de comprendre leur influence sur le comportement d'un contact macroscopique. Un modèle numérique basé sur la Dynamique Moléculaire a été utilisé pour étudier des huiles de base (alkanes) confinés sous cisaillement dans un nano-spot de l'interface du contact macroscopique.

Le travail a principalement porté sur le glissement aux parois, i.e. une différence de vitesse entre le fluide et le solide à l'interface. Un modèle de prédiction a été développé pour quantifier ce phénomène en fonction du couple lubrifiant-parois. Les surfaces ont été caractérisées par une technique de scanning, qui ensuite a été reliée à la contrainte tangentielle à l'interface et au frottement local. La rhéologie du lubrifiant sous confinement a été comparée au propriétés "bulk". Les natures des surfaces et du fluide ont été intégrées dans un modèle de glissement valable pour des alkanes linéaires (huiles de base) confinés entre des surfaces métalliques simples ou complexes. Enfin, l'impact des conditions opératoires locales sur le glissement a été étudié à travers des études paramétriques sur la vitesse, l'épaisseur de film et la pression, et quantifié au moyen d'une loi analytique.

Ces résultats ont finalement été intégrés dans une approche multi-échelle, appelée nano-EHL, pour l'étude d'un contact macroscopique. En particulier l'équation de Reynolds classique a été modifiée pour inclure les effets de glissement sur une surface. L'approche a ensuite été appliquée à un contact élasto-hydrodynamique comportant un fluide à très faible viscosité, et par conséquent une épaisseur de film nanométrique. L'apparition du glissement dans la zone centrale du contact cause une modification significative de l'épaisseur du film. Par exemple, si la surface glissante entraine le fluide, une augmentation locale d'épaisseur (dimple) compense la décéleration du lubrifiant et assure la continuité du débit. De plus, le taux de cisaillement et le frottement dans la zone centrale sont réduits par rapport au cas sans glissement. Au contraire, si la surface mouillante entraine le fluide, l'épaisseur de film diminue pour compenser l'accélération du lubrifiant, et le frottement augmente.

Enfin, la problématique de réduction de la quantité de lubrifiant a été poussée à ses limites jusqu'à atteindre la rupture locale du film et le contact direct entre solides. Lorsque deux surfaces lisses sont présentes, le lubrifiant se structure en couches parallèles aux parois. De plus, le cisaillement du système dépend de l'organisation spatiale des molécules. Lorsque peu de ponts se forment entre les couches, ce qui correspond à des configurations ordonnées, le frottement est faible. Quand par contre les molécules sont enchevêtrées le fluide résiste d'avantage au cisaillement et le frottement devient élevé. Ces configurations désordonnées sont favorisées par la présence de ramifications dans le fluide ou de surfaces nano-rugueuses. Par contre, le cisaillement du système se produit à l'interface fluide-solide en pré-

sence de surfaces non mouillantes : un phénomène de glissement aux parois apparait, limitant le frottement à une valeur faible et constante. Enfin, le maximum de frottement a été atteint pour le contact direct entre les solides, où les forces d'adhésion entre atomes des surfaces métalliques dominent.

En conclusion, ce travail montre l'importance d'une étude multi-échelle nano-macroscopique pour une bonne compréhension des mécanismes où la réduction de la quantité de lubrifiant entraine la présence de films confinés. L'analyse effectuée ici peut être étendue dans le futur à d'autres phénomènes ou configurations. Par exemple à l'échelle nanométrique des lubrifiants complexes avec des molécules polaires, telles que les acides gras, des additifs ou des liquides ioniques peuvent être considérés. Le phénomène de rupture du film peut être approfondie afin d'analyser et quantifier les déformations nanométriques des solides. Les effets thermiques dus au fort cisaillement du fluide sous confinement extrême peuvent aussi être explorés.

A l'échelle macroscopique, l'approche nano-EHL peut être étendue à des propriétés non-Newtoniennes du fluide, à une analyse thermique, ainsi qu'à la présence de rugosités microscopiques sur les surfaces. Dans ce dernier cas, il serait intéressant d'étudier les contacts possibles entre les pics d'aspérités. Un modèle à l'échelle micrométrique permettrait de caractériser chaque spot de contact, en faisant appel aux résultats des simulations atomistiques pour comprendre le comportement des dernières couches de lubrifiant séparant les surfaces. Enfin, toutes ces connaissances pourraient être intégrées dans une approche globale appelée nano-micro-EHL, afin de créer un outil numérique pour la simulation des mécanismes lubrifiés opérant sous conditions extrêmes de réduction d'épaisseur de film.

ii Zusammenfassung

ii.1 Einleitung

Eines der wichtigsten Ziele der Industrie und der Forschung in der Tribologie ist die Entwicklung von Systemen, die extreme Leistungen, Drücke und Temperaturen ertragen können. In diesem Rahmen ist eine gute Schmierung der Mechanismen notwendig, um ihre Effizienz und Lebensdauer durch eine Verminderung von Reibung und Verschleiß zu maximieren [1]. Deswegen beinhalten die meisten Anwendungen wie z.B. Lager einen Schmierfilm, der die Oberflächen im Kontaktbereich trennt. Diese Betriebsart wird Elasto-Hydrodynamik (EHD) genannt, und wird klassischerweise durch die Kopplung zwischen der Reynolds-Gleichung für das Fluidverhalten im Kontakt [2] und der Elastizitätsgleichungen für die Verformung der Festkörper unter hohem Druck beschrieben. In zahlreichen Studien wurde diese Theorie verwendet, um ein detailliertes Verständnis der Phänomene zu erreichen und um tribologische Mechanismen zu optimieren.

Allerdings zwingen heutige Umweltschutznormen zu einer Verminderung der Ölmenge. Außerdem werden im Rahmen des Downsizing separate Schmiersysteme aufgegeben, um die Größe der Mechanismen zu reduzieren: In diesem Fall werden Betriebsfluide mit niedriger Viskosität zur Schmierung des Systems verwendet, wie zum Beispiel Kühlmittel oder Treibstoffe.

Folglich nimmt die Dicke des Schmierfilmes stark ab: die Spalthöhe kann lokal die Größenordnung von Nanometern erreichen [1], was der Dimension der Moleküle entspricht (Abbildung ii-1). Die Eigenschaften von Schmierstoffen bei kleinen Filmdicken sind stark von atomaren Parametern abhängig, wie z.B. der Struktur der Fluidmoleküle oder der Zusammensetzung der Oberflächen. Es ist deswegen notwendig, diese Nanometer-Effekte quantitativ zu bestimmen, weil sie das Globalverhalten eines Kontaktes beeinflussen können.
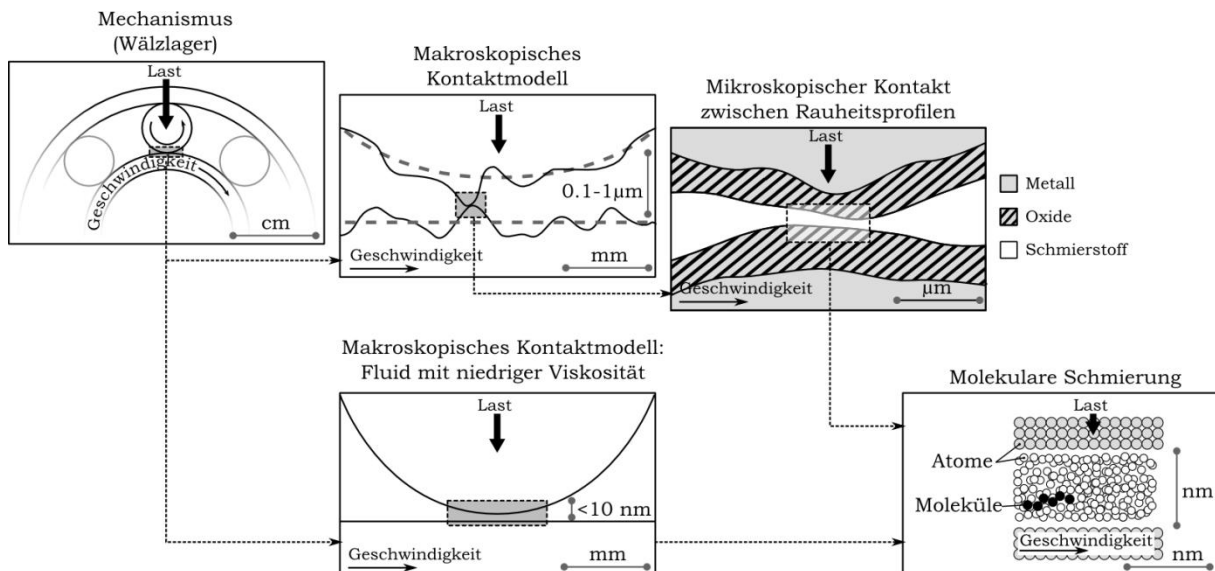
Abbildung ii-1: Mehrskaliger-Charakter eines geschmierten Kontaktes, in dem die Schmierstoffmenge sehr gering ist und die Spalthöhe im Nanometer-Bereich liegt.

ii.2   Stand der Technik und Ziele der Doktorarbeit

ii.2.1   *Molekulare Schmierung*

Molekulare Schmierung liegt vor, wenn nur wenige Schmierstoffmoleküle die Oberflächen trennen und die Spalthöhe in der Größenordnung von Nanometern liegt. Im Allgemeinen ist eine makroskopische Beschreibung nicht detailliert genug, um diesen Zustand zu charakterisieren. Deshalb wurden neue Messgeräte entwickelt, um das Verhalten in Nanometer-Spalten zu untersuchen: beispielhaft seien der „Surface Force Apparatus" (SFA) [3] und das Rasterkraftmikroskop [4] genannt. Außerdem erlauben Methoden wie Moleküldynamik [5] die Bewegung von den einzelnen Atomen zu simulieren und folglich ihre Anordnung und Geschwindigkeit in sehr dünnen Schmierfilmen zu bestimmen. Mit Hilfe dieser Methoden wurden drei Hauptphänomene identifiziert: Struktureffekte, die Nano-Rheologie und die Geschwindigkeitsrandbedingung an der Fluid-Wand-Grenzfläche.

ii.2.1.a   *Struktureffekte*

Experimente haben gezeigt, dass die Kraft eines Fluides auf die Berandung bei sehr dünnen Filmddicken räumlich oszilliert; dabei entspricht ihre Periodizität dem Durchmesser der Moleküle [3]. Dieses Phänomen wird Solvatation genannt und ist mit der Anordnung des Fluides in Molekülschichten („layering") parallel zu den Wänden verbunden. Die Molekülposition wird von Potentialen beider Oberflächen beeinflusst, und eine räumliche Organisation findet in der Spalthöhe statt. Dieser Effekt führt zu lokalen Schwankungen der Dichte, wie sich beispielsweise in Moleküldynamik-Simulationen beobachten lässt (Abbildung ii-2) [6]: die lokalen Maxima entsprechen dabei Molekülschichten, Minima ergeben sich durch die praktische Atomfreien intermolekularen Bereiche.

Diese Struktureffekte hängen von der Zusammensetzung des Schmierstoffs und der Wände ab. Sphärische Moleküle oder kürze Kette werden stark von Solvationskräften beeinflusst [7]. Außerdem wird die Anordnung in Schichten sowohl in der Spalthöhe als auch parallel zur Oberfläche von Wänden verursacht, die eine geometrische und energetische Affinität mit dem Fluid zeigen [8]. Andererseits vermindern die Gegenwart von Nanorauheit [9] oder Verzweigungen [10] die Fluidordnung.
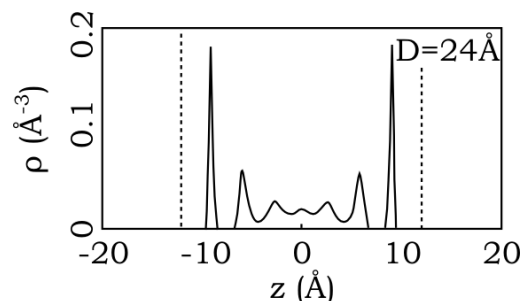
Abbildung ii-2: Dichte-Maxima entsprechend der Entstehung von Molekülschichten in einem Fluid bei sehr geringer Filmdicke. Die gepunkteten Linien stellen die Oberflächen dar, deren Abstand hier 2.4 nm ist.

ii.2.1.b   Nano-Rheologie

Die vorgenannte Schichtung der Moleküle über der Spalthöhe ist mit einer Veränderung der Rheologie unter Scherungsbelastung verbunden. Beispielsweise konnte eine Viskositätserhöhung experimentell beobachtet werden, wenn die Dicke des Schmierfilmes kleiner als 5-6 Molekülschichten ist [11]. Außerdem findet ein reversibler Übergang zu einem kristallisierten Zustand der Moleküle statt, wenn die Spalthöhe weiter reduziert wird [12]. Diese Phänomene werden jedoch durch die sog. Scherverflüssigung wieder vermindert, wobei die Viskosität unter hohen Scherraten ein Plateau erreicht [13].

Ähnlich zum Struktureffekt tritt auch die Viskositätsveränderung im Vergleich zu verzweigten Fluidarchitekturen oder in Gegenwart von nanorauen Oberflächen [9, 14] deutlicher zu Tage, wenn sphärische Moleküle oder kurze Ketten vorliegen [6].

ii.2.1.c   Einfluss der Geschwindigkeitsrandbedingungen an der Fluid-Wand-Grenzfläche

Die dritte Eigenschaft Fluiden in extrem engen Spalten ist die besondere Fluiddynamik in der Spalthöhe. Die klassische Haftbedingung verschwindender Relativgeschwindigkeit zwischen Fluid und Wand ist nun i.a. nicht mehr gültig: vielmehr ist oftmals zu beobachten, dass die direkt mit der Oberfläche im Kontakt stehende Molekülschicht über die Wand gleitet [15].

Dieser Effekt ist typisch für nicht-benetzbare Oberflächen, die schwache Interaktionen und geringe geometrische Affinität zu den Fluidmolekülen zeigen [8]. Außerdem steigt der Geschwindigkeitsunterschied an der Wand-Fluid-Grenzfläche in Gegenwart langer oder verzweigter Moleküle [16]. Höhere Scherraten und Drücke [17], sowie geringe Filmdicken [18] führen auch zu größerem Wandschlupf. Im Gegenteil hierzu unterdrücken nanoraue Oberflächen das Phänomen eher [9]: es können mehrere Molekülschichten an den Wänden haften, was als „locking" bezeichnet wird [19].

Der Stand der Technik zeigt, dass die Eigenschaften dünner Schmierfilme mit Filmdicken im Nanometerbereich deutlich von den makroskopischen Fluideigenschaften abweichen können. Es ist deswegen interessant, diese lokal bedingten Effekte in makroskopische Modelle für die Bestimmung des globalen Kontaktverhaltens einzufügen.

ii.2.2   Integration molekularer Effekte in kontinuierliche Modelle

Auf Grund der beschränkten Berechnungskapazitäten moderner Computer können im Rahmen von moleculardynamischen Modellen nur einigen Tausend Atome simuliert werden. Hierdurch bleibt die physikalische Ausdehnung berechenbarer Bereiche auf die Nanometer-Skala begrenzt und realistische Kontaktbereiche in der Größenordnugn von Millimetern können auf absehbare Zeit nicht charakterisiert werden. Ein mehrskaliger Ansatz zur Kopplung von atomistischen Simulationen und Kontinuumsmodellen bietet hier einen möglichen Ausweg.

In der Literatur wird vorgeschlagen, die durch die molekulare Struktur induzierten Phänomene in sehr dünnen Filmen durch analytische Gesetze zu approximieren. Zum Beispiel wurden Solvatationseffekte durch eine zusätzliche oszillierende Kraftkomponente zwi-

schen den Oberflächen beschrieben [20]. Folglich konnte die Spalthöhe in der Mitte des Kontaktes nur bestimmte Werte erreichen, die einer Ganzzahl von Molekülschichten entsprechen [21].

Die Veränderung der Haftbedingung an den Wänden kann auch das globale Verhalten eines Kontakts beeinflussen. Zum Beispiel führt ein konstanter Wandschlupf im ganzen Kontaktbereich zu einer Verminderung der Spalthöhe bei einer gegebenen Last [22]. Schließlich wurden in [18] Gesetze abgeleitet, die die Abhängigkeit des Wandschlupfes vom lokalen Druck, der lokalen Geschwindigkeit und Spalthöhe beschreiben. Solche Ansätze wurden in ein EHD-Kontaktmodell eingefügt, und erlaubten die detaillierte Untersuchung eines Dimpels, d.h. eines lokalen Anstiegs der Spalthöhe bei gleichzeitiger Verminderung der Reibung unter hohen Scherraten.

ii.2.3   Ziele der Doktorarbeit

Gegenstand dieser Arbeit ist die Untersuchung von Phänomenen, welche in Schmierfilmen mit Filmdicken im Nanometerbereich auftreten können. Der verfolgte Ansatz umfasst dabei zwei Schritte:

- Zuerst wird das Verhalten von Fluiden bei extrem geringen Filmdicken durch atomare Simulationen analysiert, um die Stoffeigenschaften unter typischen Arbeitsbedingungen eines elastohydrodynamischen Verlaufs zu charakterisieren.
- In einem zweiten Schritt wurde ein mehrskaliger Ansatz entwickelt, um die molekularen Effekte in makroskopische Modelle einfügen und ihren Einfluss auf das gesamten Kontaktverhalten verstehen zu können.

Zuerst werden Moleküldynamik-Simulationen für die Scherung sehr dünner Schmierfilme entwickelt (Abschnitt ii.3). Dann wird dieses Modell verwendet, um den Wandschlupf in einer typischen Kontaktgrenzfläche (Abschnitt ii.4) zu quantifizieren. Hierzu werden analytische Gesetze abgeleitet, um die Abhängigkeit dieses Phänomens von der Zusammensetzung der Oberflächen, dem Schmierstoff und den lokalen Arbeitsbedingungen zu beschreiben.

In Abschnitt ii.5 wird dieser Ansatz mit einem Kontinuumsmodell gekoppelt; diese Multi-Skalen-Methode wird angewendet, um den Einfluss des Wandschlupfes auf die Spalthöhe und die Reibung in einem EHD-Kontakt zu analysieren. Schließlich wird in Abschnitt ii.6 die Ölmenge so weit reduziert, dass ein lokaler Zusammenbruch des Schmierfilmes und direkter Festkörperkontakt auftreten.

ii.3   Das Moleküldynamik-Modell

Das Modell für die Untersuchung nanometer-dünner Filme unter Scherung basiert auf der Moleküldynamik. Im Rahmen dieser Methoden werden die Atome als Massenpunkte modelliert und die interatomatoren Kräfte durch nichtlineare Potentiale beschrieben. Diese numerische Methode löst explizit die Bewegungsgleichungen für alle Atome im System. Die Berechnung umfasst im Wesentlichen aus vier Schritten [5].

- In jedem Zeitschritt wird die auf jedes Atom wirkende Kraft aus den Interaktionen mit den Nachbarn unter Verwendung nichtlinearer Potentialfunktionen berechnet.
- Dazu werden zusätzliche Kräfte addiert, die den Randbedingungen in Druck, Scherung und Temperatur entsprechen.
- Mit dem zweiten Newtonschen Gesetz kann die Beschleunigung der einzelnen Atome bestimmt werden.
- Schließlich werden die neuen atomaren Positionen durch eine doppelte Integration mit dem Verlet-Algorithmus berechnet [5].

Durch diese Vorgehensweise kann die Bewegung aller Atome und Moleküle im System simuliert werden; aufgrund der Rechen- und Speicherkapazitäten moderner Computer liegen die Grenzen berechenbarer Modelle derzeit bei räumlichen Ausdehnungen im Nanometerbereich (10^4 Atome) und Zeitintervall von Nanosekunden (10^6 Zeitschritten).

ii.3.1 Atomistische Simulationen von Fluiden bei sehr dünnen Filmen

Im Rahmen des atomistischen Modells wird ein Kontaktbereich betrachtet, bei dem Ausdehnung und Spalthöhe im Bereich weniger Nanometer liegen (siehe Abbildung ii-3). Durch Forderung periodischer Randbedingungen in x und y wird das System unendlich in diese beiden Raumrichtungen fortgesetzt.
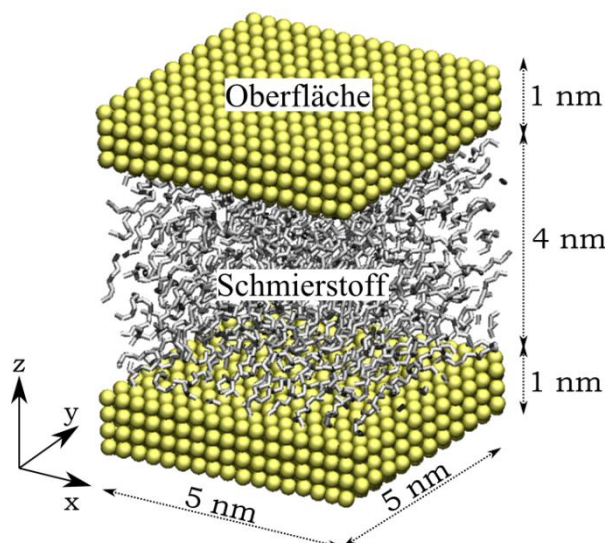
Abbildung ii-3: Überblick des Moleküldynamik-Systems, das ein Nanometer-Bereich der Kontaktfläche mit verengtem Fluid darstellt.

Die Oberflächen bestehen aus den jeweils letzten Atomschichten der Festkörper, die direkt das Fluid berühren. Ihre Materialeigenschaften entsprechen denen von Metallen oder Metall-Oxiden: solche Werkstoffe werden durch reguläre Kristallgitter modelliert, die kanonisch oder komplex sein können. Die elastischen Verformungen des Gitters werden durch lineare Federn zwischen den Atomen simuliert, deren Steifigkeit so angepasst wird, dass ein realistischer Kompressionsmodul des Werkstoffs unter reiner Druckbelastung resultiert [23].

Das Fluid besteht aus Alkanen, welche repräsentativ für typische Basis-Öle in EHD-Kontakten stehen. Jedes Molekül wird durch eine flexible Atomkette dargestellt: dabei wir-

ken zwischen den einzelnen Atomen nichtlineare Kraftfelder, welche vom relativen Abstand, der Winkeländerung und der Torsion abhängen [24]. Zur Beschreibung der intermolekularen van-der-Waals-Interaktionen zwischen Atomen verschiedener Molekülen werden Lennard-Jones-Potentiale verwendet [5]. Das Interaktionspotential zwischen Wand und Fluid wird mit Hilfe von zwei Methoden parametrisiert: bei der ersten Methode wurde die Parametrisierung so vorgenommen, dass experimentell bestimmte Adsorption/ Desorption-Energien für Alkane auf Metalloberflächen korrekt dargestellt werden [25]; die zweite Methode basiert auf dem Zusammenhang zwischen der makroskopischen Oberflächenenergie und den atomaren Interaktionen [26].

ii.3.2   Arbeitsbedingungen

Mit Hilfe des zuvor beschriebenen Modells soll die Scherung des Fluids unter gegebenen mechanischen und thermodynamischen Randbedingungen untersucht werden. Der Druck auf die Kontaktfläche, die Wandgeschwindigkeit und die Temperatur werden dabei in Anlehnung an für einen elasto-hydrodynamischen Kontakt typische Werte gewählt. Bei der Simulation eines Betriebspunktes werden dabei folgende drei Schritte vorgenommen.

Zunächst wird das Volumen des Fluidfilms mit einer gegebenen Anzahl zufällig verteilter Moleküle gefüllt: mittels einer Energieminimierung wird eine nahegelegene konsistente und damit realistische Konfiguration ermittelt. Es folgt eine Kompression des Films, während der der Druck auf die externen Atomschichten der Wände aufgebaut wird, bis sich eine stationäre Spalthöhe einstellt. Für den Rest der Simulation wird der Druck konstant gehalten. Im letzten Schritt wird den Wänden eine Tangentialbewegung aufgeprägt und das Fluid wird geschert. Unter diesen Bedingungen wird ein Zeitintervall von wenigen Nanosekunden berechnet, in dem ein stationärer Zustand erreicht werden kann.

Die meisten Simulationen werden mit konstanter Wandtemperatur durchgeführt, die mit Hilfe eines Langevin-Thermostats geregelt wird [27]. Dieses Verfahren erlaubt die durch die Fluidscherung erzeugte Energie abzuführen. Eine komplexere Energieabfuhrmethode [28] wird in Abschnitt 0 verwendet, um thermische Effekte und die Steigung der Temperatur unter extremer Spaltverengung zu untersuchen.

ii.3.3   Ausgangsgrößen des Modells

Die Ausgangsgrößen des Moleküldynamik-Modells sind die Positionen und Geschwindigkeiten aller Atome. Diese Daten können zeitlich und räumlich gemittelt werden, um die tribologischen Standardgrößen zu berechnen, wie z.B. die Dicke und Dichte des Schmierstoffs.

Ein Sampling der atomaren Anordnung und Dynamik in Schichten parallel zur Oberfläche erlaubt, die Dichten- und Geschwindigkeitsprofile in der Spalthöhe zu berechnen. Schließlich können die Schubspannung und die Reibung im System aus den tangentialen Komponenten der Wandkräfte ermittelt werden.

ii.4   Analyse des Wandschlupfes durch Moleküldynamik

Ein typisches Phänomen in Fluiden sehr geringer Filmhöhe ist der sog. Wandschlupf: hierunter versteht man das Auftreten einer Relativbewegung zwischen der wandnächsten Fluidschicht und der Wand, sodass die sonst übliche Haftbedingung nicht mehr gültig ist (Abbildung ii-4). Wandgleiten wird durch einen dimensionslosen Parameter s (für „*slip*") quantifiziert, der aus der auf das System angelegten Scherrate, sowie aus der dynamischen Reaktion des verengten Fluides ermittelt wird. Alternativ kann die Gleitlänge L_s (Abbildung ii-4) verwendet werden.
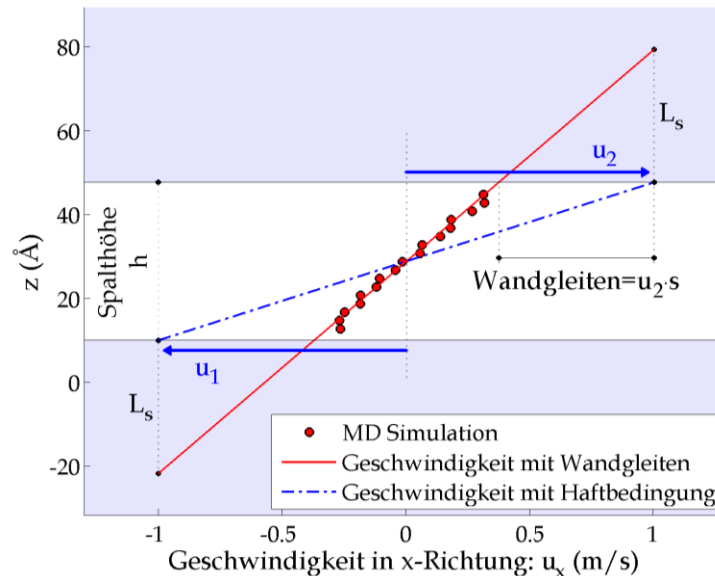
Abbildung ii-4: Wandschlupf bei einem Fluid mit sehr geringer Filmhöhe: die blauen Pfeile stellen die Wandgeschwindigkeiten u_1 und u_2 in der x-Richtung dar, während die Geschwindigkeit des Fluides aus MD-Simulationen von den roten Punkten gezeigt wird.

ii.4.1   *Einfluss der Paarung Oberfläche-Schmiermittel: ein Vorhersagemodell für Wandschlupf*

Zwei Haupteinflussgrößen für den Wandschlupf sind die Zusammensetzung der Wände sowie die Struktur der Fluidmoleküle. Abbildung ii-5a zeigt, dass verschiedene Oberflächen unterschiedliche Geschwindigkeitssprünge an der Grenzflächen aufweisen; außerdem verstärkt sich das Schlupfphänomen mit der Kettenlänge der Alkane (Abbildung ii-5b).

In einem geschmierten Kontakt können aufgrund lokaler Veränderungen der Zusammensetzung der Oberflächen zahlreiche Fluid-Wand-Paarungen auftreten. Eine Charakterisierung jeder denkbaren Konfiguration mit Hilfe der Moleküldynamik würde enorme Berechnungskosten und Zeiten mit sich bringen. Das Ziel dieses Abschnitts ist daher die Formulierung eines Modells für den Wandschlupf, das auf dem Gegensatz zwischen der Natur des Fluides (lineare Alkane, repräsentativ für Basis-Öle) und der Oberflächen (Metalle und Metalloxide) basiert.
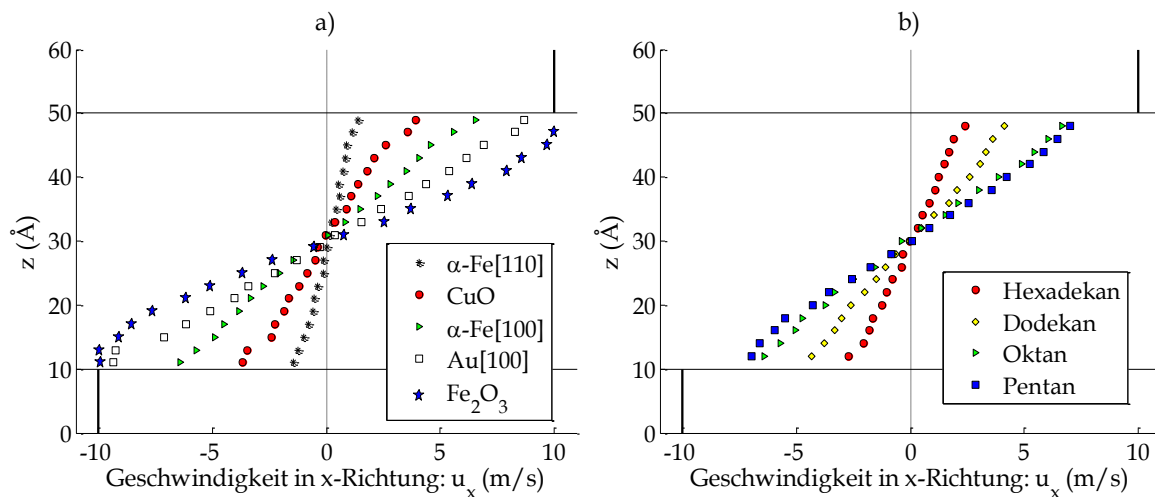
Abbildung ii-5: Abhängigkeit des Wandschlupfes von der Wand-Fluid-Paarung. Die Geschwindig-keitsprofile sind hier dargestellt für: a) einen sehr dünnen Hexadekan-Film zwischen verschie-denartigen Metalloberflächen, und b) zwei kanonische Wände mit verschiedenen linearen Alka-nen. Die Wandgeschwindigkeiten betragen jeweils ±10 m/s.

ii.4.1.a   Charakterisierung der Oberflächen

Zur Charakterisierung des Einflusses der Wände wurde eine Scanning-Methode ent-wickelt, die sowohl für kanonische als auch komplexe Kristallgitter angewandt werden kann (Abbildung ii-6). Jede Oberfläche wird dabei mit Hilfe eines Atom abgetastet, dessen Größe und energetische Eigenschaften denen einer Kohlenwasserstoffgruppe der Alkan-Kette ent-sprechen. Dabei werden lediglich die Koordinaten (x, y) vorgegeben während sich das Atom in vertikaler Richtung in das lokale Potentialminimum bewegen kann, sodass eine Folge von Gleichgewichtszuständen betrachtet wird. Durch die Wiederholung dieser Vorgehensweise auf der ganzen Oberfläche kann man ein Potentialfeld (Abbildung ii-6) und eine Gleichge-wichtshöhe ermitteln. Diese Daten werden schließlich mit der energetischen Wand-Fluid-Wechselwirkung (Korrugation) und der geometrischen Affinität zwischen den Molekülen und dem Kristallgitter (Kommensurabilität) in Verbindung gesetzt und zum Charakterisie-rungsparameter ζ_{surf} zusammengefasst.
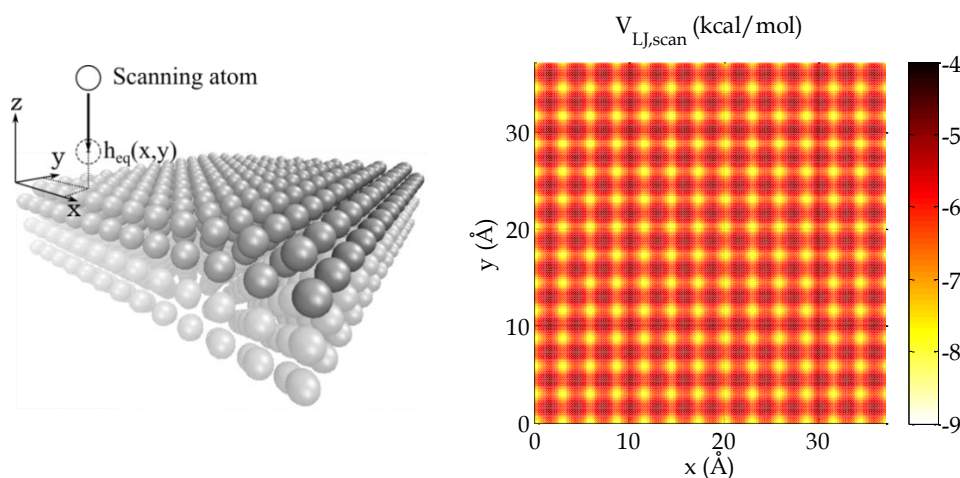
Abbildung ii-6: Scanning-Methode und Abtastung einer α-Fe[100] Oberfläche. Das entsprechende Potentialfeld ist in der rechten Teilabbildung dargestellt.

Diese Kenngröße quantifiziert die tangentiale Impulsübertragung an der Grenzfläche und erlaubt, die Oberflächen entsprechend ihrer Fähigkeit zur Impulsübertragung auf das Fluid zu klassifizieren. Die Abhängigkeit der Grenzschubspannung τ_{zx} von ζ_{surf} ist in Abbildung ii-7 für verschieden Oberflächen-Alkan-Paare dargestellt. Für kleine Werte des Parameters ζ_{surf} wird die Spannung von den schwachen Wand-Fluid-Wechselwirkungen begrenzt, und Wandschlupf tritt auf. Dann steigt τ_{zx} mit ζ_{surf}, bis ein Plateau erreicht wird. In diesem Fall ist die Schubspannung von der vollen Scherung des Fluides begrenzt. Die Kurven $\tau_{zx}(\zeta_{surf})$ werden schließlich durch analytische Formeln beschrieben, die für lineare Alkane zwischen kanonischen und komplexen Metalloberflächen gültig sind.
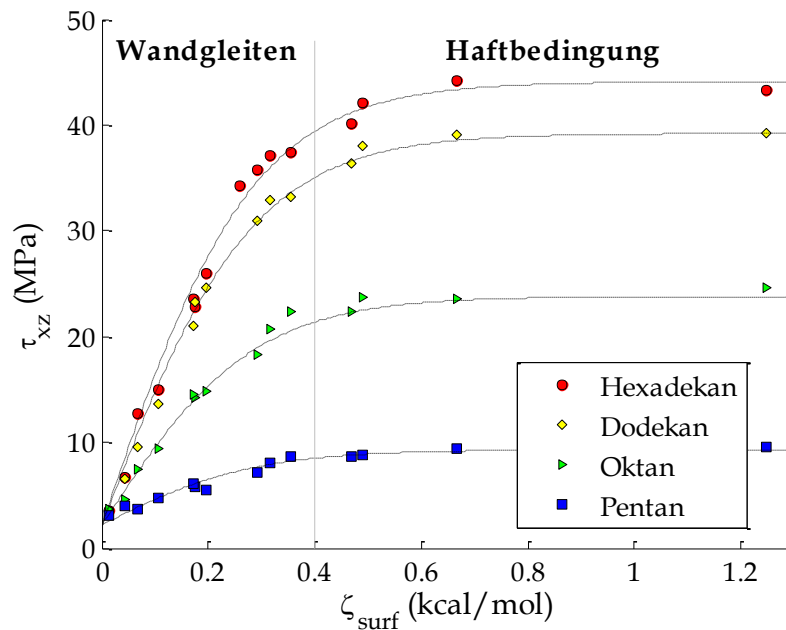
Abbildung ii-7: Schubspannung in Abhängigkeit von ζ_{surf}, für verschiedene lineare Alkane. Jeder Punkt entspricht dem Ergebnis einer Moleküldynamik-Simulation.

ii.4.1.b   Charakterisierung des verengten Fluides

Die Rheologie des Fluides bei sehr dünnen Filmddicken wird durch die effektive Viskosität η_{eff} gekennzeichnet. Ein Vergleich mit Moleküldynamik-Simulationen von n-Alkanen im nicht verengten Zustand zeigt, dass η_{eff} durch eine Bulk-Viskosität η_{bulk} approximiert werden kann, wenn die Spalthöhe größere als 2-3 nm ist und kein Übergang zum Festkörperverhalten im Schmierstoff stattfindet. Die Viskosität $\eta_{bulk}(\tau_{zx},P,T)$ hängt nur von den Arbeitsbedingungen in Druck, Temperatur und Schubspannung τ_{zx} ab.

ii.4.1.c   Das Vorhersagenmodell für Wandgleiten

Schließlich wird der Einfluss der Oberflächenmorphologie und der molekulare Struktur des Fluides in ein Vorhersagenmodell für Wandgleiten eingefügt. Für den Wandschlupfparameter gilt hierbei

$$s = 1 - \dot{\gamma}_{app}^{-1} \frac{\tau_{zx}(\zeta_{surf})}{\eta_{bulk}(\tau_{zx},P,T)}$$

$\dot{\gamma}_{app}$ ist die durch die Arbeitsbedingungen angelegte externe Scherrate. Die Schubspannung $\tau_{zx}(\zeta_{surf})$ wird durch die Kurven von Abbildung ii-7 in Abhängigkeit vom Oberflächen-charakterisierungsparameter aus der Scanning-Mehode bestimmt. Die Viskosität η_{bulk} des Schmiermittels kann mit Modellen aus der Literatur beschrieben werden. Dieses Vorhersagemodell für Wandschlupf ist gültig für lineare Alkane, die zwischen kanonischen und komplexen Metalloberflächen verengt sind.

ii.4.2   Einfluss der Betriebsbedingungen: ein analytisches Gesetz für Wandschlupf

Das vorherige Modell für Wandgleitvorhersagen wurde für ein einzelnes Set von Betriebsbedingungen hergeleitet. Allerdings kann die kinematische Randbedingung an der Grenzfläche auch von dem Wandgeschwindigkeitsunterschied Δu, der Dicke des Schmierfilmes h und dem Druck P abhängen. Da diese Größen über das ganze Kontaktgebiet variieren, ist es notwendig, ihren Einfluss auf den Wandschlupf zu untersuchen.
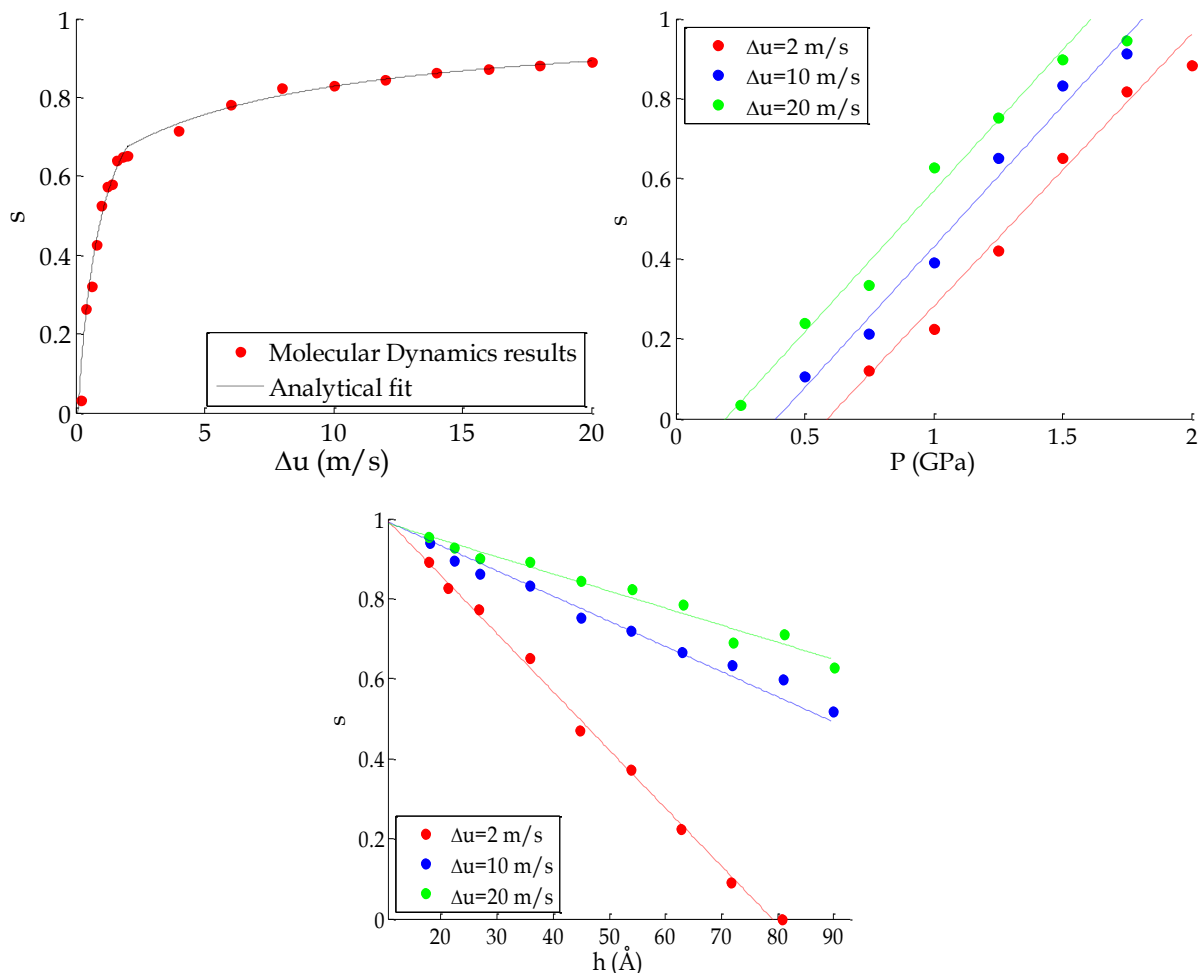
Abbildung ii-8: Abhängigkeit des Wandschlupfes von der Schergeschwindigkeit, der Verengung des Fluides und dem lokalen Druck, für ein schwach wechselwirkendes Wand-Fluid-Paar. Die Punkte stellen Moleküldynamik-Ergebnisse dar, und die Linie entspricht dem analytischen Gesetzt für Wandgleiten.

Folglich werden Moleküldynamik Parameterstudien über Δu, h und P für ein Ober-flächen-Schmierstoff-Paar mit schwachen Interaktionen durchgeführt. Der untersuchte Wertebereich entspricht typischen Arbeitsbedingungen eines elasto-hydrodynamischen Kontaktes. Es zeigt sich, dass das Wandgleiten mit zunehmender Schergeschwindigkeit und Druck sowie abnehmender Schmierspalthöhe ansteigt (Abbildung ii-8); diese Ergebnisse korrespondieren mit der Literatur [17, 18, 29]. Die Abhängigkeit des Gleitparameters s (bzw. der Gleitlänge L_s) von den Arbeitsbedingungen wird schließlich durch ein analytisches Gesetz

$$s = s(\Delta u, h, P)$$
$$L_s = \frac{h}{2} \cdot \left(\frac{1}{1 - s(\Delta u, h, P)} - 1 \right)$$

aus den Ergebnissen atomistischer Simulationen quantitativ bestimmt.

Dieser Abschnitt hat sich mit der Quantifizierung des Wandschlupfes in Abhängigkeit von den Hauptparametern einer Kontaktgrenzfläche beschäftigt. Analytische Gesetze und Vorhersagemodelle wurden für viele verschiedene Wand-Fluid-Paarungen und typische Arbeitsbedingungen von EHD-Kontakten hergeleitet. Diese Ansätze erlauben nun eine einfache und effiziente Integration von Phänomenen auf molekularer Ebene in makroskopische Kontinuumsmodelle.

ii.5 Die Kopplung zwischen Effekten auf molekularer Ebene und makroskopischen Kontinuumsmodellen

Das zweite Ziel dieser Doktorarbeit ist, den Einfluss von Molekularphänomenen auf das globale Verhalten von geschmierten Kontakten bei sehr geringen Schmierfilmhöhen zu untersuchen. Aus diesem Grund wird ein mehrskaliger Ansatz (Nano-EHD) entwickelt, um atomistische Simulationen auf molekularer Ebene mit klassischen EHD-Modellen zu koppeln.

ii.5.1 Der Nano-EHD-Ansatz

Die folgende Studie ist hauptsächlich auf den Wandschlupf bei EHD-Linienkontakten fokussiert: hierzu wird die klassische Reynolds-Gleichung für den Fluiddruck im Kontaktgebiet geeignet verändert, um dieses Phänomen zu berücksichtigen. Hierbei wird angenommen, dass der Wandschlupf nur an einer der beiden Oberflächen auftritt: die klassische Haftbedingung wird an der unteren Oberfläche durch eine Navier-Randbedingung [30] ersetzt. Analog zum üblichen Vorgehen lässt sich die Reynolds-Gleichung mit Wandschlupf (wall slip) abgeleitet:

$$\frac{\partial}{\partial x}\left(\frac{\rho}{12\eta}\left(h^3 \frac{h+4L_s}{h+L_s} \right)\frac{\partial P}{\partial x} \right) = \frac{\partial}{\partial x}\left(\frac{\rho h^2}{2(h+L_s)}u_1 + \frac{\rho h(h+2L_s)}{2(h+L_s)}u_2 \right)$$

Diese Gleichung gilt für einen Linienkontakt mit Newtonschem Fluid unter stationären und isothermen Bedingungen. Die Gleitlänge L_s in Abhängigkeit von Druck, Wandgeschwindigkeit und Dicke des Schmierfilmes wird durch die analytischen Gesetze aus Abschnitt ii.4 beschrieben. Der nano-EHD-Ansatz basiert auf der gekoppelten Lösung der Rey-

nolds-Gleichung und der Gleichungen, welche den Wandschlupf beschreiben. Zusätzlich werden die Elastizitätstheorie für die Verformung der Festkörper, die Viskosität-Druck- bzw. die Dichte-Druck-Ansätze (Roelands bzw. Dowson-Higginson) für das Fluidverhalten, die Definition der Spalthöhe und das Lastengleichgewicht im Modell eingefügt. Dieses Gleichungssystem wird mit der Finite-Elemente-Methode in Comsol Multiphysics gelöst, wobei alle physikalischen Phänomene stark miteinander gekoppelt sind.

ii.5.2 Anwendung auf einen EHD-Kontakt mit sehr geringer Schmierspalthöhe

Das zuvor beschriebene Nano-EHD-Modell wird nun auf einen elasto-hydrodynamischen Linienkontakt angewendet: hierbei wird ein Fluid mit sehr geringer Viskosität genutzt, wodurch in der Mitte des Kontakts eine minimale Filmdicke von nur wenigen Nanometern hervorgerufen wird. Außerdem zeigt die untere Oberfläche nur sehr schwache Wand-Fluid Wechselwirkungen: folglich tritt ausgeprägter Wandschlupf in der Mitte des Kontaktes auf. Dieser Effekt verursacht eine starke Veränderung der Spalthöhe, der Dynamik des Schmierstoffes und der Reibung im Vergleich zur klassischen EHD-Schmierungstheorie.

Da die Geschwindigkeitsrandbedingungen an den Wänden unterschiedlich sind (es gibt sowohl eine gleitende als auch eine anhaftende Oberfläche), müssen zwei Konfigurationen berücksichtigt werden. Im ersten zu betrachtenden Fall bewegt sich die gleitende Oberfläche schneller und reißt das Fluid innerhalb und außerhalb des Kontakts mit. Ein Dimpel (d.h. eine lokale Vergrößerung der Spalthöhe) kann in der Mitte des Kontaktbereichs beobachtet werden (Abbildung ii-9a). Eine Erhöhung des Wandgeschwindigkeitsunterschieds, hier durch den SRR-Parameter (Slide-to-Roll-Ratio) beschrieben, verursacht einen Anstieg des Wandschlupfes und folglich größere Amplituden des Dimpels.
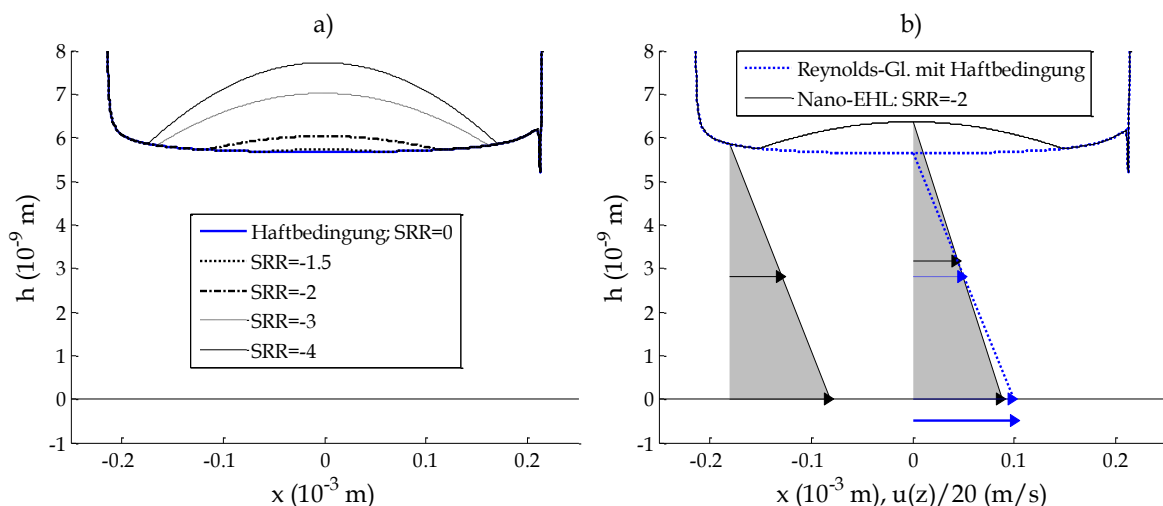
Abbildung ii-9: Ergebnisse des Nano-EHL-Modells mit einer einzigen Gleitfläche, die das Fluid innerhalb und außerhalb des Kontaktes mit reißt. a) Ein Dimpel, dessen Amplitude von dem Wandgeschwindigkeitsunterschied abhängt, bildet sich in der Mitte der Kontaktzone. b) Geschwindigkeitsprofile in der Spalthöhe.

Die Veränderung der Schmierfilmdicke wird durch eine Analyse der Fluidgeschwindigkeit im verengten Bereich erklärt. Abbildung ii-9b zeigt, dass das Wandgleiten die Ge-

schwindigkeit des Fluides in der Mitte des Kontakts im Vergleich zur Einlaufzone herabsetzt. Um dennoch entlang des Schmierspaltes die Massenerhaltung trotz geringerer Wandgeschwindigkeit zu gewähren muss bei Vorliegen eines linearen Geschwindigkeitsverlaufes die Schmierspalthöhe zunehmen.

Das gegensätzliche Phänomen tritt auf, wenn die obere Wand (mit Haftbedingung) schneller ist und das Fluid mitreißt (Abbildung ii-10a). Das Wandgleiten von der unteren Oberfläche bewirkt eine höhere Geschwindigkeit des Schmierstoff an der unteren Grenzfläche(Abbildung ii-10b): um dennoch die Massenerhaltung zu erfüllen muss daher die Schmierspalthöhe im Zentrum des Kontaktes abnehmen. Es ist sogar zu beobachten, diese Einschnürung stärker sein kann als die am Ausgang der Hochdruckzone, sodass die kritische minimale Schmierfilmhöhe in diesem Fall mitunter im Zentrum auftritt.
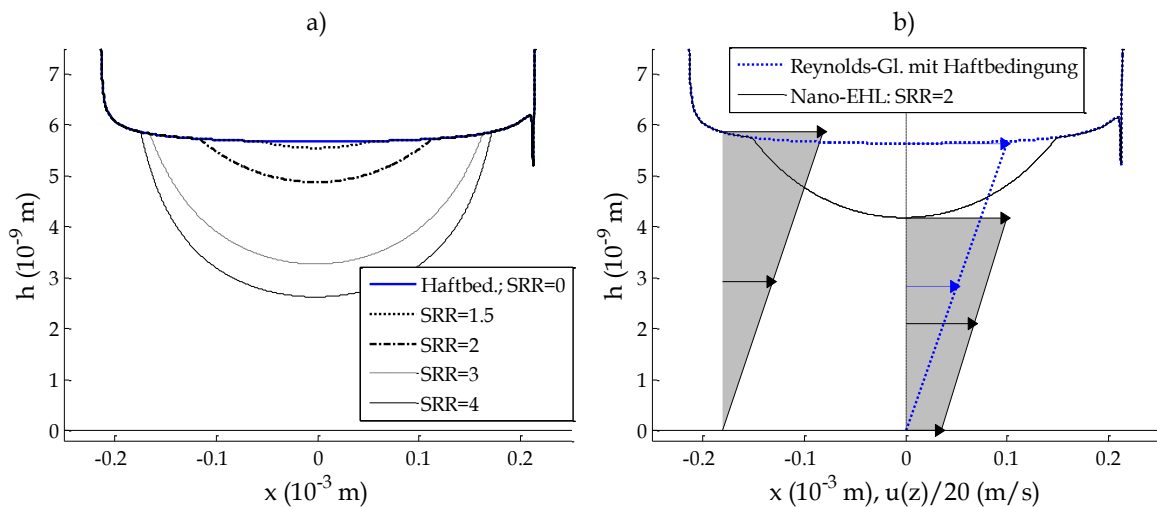
Abbildung ii-10: Ergebnisse des Nano-EHL-Modells: Wandschlupf tritt an der ruhenden Oberfläche auf, die andere Oberfläche bewegt sich tangential. a) Eine lokale Verminderung der Schmierfilmdicke, deren Amplitude von dem Wandgeschwindigkeitsunterschied abhängt, kann in der Mitte der Kontaktzone betrachtet werden. b) Geschwindigkeitsprofile in der Spalthöhe.

Wandschlupf kann auch die Reibung beeinflussen (Abbildung ii-11). Laut der klassischen EHD-Theorie für einen stationären und isothermen Zustand mit newtonschem Fluid ist der Reibungskoeffizient proportional zum Geschwindigkeitsunterschied der Wände. Abweichungen hiervon werden allerdings in Gegenwart von Wandschlupf betrachtet. Wenn die Oberfläche mit Wandschlupf sich tangential bewegt, so ist die Reibung kleiner, weil die Vergrößerung der Spalthöhe zu geringeren Scherraten und Schubspannungen führt. Im Gegenzug steigt die Reibungskraft wegen vergrößerter Scherraten und Schubspannungen, wenn die Wand mit Haftbedingung das Fluid mitreißt und die Dicke des Schmierfilmes abnimmt.
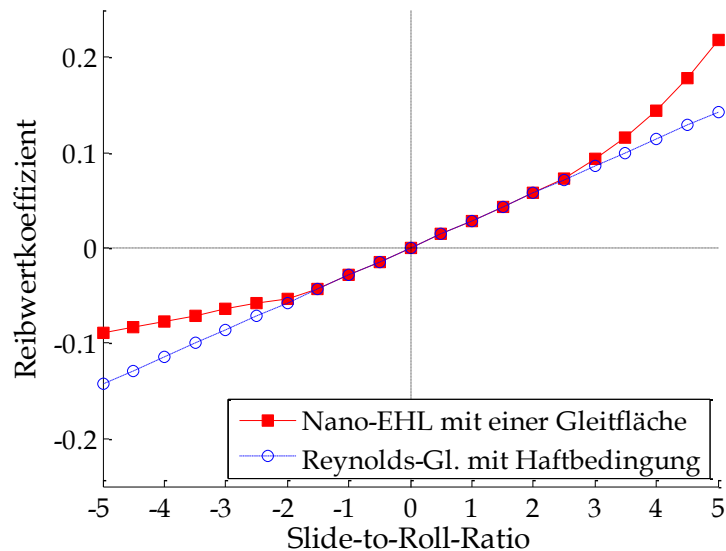
Abbildung ii-11: Reibungskoeffizient als Funktion des *slide-to-roll-ratio*.

Abschließend wird eine Oberfläche betrachtet, deren Eigenschaften (also bspw. Korrugation, Kommensurabilität) über der Kontaktlänge variieren. Dies ist beispielsweise der Fall, wenn die Kontaktfläche aus den Oberflächen verschieden orientierter Körner besteht: jedes Korn zeigt dabei unterschiedliche Materialeigenschaften und unterschiedlich stark ausgeprägten Wandschlupf an der Grenzfläche. Die Spalthöhe variiert lokal und folgt die Struktur der Oberfläche, mit starken Sprüngen an den Rändern der Körner (Abbildung ii-12).
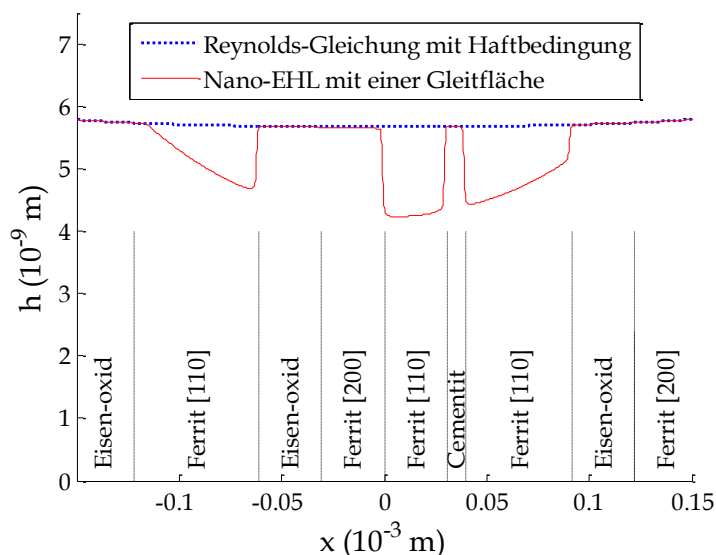
Abbildung ii-12: Ergebnisse des Nano-EHL-Modells in Gegenwart von Körnern mit unterschiedlichen Oberflächeneigenschaften in der Oberfläche an der Wandschlupf vorliegt.

Zusammenfassend hat der Multi-Skalen-Ansatz erlaubt, den starken Einfluss von Wandgleiten in nanometer-dünnen Schmierfilmen auf die Spalthöhe und Reibung eines gesamten Kontakts zu bestimmen. Jedoch können andere Phänomene auf der Nanometer-

Ebene betrachtet werden und in makroskopische Modelle eingefügt werden. Die Folgen einer extremen Verminderung der Ölmenge in einem Kontakt werden im nächsten Abschnitt untersucht.

ii.6 Untersuchung der Aufspaltung des Schmierfilmes mit Moleküldynamik

Heutzutage werden Schmiersysteme so gestaltet, dass sie mit immer geringeren Ölmengen funktionieren können. Folglich steigt die Wahrscheinlichkeit, dass der Schmierstoff im Kontaktbereich lokal nicht mehr reicht, um die Festkörper völlig zu trennen: es können sich dann direkte Kontaktstellen zwischen den Oberflächen bilden, sodass im Kontakt simultan Fluid- und Festkörperreibung vorliegen. Die Charakterisierung eines solchen Mischreibungskontaktes benötigt ein besseres Verständnis der Aufspaltung des Schmierfilmes. Folglich werden Moleküldynamik-Simulationen durchgeführt, in denen die Ölmenge im Nanometer-Kontaktbereich extrem verringert wird, bis eine direkte Wechselwirkung zwischen den Oberflächen auftritt.

ii.6.1 Anordnung des Fluides und Reibung für glatte Oberflächen

Zunächst werden zwei glatte benetzbare Oberflächen gewählt, die starke Wechselwirkungen mit dem Fluid aufweisen, wobei n-Hexadecan als Schmierstoff verwendet wird. Wegen der extrem dünnen Spalthöhe ordnen sich die Fluidmoleküle parallel zu den Wänden in einer ganzen Zahl von Schichten an. Die Dicke des Schmierfilms verändert sich folglich in Anhängigkeit von der Ölmenge stufenartig (Abbildung ii-13), und die Höhe der Sprünge entspricht dem Moleküldurchmesser.
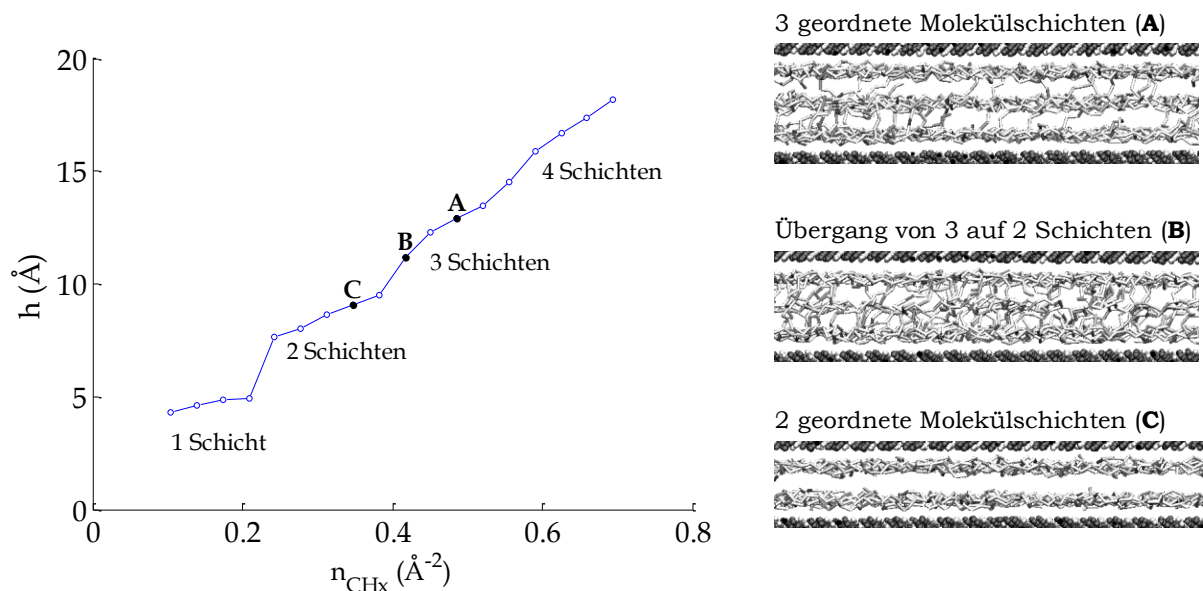
Abbildung ii-13: Spalthöhe in Abhängigkeit von der Fluidmenge zwischen zwei glatten Oberflächen. Die Konfigurationen A, B und C zeigen exemplarisch den Übergang zwischen Konfigurationen mit strukturierten Molekülschichten (A,C) über das Zwischenstadium eines ungeordneten Zustands (B).

Außerdem sind zwei Arten von Konfigurationen möglich: einerseits zeigen die Zustände **A** und **C** in Abbildung ii-13 geordnete Strukturen, mit separierten Molekülschichten ohne viele Brückenbindungen, das heißt Moleküle, die zwischen zwei Schichten aufgeteilt sind. Andererseits werden Übergangszustände (**B**) durch eine ungeordnete Molekülaufteilung charakterisiert, in denen die mittleren Schichten sich vermischen und die Moleküle verflochten sind.

Sprünge in den Geschwindigkeitsprofilen im Schmierstoff weisen darauf hin, dass die Scherung nur zwischen den Molekülschichten stattfindet. Folglich ist der Begriff der bulk-Viskosität mit einer gleichmäßigen Scherung des Fluides nicht mehr anwendbar, und ein reversibler Übergang zu einem Festkörperverhalten tritt auf. Außerdem ist die Reibung des Systems mit dem Ordnungsgrad der Moleküle und der Anzahl der Brücken zwischen den Schichten verbunden (Abbildung ii-14). Schubspannungsminima entsprechen geordneten Konfigurationen, in denen die Schichten leicht übereinander gleiten. Reibungsmaxima hingegen entsprechen Übergangszuständen, da die verflochtenen Moleküle der Scherung widerstehen. Das absolute Maximum wird bei Vorliegen einer einzigen Molekülschicht zwischen den Oberflächen erreicht. In diesem Fall entsteht beiderseitiges Wandgleiten und das System wird an der Grenzfläche trotz der starken Wand-Fluid-Wechselwirkungen geschert.

Hohe Scherraten und Schubspannungen verursachen eine hohe Wärmeerzeugung, und die Oberflächen- und Fluidtemperaturen steigen rasch. Allerdings sind thermische Effekte in niedrigen Reibungskonfigurationen begrenzt, und die Temperatur bleibt konstant.
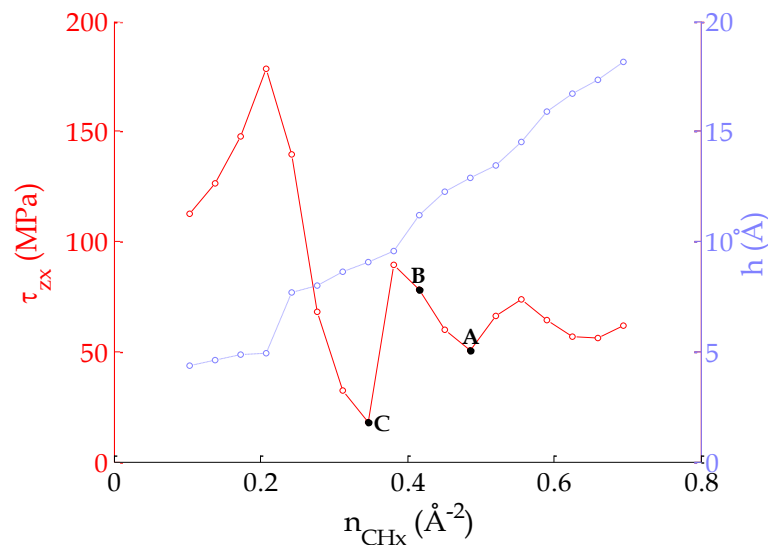
Abbildung ii-14: Schubspannung und Spalthöhe in Abhängigkeit von der Fluidmenge zwischen zwei glatten Oberflächen.

ii.6.2 *Einfluss des Schmiermittels*

Die Zusammensetzung des Fluides hat auch einen Einfluss auf das lokale Kontaktverhalten. Sphärische Moleküle wie Methan sind sehr empfindlich gegenüber Verengung, folglich sind die Sprünge in Spalthöhe deutlicher im Vergleich zu linearen Molekülen (Abbildung ii-15a). Außerdem können Brücken zwischen Schichten nicht entstehen, was zu einer sehr geringen Reibung führt (Abbildung ii-15b).

Zusammenfassung

Andererseits begünstigen Verzweigungen auf den Molekülketten die Gegenwart von Brücken und verflochten Zuständen. Deswegen verschwinden die geordneten Konfigurationen, die charakteristisch für linearere Moleküle sind. Die Spalthöhe zeigt keine Stufen, und die Reibung bleibt im Allgemeinen hoch mit geringen Schwankungen.
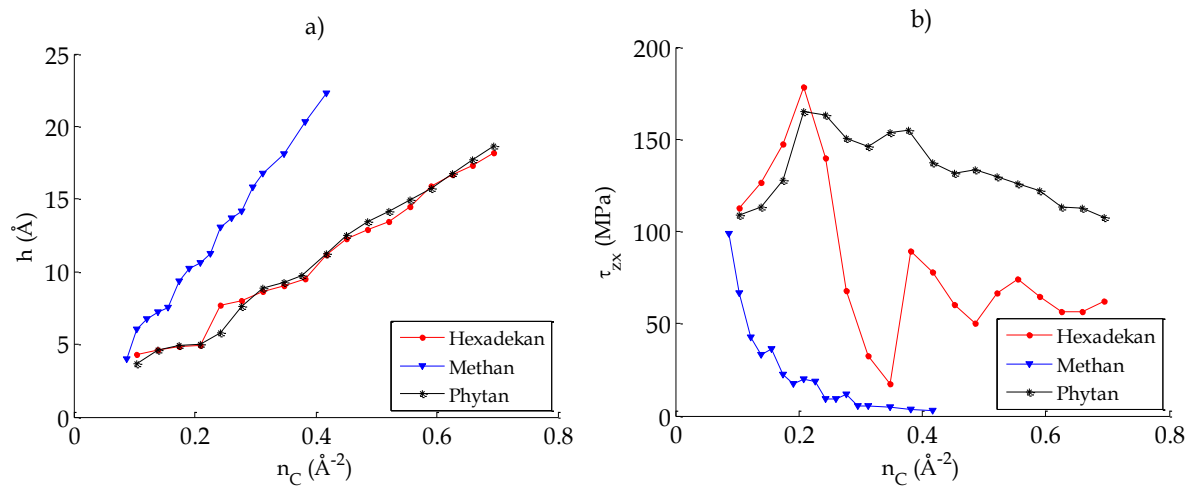
Abbildung ii-15: Spalthöhe (a) und Schubspannung (b) für verschiedene Schmierstoffe mit linearen, sphärischen und verzweigten Molekülen in Abhängigkeit von der Fluidmenge zwischen zwei glatten Oberflächen.

ii.6.3 Einfluss der Oberflächen: Nanorauheit und Wand-Fluid-Wechselwirkung

Ähnlich wie verzweigte Moleküle verursacht Nanorauheit auf den Wände einen ungeordneteren Zustand bei geringen Schmierspalthöhen (Abbildung ii-16, Konfiguration **D**): deshalb ist die Reibung in solchen Situationen im Allgemeinen hoch. Außerdem wandern die letzten noch vorhandenen Moleküle bei einer extremen Verminderung der Schmierstoffmenge in die Kavitäten des Rauheitsprofils. Folglich können die Rauheitsspitzen direkt mit der anderen Wand wechselwirken, obwohl noch Restmengen von Schmierstoff vorhanden sind (Konfiguration **E**). Das Reibverhalten ist typisch für trockene Reibung, mit starken Adhäsionskräften, hohen Schubspannungen, und der Verformung der Rauheit. In diesem Zustand wird das Reibungsmaximum erreicht.

Indem die Benetzbarkeit der Oberflächen reduziert wird, und somit auch die molekularen Wechselwirkungen mit dem Fluid, wird das System an der Grenzfläche geschert. In der Folge tritt Wandschlupf auf, wodurch die Reibung auf einen niedrigen konstanten Wert beschränkt wird (Abbildung ii-16). Allerdings wird Wandschlupf von Nanorauheit auf nicht benetzbare Oberfläche stark reduziert, und hohe Reibwerte treten auf.
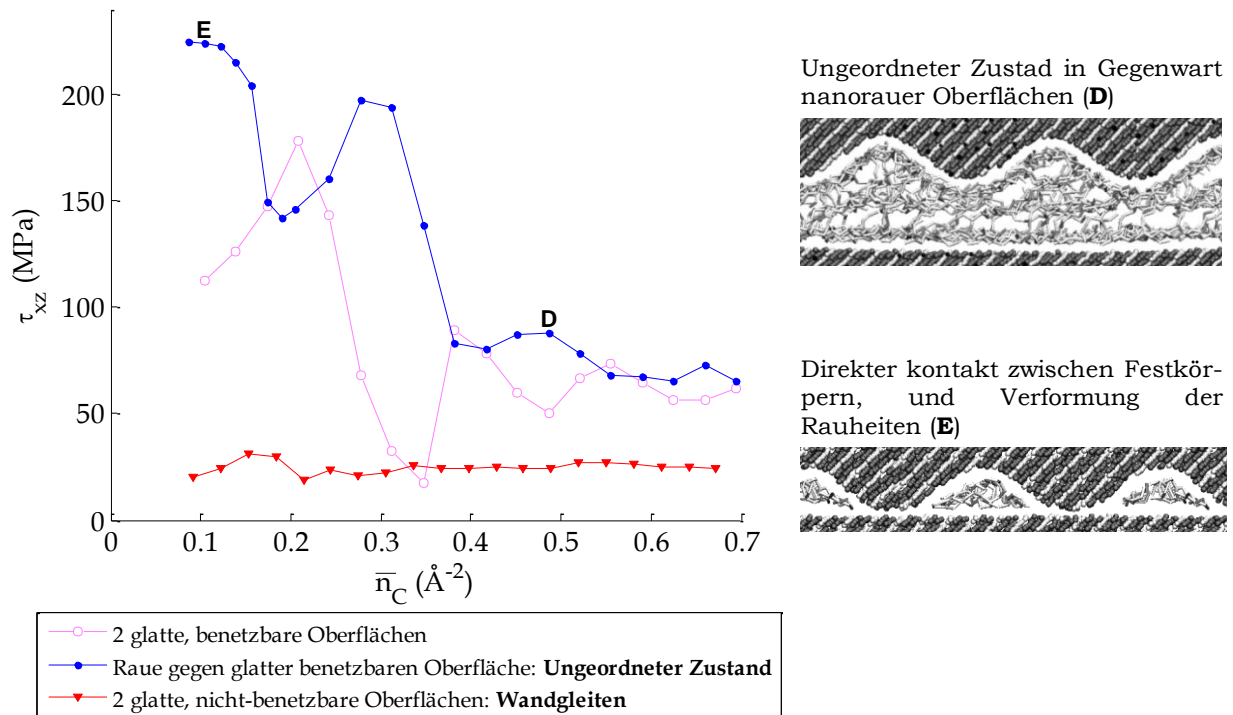
Abbildung ii-16: Schubspannung für verschiedene Morphologien und Nanorauheiten der Oberflächen

ii.7 Zusammenfassung und Ausblick

Die heutigen Trends in der tribologischen Entwicklung führen zu einer Reduzierung der Ölmenge in geschmierten Mechanismen. Folglich nimmt die Schmierfilmdicke zwischen Festkörpern stark ab und erreicht oftmals Größenordnungen weniger Nanometer. Die Eigenschaften von Fluiden bei derartig kleinen Schmierspalthöhen können stark von den normalen des „bulk"-Zustands bei großen Schmierspalthöhen abweichen: typische Phänomene sind die Anordnung des Schmiermittels in Molekülschichten („layering"), eine vergrößerte Viskosität und das Auftreten von Wandschlupf in der Wand-Fluid-Grenzfläche statt der klassischen Haftbedingung.

Folglich ist das Ziel dieser Doktorarbeit, Molekularphänomene in nanometer-dünnen Schmierfilmen zu charakterisieren und ihren Einfluss auf das Globalverhalten eines makroskopischen Kontaktes zu berücksichtigen. Dafür wurden Moleküldynamik-Simulationen verwendet, um die Scherung von Basis-Öle (Alkane) zwischen Metalloberflächen bei extrem dünnen Filmhöhen in einem Nano-Bereich des Kontakts zu untersuchen und somit spezifische Materialcharakteristika für die Makroebene abzuleiten.

Die Arbeit fokussiert sich auf das Phänomen des Wandschlupfes, das heißt auf den Geschwindigkeitsunterschied zwischen dem Fluid und der Wand an der Grenzfläche. Ein Vorhersagemodell wurde entwickelt, um dieses Phänomen in Abhängigkeit von der Oberflächen-Schmiermittel-Paarung zu quantifizieren. Die Wände wurden hierbei durch einen Charakterisierungsparameter aus einer Scanning-Methode beschrieben, der die Ermittlung der lokalen Schubspannung an der Grenzfläche erlaubt. Die Rheologie des Fluides bei sehr

Zusammenfassung

geringen Spalthöhen wurde mit „bulk"-Eigenschaften verglichen. Die Zusammensetzung der Oberflächen und des Schmierstoffs wurden in einem Modell für Wandschlupf eingeführt, das für lineare Alkane (Basis-Öle) zwischen kanonischen und komplexen Metalloberflächen gültig ist. Schließlich wurde durch Parameterstudien der Einfluss der angelegten Wandgeschwindigkeit, der Spalthöhe und des Ducks auf Wandschlupf untersucht, und durch ein analytisches Gesetzt beschrieben.

Diese modellhaften Beschreibungen der makroskopischen Wirkungen von Phänomenen auf der Nanoskala wurden im Sinne eines Multi-Skalen-Modells für die Analyse eines makroskopischen EHD-Kontaktes eingefügt (Nano-EHL). Insbesondere wurde die klassische Reynolds-Gleichung verändert, um auch das Wandgleiten auf einer der beiden beteiligten Oberflächen zu berücksichtigen. Anhand dieses Nano-EHL-Modells konnte ein EHD-Kontakt mit niedrig-viskosem Fluid – und folglich mit einer Schmierfilmdicke im Nanometerbereich – untersucht werden. Hierbei zeigte sich, dass das Auftreten des Wandschlupfes in der Mitte des Kontaktes eine Veränderung der Spalthöhe verursachen kann. Für den Sonderfall dass eine der beiden Oberflächen ruht lassen sich folgende Fälle unterscheiden: falls der Wandschluf an der sich bewegenden Oberfläche auftritt tritt im Zentrum der Hochdruckzone eine Vergrößerung der Schmierfilmdicke auf (Dimple). In diesem Fall sind auch die Scherrate und Reibung kleiner im Vergleich zur Konfiguration mit einer klassischen Haftbedingung auf beiden Wänden. Im Gegensatz dazu wird die Spalthöhe niedriger und die Reibung höher, wenn an der sich bewegenden Oberfläche zwischen Fluid und Oberfläche die Haftbedingung gültig ist.

Schließlich wurde eine extreme Verminderung der Ölmenge bis hin zum lokalen Zusammenbrechen des Schmierfilms dem damit verbundenen direkten Festkörperkontakt untersucht. In Gegenwart von zwei glatten Oberflächen können sich über die Spalthöhe Molekülschichten ausbilden, die parallel zu den Wänden liegen. Außerdem hängt die Scherung im System von der Anordnung der Moleküle ab. Treten die Molekülschichten geordneten Zuständen mit wenigen Brücken zwischen den Schichten auf, so ist die Reibung niedrig. Wenn die Moleküle zwischen den Schichten aber verflochten sind, widerstehen sie der Scherung des Schmierstoffes, und höhere Reibwerte werden erreicht. Diese ungeordneten Zustände treten bevorzugt in Gegenwart von verzweigten Fluiden und nanorauen Oberflächen auf. Im Gegenteil hierzu findet die Scherung an der Wand-Fluid-Grenzfläche in Gegenwart glatter, nicht-benetzbarer Oberflächen statt: Wandschlupf entsteht und begrenzt die Reibung zu einem niedrigen, konstanten Wert. Schließlich wird das Reibungsmaximum bei direktem Festkörperkontakt erreicht, wenn starke Adhäsionskräfte zwischen den Wänden wechselwirken.

Abschließend zeigt diese Arbeit die Wichtigkeit einer Multi-Skalen-Analyse zwischen den Nano- und Makro-Ebenen, um ein besseres Verständnis geschmierter Mechanismen mit verengten Fluiden zu erreichen. Diese Studie kann in der Zukunft um andere Phänomene oder Konfigurationen erweitert werden: Zum Beispiel können polare Moleküle (wie z.B. Fettsäure, Additive und ionische Fluide) auf atomarer Ebene betrachtet werden. Die lokale Aufspaltung des Schmierfilmes kann vertieft werden, um die Verformungen der Nano-Rauheit zu quantifizieren. Auch Thermische Effekte unter hoher Scherung könnten weiter untersucht werden.

Auf der makroskopischen Ebene kann der Nano-EHL-Ansatz um nicht-Newtonsche Eigenschaften des Fluides, eine thermische Betrachtung, sowie die Gegenwart mikroskopischer Rauheit auf den Oberflächen erweitert werden. Im letzten Fall würde eine Analyse der Kontakte zwischen Rauheitsspitzen notwendig sein. Ein Mikrometer-Modell würde erlauben, einzelne Kontaktstellen mit Hilfe atomistischer Simulationen für das Verhalten der letzten Molekülschichten zwischen den Oberflächen zu charakterisieren. Schließlich sollte ein Nano-Mikro-EHL-Ansatz alle diese Kenntnisse-integrieren, um ein erweitertes numerisches Modell zur Simulation geschmierter Mechanismen unter extremer Verminderung der Ölmenge zu entwickeln.

Nomenclature

Roman symbols

a	[Å]	Dimension of the lattice cell along the 1st primitive vector
A	[nm]	Asperity amplitude for nano-rough surfaces
b	[Å]	Dimension of the lattice cell along the 2nd primitive vector
b_h	[m]	Half contact width from the Hertzian theory
c	[Å]	Dimension of the lattice cell along the 3rd primitive vector
c_f	Dimensionless	Friction coefficient
$\bar{d}$	[Å]	Mean distance to the nearest atom in the crystal lattice
(d_x, d_y)	[m]	Displacement field within a solid body along the x- and z- directions
E	[GPa]	Young's modulus
E'	[GPa]	Reduced Young's modulus
E_c	[GPa]	Young's modulus of the cylinder
E_{eq}	[GPa]	Equivalent Young's modulus
E_p	[GPa]	Young's modulus of the plane
F	[kcal/mol.Å]	Drag force along the minimum-force-path from the scanning technique
F_{corr}	[kcal/mol.Å]	Corrugation force from the scanning technique
F_i	[kcal/mol.Å]	Total force acting on atom i
$F_{x,i}$	[kcal/mol.Å]	Resistive force along the shearing direction on an atom i in the control domain
$F_{z,i}$	[kcal/mol.Å]	Normal force applied on an atom i in the control domain
h	[m], [nm]	Film thickness
H	Dimensionless	Dimensionless film thickness
h_0	[m]	Solid body displacement
H_0	Dimensionless	Dimensionless solid body displacement
h_{comm}	[Å]	Commensurability height from the scanning technique
h_{avg}	[nm]	Average film thickness for nano-rough surfaces
h_{eff}	[nm]	Effective film thickness for nano-rough surfaces
h_{eq}	[Å]	Equilibrium height from the scanning technique
$\bar{h}_{eq}$	[Å]	Average equilibrium height from the scanning technique
$\hbar$	[J/s]	Planck's constant
k_b	[J/K]	Boltzmann constant
K_{angle}	[kcal/mol.Å²]	Spring stiffness of the angle bending potential
K_{bond}	[kcal/mol.deg²]	Half spring stiffenss of the harmonic bond potential

Nomenclature

$K_{torsion}$	[kcal/mol]	Spring stiffness of the torsion potential
l	[Å]	Bond length
l_0	[Å]	Equilibrium bond length
L_s	[Å]	Slip length
$\bar{L}_s$	Dimensionless	Dimensionless slip length
L_{lock}	[Å]	Locking length
$L_{lock,peak}$	[Å]	Locking length above the asperity peaks
$\bar{L}_{lock,peak}$	Dimensionless	Dimensionless locking length above the asperity peaks
L_x	[nm]	Length of the Molecular Dynamics simulation box
L_y	[nm]	Width of the Molecular Dynamics simulation box
m_i	[a.m.u.]	Mass of atom i
$m_{mol,i}$	[a.m.u.]	Mass of molecule i
M_X	[kcal/mol.Å.fs^3]	Momentum transfer in the Müller-Plathe method
n	Dimensionless	Multiplicity of the torsion potential
N	Dimensionless	Exponent for the shear thinning behavior in fluids
n_C	Dimensionless	Number of atoms in the control domain of the walls, where the operating condtions of the atomistic simulations are applied
$\bar{n}_{CHx}$	Dimensionless	Number of hydrocarbon groups per surface area
$n_{CHx,mol}$	Dimensionless	Number of hydrocarbon groups per alkane molecule
n_{mol}	Dimensionless	Number of fluid molecules in the system
P	[Pa]	External pressure
$\bar{P}$	Dimensionless	Dimensionless external pressure
P_{adh}	[Pa]	Normal pressure due to adhesion
P_{crit}	[Pa]	Critical pressure for the onset of slip
P_h	[Pa]	Hertzian contact pressure
P_R	[Pa]	Roelands pressure
r	[Å]	Interatomic distance
r_i	[Å]	Position of atom i at instant t
$\ddot{r}_i$	[Å]	Acceleration of atom i at instant t
R	[m]	Reduced contact radius
R_i	[m]	Radius of curvature of surface i
s	Dimensionless	Slip parameter
S	[nm^2]	Area of the contact nano-patch in the Molecular Dynamics simulation
SRR	Dimensionless	Slide-to-Roll-Ratio
t	[s]	Time
t_{rel}	[s]	Relaxation time of the fluid
T	[K]	Fluid temperature
T_D	[K]	Debye temperature of the crystal lattice

T_{wall}	[K]	Imposed wall temperature
u	[m/s]	Fluid velocity along the shearing (x-) direction
u_i	[m/s]	Velocity of wall i along the shearing (x-) direction
V	[m³]	Volume
V_{angle}	[kcal/mol]	Angle bending potential
V_{bond}	[kcal/mol]	Harmonic bond potential
V_i	[kcal/mol]	Total potential acting on atom i
V_{LJ}	[kcal/mol]	Non-bonded Lennard-Jones potential
$V_{LJ,scan}$	[kcal/mol]	Lennard-Jones potential from the scanning technique
$V_{torsion}$	[kcal/mol]	Dihedral torsion potential
w	[N/m]	Line load
W	[J]	Work
X	Dimensionless	Dimensionless contact abscissa
z_R	Dimensionless	Roelands exponent

Greek symbols

α	[m²/s]	Thermal diffusivity
α_R	[1/Pa]	Roelands coefficient
β	[deg]	Phase shift of the torsion potential
γ_i	[J/m²]	Surface energy of material i
γ_{ij}	[J/m²]	Surface energy at the interface between materials i and j
$\dot{\gamma}_{app}$	[1/s]	Apparent shear rate
$\dot{\gamma}_{eff}$	[1/s]	Effective shear rate
δt	[fs]	Time step of the Molecular Dynamics simulation
$\langle \delta r^2 \rangle$	[Å]	Average mean square displacement of the atoms in the system
δ	[m]	Elastic deformation
$\bar{\delta}$	Dimensionless	Dimensionless elastic deformation
Δu	[m/s]	Wall velocity difference
Δx	[Å]	Sampling interval of the scanning technique along the x-direction
Δy	[Å]	Sampling interval of the scanning technique along the y-direction
$\bar{\bar{\varepsilon}}$	Dimensionless	Strain tensor
ε	[kcal/mol]	Lennard-Jones energy interaction parameter
ε_f	[kcal/mol]	Average LJ energy interaction parameter of the fluid
ε_w	[kcal/mol]	LJ energy interaction parameter of the wall atoms
ε_{w-f}	[kcal/mol]	Wall-fluid LJ energy interaction parameter
ε_{scan}	[kcal/mol]	Lennard-Jones energy interaction parameter for the scanning atom

Nomenclature

ζ_{surf}	[kcal/mol]	Surface characterization parameter
η , η_{bulk}	[mPa.s]	Fluid viscosity in bulk conditions
$\bar{\eta}$	Dimensionless	Dimensionless fluid viscosity
η_0	[mPa.s]	Fluid viscosity at ambient pressure and temperature
η_{eff}	[mPa.s]	Effective fluid viscosity under confinement
θ	[deg]	Angle between three consecutively bonded atoms
θ_0	[deg]	Equilibrium angle of the angle bending potential
κ	Dimensionless	Ratio of the wall-fluid and fluid-fluid LJ interaction parameters
λ	[nm]	Asperity wavelength for nano-rough surfaces
Λ	[W/m.K]	Thermal conductivity
μ	[mPa.s]	Fluid viscosity of the Newtonian plateau
ν_c	Dimensionless	Poisson's coefficient of the cylinder
ν_{eq}	Dimensionless	Equivalent Poisson's coefficient
ν_p	Dimensionless	Poisson's coefficient of the plane
ρ	[kg/m^3]	Average lubricant density in the film
$\bar{\rho}$	Dimensionless	Dimensionless lubricant density
ρ_0	[kg/m^3]	Lubricant density at ambient pressure and temperature
ρ_{avg}	[kg/m^3]	Average film thickness for nano-rough surfaces
$\bar{\bar{\sigma}}$	[Pa]	Stress tensor
σ	[Å]	Lennard-Jones distance parameter
σ_{scan}	[Å]	Lennard-Jones distance parameter for the scanning atom
τ_{zx}	[Pa]	Shear stress
τ_{max}	[Pa]	Maximum shear stress for the fluid
φ	[deg]	Dihedral between four consecutively bonded atoms
ϕ_m	[kg/s]	Mass flow in the contact
ψ	Dimensionless	Viscosity enhancement term under confinement
ω_d	[rad/s]	Debye frequency of the crystal lattice

General introduction

One of the major goals of modern technology is to design high performance systems with a long life span. Being able to safely operate machine components under severe conditions without the need to replace them leads to significant cost savings, environmental benefits, and is the key to remain competitive in the industry.

However, the efficiency and reliability of mechanisms can be hampered by tribological phenomena occurring in every contact between moving bodies. Friction is responsible for high energy losses, while wear and surface degradation significantly increase the risk of failure of machine components. Hence, engineers and researchers alike are striving to minimize these undesired effects.

The most common solution to control friction and wear is to separate the surfaces through a thin lubricant film. Achieving optimum performance requires nevertheless a deep understanding of the phenomena occurring in lubricated contacts and their dependence on many parameters, like for instance the body kinematics, operating conditions, materials etc. Thus, engineers and researchers alike have been constantly developing several theories, numerical models and experimental setups to answer this challenge.

This is especially important in the current industrial context, where lubricated devices must cope with more and more severe operating conditions. In fact the applied loads, temperatures and speeds are constantly increasing, while the quantity of oil separating the surfaces is being reduced due to environmental constrains or downsizing of the mechanisms.

In particular extremely thin films, whose thickness is comparable to the size of the fluid molecules, can be often found in the contact zones during the normal running process. Under this state of severe confinement, the lubricant behavior becomes dependent on nanometer-scale parameters like the molecular architecture of the fluid, the physico-chemical composition of the surfaces, and the atomic interactions.

Understanding these molecular effects and their impact on macroscopic contacts is becoming a critical issue for improving the reliability and efficiency in modern mechanisms, which rely more and more on the presence of confined films. Hence, the following research work will explore this issue through a detailed numerical analysis of nanometer-scale contact behavior, as well as the development of a multi-scale approach for the integration of molecular phenomena into continuous lubrication models.

I Context and state of the art

Since the beginning of history Man has known about the existence of friction and sought ways to reduce it. For instance, the use of primitive lubrication means like water, sand or animal fat dates to earlier than 4000 b.C. [1]. Throughout time this phenomenon has sparked the interest of great scientists. During the Renaissance, Da Vinci was the first to perform quantitative experiments on the dry contact between two surfaces. He introduced the notion of friction coefficient, defined as the ratio between the friction force and the applied normal load, and observed its independence with the contact area. His discoveries were confirmed two centuries later by Amontons, and were completed by Coulomb, who reported the invariance of the friction coefficient with the sliding velocity. Despite these advances, tribology was not yet considered a separate science, and only sporadic attempts were made to understand in detail the nature of contact problems.

Instead, the first significant studies concerning lubrication started during the industrial revolution in the 19th century, spurred by the need for efficient and reliable machinery. After preliminary experimental work by Hirn [1], Tower [31] showed that the solid bodies in a hydrodynamic bearing were fully separated by a lubricant film. This thin layer of oil governed exclusively the friction forces in the contact.

A milestone occurred in 1886: Reynolds developed his eponymous equation [2], which constitutes the base for all modern lubrication theories. By simplifying the Navier-Stokes equations [32], he described the viscous, laminar flow of a Newtonian, incompressible fluid in a contact. In particular, he was able to relate body kinematics and geometry to the pressure build-up in the lubricant and the resulting hydrodynamic lift (Figure I-1). These phenomena are essential to the formation of a fluid film which fully separates the surfaces and reduces friction and wear.
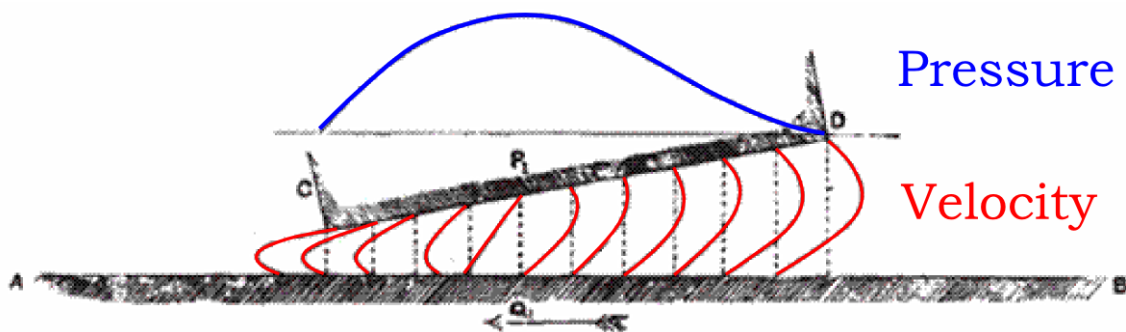
Figure I-1: Velocity and pressure profiles in a thrust pad due to the convergent geometry of the moving surfaces. Results from Reynolds [2].

I.1   Lubrication regimes

In 1902, Stribeck [33] studied the friction coefficient for a significant number of lubricated contacts under varying operating conditions. He then traced its qualitative dependence as a function of the film thickness, which is related to the velocity, the load, and the nature of the lubricant. From this qualitative representation (Figure I-2) it becomes possible to define three main lubrication regimes, depending on both the friction coefficient and the

underlying tribological mechanisms: full-film lubrication, mixed lubrication and boundary lubrication.
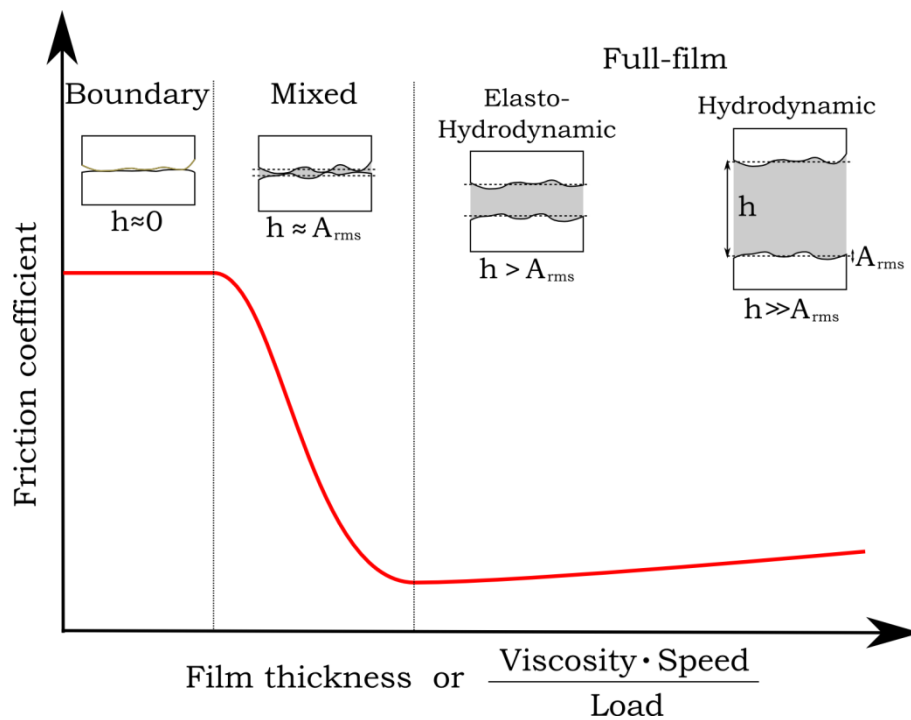
Figure I-2: Stribeck curve, representing the qualitative dependence of the friction coefficient with the film thickness. A comparison between the film thickness *h* and the root mean square roughness amplitude *A$_{rms}$* of the solids is also shown.

I.1.1   Full film lubrication

Full-film lubrication is located at the right side of the Stribeck curve. In this regime, the external load is fully supported by the hydrodynamic lift generated in the contact. The lubricant film is sufficiently thick to guarantee the complete separation of the surfaces. As a consequence, the friction force depends only on the shearing of the fluid and is in general very low. Moreover, wear is virtually absent, making full-film the ideal lubrication mode for many applications, like for instance bearings.

Two sub-regimes can be identified, mainly depending on the contact geometry. Hydrodynamic lubrication is typical of systems with conforming surfaces (Figure I-3a), such as journal bearings. In this case the load is spread on a large contact area, the resulting fluid pressure is of the range of 0.1 - 10 MPa, and no significant deformation of the bodies occurs.

On the other hand, non-conforming geometries (Figure I-3b) lead to very small contact areas and high pressures (500 MPa - 5GPa). An elasto-hydrodynamic lubrication (EHL) regime ensues, where the elastic deformations of the surfaces are of the same order of magnitude of the film thickness and modify the contact geometry. This mode is common in applications such as rolling element bearings, cam tappets, gears etc.
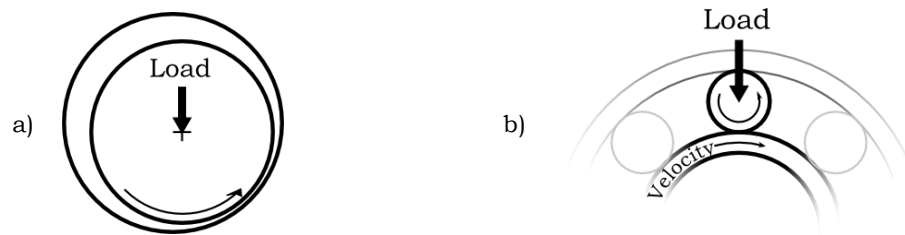
Figure I-3: Schematic representation of contacting geometries. a) Conforming: shaft rotating in a journal bearing. b) Non-conforming: Roller-raceway contact in a bearing

The understanding of the EHL regime proves more difficult to model than hydrodynamic lubrication due to its multi-physical nature. The solid body deformation [34] must in fact be coupled with fluid flow in the contact [35-37]. As a result of the high pressures, the lubricant properties change due to piezoviscous [38-40] and compressibility effects [37]. Shear thinning effects also modify the fluid viscosity at high shear rates [41]. Finally, heat flow must be modeled in the contact, along with the temperature dependence of the fluid properties [42, 43], to accurately predict the frictional behavior [44-46]. The resolution of EHD problems has progressed significantly in the last years with the development of fast and accurate computational techniques [47-49] and fully coupled multi-physical approaches [44, 45].

I.1.2 Mixed lubrication

The full-film regime is ideal for applications where minimal friction and wear are required, since the lubricant fully separates the surfaces. Several factors can nevertheless result in a decrease of the film thickness. In example, lower speeds during start-up and stopping of mechanisms hamper the hydrodynamic lift generation. Furthermore, a reduction of the fluid quantity can lead to starvation and sub-optimal lubrication of the contact zone. Finally, lower viscosity fluids such as coolants may not be able to fully support the external load. As a consequence, a transition to the mixed regime in the central part of the Stribeck curve occurs. In this case, the film thickness reaches the same order of magnitude as the undeformed surface roughness. The asperity peaks come into contact forming junctions that support a part of the load.

Friction depends on the shearing of both the fluid and these spots [50, 51]. A minimum is found at the transition with the full-film EHL case, where the number of interacting asperities is very small. As the lubricant quantity in the contact is reduced, more junctions are formed: the friction coefficient increases towards values characteristic of a non lubricated case.

I.1.3 Boundary lubrication

At very low speeds and high loads, the hydrodynamic lift becomes negligible, the fluid is squeezed out of the contact and the load is entirely supported by the interactions between solid bodies.

Direct surface contact was first studied by Da Vinci, Coulomb and Amonton, who experimentally observed the invariance of the friction coefficient with speed and load [1].

More detailed studies by Holm [52] and the formulation of the adhesion theory of friction by Bowden and Tabor [53] provided further insight on the mechanisms of this regime. It was shown that the contact spots between asperities undergo plastic deformation. The shearing of these junctions is responsible for the friction force; furthermore, high surface degradation and wear of the interacting asperities occur.

It may also happen that a residual quantity of lubricant remains trapped between the contacting bodies. Tribo-chemical reactions triggered by the extreme pressures and temperatures lead to the adsorption of thin layers of oil and additives on the surfaces [54, 55]. These tribofilms determine the behavior of the asperity junctions under shearing and can provide wear protection. Such regime is called boundary lubrication: friction is generally high and independent from the load and velocity.

I.2   The multi-scale nature of film thickness reduction

Classically, lubricated applications such as rolling element bearings were designed to operate under full-film conditions, as this prevents surface contact and ensures the maximum longevity of the mechanical components. The mixed and boundary regimes, involving higher wear and friction losses, were found only in particular cases such as startup and stopping, or abnormal situations rapidly leading to system failure.

Nowadays, bearing design is nevertheless becoming a challenging compromise between coping with more and more severe conditions, while keeping performance and reliability unchanged. On one hand, the loads, temperatures and transferred power are increasing. On the other hand, the quantity of oil and additives in the contacts is being decreased due to environmental constraints. Furthermore, weight reduction and downsizing are becoming standard practices in the industry. Hence, heavy and cumbersome separate lubrication circuits are being abandoned, while low viscosity operating fluids like coolants or fuels are used instead of traditional oil.

As a consequence the normal operating window for the rolling element bearings is shifted at the limit between EHD and mixed lubrication in the Stribeck curve of (Figure I-2). Thinner oil films separate the surfaces, whose thickness can decrease significantly down to a few nanometers or less between the roughness asperities, as shown schematically in Figure I-4.
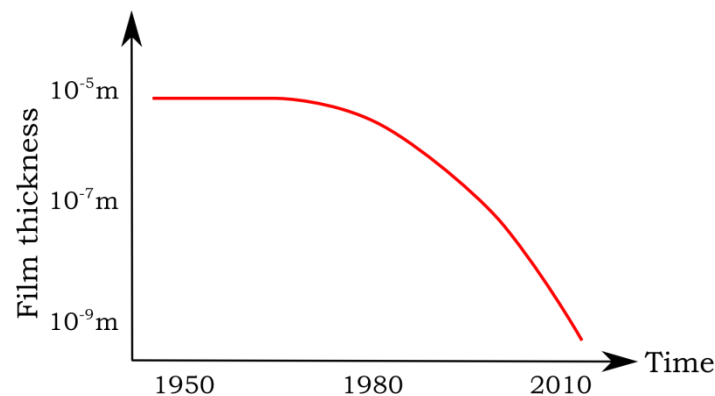
Figure I-4: Predicted evolution of the film thickness with time, inspired by Dowson [1].

In this configuration, local nanometer-scale phenomena occurring at the asperity junctions become dominating factors for the contact behavior [56]. A zoom in the contact zone helps to understand the complexity of the problem and its multi-scale nature. This is schematically shown for a typical roller-element bearing in Figure I-5.
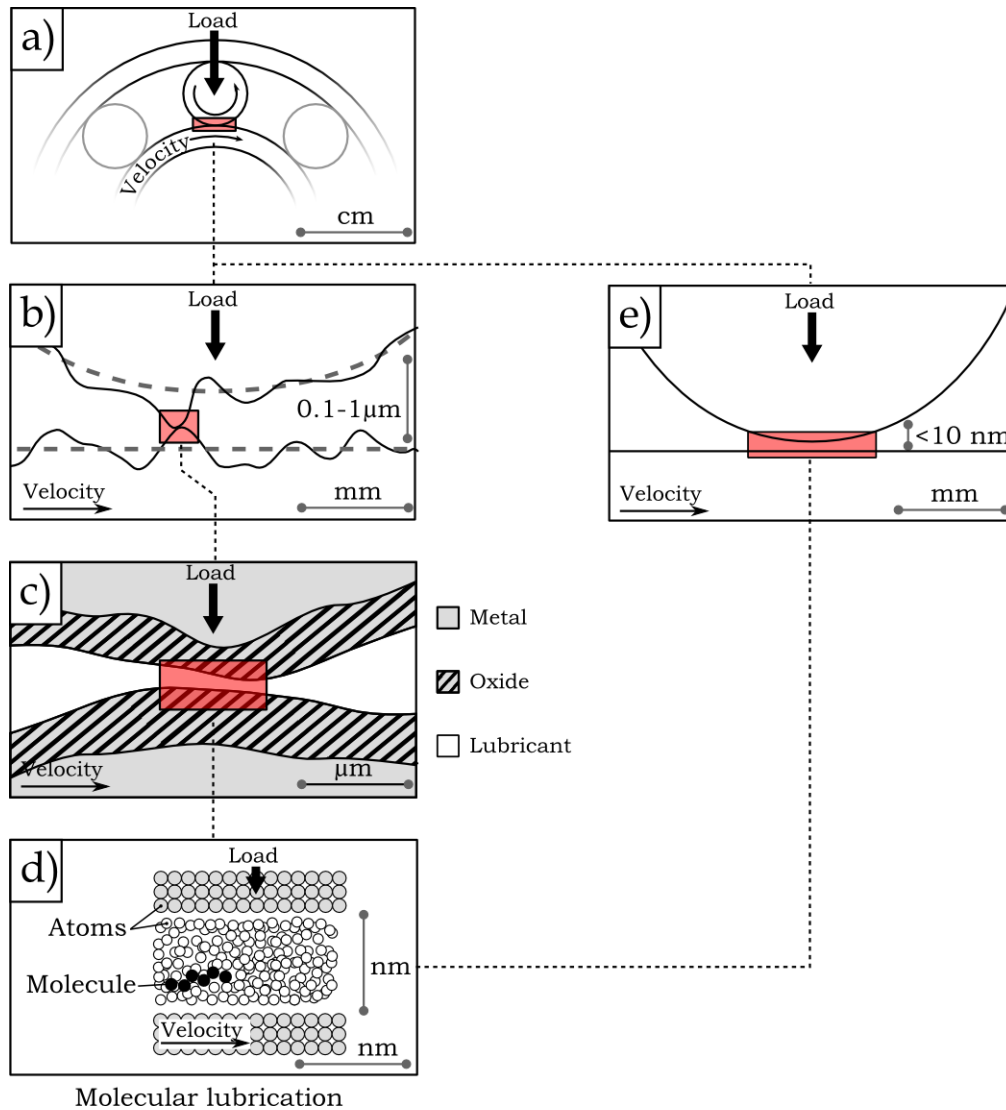
Figure I-5: Multi-scale nature of a contact problem with film thickness reduction: from a macroscopic application to molecular lubrication

Figure I-5a represents the whole mechanism. The radii of the contacting elements are of a few millimeters, while the kinematics involve time scales of a few milliseconds. The classical EHL theory, based on the assumption of a fully flooded contact, predicts a film thickness down to roughly 0.1 µm (Figure I-5b). Lower values can nevertheless be expected when the operating conditions become more severe or the lubricant quantity is reduced [57]. Furthermore, roughness with an RMS amplitude between 1 nm and 1 µm present on typical engineered surfaces [58] depending on the finishing process. Hence, at the transition between EHD and mixed lubrication, the asperity peaks start to interact.

A zoom on these contact spots (Figure I-5c), featuring areas of a few square micrometers, reveals a complex landscape. The surfaces present a grain structure featuring varying composition, as oxidation phenomena in contact with the lubricant [55]. Moreover, reactive molecules like additives can be physi- and chemisorbed on the surfaces forming protective layers [59].

One of the most important aspects is the presence of nanometric lubricant film trapped between the asperities. Figure I-5d shows schematically that its thickness is comparable to the size of the fluid molecules: hence, the lubricant is in a state called molecular confinement due to the close vicinity of the surfaces. Such extremely thin films determine the properties of the asperity junctions under shearing, as well as friction in the whole contact zone. Hence, a new lubrication sub-regime describing their structural and rheological properties can be identified, called *molecular lubrication*.

Its importance in lubricated applications is increasing, due to the current trends in film thickness reduction. In fact, it is nowadays possible to design applications that rely massively on molecularly confined fluids to ensure the separation of the surfaces in the whole contact. As an example for rolling-element bearing, Habchi [60, 61] showed that a nanometer film thickness could be reached by using low viscosity cooling fluids in a contact with smooth surfaces (Figure I-5e).

Hence, understanding molecular lubrication is becoming a priority in the current industrial context. Nevertheless, due to the extremely small scale of the system and the underlying physical phenomena, standard experimental setups and numerical methods cannot be used. Existing studies on this challenging task will be reviewed hereafter.

I.3   Molecular lubrication

In molecular lubrication only a few fluid molecules separate the surfaces. Under this state of severe confinement, the continuum hypothesis classically used to characterize the behavior of bulk fluids can be questioned. In fact, the properties of extremely thin lubricant films become dependent on local phenomena occurring at the nanometer scale.

Nanometer-range atomic interactions rule structural and rheological properties of the lubricant. Moreover, the physico-chemical composition of the surfaces become dominant factors for the flow of the confined fluid. Complex effects may also intervene due to severe operating conditions in pressure, shearing and temperature, which modify the local tribological behavior in the contact.

Hence, new experimental and numerical techniques have been developed to provide a deep insight on these molecular phenomena.

I.3.1   Techniques for the analysis of molecular lubrication

I.3.1.a   Experimental studies

A significant breakthrough in the understanding of confined fluids was the invention of the Surface Force Apparatus (SFA) by Israelachvili and coworkers in 1961. In this device a

cross-cylinder setup is used to determine precisely surface-surface interactions [3]. The cylinders are precisely positioned through piezoelectric crystals; the distance between the surfaces and the contact area is measured through optical interferometry [4] or capacitive methods [62]. These very sensitive techniques allow resolutions to 0.1 nm for the distance and 10^{-8} N for the force, which gives access to quantities at the atomic scale. The surfaces are typically constituted of atomically smooth mica, but other materials can be deposited on this substrate. Furthermore it is possible to use the SFA in controlled environments or immersed in fluids, making this device ideal for the study of nano-confined lubricants.

The Atomic Force Microscope (AFM) is also widespread for the characterization of interactions at the molecular scale. In this case, a nanometer scale tip fixed on a cantilevered spring is dragged either in direct contact or above a flat surface [63]. During the scanning procedure the bending of the cantilever is measured using laser beam deflection or interferometry techniques with an accuracy of 0.01 nm. This allows force measurements in the range of 0.1-1 nN [4]. The spatial resolution depends on the tip size, which can vary from 10 to 100 nm. Smaller tip radii are preferred as they provide better detail of the surface topology. However the tip can deform elastically or plastically during the measurement, thus its geometry and the distance from the surface is not really known [4]. Nevertheless AFM devices can be used to study a large variety of interactions like van der Waals, electrostatic, solvation forces etc. in many controlled environments or in presence of fluids.

From their invention, both the SFA and the AFM have been constantly improved for the characterization of nano-confined liquids, allowing for the measurement of lateral friction forces [4, 63] and the fluid viscosity [12, 64, 65] under shear.

I.3.1.b   Numerical simulations

Parallel to the experimental techniques, the rise in performance of computers allowed the development of simulation tools to study molecular lubrication.

In general, a thermodynamic ensemble containing some thousands of atoms is observed [5]: its total energy can be computed as the sum of the kinetic and potential contributions. The first depends mainly on thermal agitation of the atoms, whereas the second is related to the interactions between molecules governed by force fields.

Two approaches related to this definition of system energy have become very widespread. Monte Carlo [66, 67] is a simulation method based on statistical mechanics. Atomic configurations are generated randomly and either accepted or rejected depending on their energy state. Since only the potential energy is calculated, and not the interatomic forces, Monte Carlo is very efficient to determine the equilibrium state and structural properties of systems with large numbers of atoms. However this method features no notion of time. Hence, the simulation of non-equilibrium phenomena such as fluid flow and the related coefficients like viscosity remains difficult.

On the other hand, Molecular Dynamics (MD) is a deterministic method where the evolution of the system over time is calculated explicitly by solving Newton's equations of motion [5]. During an iteration, the forces acting on each atom and its individual acceleration are calculated from force fields which describe the intermolecular interactions. Through numerical integration it becomes possible to obtain the new atomic positions.

As the notion of time is present in Molecular Dynamics, both equilibrium and non equilibrium states can be simulated. In particular, transfer coefficients such as diffusion rates, thermal conductivity, or the viscosity of a lubricant can be determined. Molecular Dynamics will therefore be considered in this work to characterize the behavior of highly confined films under shearing: more details on these simulations will be provided in the next chapter.

In the following both numerical and experimental studies of molecular lubrication will be reviewed. Three main aspects will be described: solvation forces and the ensuing lubricant ordering, fluid nano-rheology and interfacial flow.

I.3.2   Properties of molecularly thin films

I.3.2.a   Solvation forces and lubricant ordering

While a fluid is a structureless continuum in its bulk state, this is no longer valid under molecular confinement. In fact, the presence of surfaces in close proximity generates structural effects which deeply influence the ordering of the lubricant molecules.

Using a Surface Force Apparatus, Horn and Israelachvili [3] studied OTMCS (a liquid with quasi-spherical molecules) for film thicknesses under 10 molecular diameters. They showed that the force between two surfaces does not evolve smoothly with the distance as predicted by the van der Waals theory (Figure I-6). Instead, the wall-wall interaction varies between repulsion and attraction states with a periodicity roughly equal to the molecular diameter. This oscillatory component was called solvation force. Further studies on linear alkanes [7, 68, 69] showed a similar behavior, with the periodicity corresponding to the width of the alkane chains (0.4 nm).
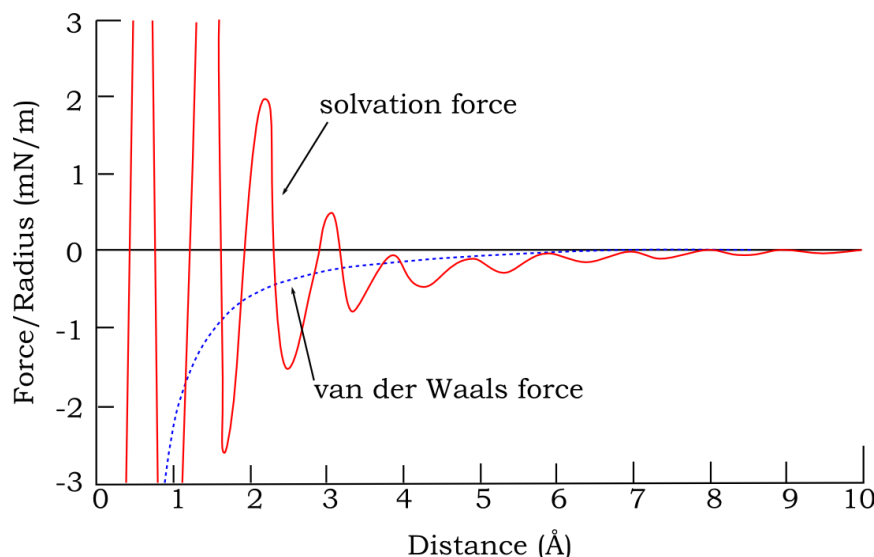
Figure I-6: Wall-wall force as a function of surface separation between two mica substrates with confined OTMCS molecules, measured with an SFA. The van der Waals interaction predicted by the continuum theory is also represented. Results from Horn et al. [3].

The origin of the solvation force is related to the ordering effect of the substrate potential on the neighboring lubricant molecules. Under confined conditions, the fluid form layered structures parallel to the walls. While full layers are energetically and entropically

stable configurations, corresponding to potential minima, fractional ones are disfavored. These variations in the free energy are reflected onto the surface force oscillations.

The presence of ordered structures in molecular films was confirmed by Monte Carlo simulations of confined Lennard Jones liquids [70, 71]. The numerical work was later extended through Molecular Dynamics calculations for various surfaces and lubricants [6, 8, 14, 15, 72] (Figure I-7). For thicknesses between 6 to 10 molecular diameters, strong density peaks are observed near the surfaces, corresponding to organized layer structures; their periodicity is roughly equal to the molecular diameter. On the other hand, the oscillations are attenuated in the center of the film, which is characterized by a disordered configuration.

Reducing surface separation leads to the formation of structures across the whole film thickness [6]. When the surfaces are pressed together, all the layers are compressed until a full one is squeezed out [3, 6]. These sudden transitions to a new stable state explain the oscillations in the solvation force. Recent simulation work by Persson et al. [73-77] has confirmed these trends through an analysis of the dynamic squeeze-out of the lubricant from an asperity contact under increasing pressure.
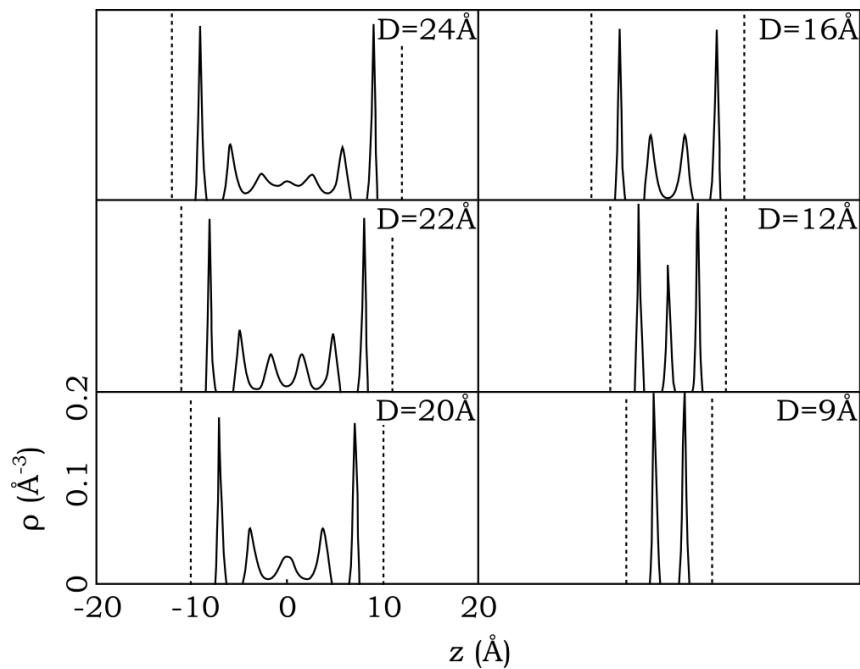
Figure I-7: Density profiles across the lubricant film (z-direction) for a confined Lennard-Jones fluid. The distance D between the walls (dotted lines) is varied from 24 to 9 Ångstroms, corresponding to 7 to 2 molecular layers. Results from Gao et al. [6].

Ordering effects in confined fluid are also related to its molecular architecture. Surface Force Apparatus tests [7] showed that the number of density oscillations near each surface is smaller for linear alkanes (5-6) than for spherical molecules (9-10). Molecular Dynamics [10, 14, 16] and experimental [78] studies revealed that the presence of branching frustrates the layering phenomenon significantly. In this case the solvation force becomes mainly repulsive and is in general stronger compared to linear alkanes [14, 79].

Changing surface nature has a profound impact on structural effects in confined lubricants. Thompson and Robbins [8] analyzed the influence of lattice spacing and the

strength of the wall-fluid potential on a Lennard Jones fluid confined between smooth crystalline surfaces. In addition to the formation of layers across the film thickness, they showed the existence of epitaxial (in-plane) ordering parallel to the walls depending strongly on surface-fluid commensurability.
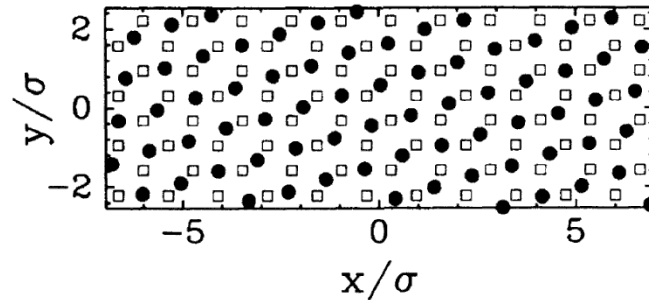
Figure I-8: Epitaxial ordering: formation of an in-plane structure in the first layer of a confined Lennard-Jones fluid (black circles), commensurate with the neighboring surface lattice (white squares). Results from Thompson et al. [8].

In commensurate cases, where the densities of fluid and wall atoms are similar, the fluid disposes itself in an ordered structure matching the adjacent crystal lattice (Figure I-8). On the other hand, increasing wall density by reducing lattice spacing frustrated the epitaxial ordering (Figure I-9). The same trends were obtained through the semi-analytical approach of Barrat and Bocquet [30, 80], who used a structure factor related to lattice spacing to explain the occurrence of in-plane ordering. Recent simulation work [81] confirmed these results for more complex fluids.
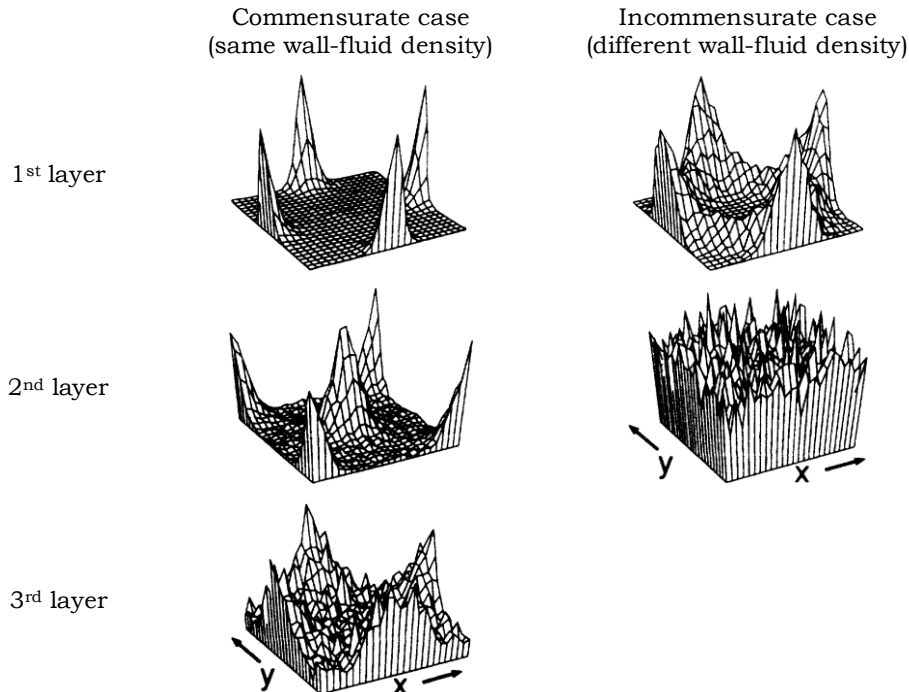
Figure I-9: Probability distribution of a Lennard-Jones fluid in proximity of a substrate. Sharp peaks are characteristic of ordered structures, commensurate to the lattice structure, whereas disordered configurations feature a more uniform distribution. Results from Thompson et al. [8].

Furthermore, the structural effect of the wall can extend more or less deeply across the fluid thickness depending on the strength of the energy interaction. This trend was also confirmed by Berro [23], who related the adsorption potential of the surfaces to the ordering across the lubricant thickness. Finally, the effect of nanometer scale roughness was investigated through Molecular Dynamics by Gao [9], who reported a severe reduction of the density peaks and the suppression of the oscillatory solvation force.

In conclusion, a state of confinement has a profound influence on the ordering of the lubricant. However, a modification of the dynamic behavior under shearing can also occur together with structural effects. In the following, the nano-rheology response of molecular films will be analyzed in more detail.

I.3.2.b   Rheology of nano-confined fluids

In classical rheological models the resistance to flow of a lubricant is characterized by its shearing viscosity η. In a bulk state, this property depends only on a fluid and its response to variations in operating conditions in pressure, temperature, and shear rate: $\eta = \eta(P, T, \dot{\gamma})$. Under confinement, however, non-intrinsic factors such as the proximity of the surfaces and the ensuing structural effects also influence fluid dynamics as shown in the following. Hence, the traditional notion of bulk viscosity is inappropriate in molecular lubrication. Most works on nano-rheology define the flow resistance in molecularly thin flow as the ratio between the shear stress and shear rate in the system. The resulting "effective viscosity" η_{eff}, with the units of a standard bulk viscosity, is then used to describe the profound transformations occurring in the dynamic behavior of confined fluids.

One of the most striking examples is the significant increase of effective viscosity with confinement compared to bulk values. This phenomenon was reported for different alkanes by Granick and coworkers [11, 82-85], who used a modified Surface Force Apparatus capable of measuring dissipative lateral forces occurring under an oscillatory shear motion of the surfaces (Figure I-10). Numerous studies enabled to further understand the effect of confinement on nano-rheology and establish three sub-regimes in molecular lubrication.
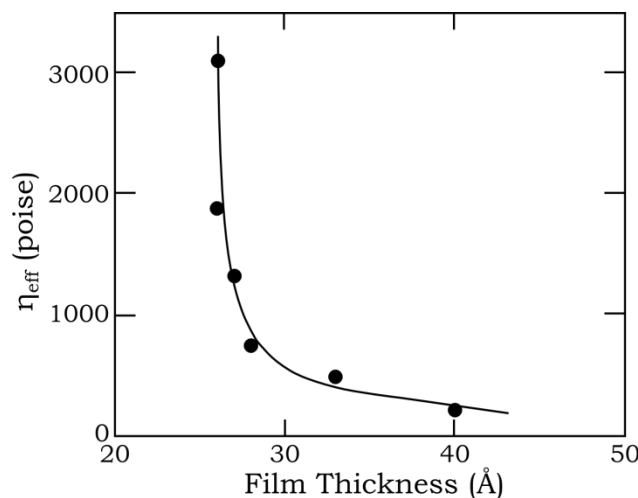
Figure I-10: Effective viscosity increase with the film thickness reduction, for an n-dodecane film confined between mica surfaces. Results from Granick et al. [11].

Chan and Horn [65] showed that the continuous theory for bulk fluids can appropriately describe drainage for spherical and linear molecules at surface separations down to 50 nm. Furthermore, when the lubricant film is thicker than roughly 10 molecular diameters and its center remains a structureless medium, the effective viscosity is within 10% of the bulk value [86].

However, as the surface separation decreases, long range structures form across the whole film thickness due to the ordering effect of the wall fluid potential. An intermediate regime occurs in correspondence with a significant viscosity enhancement [11, 64, 84, 85].

Finally, at 2-3 molecular diameters the film undergoes a reversible glass transition and assumes a solid-like behavior [12, 64, 84, 87]. In this state, the effective viscosity is several orders of magnitude larger than bulk values [88]. Furthermore, a stick-slip behavior under shearing was observed both experimentally [12] and through atomistic simulations [89, 90]. The molecules undergo a series of crystallized (stick) and molten (slip) configurations (Figure I-11).
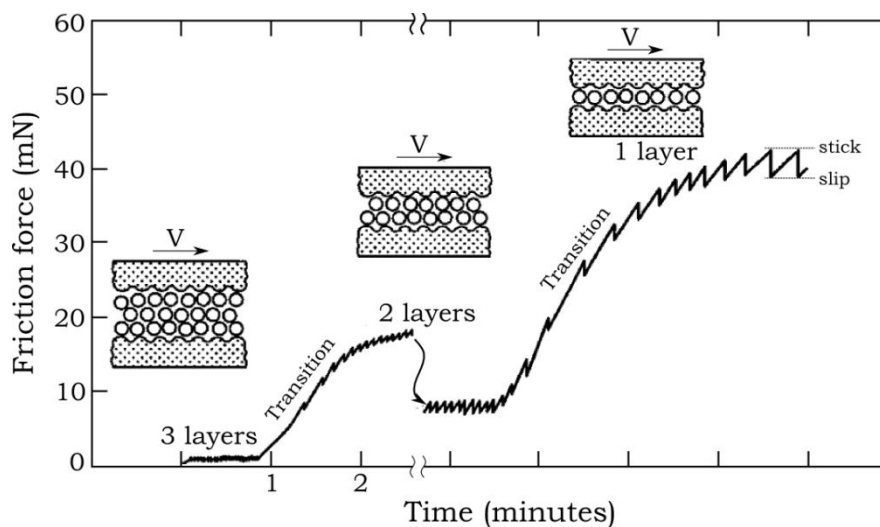
Figure I-11: Changes in friction during layering transitions towards a glass-like state for an OMTCS liquid under low shearing velocity. The oscillations in the friction force are due to stick-slip in the confined lubricant. Results from Gee et al. [12].

The resistance to shearing of the lubricant in this solid-like state is deeply influenced by pressure. At constant film thickness, both the effective viscosity [64] and diffusion times [90] increase with load. Furthermore, the flow resistance in nano-pores oscillates with the pore diameter similarly to the solvation pressure (Figure I-12) [91].

The glass transition under confinement depends strongly on the molecular shape and surface structure. For spherical molecules crystallized structures are formed within films smaller than 5-6 molecular diameters [6]. Although similar trends were observed for alkane chains [11] with the formation of crystalline bridges between layers [92], the glass transition occurs for thinner films and higher loads. The presence of branching prevents the formation of regular structures within the film thickness and the fluid remains liquid-like [14, 16]. Finally, the glass transition and viscosity enhancement are also frustrated by the presence of nanometer-scale roughness [9, 93].
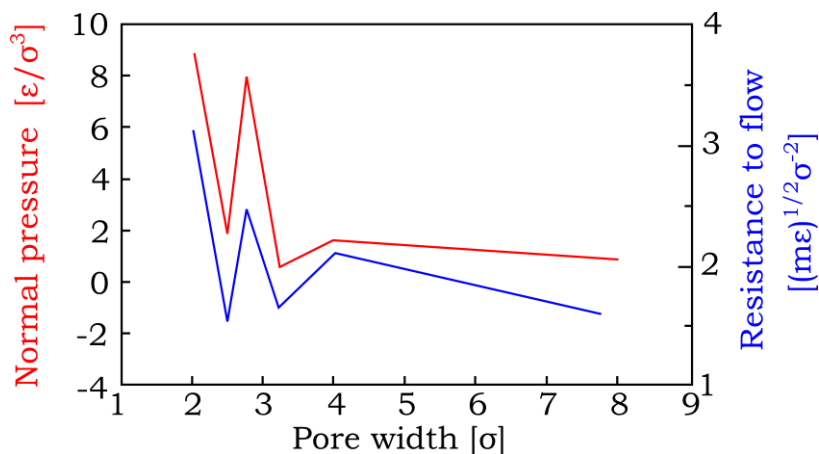
Figure I-12: Solvation pressure and flow resistance of a Lennard-Jones fluid in a nanopore as a function of its width, in reduced units. σ, ε and m correspond to the atomic radius, interaction energy and mass respectively. Results by Somers et al. [91].

The rheology of molecularly confined films can be modified by the applied shear rate. At low levels of shearing, the transition from a solid- to a liquid-like state occurs when a critical yield stress is exceeded [13, 85], and the Newtonian plateau typical of a bulk state is reached (Figure I-13). The ensuing viscosity decrease can be expressed by a general law where $\eta_{eff} \propto \dot{\gamma}^{-N}$, with exponents N between $1/2$ and 1 [11, 85, 90, 94].
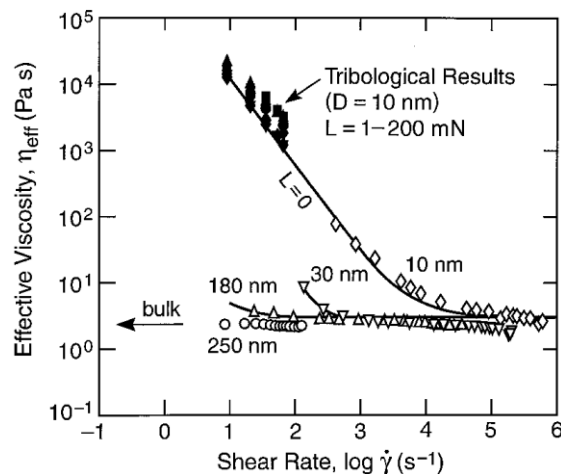
Figure I-13: Viscosity dependence of the effective viscosity with shear rate in a polybutadiene film for 4 surface separations. The white points represent a liquid-like behavior, whereas the black ones a solid-like state. Results from Luengo et al. [13].

This behavior is characteristic of confined films only, and should therefore not be confused with non-Newtonian shear thinning effects occurring in either a bulk state [41] or under molecular confinement [95] at very high shear rates. All these results were summarized by Luengo [96] in a generalized map representing the effective viscosity in confined films as a function of the shear rate and the degree of confinement (Figure I-14).
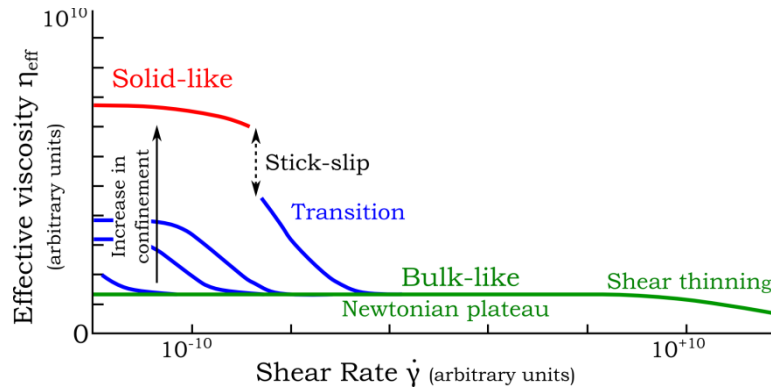
Figure I-14: Generalized map in arbitrary units for the effective viscosity of confined films as a function of the shear rate, load and film thickness. Inspired by Luengo et al. [13].

I.3.2.c   Flow at the wall-fluid interface

The no-slip boundary condition, where the lubricant moves at the same speed as the neighboring solids, is often used in the classical lubrication theory and fluid dynamics. In molecularly thin films, the fluid velocity in proximity of the surfaces can nevertheless be very different from the imposed wall velocity, due to the significant change in the nano-rheology and the strong ordering effects under confinement. This deviation from the no-slip boundary condition will be described from now on through the term "interfacial flow".

One of the most striking phenomena is the occurrence of wall slip at the surface-lubricant interface (Figure I-15). This phenomenon was observed in capillary and plate visco-simeters [97, 98]. As interfacial slip leads to a lower effective shear rate in the fluid compared to the expected bulk values, a reduction in friction ensues. This effect occurs at relatively low shear rates and could therefore not be explained through non-Newtonian shear thinning of the lubricant. The presence of wall slip was confirmed for polymers confined between non-wettable surfaces through local velocity measurements [99]. However, local dynamics in na-nometric films under severe operating conditions are difficult to access through experiments. Significant progress in the understanding of interfacial flow was therefore achieved through numerical simulations.
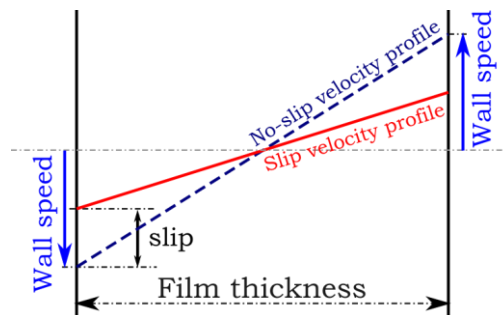
Figure I-15: Schematic representation of wall slip in a nano-confined fluid under shearing.

Wall slip was reported to be strongly dependent on the operating conditions. Fillot showed that larger pressures or a reduction in the film thickness favoured its occurrence [18]. The impact of the applied shear rate on slip was studied by many authors [29, 100, 101]. Bar-rat and Bocquet [30, 80, 102] reported that the slip length stays constant in the case of New-tonian fluids at low wall speeds. On the other hand, Martini [103] showed that at high levels

of shearing slip increases significantly up to a maximum value depending on wall stiffness. Priezjev [104] formulated general laws describing the dependence of wall slip on shear rate for shear and pressure driven flows.
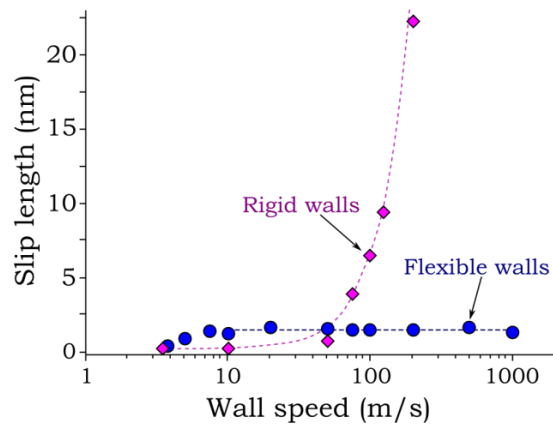
Figure I-16: Wall slip dependence on wall velocity, for n-decane confined between rigid and flexible walls. Results from Martini et al. [103].

The interfacial velocity difference at the surface-fluid boundary also depends on the architecture of the lubricant molecules. Wall slip was shown to increase with fluids featuring longer chains and branched molecules [16, 23, 105], which exhibit a higher effective viscosity under confinement. The presence of polar additives physisorbed on the surfaces, however, leads to a wall slip reduction [106] (Figure I-17).
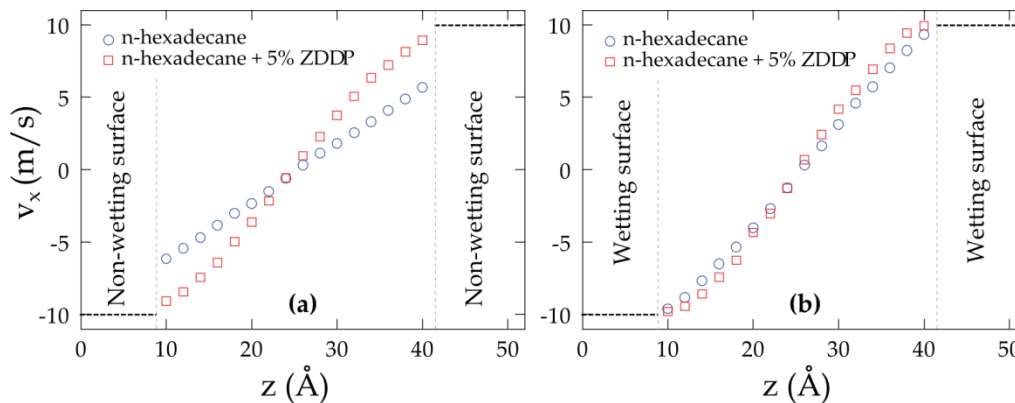
Figure I-17: Velocity profiles for pure hexadecane and an hexadecane-ZDDP mixture under confinement. Non-wettable (a) and wettable (b) surfaces are obtained by changing the wall-fluid interaction potential. Interfacial flow is modified by the physisorption of the antiwear additives (ZDDP) and surface wettability. Results from Berro et al. [106].

The affinity between the wall and fluid in terms of interaction energy and surface morphology also plays an important role on interfacial flow [8, 81, 101]. Stevens and Thompson showed that stronger wall potential reduced the occurrence of wall slip; Berro [23] reported the same trends for complex surface lattices through an analysis of the corrugation potential. Furthermore, different surface morphologies can feature large variations in interfacial flow (Figure I-18).
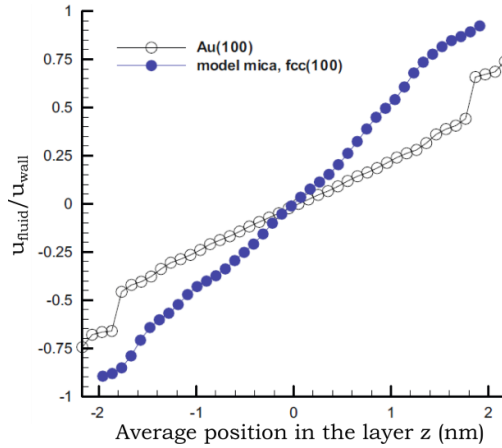
Figure I-18: Velocity profiles for hexadecane confined between smooth mica (commensurate) and gold (incommensurate) surfaces. While a no-slip boundary condition is valid for mica, wall slip is observed for gold. Results by Jabbarzadeh et al. [81].

For example, structureless and potentially smooth walls were characterized by a total slip boundary condition where the fluid was not entrained [107]. On the other hand, surfaces created from crystalline structures featured a more realistic interaction with the fluid molecules, in which slip may or may not occur. In particular, the formation of epitaxial structures in commensurate solid-fluid pairs leads to significantly smaller wall slip than incommensurate cases [8, 81, 102]. Finally, nano-rough surfaces feature a strong reduction or the total suppression of the slip effect [9, 108].

In molecular lubrication the opposite phenomenon of wall slip, called locking, can also occur. One or more interfacial fluid layers become pinned on the surfaces and move with the imposed wall speed. This was observed by Chan and Horn [65] in drainage experiments of nano-confined films between 10 and 50 nm. Locking was also obtained in presence of surfaces with a very strong wall-fluid interaction potential [8, 23, 100]. Experimental [109] and numerical [19] studies reported the formation of one pinned layer on top of the asperity peaks near nano-rough surfaces, which leads to an increase in friction during shearing.

In conclusion, many interesting properties characterize severely confined films, which cannot be described through the continuous theories for bulk fluids. While the aforementioned literature provides already a deep understanding of the mechanisms occurring in nanometer scale lubrication, this regime remains an open field of study. The design of modern devices requires in fact the characterization of more and more complex systems, with real surface materials as well as an accurate physico-chemical description of the lubricant and additives [59, 110]. Furthermore, the integration of these phenomena into macroscale models is of capital importance for the design of modern lubricated applications. In the following the most significant attempts at linking molecular lubrication to simulations at larger scale will be reviewed.

I.4   Toward a multi-scale model

Most numerical simulation methods for molecular lubrication can probe space and time scales of the order of magnitude of nanometers and nanoseconds. However, a domain

of a few millimeters, consisting of billions of atoms, should be considered to characterize a whole contact, like for instance between the ball and raceway in a bearing. This lies outside of the capabilities of modern computers, due to the high computational costs of Molecular Dynamics calculations. Hence, there has recently been a significant development of coupling techniques between atomistic simulations and macroscale methods based on the continuum theory.

A direct coupling has been performed through various methods in the case of solid materials (see [111] for a comprehensive review). This allowed the investigation of phenomena such as plasticity, asperity contact, nano-indentation, crack propagation, wear or the behavior of structures like carbon nanotubes and their influence onto bulk solids [111]. In general, a Finite Element method is employed to characterize the bulk behavior, whereas atomistic approaches are used to provide a finer resolution for the study of local effects. The coupling is then performed either by making the Finite Element nodes correspond to the atomic positions (Figure I-19a) [112], using optimized intermediate coarse grain formulations (Figure I-19b) [113], or projection operators between the two scales on a superimposed domain (Figure I-19c) [111].
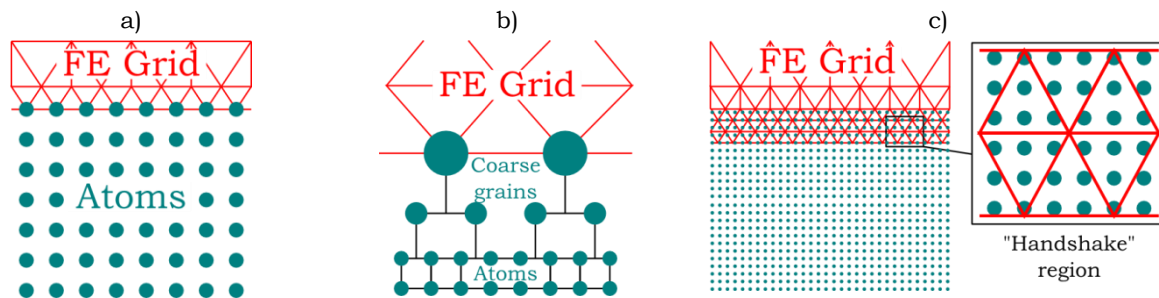
Figure I-19: Schematic representation of the direct coupling methods between atomistic and continuum simulations for solid bodies. a) One-to-one mapping between atoms and Finite Elements [112]. b) "Smartblock" method with intermediate coarse grains [113]. c) "Handshake" method with superimposed atomistic and Finite Element regions [111].

In the case of nano-confined lubricants, a direct coupling between atomistic simulations and macroscopic models is more difficult. Due to the disordered nature of the fluids, an extremely wide variety of responses is found in a whole contact. In fact, the fluid rheology depends locally on the degree of confinement, the operating conditions, the surface nature and the nano-geometry. Such responses are not simulated directly for all the possible configurations, which would require huge computational costs; instead, they are integrated into multi-scale simulations through laws issued from a limited number of atomistic simulations or experiments.

In example, Bencoe et al. [114, 115] studied rough surfaces coated with solid organic films during running-in process and reported a reduction in the coefficient of friction. They fitted experimental data [116] to model the shear behavior of the interfacial layers with pressure. Recently, Vakis et al. [117] integrated the stiffness of solid lubricants under normal load and shearing in an asperity contact model for hard disk drives. The resulting model could capture three main regimes: substrate contact, lubricated contact and the transition between

the two. The results were in agreement with experimental data and showed that the presence of lubricant improved the normal load capability without increasing friction.

Results for confined lubricants in a liquid-like state were included into classical full-film lubrication models. Structural effects were explored by Kato et al. [20] through the addition of the van der Waals and solvation forces for an OMCTS fluid under a nanometric film thickness [65, 118]. In the hydrodynamic regime, they showed that an oscillatory force occurs in the pressurized zone, corresponding to molecular density variations (Figure I-20a). When the surfaces are closer under higher loads, the adhesion and solvation components in the central part of the contact may become much larger than the applied pressure. Elastic surface deformation ensues, such as the flattening in Figure I-20b.
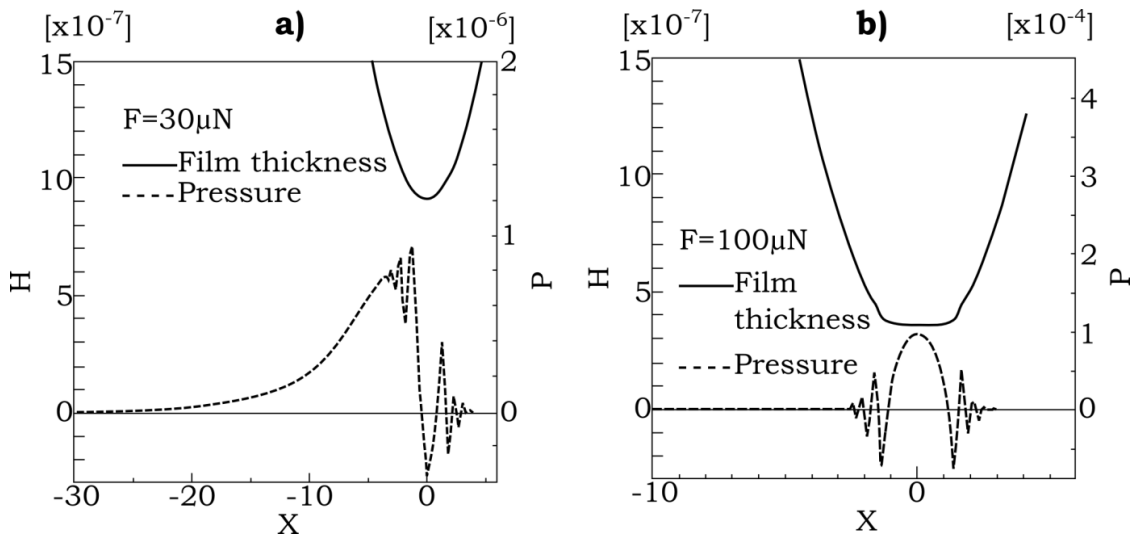
Figure I-20: Film thickness and pressure in a full-film contact including solvation and van der Waals forces, under two different loads. Results from Kato et al. [20].
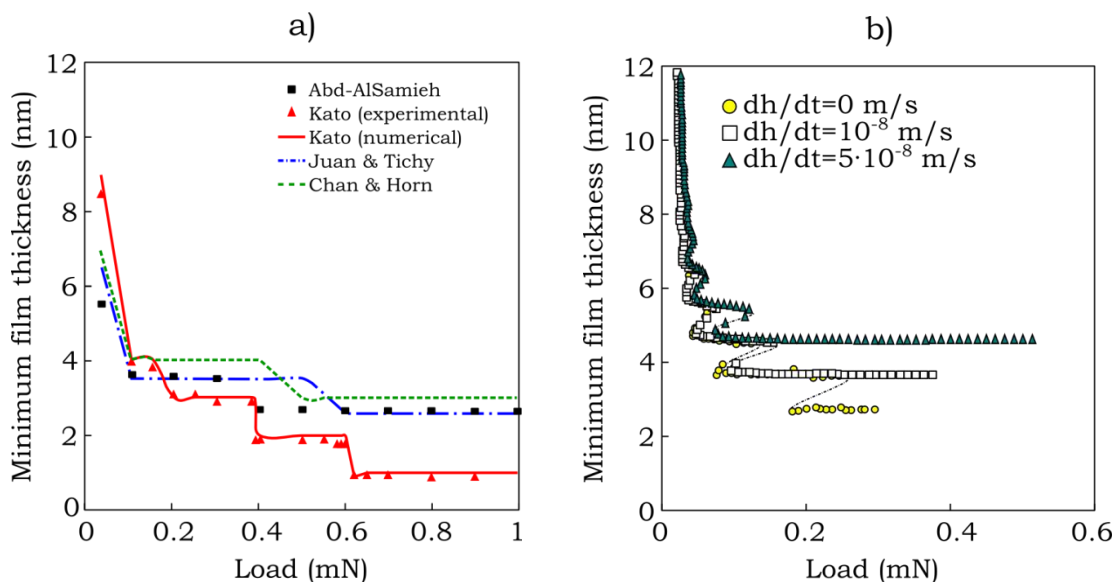
Figure I-21: Dependence of the minimum film thickness with load in a full-film contact including solvation and van der Waals forces. a) Under stationary conditions. Results from Abd-AlSamieh et al. [120]. b) Under transient conditions for three different surface approach velocities. Results by Teodorescu et al. [21].

Furthermore, the minimum film thickness becomes quantized with the load [20, 119, 120]: only some discrete values can be reached, corresponding to an integer number of molecular layers separating the surfaces (Figure I-21a). Finally, Teodorescu [21] reported that solid body inertia reduces the effect of the solvation force in transient contact dynamics. In fact, for fast surface approaches the film thickness is governed by the lubricant squeeze-out instead of the molecular interactions, and is higher compared to a stationary case (Figure I-21b).

Nano-rheology effects were introduced in an elasto-hydrodynamic lubrication model by Martini and coworkers [121]. They fitted Molecular Dynamics data to characterize the viscosity of a linear alkane as a function of confinement, and observed oscillatory values with surface separation. In a macroscopic contact under EHL conditions, this lead to a viscosity decrease in the inlet zone, thus impacting the formation and thickness of the lubricant film. Sham and Tichy [122, 123] also used Molecular Dynamics to understand the influence of neighboring surfaces on the effective viscosity in molecularly thin shear flow. In particular, strong wall-fluid interaction energies resulted in a viscosity increase near the walls. These results were implemented in a finite element model of a wedge contact: the ensuing pressure generation was much larger than in the standard Newtonian case (Figure I-22).
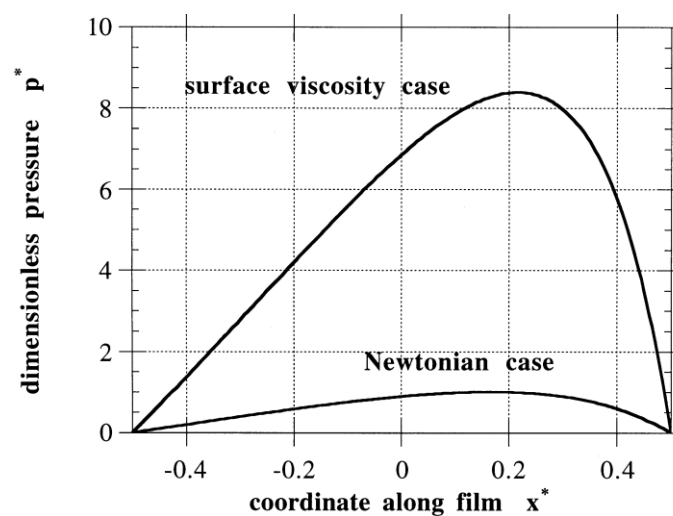
Figure I-22: Pressure generation in a wedge contact with or without the viscosity increase in proximity of surfaces due to the wall-fluid interactions. Results from Sham and Tichy [122].

The effective viscosity increase near the walls corresponds to locking. This phenomenon, as well as wall slip, can be modeled through a modification of interfacial flow under confinement. These non-standard boundary conditions were often studied in the literature, though without a direct link to molecular lubrication. For example, Navier [30] related the interfacial slip velocity and shear rate through a constant proportionality coefficient called slip length. The slip boundary condition was also implemented in the Reynolds equation to model porous journal bearings [124]. An alternative formulation with a limiting shear stress between the fluid and the wall on the slipping surface was developed by Spikes [125]. Finally, Meurisse [126] created a model based on the standard Reynolds equation with three layers across the film thickness. The viscosity and thickness of the external layers could be pa-

rametrized compared to the central ones to yield both locking and slipping boundary conditions.

While these models were not integrated directly into multi-scale approaches, there have been recent attempts to couple them with data issued from molecular lubrication studies. Chu [22] used a constant slip length in the resolution of a modified Reynolds equation including the effects of Navier slip and flow rheology. It was shown that an increase of the slip length on the moving surfaces resulted in a severe film thickness decrease. In fact, the lubricant was less entrained in the contact by slipping surfaces compared to a standard no-slip case (Figure I-23). A modification of the pressure profile with a reduction of the typical EHL spike and a larger central pressure were also reported.
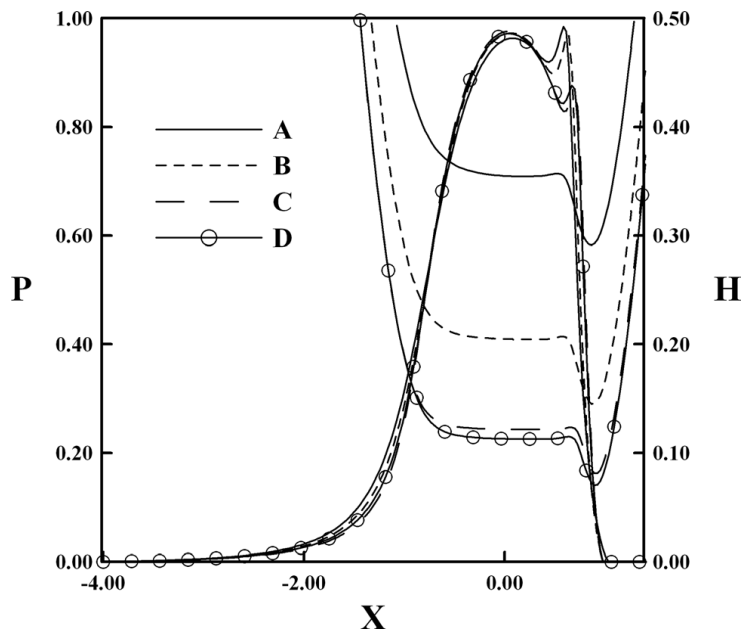
Figure I-23: Pressure and film thickness in dimensionless units for an EHL contact with different slip lengths values: A (no slip), B (0.26, 0), C (0.52, 0), and D (0.26, 0.26). The values in brackets correspond to the slip lengths on the upper and lower surfaces respectively. Results from Chu et al. [22].

Fillot [18] simulated the occurrence of wall slip through Molecular Dynamics in molecularly thin shearing flow under pressures, wall speeds and film thicknesses characteristic of an EHL contact. These results were used to formulate several laws characterizing slip as a function of the operating conditions and degree of confinement, which were then directly coupled with the resolution of the Reynolds equation.

The composite model showed the formation of dimples in the central part of the contact under moderate to high shear velocities (Figure I-24a). The modification of interfacial flow due to slip in the high pressure zone prevents the evacuation of the fluid and larger film thickness ensues. Finally, the occurrence of slip limits the friction increase with larger wall velocity differences (Figure I-24b).
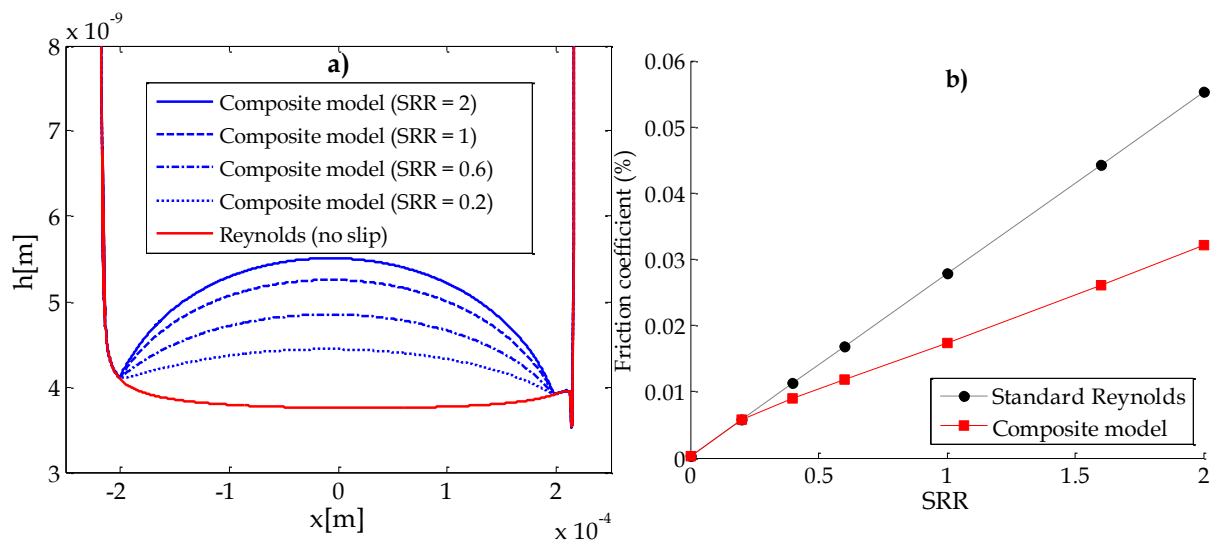
Figure I-24: Film thickness (a) and friction (b) dependence with Slide-to-Roll-Ratio (SRR) for the classical no-slip and composite models. SRR is the ratio between the wall velocity difference and the mean wall speed. Results by Fillot et al. [18].

In conclusion, these first multi-scale studies show the importance of integrating molecular lubrication in the simulation of modern industrial applications. Structural effects, changes in the nano-rheology and molecularly thin flow occurring in confined fluids translate into a modification of the film thickness, pressure distribution and friction in macroscale contacts. Furthermore, the characterization of molecular effects through analytical laws issued from atomistic simulations opens interesting possibilities. This procedure allows a fast integration into larger scale models, thus avoiding the significant computational costs of a direct coupling. However, it requires a deep understanding of molecular phenomena to account for the complex landscape of materials, lubricants and operating conditions which are found in a real contact.

I.5   Objectives of this work

The current trends in film thickness reduction are leading to an increasing importance of molecularly thin films in modern lubricated applications. Their characterization has revealed a significant number of phenomena which contradict the classical behavior of bulk fluids, like for instance structural effects or modifications of the nano-rheology and interfacial flow. Moreover, new multi-scale approaches showed that these molecular effects have a profound impact on the behavior of macroscopic contacts.

In this framework, the research work will focus on the consequences of the film thickness reduction in the case of elasto-hydrodynamic applications, like for instance rolling-element bearings. In particular, it will focus on the characterization of molecular scale phenomena and their integration into continuous models. Such research work will follow three main directions.

I.5.1   Characterization of wall slip in confined fluids

The first problem concerns one of the most peculiar phenomena in molecularly confined fluids: the occurrence of wall slip effects. The literature provides a good insight on the different factors influencing the modification of interfacial flow, like for example the morphology of the surfaces, the lubricant architecture or the operating conditions.

Nevertheless, real contact interfaces present a wide variety of surface compositions, geometries and lubricant types, as well as significant variations in pressure, shearing and film thickness. Hence, each spot in the contact region may feature different interfacial flow conditions. Accounting for all these possible configurations is necessary to understand the behavior of macroscopic contacts with nanometric film thicknesses. However, this poses at least two issues. First, the literature often focuses on canonical cases with simple surfaces and fluids. Second, a very large amount of atomistic simulations would be required, leading to high computational costs.

Hence, the first objective of this work is to further analyze the influence of the operating conditions, surface and lubricant nature on interfacial flow. In particular, quantitative models should be proposed to predict the occurrence of slip for different wall-fluid configurations. Moreover, a comprehensive law describing the wall slip dependence on all the aforementioned parameters should be formulated to account for nanometer-scale effects in real contact interfaces.

I.5.2   Integrating molecular effects into macroscopic contacts

The second problem concerns the integration of molecular effects into continuous models. It was previously shown that the tools for the characterization of severely confined films are limited to the nanometer scale, and therefore cannot be used to characterize a whole contact zone. To solve this issue, promising multi-scale approaches have been developed: molecular phenomena are described through simple laws, which can then be directly integrated into modified continuum equations. Nevertheless, the number of studies on this topic remains limited, particularly on contacts under elasto-hydrodynamic conditions.

Hence, the second objective of this work is to further develop multi-scale coupling techniques focusing on typical EHL operating conditions. In particular, the lubrication through ultra-low viscosity operating fluids is considered, as it results in a nanometer film thickness under normal running conditions. In this scenario, the classical Reynolds equations modeling the lubricant flow in the contact can be modified including the aforementioned wall slip effects. Thus, the impact played by molecular phenomena on the surface separation, friction, and lubricant dynamics in macroscopic contacts can be analyzed.

I.5.3   Towards local film breakdown

The third problem is also related to the film thickness reduction typical of modern lubricated mechanisms. Despite the presence of confined fluids, most of the nano- and macroscale systems reviewed in the state of the art featured a complete separation of the surfaces, akin to a full-film lubrication regime. Nevertheless, the decrease in the oil quantity may leave

some sub-regions of the contact without lubrication: in this case, the wall-wall interactions dominate the friction process.

Moreover, the state of the art showed that during the transition from a molecularly thin lubricant film to direct surface contact, the lubricant can assume a solid-like state due to strong structural effects. The third objective of this research is to study this process, called local film breakdown, under shearing conditions. In particular, the ordering effects, nano-rheology and friction in the last molecular layers separating the surfaces should be analyzed as a function of confinement, as well as surface and lubricant nature.

I.6   Outline of the manuscript

In order to characterize in detail the local behavior of molecularly thin films, a numerical model based on the Molecular Dynamics approach will be developed in the following Chapter. This will allow simulating the shear behavior of typical base oils confined between realistic tribological surfaces in a nano-patch of the contact. All the elements in the system will be parametrized to yield realistic properties for the wall materials, the fluid and the interface. Moreover, the typical outputs of the Molecular Dynamics simulations will be linked to the classical tribological quantities of lubrication models.

The model will be used in Chapter III to study wall slip under molecular confinement. First, a particular focus will be placed on the role played by surface and lubricant natures. A predictive model for interfacial flow will be proposed, based on the competition between these two parameters. In particular, a novel surface characterization will be developed to relate the wall-fluid interactions to local friction in the system. Moreover, parametric studies on the level of shearing, confinement and the applied pressure will allow the formulation of analytical laws characterizing the dependence of wall slip on the operating conditions.

In Chapter IV a multi-scale approach, called nano-EHL, will be developed to integrate molecular effects into macroscopic lubrication models. The classical elasto-hydrodynamic theory will be modified to include interfacial slip, quantified as a function of the contact conditions through the analytical laws obtained in Chapter III. The new approach will be applied on a typical roller-raceway contact in a bearing, lubricated through a low viscosity fluid under confined conditions. The observed changes in film thickness and friction compared to the standard theory will be related to the modification of lubricant flow due to slip effects in the central zone of the contact.

As an ultimate step, the reduction of the lubricant quantity will be pushed to its limits in Chapter V, up to the occurrence of local film breakdown and direct surface contact. This process will be studied by considering thinner and thinner film thicknesses in atomistic simulations. Structural effects representative of the transition towards a solid like behavior will be analyzed as a function of the degree of confinement. Friction results will be interpreted as a function of the degree of organization and shape of the fluid molecules, as well as the nano-geometry and composition of the surfaces. The limits of the current simulations will then be reached as the direct contact between the surfaces occurs.

Finally, after a summary of this research work on the characterization of molecular effects and their integration into continuous models, some recommendations for future work inspired by the results of this research will be presented.

II The Molecular Dynamics model

The state of the art in the previous Chapter highlighted the capabilities of Molecular Dynamics simulations for the characterization of nano-confined fluid films. Unlike classical models, this approach where all atomic trajectories and interactions in a system are simulated, allows observing deviations from bulk-like behavior and the modification of the dynamic properties of the lubricant. Furthermore, the fluid flow under confinement can be characterized depending on the surface and lubricant nature. In fact, phenomena such as wall slip and locking stem directly from the interatomic interactions which are explicitly modeled in Molecular Dynamics.

Despite these capabilities, the number of atoms in the system is limited to a few thousands due to computational limits. It is therefore impossible to simulate a whole lubricated device, and only a nano-patch in the contact area, where the film thickness and lateral dimensions are of the order of magnitude of a few nanometers, will be considered. The Molecular Dynamics model used to study the local tribological behavior under shearing of confined lubricants will be detailed in the following. Its construction and parametrization is inspired by the PhD work of Berro [23]

First, the principle and resolution algorithms of the numerical method will be described. After an overview of the system, further details on the nano-scale modeling of the surfaces, the lubricant and the wall-fluid interaction will be given. Finally, the main outputs of the model as well as the relationship with macroscopic quantities will be presented.

II.1 The numerical method and resolution algorithm

Molecular Dynamics is an explicit method based on the resolution of Newton's equation of motion to determine the evolution of a system of atoms through time. The main steps are shown in the flowchart in Figure II-1. At the time t, the position r_i of each atom i in the simulation box is known. The potential energy V_i can then be determined as a function of the interatomic distances and interactions described by force fields. The force F_i acting on an atom is computed as the gradient of the total potential energy [5]:

$$F_i = -\nabla V_i \tag{II.1}$$

Thermodynamic constraints representing the external operating conditions are added to F_i (see Section II.2.5). Then, the acceleration can be calculated by using Newton's second law of motion:

$$\ddot{r}_i = \frac{F_i}{m_i} \tag{II.2}$$

with m_i being the atomic mass. Finally, a double integration is performed through the Verlet algorithm to compute the atom position at the new time $t + \delta t$ [5]:

$$r_i(t + \delta t) = 2r_i(t) - r_i(t - \delta t) + \delta t^2 \ddot{r}_i(t) \tag{II.3}$$

As this procedure is looped for each time step δt, the system evolves deterministically. The choice of the time step influences the integration error in Equation (II.3), of the order of δt^2. Hence, this parameter is critical for the stability of the resolution and energy conservation in the system [5, 23]. Furthermore, the Verlet algorithm is based on the hypothesis

that the atomic forces and positions do not vary significantly between successive steps. The thermal agitation of the atoms occurs over a time scale of 10^{-12} s; hence, time steps of the order of magnitude of the femtosecond (10^{-15} s) are typically used to ensure energy conservation in the thermodynamic ensemble [5].

As the forces and trajectories are calculated on a per atom base, Molecular Dynamics is a computationally expensive method. In general, a few million time steps are computed, corresponding to simulated times of nanoseconds. This small duration is nevertheless sufficient to capture many phenomena occurring in molecular lubrication.
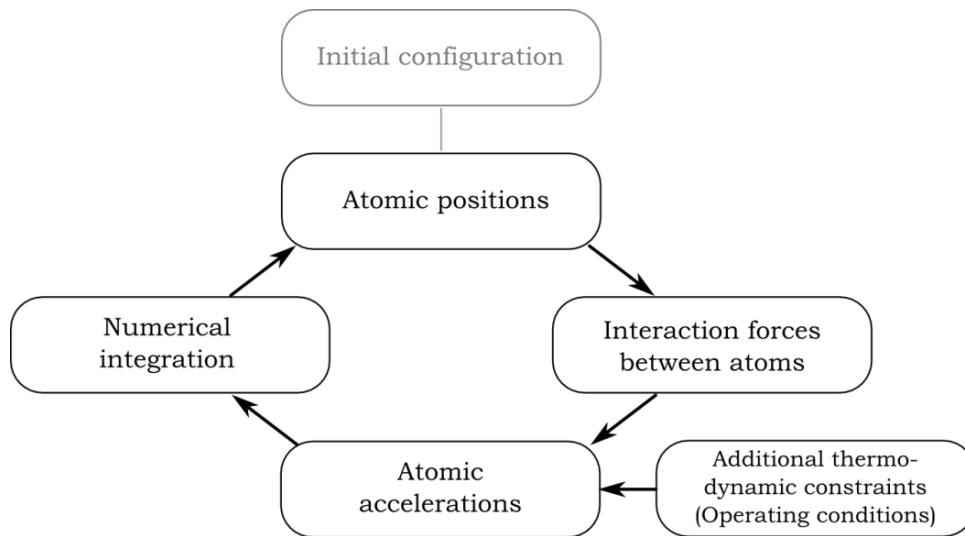
Figure II-1: Flow chart of the Molecular Dynamics method showing the calculations during one timestep.

II.2 The model for the simulation of confined fluids

The objective of the Molecular Dynamics model is to simulate the behavior under shearing of lubricants confined between two solid substrates. An overview of the typical simulation box is shown in Figure II-2. Its size is roughly 5 by 5 nanometers in length (x-direction) and width (y-direction). In the following, the film thickness along the z-direction is of the order of magnitude of a few nanometers, corresponding roughly to ten molecular layers. However, it will be reduced in Chapter V to achieve local film breakdown and direct surface contact.

Periodic boundary conditions are applied along x and y: the simulation box is then repeated in these directions creating effectively infinite surfaces. This hypothesis is justified by the fact that, in the center of a lubricated contact, the film thickness is infinitely small compared to the other dimensions. Hence, the outflow of the fluid molecules during shearing is prevented, which ensures the integrity of the Molecular Dynamics model.

Further details on the main elements of the system are presented in the following. First, the solid surfaces are generated from regular crystalline structures and parametrized through a comparison with mechanical bulk properties. The architecture of the lubricant,

governed by force fields which account for all the inner degrees of freedom of the molecules, will be discussed. The wall-fluid interaction will be briefly discussed, with an in depth analysis provided in Appendix A. The application of the operating conditions in pressure, shearing and temperature through thermodynamic constraints will be presented.
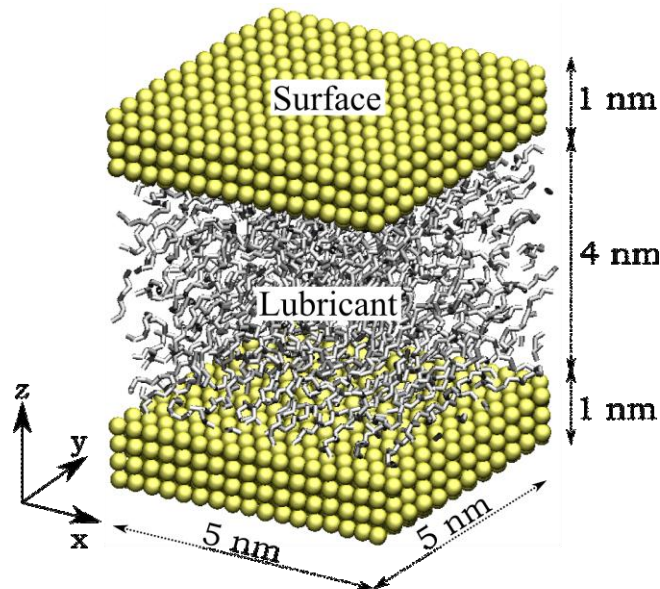
Figure II-2: Overview of the simulation box, representing a nano-patch of the contact zone.

II.2.1 *Solid walls and crystalline structures*

Though the main goal in molecular lubrication is to characterize the behavior of nano-confined fluids, it was shown in the previous Chapter that the choice of realistic surface models is crucial. For example, potentially smooth walls fail to represent the complex interaction effects between wall atoms and fluid molecules [8, 107]. Furthermore, the geometry [8, 81] and corrugation potential [23] of the surfaces influence substantially interfacial flow and friction in the contact.

In the Molecular Dynamics model, the walls are roughly 1 nm thick and correspond to the last layers of atoms in direct contact with the fluid. Hence, the chosen materials are representative of the composition at the interface. In addition to existing materials, canonical structures with arbitrary geometrical parameters are also chosen to provide a broader range of results. In all cases the properties of the walls are representative of metals and metal oxides. Regular crystalline lattices, with the atoms initially placed in the equilibrium positions, are used to generate the surfaces. Canonical structures, such as cubic (C), body-centered cubic (BCC) or face-centered-cubic ones (FCC) are typical of pure metals [127, 128]. On the other hand, more complex lattices describe oxide compounds, with atoms placed also in the interstitial sites [129, 130]. Figure II-3 shows some typical examples of these structures, while Table II-1 summarizes the lattice parameters of the materials used throughout this work.
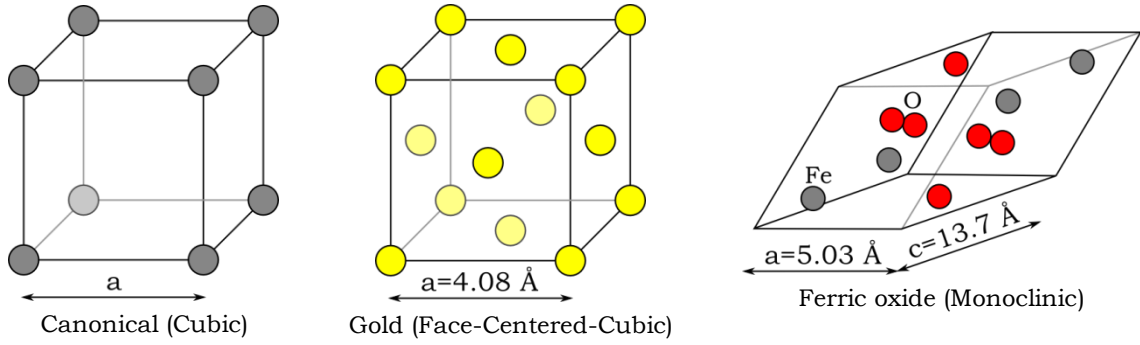
Figure II-3: Examples of unit cells of crystalline structures, which are repeated in the three spatial directions to generate the solid bodies.

Surface	Structure	Lattice constants (Å)	Bulk modulus (GPa)	Spring stiffness K_{bond} (Kcal/mol)
Compound				
Gold (Au)	Face-centered-cubic	a = 4.08	79	9.93
Ferrite iron (α-Fe)	Body-centered-cubic	a = 2.867	210	22.7
Iron oxide (Fe_2O_3)	Rhombohedral	a = 5.029 c = 13.730	210	22.7
Cementite (Fe_3C)	Orthorombic	a = 5.06 b = 6.74 c = 4.51	142	18.0
Copper oxide (CuO)	Monoclinic	a = 4.65 b = 3.42 c = 5.12	124	16.0
Silicon Nitride (Si_3N_4)	Hexagonal	a = 7.533 c = 2.934	320	27.0
Canonical				
Cubic (CC)	Cubic	a = 2, 2.5, 3, 3.5, 4	79	9.93
Face-centered-cubic (FCC)	Face-centered-cubic	a = 3, 3.5, 4, 4.5, 5, 5.5	79	9.93

Table II-1: Lattice structure and constants, bulk Young's modulus and interatomic bond stiffness for different surface materials [127, 129-132]. The mechanical properties of canonical surfaces are chosen the same as gold.

To generate geometrically smooth surfaces, the crystalline structures are cut by a plane whose orientation is described through Miller indexing. Due to the discrete nature of the walls an atomic roughness is still present. Its wavelength corresponds to the lattice spacing and is typically of a few Ångstroms. Alternatively, nano-scale roughness profiles can also be carved into the crystalline structure. In this work, sinusoidal asperities along the x-direction with a wavelength λ and amplitude A of a few nanometers will be considered in Chapter V and Appendix C to study the influence of wall geometry in molecular lubrication.

Another important factor influencing the interfacial flow of nano-confined lubricants is wall stiffness [103]. This parameter is ruled by the interactions between the atoms in the surfaces, which are usually described through three types of potential. In harmonic bonds [5], the atoms are linked by unbreakable springs which can deform elastically. On the other

hand, the Lennard Jones potential describes the attractive (van der Waals) and repulsive (Pauli) forces due to electronic cloud interaction on a per atom basis [133]. The Embedded Atom Method [128] (EAM) uses an energy function depending on electron density to model interactions in metals and alloys. Additional terms, such as Coulombic interactions, partial polarization, as well as combinations of different contributions can be used to model more complex materials [134].

Lennard Jones and EAM potentials allow the computation of plastic deformation and the formation of dislocations within the lattice. Harmonic bonds cannot capture these phenomena; nevertheless, in this study shearing occurs in the confined fluid and surface deformation remains limited to the elastic domain. Furthermore, by employing harmonic bonds, the number of neighboring atoms is fixed during a simulation compared to the other potentials. As a result, the computations are 5 to 10 times faster [23]. Finally, this method can be easily applied to complex materials such as metal oxides, and will be used throughout this work. The harmonic potential between two atoms is given by [5]:

$$V_{bond} = K_{bond}(l - l_0)^2 \qquad (\text{II}.4)$$

Here l represents the interatomic distance, whereas l_0 is the bond length at equilibrium obtained from an undeformed lattice.

The spring stiffness $2 \cdot K_{bond}$ must then be parametrized to yield realistic mechanical properties for the walls. There are three guidelines for this operation, which must be performed for each surface material. First, the lower limit for the stiffness parameter is given by the Lindemann criterion related to the melting point of solids [135]:

$$\left\langle \delta r^2 \right\rangle \leq \left(0.18 \cdot \bar{d} \right)^2 \qquad (\text{II}.5)$$

This prevents an excessive vibration by limiting the mean square displacement $\left\langle \delta r^2 \right\rangle$ of the atoms from their equilibrium positions in the crystal lattice, compared to the average interatomic distance $\bar{d}$. Hence, the integrity of the crystalline structure is ensured. Second, the Debye frequency ω_D, which is the maximum vibration frequency of the crystal, must not be exceeded [136]. The upper value for the spring stiffness is given by [137]:

$$K_{bond,\max} = \frac{\bar{m} \cdot \omega_D^2}{2} = \frac{\bar{m}}{2}\left(\frac{k_B T_D}{\hbar} \right)^2 \qquad (\text{II}.6)$$

where k_B and $\hbar$ are the Boltzmann and the Planck constants respectively, $\bar{m}$ represents the mean atomic mass and T_D is the Debye temperature. While the Lindemann and Debye criteria give good guidelines for the parameterization of K_{bond}, the minimum and maximum can differ of a few orders of magnitude [23].

More precise values can be obtained by considering the actual mechanical properties of the solid material. Molecular Dynamics compressibility simulations are performed by applying a slight pressure change δP on the lattice. A small volume variation δV ensues, which can be linked to the bulk modulus E of the material by [23]:

$$E = -V \frac{\delta P}{\delta V} \qquad (\text{II}.7)$$

The spring stiffness is adjusted to match results from the Molecular Dynamics simulations with data from the literature. The obtained values usually range between 10 and 50 kcal/mol for metals and metal oxides (see Table II-1), which complies with both the Lindemann and Debye criteria.

The stiffness of the harmonic bonds also governs heat conduction within the solid body. The corresponding thermal conductivity Λ can be determined through reversible non equilibrium simulations [138]. It was shown that Λ is significantly underestimated compared to bulk values from the literature, because heat transfer through the movement of electrons within the metal lattice is not simulated [23]. More complex potentials, such as Lennard Jones or EAM do not show an improvement compared to harmonic bonds. As a result, energy dissipation from the system and the formation of temperature gradients across the surfaces may be influenced. This issue is also strongly influenced by the choice of thermostating techniques for temperature regulation, and will be discussed more in detail in Section II.2.5. In the following the description of the Molecular Dynamics model will continue with a particular focus on lubricant architecture.

II.2.2 *Molecular structure and force fields*

Liquid lubricants are generally more complex and difficult to model than solid materials. In fact they are made of flexible chains which in general do not feature a global ordering, and are characterized by a large number of degrees of freedom. According to the literature [5, 24, 139], this complex behavior is usually modeled through force fields governing the intra- and intermolecular interactions. In the following, a particular focus is placed on the architecture of alkanes, which are representative of lubricant base oils and will be considered for the rest of this work.

Intramolecular interactions shown schematically in Figure II-4a, include covalent bond stretching from Equation (II.4), angle bending and torsion [5]. Covalent angle bending between three consecutive atoms along the molecular chain is modeled through an angular spring potential:

$$V_{angle} = K_{angle} \left(\theta - \theta_0 \right) \tag{II.8}$$

with $\theta - \theta_0$ the deviation from the equilibrium angle and K_{angle} the stiffness parameter. Dihedral interactions are represented through torsion potentials between four consecutive atoms along the molecular chain:

$$V_{torsion} = K_{torsion} \left[1 + \cos\left(n\varphi - \beta \right) \right] \tag{II.9}$$

Here, $K_{torsion}$ is the dihedral energy barrier, n the multiplicity of the equilibrium positions, φ the torsion angle and β the phase shift.

Atoms belonging to different molecules, or separated by more than 4 atoms along the molecular chain, are non-bonded. In this case, a 12-6 Lennard-Jones potential with a cutoff distance of 10 Ångstroms, representing the van-der-Waals interactions, is used:

$$V_{LJ} = 4\varepsilon \left[\left(\frac{\sigma}{r} \right)^{12} - \left(\frac{\sigma}{r} \right)^{6} \right] \tag{II.10}$$

In Equation (II.10) r is the distance between the nuclei of the atoms, σ the gap at which the potential changes from positive to negative, whereas ε quantifies the energy minimum at the equilibrium position $r_{eq} = 2^{1/6}\sigma$. These parameters are generally given for two interacting atoms of the same species. In the case of atoms of different nature A and B, the Lennard-Jones parameters are calculated through the Lorentz-Berthelot mixing rules [5]:

$$\varepsilon_{AB} = \sqrt{\varepsilon_A \cdot \varepsilon_B} \qquad \text{and} \qquad \sigma_{AB} = \frac{\sigma_A + \sigma_B}{2} \qquad (II.11)$$

Finally, long range electrostatic forces are considered in this work since alkane molecules are non-polar.
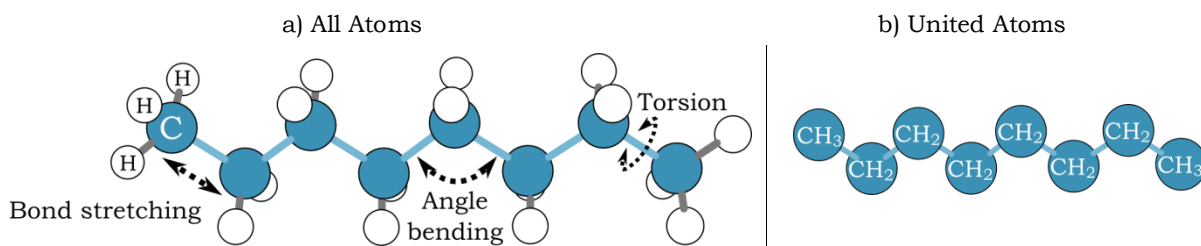
Figure II-4: Schematic representation of a linear alkane (n-octane). A) All-Atom formulation, showing also the intra-molecular degrees of freedom. B) United-Atom formulation.

In MD simulations, the totality of atoms in the fluid molecules is explicitly modeled most of the time. As the name suggests, this is the case for an All-Atom (AA) representation shown in Figure II-4a. However, simplifications in the molecular structure can be introduced for instance in the case of alkanes, where single Hydrogen and Carbon atoms are combined into CH_2 and CH_3 segments (Figure II-4b). In this formulation, called United-Atom (UA) [94], the number of degrees of freedom is greatly reduced, which allows the choice of a bigger time step and leads to significantly faster computational times. Hence, the United-Atoms formulation will be chosen in this work: the corresponding interaction parameters for alkanes are summarized in Table II-2.

Bonded interactions		
Potential	**Neighbors**	**Parameters**
Bond stretching	CH_2–CH_3 CH_2–CH_2	K_{bond} = 268.09 kcal/mol/Å^2 l_0 = 1.54 Å
Angle bending	CH_x–CH_2–CH_2	K_{angle} = 62.067 kcal/mol/deg^2 θ_0 = 114 deg
Torsion	CH_x–CH_2–CH_2–CH_2	$K_{torsion}$ = 1.499 kcal/mol n = 3 β = 0.0 deg
Non-bonded interactions (Lennard-Jones potential)		
Atom	**Mass (a.m.u.)**	**σ (Å)** **ε (kcal/mol)**
CH_2	14.027	3.93 0.0933
CH_3	15.035	3.93 0.2264

Table II-2: Parameters of the bonded and non-bonded interaction potentials for alkanes, from an OPLS-CHARMM United Atoms force field [24, 139].

II.2.3 Wall-fluid interaction

A further element of the Molecular Dynamics model is the interaction between lubricant molecules and the solid walls. In general, forces of different natures characterize the wall-fluid interface. Short range van der Waals interactions, as well as long range electrostatic ones in the case of polar molecules can describe how the molecules are physisorbed on the surfaces [106]. Furthermore, complex tribo-chemical reactions can lead to chemisorption phenomena, which cause a significant modification of the wall-substrate interactions [59].

In this work, the parameterization concerns mainly the van der Waals forces between alkane molecules and the walls, which are modeled through a Lennard-Jones potential in Equation (II.10). In particular, it was shown in Chapter I that the wall-fluid energy parameter ε_{w-f} is critical for interfacial flow and the occurrence of velocity slip [8, 23, 101]. However, there are very little references in the literature for the interaction strength of real surface materials with alkane molecules.

In general, ε_{w-f} can be expressed as a function of the average well depth of the Lennard-Jones potential for the fluid ε_f:

$$\varepsilon_{w-f} = \kappa \cdot \varepsilon_f \qquad (II.12)$$

ε_f can be calculated from the force fields describing the non-bonded interactions in the lubricant (see Appendix A), and is typically of the order of magnitude of 0.1 kcal/mol for alkanes. According to the literature, the factor κ ranges from 0.4 to 10, covering weakly to highly adsorbing surfaces. However, a more accurate choice for this parameter should be made for real surface materials to capture adequately the fluid dynamics in molecularly confined films.

In Appendix A two methods are described in detail and compared. The first one suggests tuning κ to fit the experimental measurement of adsorption and desorption energies of CH_x groups on different metal surfaces [23, 25, 81]. A more general formulation stemming from the definition of surface energy will then be presented. Both methods deliver similar results: in particular, it is found that $\kappa =5$ can adequately describe the wall-fluid interaction for most configurations with metal surfaces and alkane molecules.

As detailed in Appendix A, the potential well-depth for the wall atoms ε_w can finally be obtained through the Lorentz-Berthelot mixing rules from Equation (II.11):

$$\varepsilon_w = \kappa \cdot \varepsilon_{w-f} = \kappa^2 \cdot \varepsilon_f \qquad (II.13)$$

The values for the surface materials used throughout this work are reported in Table II-3.

Atom	Mass (a.m.u.)	σ (Å)	ε (kcal/mol)
Au	196.97	2.655	2.625
Fe	55.845	2.321	0.945 (pure) 4.041 (carbide) 9.518 (oxide)
Cu	63.546	2.741	4.679
C	12.000	3.400	0.0854
O	15.999	2.960	0.210
Si	28.086	3.826	1.486
N	14.007	3.328	0.267
Canonical	196.97	2.655	1.000

Table II-3: Parameters of the non-bonded interactions for wall atoms [24, 133, 140].

II.2.4   *System initialization*

After the parametrization of all the molecular interactions in the system, it is necessary to define the initial configuration of the atoms. The fluid is confined between two surfaces, in a configuration similar to Figure II-2. However, the size of the simulation domain must be chosen appropriately to provide meaningful results.

Along the x- and y-directions, the box must be big enough to prevent a molecule from interacting with itself over the periodic boundaries. To ensure this condition, the system size must be larger than the backbone length, plus the cutoff distance of the Lennard-Jones potential on each end of the chain. In order to simulate alkanes up to 20-25 CH_x segments, which are 2.5 nm long when fully deployed [95, 108], a box length of L_x =5 nm and width of L_y =5 nm are therefore chosen.

The size in the z-direction is determined by both the film and wall thickness. While the surfaces are in reality some millimeters thick, only 1 nanometer is considered, which corresponds to the last layers in direct contact with the fluid. This height is equal to the cutoff distance of the Lennard-Jones potential, therefore the wall-fluid van der Waals interactions are fully accounted for.

The film thickness h is not imposed in the simulations; instead, a constant external load is applied (Section II.2.5). Under compression, the outflow of the fluid molecules is prevented, as infinite surfaces are simulated through the periodic boundary conditions along the x- and y-directions. An equilibrium state is reached as the repulsive forces in the system balance the external load. Hence, h depends only on the applied pressure and the number of lubricant molecules. Typically, the initial lubricant density is chosen to be similar to the equilibrium one [23], for example using bulk compressibility laws as a guideline [37]. As a consequence, the thickness varies only slightly once compression is applied. This allows setting target values for the film thickness to study the effect of confinement on the fluid. Once the system initialization is complete, it is possible to simulate the shearing of the lubricant.

II.2.5 *Thermodynamic ensemble, simulation steps and operating conditions*

The simulations are run using an NVE (micro-canonical) thermodynamic ensemble. Hence, the number of molecules, the volume and the total energy in the system remain constant during the whole simulation. Moreover, the operating conditions in load, wall speed and temperature are applied through additional thermodynamic constraints. In particular, three main steps are simulated to determine the lubricant behavior under molecular confinement: relaxation, compression and shearing.

As the lubricant molecules are initially randomly disposed, an energy minimization phase is required to reach a realistic configuration characteristic of an equilibrium state. A compression step follows: the external load is applied symmetrically to control domains located on the outer atomic layers of the surfaces (Figure II-5). In particular, the local pressure P acting on the nano-patch is set through atomic forces acting in the z-direction:

$$F_{z,i} = \frac{P \cdot S}{n_C} \tag{II.14}$$

with $S = L_x \cdot L_y$ the area of the contact patch and n_C the number of atoms in the control domains of the walls. After roughly 0.5 ns, a stable value for the film thickness is reached; the distributed load is then kept constant throughout the rest of the simulation. The local pressure values on the nano-patch are typically chosen from an elasto-hydrodynamic lubrication case, and range from roughly 0.1 to 5 GPa.
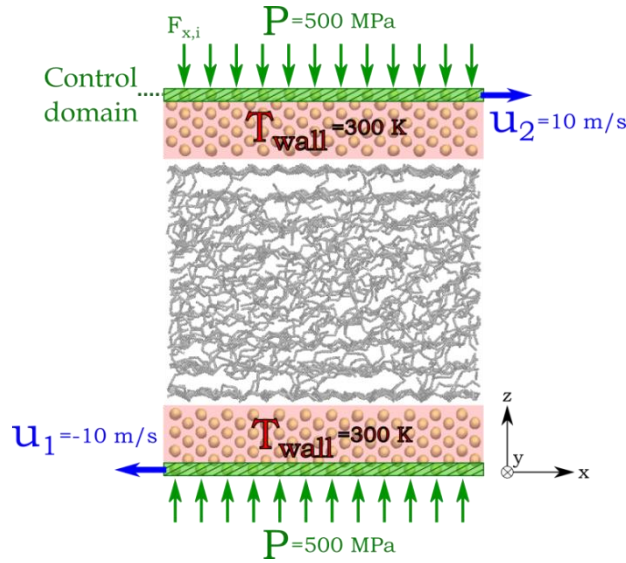
Figure II-5: Application of the operating conditions in pressure, wall speed and temperature. The control domains for P, u_1 and u_2 are the external atomic layers (green hashed area), where the walls in the Molecular Dynamics simulation are coupled with the bulk solid bodies. The temperature is applied on the whole surfaces (red shaded area).

Finally, the velocities u_1 and $u_2 = -u_1$ are imposed in the x-direction to the lower and upper surfaces respectively, generating a shear-driven (Couette) flow in the lubricant. For this phase 5 to 10 nanoseconds are simulated, which is generally sufficient to achieve a steady state regime: the behavior of the nano-confined fluid can then be characterized. The values for u_1 and u_2 are usually in the range from 1 m/s to 10 m/s [18, 23].

Another important thermodynamic constraint is the regulation of the temperature during the simulation. In fact, while the chosen NVE thermodynamic ensemble entrains a constant energy condition, the external operating conditions typically involve an imposed temperature. Furthermore, during the shearing of the lubricant heat is generated and is normally evacuated by the surfaces. However, all the interactions in the system are conservative, and no thermal dissipation can take place. It is therefore necessary to use thermostating techniques to remove energy from the system and avoid an unrealistic temperature increase.

While the temperature T in the fluid is left free to evolve during the simulation, the one in the surfaces (T_{wall}) is regulated through a Langevin thermostat [27] issued from Brownian mechanics. A friction and a random force are added to the equations of motion to represent respectively the influence of the surrounding medium on the thermal agitation of the atoms, and the interactions with a heat bath at the operating temperature. As this technique acts on a per-atom basis no temperature gradient forms across the surfaces [23], effectively simulating an infinite thermal conductivity in the walls. This hypothesis can be justified by the fact that the simulated surfaces are extremely thin compared to the bulk solids. Hence, the issues about the underestimation of the thermal conductivity due to the parametrization of the intra-wall interactions (Section II.2.1) are solved. It should nevertheless be reminded that this procedure may influence the interfacial transport properties and flow at the interface between the confined fluid (non-thermostated) and the wall (thermostated) [23].

The target temperature of the Langevin thermostat can be set to a fixed value during the whole simulation. This method, called Sliding Boundary Temperature (SBT), is the classical energy dissipation technique in Molecular Dynamics simulations [121, 141, 142]. It will be used in most of this work with a constant imposed wall temperature T_{wall} =300 K. It was in fact shown that no significant heating occurs in confined alkanes for wall speeds up to ±10 m/s and thickness of roughly ten molecular diameters [23, 28]. In Chapter V, however, an advanced technique called Variable Boundary Temperature (VBT) algorithm [28] will be employed to study thermal effects occurring due to a severe film thickness reduction. The heat flux removed by the wall thermostat is imposed as a boundary condition on a semi-infinite solid body. The surface temperature is then calculated dynamically from the dissipated energy, thermal bulk properties of the surfaces and the temperature far away from the contact interface. Hence, heating effects occurring locally in the contact nano-patch can be simulated.

Through the application of these thermodynamic constraints the shearing of the lubricant is simulated. Once a steady state is reached, results such as the velocity profiles in the lubricant thickness or the tangential shear stress at the surfaces can be calculated through statistical averaging.

II.3 Outputs of the Molecular Dynamics simulations

The Molecular Dynamics resolution algorithm presented in Section II.1 gives the access to the position, velocity and the force acting on each atom at every time step. In order to characterize the behavior of nano-confined fluids, statistical averaging in time and space of these quantities is employed. In the following, the Molecular Dynamics results are related

to the usual tribological variables of film thickness, density, friction, viscosity and temperature. It should nevertheless be remembered that these quantities are defined locally in the nano-patch and may deviate from the typical bulk behavior.

II.3.1 *Film thickness*

The film thickness h for smooth surfaces is calculated as shown in Figure II-6. Two central planes are placed between the lubricant atoms and the neighboring surfaces [23]. The instantaneous thickness, defined as the distance between these planes, is then averaged over the shearing duration.
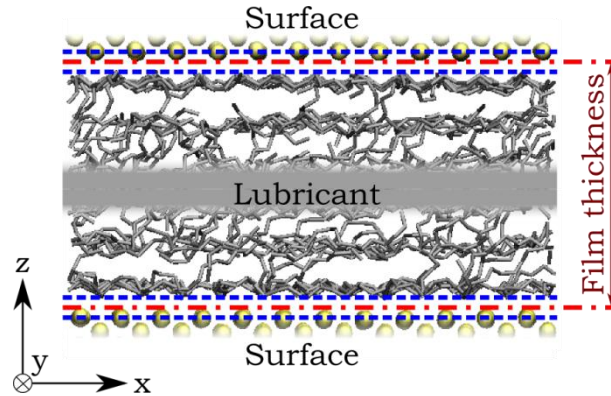
Figure II-6: Schematic representation of the film thickness calculation for smooth surfaces.

II.3.2 *Lubricant density*

The average lubricant density ρ can then be defined through the film thickness [15]:

$$\rho = \frac{\left\langle \sum_{i=1}^{n_{mol}} m_{mol,i} \right\rangle}{S \cdot h} \tag{II.15}$$

with n_{mol} the number of fluid molecules in the system, $m_{mol,i}$ the mass of each molecule, S the area of the nano-patch and $\langle \rangle$ the time average. The lubricant density can then be directly compared to the macroscopic quantity in the contact [18]. By considering the configuration of Figure II-7 as an example, the average density of the confined hexadecane is equal to $\rho = 890$ kg/m³, which corresponds to the values obtained through the Dowson-Higginson bulk law under a pressure of 500 MPa [23, 37].

The atomic positions can also be used to calculate profiles across the film thickness to visualize structural effects occurring in the nano-confined fluid. The film thickness is divided in a series of slabs with a height δh; the density in each slab is then averaged over time for the sampling duration once the steady state is reached. As an example, the typical layering structures already mentioned in the literature (see Chapter I) can be observed in Figure II-7. The density peaks near the wall correspond to well-defined layers; on the other hand the oscillations are reduced in the center of the film, where the fluid is disordered.
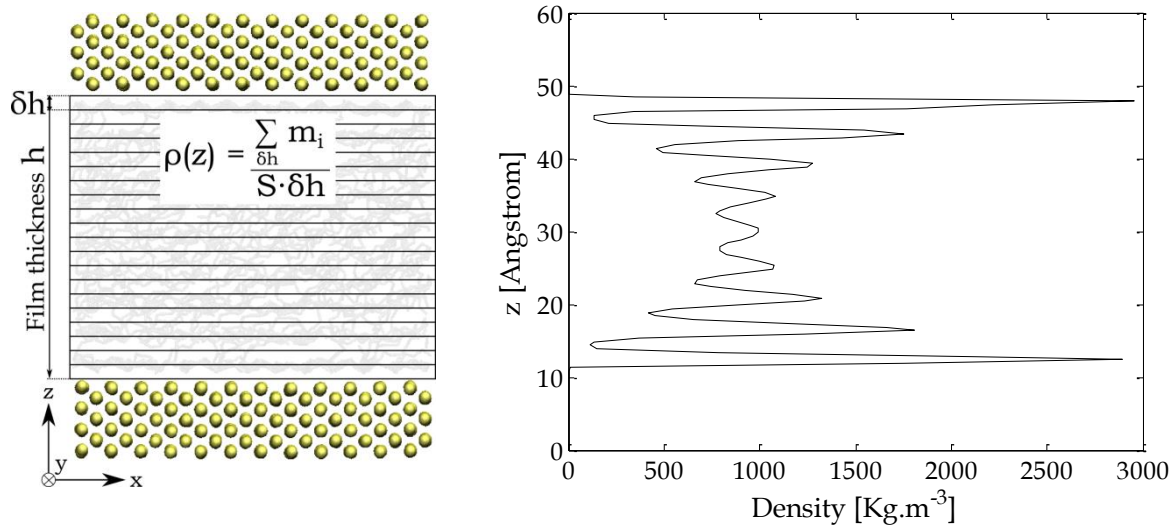
Figure II-7: Method for sampling the fluid density across the film thickness and resulting profile (Au [100] surfaces, n-hexadecane, P=500 MPa, $u_2=-u_1=10$ m/s, $T_{wall}=300K$).

II.3.3   Fluid dynamics

In order to determine the lubricant dynamics across the film thickness, a procedure similar to the one for the density is applied. Again, the gap width is divided in a series of slabs; the speed of the fluid molecules in each slab along the shearing (*x-*) direction is averaged over time during steady state conditions. A velocity profile similar to the one shown in Figure II-8 is thus obtained.
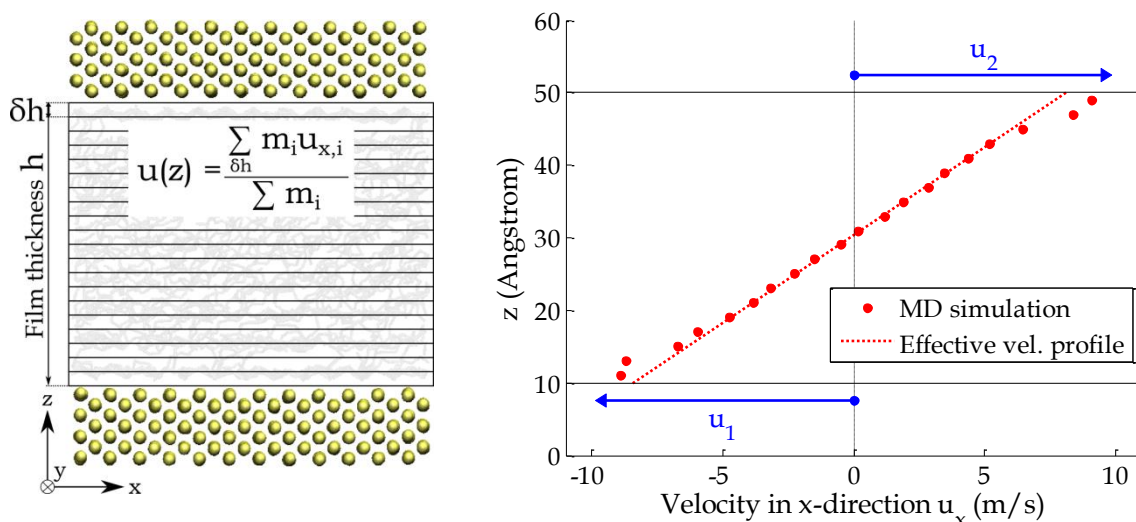
Figure II-8: Method for sampling the fluid velocity across the film thickness and resulting profile. The linear interpolation to obtain the effective shear rate is shown through the dotted line. (Au [100] surfaces, n-hexadecane, P=500 MPa, $u_2=-u_1=10$ m/s, $T_{wall}=300K$).

In the represented configuration, it can be noticed for instance that the fluid velocity is linear in the center of the film. This phenomenon is representative of a liquid-like behavior, and is typical of alkanes for surface separations down to 3-4 nanometers [11, 23, 143]. In this

case, it is therefore possible to define the effective shear rate $\dot{\gamma}_{eff}$ as the velocity gradient in the z-direction $\partial u(z)/\partial z$, obtained through an interpolation of the profile in the center of the fluid film [108].

This characterization of the lubricant dynamics across the film thickness will be further discussed and exploited in Chapter III to study interfacial flow under molecular confinement.

II.3.4 *Shear stress, friction and viscosity*

The shear stress is related to the atomic forces $F_{x,i}$ opposing the movement of the surfaces in the shearing direction per surface unit [15]:

$$\tau_{zx} = \frac{\left\langle \sum_{i=1}^{n_C} F_{x,i} \right\rangle}{S} \tag{II.16}$$

with n_C the number of atoms in the control domain where the wall velocities are applied (see Section II.2.5), S the area of the nano-patch and $\langle \rangle$ the time average. The local friction coefficient $c_f = \tau_{zx}/P$ can be obtained by dividing the shear stress by the applied pressure. Finally, the nano-rheology of the lubricant can be characterized through its effective viscosity η_{eff} [15]:

$$\eta_{eff} = \tau_{zx}/\dot{\gamma}_{eff} \tag{II.17}$$

It must be noted that all the aforementioned quantities describe an average behavior in the whole nano-patch of the contact. For example, the effective viscosity term does not capture local variations near the walls due to the layer structure and strong density variations [144]. Still, the averaging is performed over times and space scales of some nanoseconds (the simulated duration) and nanometers (the system size), which is appropriate to capture many phenomena occurring in molecularly confined films presented in Chapter I, such as structural effects, the fluid dynamics under shearing and the nano-rheology.

II.4 Conclusion

In this Chapter a Molecular Dynamics model was developed to study the shear behavior of fluids severely confined between two surfaces. A local patch of the contact area was considered, featuring a length, width, and lubricant film thickness of the order of magnitude of a few nanometers. Each element of the system was parametrized to yield realistic properties for the walls, the confined lubricant, and the surface-fluid interface. The operating conditions in pressure, wall speed and temperature were introduced through thermodynamic constraints and thermostating techniques, in order to simulate the shearing of the lubricant over some nanoseconds.

The main outputs of the Molecular Dynamics simulations consisted of the atomic positions and trajectories. These were averaged over time and space to obtain the usual tribological variables of film thickness, density, friction and viscosity, which characterize the local behavior of the contact nano-patch.

Hence, the Molecular Dynamics model presented in this Chapter can be further used to characterize many phenomena characteristic of nanometric lubricant films. In the following, a particular focus will be placed on the flow at the wall-fluid interface, which under molecular confinement can deviate from the classical no-slip condition. In particular, the wall slip phenomenon will be characterized as a function of the operating conditions, as well as surface and lubricant natures.

III Molecular Dynamics study of interfacial slip

In the introductory Chapter it was shown that interfacial flow in nano-confined fluids can significantly deviate from the classical no-slip boundary condition. Wall slip may occur depending on the operating conditions, the molecular structure of the fluid, the wall-fluid interaction energy and commensurability etc. Section I.4 reported that these effects can significantly affect the tribological behavior in macroscopic contacts and modify the pressure generation, load bearing capability, the film thickness and friction.

Hence, a detailed analysis of interfacial flow under molecular confinement is required. Though the existing numerical and experimental studies provide a deep insight on the underlying physical phenomena, further work is needed in order to implement the results in a multi-scale approach for the simulation of elasto-hydrodynamic contacts with nano-confined fluids. First, only few of the literature references in Molecular Dynamics consider operating conditions characteristic of EHD lubrication. Moreover, the surfaces are usually derived from canonical surfaces with simple crystal lattices, whereas in reality the contact interface is also composed of more complex materials like oxides.

Finally, despite being a powerful tool to characterize molecularly confined fluid, atomistic numerical simulations are computationally expensive. Hence, a direct coupling between Molecular Dynamics and macroscopic models remains difficult. As shown in the existing multi-scale approaches, it is necessary to formulate laws describing molecularly thin flows under all possible conditions of pressure, wall velocity, film thickness, wall-fluid pair etc. An additional point of interest is the creation of predictive models for wall slip. In fact, being able to foretell the occurrence of these phenomena without the need to perform additional Molecular Dynamics simulations would lead to significant computational savings. The following Chapter is developed with these two goals in mind.

The numerical model presented in Chapter II will be used to analyze the interfacial flow and rheology of molecularly confined alkanes under shearing. First, wall slip will be defined from the dynamics of the confined lubricant. A predictive model will then be formulated to foresee the impact of surface and lubricant nature on wall slip in the case of confined alkanes and smooth walls. Finally, an analytical slip law describing the influence of the operating conditions and confinement will be proposed to integrate interfacial flow effects into continuous models.

III.1 Slip characterization through Molecular Dynamics

The velocity slip of fluid molecules near the solid walls is one of the most intriguing phenomena due to confinement. In fact, it contradicts the classical no-slip boundary condition typically used in continuous models, where the fluid flows at the same speed as the neighboring solids. The occurrence of slip is clearly seen in Figure III-1 for a nano-confined alkane under operating conditions typical of an EHD contact zone: the fluid velocity at the boundary is significantly different from the imposed wall speed.
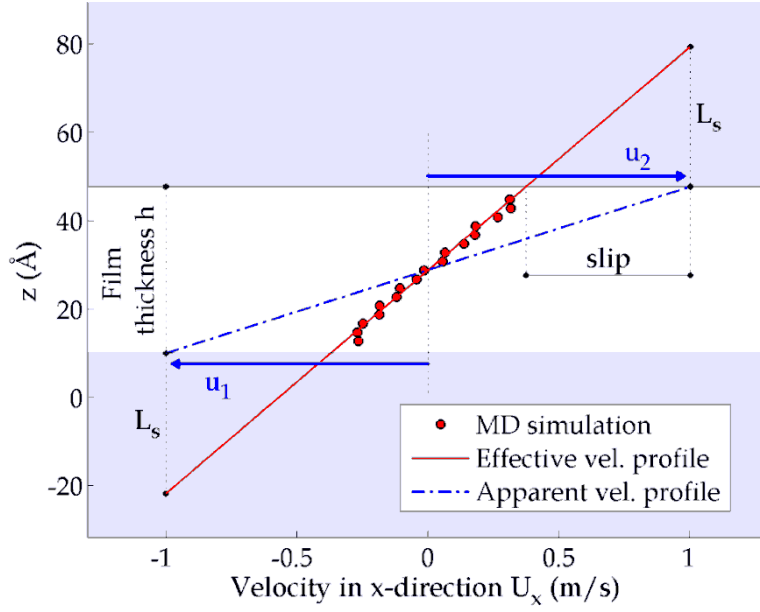
Figure III-1: Wall slip occurrence in molecularly thin shear flow. The imposed wall speeds u₁ and u₂ along the x-direction are represented by the blue arrows, whereas the fluid velocity is shown by the red dots. CuO [001] surfaces, n-octane, P=1.5 GPa, u₂=-u₁=1 m/s, Twall=300K.

A simple wall slip model is established to quantify this phenomenon through the comparison of the apparent and effective shear rates in the lubricant. The apparent shear rate $\dot{\gamma}_{app}$ is written as:

$$\dot{\gamma}_{app} = \frac{u_2 - u_1}{h} = \frac{\Delta u}{h} \tag{III.1}$$

It describes simple shearing of a fluid film with thickness h by two surfaces moving at a velocity difference $\Delta u = u_2 - u_1$. Hence, wall slip is not considered yet, and $\dot{\gamma}_{app}$ depends exclusively on the model input parameters and the chosen operating conditions. On the other hand, the effective shear rate $\dot{\gamma}_{eff}$ accounts for the actual dynamics in the confined lubricant. This term corresponds to the velocity gradient in the center of the film, as explained in Chapter II [16]. Finally, a dimensionless wall slip parameter s is obtained by combining the apparent and effective shear rates [94]:

$$s = 1 - \frac{\dot{\gamma}_{eff}}{\dot{\gamma}_{app}} \qquad \text{with} \qquad s \in [0,1] \tag{III.2}$$

The effective velocity of the fluid at each wall i is then equal to $(1-s) \cdot u_i$. When s is nil, so is the velocity difference at the boundary, corresponding to the standard no-slip condition. On the other hand, when $s = 1$ the fluid is not entrained by the surfaces and total slip occurs.

As an alternative to the dimensionless parameter s, boundary slip can also be quantified through the slip length L_s. This quantity represents the fictive distance between the wall-fluid interface and the ordinate z at which the fluid speed $u(z)$ matches the imposed wall velocity u_i (Figure III-1) [30]. In a fully symmetrical system, the slip length can be related to the dimensionless parameter s by:

$$L_s = \frac{h}{2} \cdot \left(\frac{1}{1-s} - 1 \right) \qquad \text{with} \qquad L_s \geq 0 \qquad\qquad \text{(III.3)}$$

The condition $L_s = 0$ is equivalent to the classical no-slip boundary. On the other hand, when $s = 1$ and total slip occurs, L_s tends towards infinity. Such state cannot be reached in reality, as the slip length is limited to a finite value in the case of elastic walls [103]. However, this threshold can be some orders of magnitude larger than the film thickness [29, 102, 103, 107], corresponding to s values very close to unity. Hence, $s=1$ will be chosen as the upper limit for the validity for Equation (III.2).

In the following, the dimensionless parameter s will be preferred over the slip length L_s for the quantification of the wall slip phenomenon. It should nevertheless be reminded that both quantities have been used in the literature for this purpose, and they are easily interchangeable through Equation (III.3). The definition of s in Equation (III.2) allows studying the dependence of interfacial flow on various parameters characteristic of molecularly confined films. The influence of surface and lubricant nature will be analyzed hereafter.

III.2 A predictive wall slip model for surface and fluid natures

Up to now, there have been a significant number of studies on the impact of surface morphology and lubricant architecture on wall slip. For example, simulations showed that a decrease in the solid-liquid interaction energy and commensurability favors the occurrence of this phenomenon [8, 30, 80, 102, 145, 146]. Interfacial slip was also shown to increase with longer chains or in presence of branching [16, 105]. On the other hand polar additives sticking to the surfaces led to a no-slip boundary condition by altering the potential and the geometry of the walls [106].

While these studies offer a good insight on the different parameters influencing wall slip, the impact of surface and fluid nature must be explored further. In fact, a vast variety of wall morphologies characterizes the typical contact area in lubricated applications. Such complexity can be illustrated by taking (100Cr6) steel as an example for rolling element bearings [147]. This material is mainly composed by ferrite (α-Fe), featuring a Body-Centered-Cubic crystal structure. However, austenite (Face-Centered-Cubic iron) can be present depending on the thermal treatment [148]. Furthermore, carbides such as cementite (Fe_3C) and martensite are located at the grain boundaries, whereas chromium inclusions are found in the iron structure. The surfaces can oxidize, resulting in the formation of FeO or Fe_2O_3 layers in contact with the lubricant. Finally, each of these materials may present a different crystallographic orientation at the wall-fluid interface, which can affect the energy interaction, commensurability and therefore interfacial flow.

Accounting for all possible configurations in the contact zone poses at least two issues. First, the literature often focuses only on canonical wall structures, and the proposed analyses are applicable with difficulty to more complex lattices. Second, a very large amount of simulations would be required, leading to huge computational costs.

Hence, the aim of the following work is to develop a predictive model for wall slip as a function of surface and fluid natures. The formulation should be valid for a wide variety of

geometrically smooth surfaces with properties typical of metals or metal oxides. Furthermore, it should be applicable to alkanes, which are representative of the standard base oils in lubricated applications. The starting point is the interpretation of wall slip as the consequence of the competition between surface and lubricant natures.

III.2.1 *The competition between wall-fluid interactions and fluid nano-rheology*

The Molecular Dynamics model from Chapter II is used to simulate the shearing of alkanes in a lubricated contact interface featuring a nanometer film thickness (h =4 nm). Moreover, the operating conditions in pressure (P =500 MPa) and shearing (Δu =20 m/s) are chosen representative of an elasto-hydrodynamic regime. These values are then held constant in the rest of this study, while the surfaces and fluid in the contact nano-patch are changed.

In order to understand the effect of surface nature on interfacial flow, a wide range of wall morphologies will be considered in the following. In addition to existing materials, like for instance iron and iron oxide, canonical Cubic and Face-Centered-Cubic structures with arbitrary lattice parameters are also chosen to provide a broader range of results. However, the properties of the walls remain in all cases representative of metals and metal oxides, as detailed in Chapter II. For the lubricant, n-alkanes with different chain lengths will be studied.

The resulting influence of wall morphology and fluid nature on the velocity jump at the boundary is well shown in Figure III-2 and Figure III-3. First, in Figure III-2, n-hexadecane is confined between different wall types. Interfacial flow varies significantly for each of the chosen surfaces. Some feature very large slip values, such as CuO [001] or α-Fe [110]. With other structures the velocity jump at the wall-fluid boundary is significantly reduced or completely suppressed, and locking of the first molecule layers in proximity of the surfaces takes place. This is the case for gold [100] and iron oxide [001].
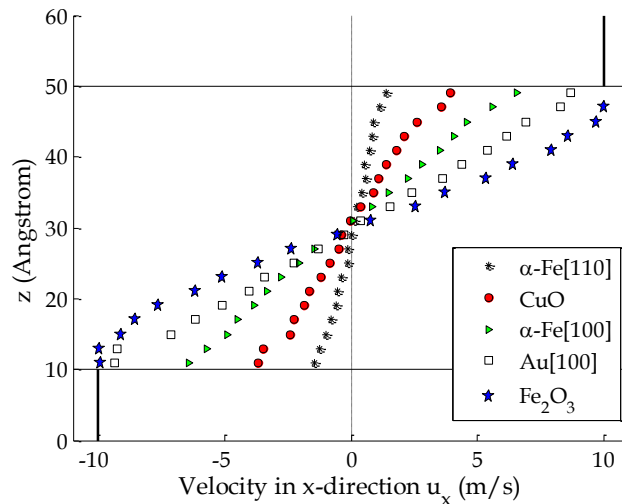
Figure III-2: Wall slip dependence on surface material and orientation, for n-hexadecane confined between smooth walls. P=0.5 GPa, u₂=-u₁=10 m/s, h=4 nm, T_wall=300K.

In Figure III-3 four linear alkanes with different chain lengths are confined between C3 walls issued from a Cubic lattice with a spacing of 3 Å. Longer chains feature higher velocity slip at the boundary, compared to shorter ones, in coherence with trends from the literature [23, 105].
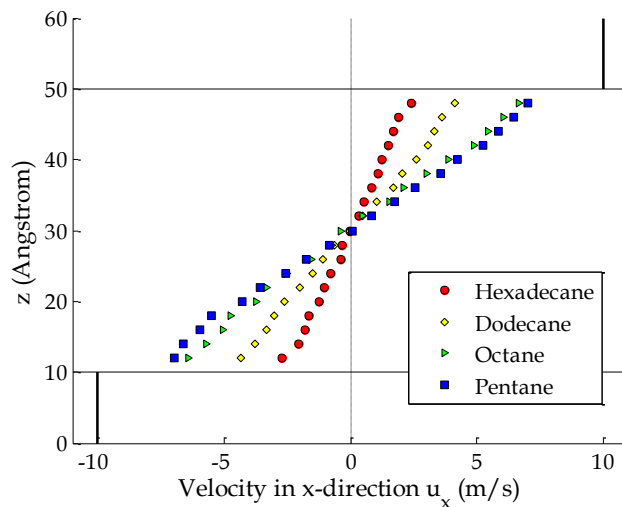
Figure III-3: Wall slip dependence on the chain length of linear alkanes confined between walls featuring a cubic strucure with lattice constant a=3Å. P=0.5 GPa, $u_2=-u_1=10$ m/s, h=4 nm, T_{wall}=300K.

To understand these results, the fluid flow in molecularly thin films must be analyzed in more detail. In Equation (III.2) slip was expressed as a function of the apparent and effective shear rates. The first describes the classical shear flow with a no-slip boundary condition. As pressure, wall speed and film thickness do not vary throughout this study, the apparent shear rate stays constant and equal to $\dot{\gamma}_{app}$ =5·10⁹ s⁻¹ under the aforementioned operating conditions. On the other hand, the effective shear rate $\dot{\gamma}_{eff}$ characterized the actual lubricant dynamics under confined conditions and shear. Further analysis of this term gives a possible interpretation for the dependence of interfacial slip on surface and fluid natures. In fact Equation (III.4) reveals the competition between two terms:

$$\dot{\gamma}_{eff} = \frac{\tau_{zx}}{\eta_{eff}} \qquad (III.4)$$

The effective viscosity η_{eff} expresses the fluid resistance to shearing under confined conditions (see Section II.3). It increases with the molecular size, because longer chains exhibit a stronger internal cohesion between layers compared to shorter ones [23, 149]. On the other hand, τ_{zx} is the shear stress measured at the walls along the shearing (x-) direction. For a given lubricant, this quantity is deeply related to the nature of the surfaces. In fact each wall is capable of transferring only a finite tangential shearing momentum to the fluid at the boundary: the limit depends mainly on both the interaction strength and the commensurability (i.e. the respective geometry) of the surface-fluid pair [8].

The competition between the effective fluid viscosity and the tangential momentum transfer capability of the surface leads to two possible states. In the first one, the maximum shear stress that the wall can transfer is not sufficient to overcome the internal cohesion of

the fluid. Hence, the latter is not fully sheared and wall slip occurs. This is the case for weak wall-fluid interactions [101], incommensurate structures [81] or lubricants featuring a high viscosity under confinement [16]. On the other hand, interfacial wall slip is reduced or absent in presence of surfaces with high momentum transfer capability or low viscosity lubricants. In fact, the fluid is fully sheared and the measured shear stress is determined by its internal cohesion. This qualitative interpretation is the base for the formulation of a wall slip prediction model as a function of surface and fluid natures. The first step is the development of a surface characterization technique.

III.2.2 A general characterization parameter for the surfaces

At the nanometer scale, the discrete nature of the walls has a deep influence on the neighboring fluid molecules. No matter how geometrically smooth, the crystal structures induce an ordering upon the first lubricant layers near the walls. In fact the discrete nature of the walls generates in-plane variations in the surface-fluid interaction potential ε_{w-f}, and the lubricant molecules tend to be attracted towards potential minima [8, 150]. Furthermore, the formation of epitaxial structures in the fluid is related to its commensurability with the crystal lattice [8, 81, 101].

A scanning technique is proposed to quantify the effect of these two main parameters. The methodology is largely inspired by Berro's work [23], and uses the principle proposed by Jabbarzadeh in [81]. The scanning method is shown in Figure III-4. The surface in contact with the lubricant is set parallel to the (x, y)-plane. A scanning atom is chosen with a size representative of the alkane hydrocarbon (CH_x) groups: $\sigma_{scan} = 3.93$ Å. Its energy interaction parameter is set to a default value ε_{scan} of 1 kcal/mol in accordance with [23]. This sphere is used to probe the surface: its coordinates in the x- and y-directions are fixed, but freedom of movement is left along the z-axis. The scanning atom finds its equilibrium position $h_{eq}(x,y)$ on top of the wall, corresponding to the minimum of the surface-atom Lennard-Jones potential $V_{LJ,scan}(x,y)$. This process is repeated on the whole surface at regular intervals Δx and Δy in the x- and y- directions respectively: both h_{eq} and $V_{LJ,scan}$ are recorded for each sampling point. The sampling steps are chosen equal to 0.1 Å, which allows a detailed mapping of the wall morphology [23].
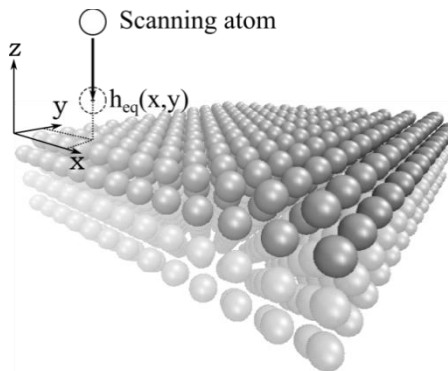
Figure III-4: Scanning technique on a ferrite α-Fe[100] surface

An example chart of the recorded potentials $V_{LJ,scan}$ is shown for canonical and complex crystal lattices in Figure III-5. The epitaxial variations in the interaction energy clearly

follow the main directions of the lattice structure for each surface in Figure III-5a. For example, the potential minima are located in correspondence with the empty spaces between wall atoms. In these zones the equilibrium height of the scanning particle is closer to the surface and interacts with more lattice sites. The same trends are obtained when analyzing a more complex crystal structure, such as iron oxide in Figure III-5b.

This method can then be considered the numerical equivalent to experimental surface characterization techniques, such as AFM. Furthermore, the use of a probing particle characteristic of a lubricant atom allows for a mapping representative of the wall-fluid interactions and commensurability. Hence, both the recorded Lennard-Jones potential and equilibrium height from the scanning technique will be related to the shear stress at the interface, according to the qualitative explanation of wall slip in Section III.2.1.

Top view of the surface	Recorded potential V$_{LJ}$ (kcal/mol)

a) Ferrite: α-Fe[100]

b) Iron oxide: Fe$_2$O$_3$[001]
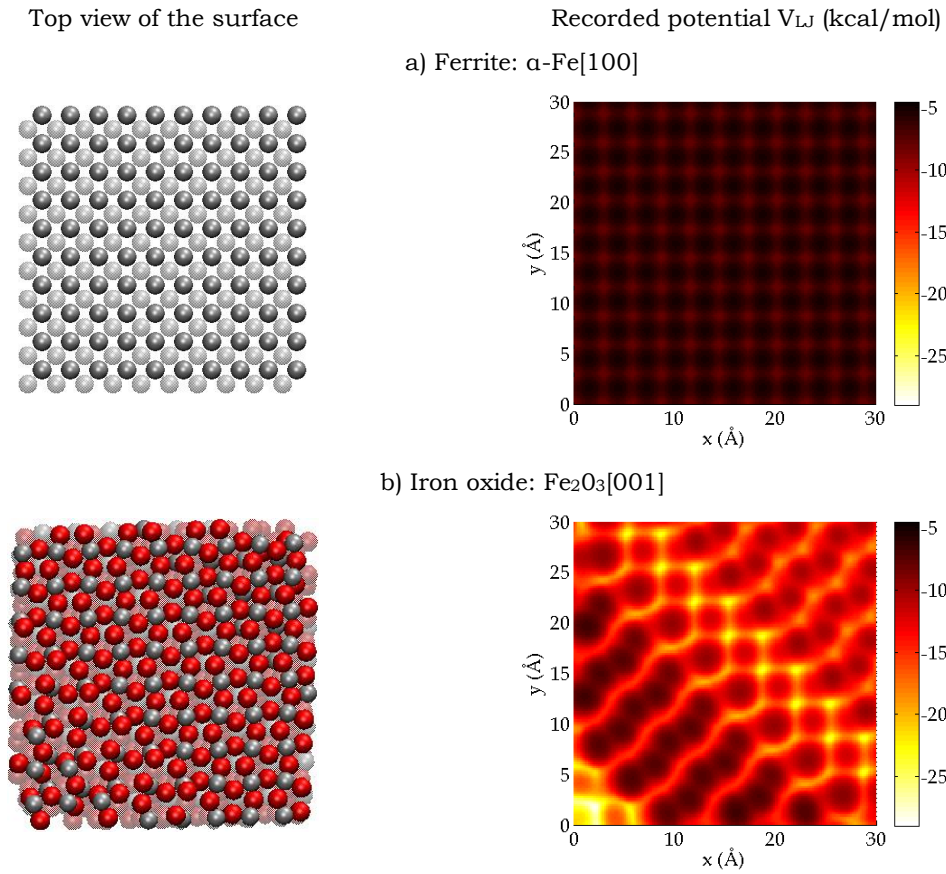
Figure III-5: Ferrite (a) and iron oxide (b) surfaces with the corresponding Lennard-Jones potential from the scanning technique. The brighter zones correspond to potential minima, where the atom is closer to the surface.

The Lennard-Jones potential $V_{LJ,scan}(x,y)$ is exploited first through a force formulation inspired by the Frenkel-Kontorova model [151]. To illustrate this procedure, Figure III-6 shows a simplified one-dimensional case, where the scanning atom slides along a sinusoidal wall potential in the shearing direction (along the x-axis). The dynamics of the particle can be described through the equation of motion [29, 150]:

$$m_{scan}\ddot{x}_{scan} + \frac{\partial V_{LJ,scan}(x,y,t)}{\partial x} = F - c_{w-f}\dot{x}_{scan}$$

(III.5)

x_{scan}, $\dot{x}_{scan}$ and $\ddot{x}_{scan}$ are the position, velocity and acceleration of the scanning atom respective to the surface, and m_{scan} its mass. The particle is driven by the force F, representative of the interaction with other fluid layers. However, its movement is slowed by the drag force $c_{w-f}\dot{x}_{scan}$, due to friction with the substrate and characterized by a viscous dissipation coefficient c_{w-f}.
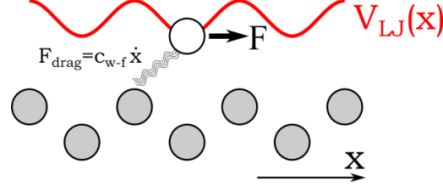
Figure III-6: Schematic representation of the scanning atom moving in a sinusoidal wall potential V$_{LJ}$, inspired by the Frenkel-Kontorova model. The particle is driven by a force F, while drag due to the interaction with the substrate is equal to a friction coefficient c$_{w-f}$ multiplied by the atomic velocity in the x-direction.

At the very onset of slip, both the velocity and acceleration of the atom respective to the wall are nil. Hence, Equation (III.5) can be simplified to:

$$F = \frac{\partial V_{LJ,scan}(x,y,t)}{\partial x} \tag{III.6}$$

Interfacial slip occurs when the driving force exceeds the maximum of the potential gradient along the shearing direction. This threshold value is therefore representative of the maximum shear stress that the wall can transfer tangentially to the fluid molecules before the occurrence of wall slip. As it is related to energetic interactions between the surface and the lubricant, it will be called corrugation force F_{corr} to be consistent with the literature [23, 25, 146, 151]:

$$F_{corr} = \max\left(\frac{\partial V_{LJ,scan}(x,y,t)}{\partial x}\right) \tag{III.7}$$

The calculation of the forces F and F_{corr} in the case of two-dimensional surfaces found in real interfaces cannot always be expressed through analytical functions, as opposed to canonical lattices typically used in the literature [8, 29, 80]. For example, structures like oxides are characterized by a very complex potential landscape (Figure III-5b). Furthermore, the lattice directions may be skewed compared the x- and y- axes of the system. A general formulation is therefore proposed. It is based on the free movement of the fluid molecules perpendicular to the sliding direction (along the y-axis): during the sliding motion the alkane CH$_x$ groups can travel around the potential peaks [150]. Therefore, a minimum-force path is calculated, based on the assumption that the atoms try to slip in the direction opposing the least resistance to their movement. The force acting at each point in the x-direction is then given by minimum slope of the Lennard-Jones potential:

$$F = \min\Big|_{\Delta y} \frac{V_{LJ,scan}(x+\Delta x, y+\Delta y) - V_{LJ,scan}(x,y)}{\Delta x + \Delta y} \tag{III.8}$$

An example for the minimum force path on a canonical Face-Centered-Cubic surface is given in Figure III-7, which shows the motion of the scanning atom around the potential peaks.

Finally, the maximum resistance to the sliding of the atom is quantified by the corrugation force F_{corr}, according to Equation (III.7). Table III-1 summarizes the F_{corr} values for the wall types considered in this work, featuring both canonical crystal lattices and complex ones.
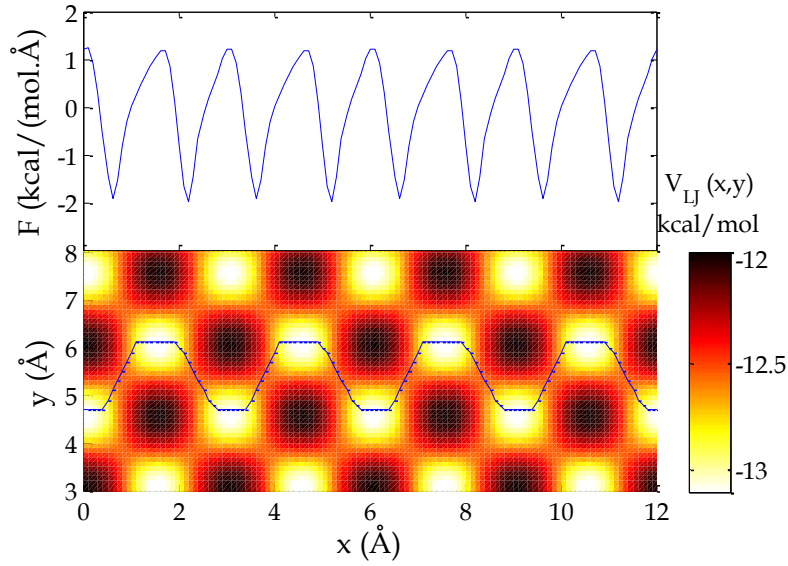
Figure III-7: Force F from Eq. (III.8) and corresponding minimum-force-path for a canonical face-centered-cubic surface with a lattice constant a=3Å.

Surface (canonical)	F_{corr} (kcal/mol/Å)	h_{comm} (Å)	ζ_{surf} (kcal/mol)
Cubic 2 (a=2Å)	0.640	0.0229	0.0147
Cubic 2.5 (a=2.5Å)	0.990	0.0666	0.0659
Cubic 3 (a=3Å)	1.348	0.131	0.176
Cubic 3.5 (a=3.5Å)	1.518	0.208	0.316
Cubic 4 (a=4Å)	1.642	0.299	0.491
FCC 3 (a=3Å)	1.277	0.0335	0.0428
FCC 3.5 (a=3.5Å)	1.6115	0.0660	0.106
FCC 4 (a=4Å)	1.777	0.110	0.195
FCC 4.5 (a=4.5Å)	1.812	0.162	0.293
FCC 5 (a=5Å)	2.148	0.219	0.470
FCC 5.5 (a=5.5Å)	2.354	0.283	0.665
Surface (material)	**F_{corr} (kcal/mol/Å)**	**h_{comm} (Å)**	**ζ_{surf} (kcal/mol)**
Au [100]	3.009	0.1177	0.354
Au [110]	5.044	0.2475	1.248
Fe [100], [200]	1.8829	0.1376	0.259
Fe [110]	0.8199	0.0631	0.0517
CuO [001]	1.7479	0.0989	0.173
Fe_2O_3 [001]	6.1429	0.4000	2.457
Fe_3C [001]	5.8203	0.4457	2.594
Si_3N_4 [001]	4.980	0.2900	1.418

Table III-1: Corrugation force, commensurability height and surface interaction parameter for the chosen wall typologies

The wall-fluid commensurability must now be characterized. This parameter is related to the geometry of the lattice and the fluid, and influences the epitaxial ordering of the molecules near the surfaces [8]. To quantify it, the equilibrium distance $h_{eq}(x,y)$ between the probing atom and the surface in the scanning technique is used. Figure III-8 shows how the in-plane variations of $h_{eq}(x,y)$ are related to the ordering of the fluid molecules near the wall. In a commensurate case, the size of CH_x groups is similar or smaller than the lattice constants, and they will be able to fit between the wall atoms: hence, big variations in the equilibrium height will be recorded. Furthermore, epitaxial ordering along the lattice directions is favored in this case and the surface can transfer a high shear stress (Figure III-8a). On the other hand, a reduction in the lattice spacing leads to incommensurate fluid-wall pairs [8], less penetration of the CH_x groups between lattice sites, and smaller oscillations in the equilibrium height. In this case, in-plane ordering of the fluid parallel to the vectors of the crystal lattice is frustrated. The molecules align themselves mainly in the shearing direction and the tangential momentum transfer capability of the wall is reduced (Figure III-8b). A commensurability height parameter h_{comm} is then introduced in order to quantify the variations of $h_{eq}(x,y)$ and account for the commensurability of the wall-fluid pair, similarly to [81]:

$$h_{comm} = \sqrt{\frac{1}{N}\sum_{i=1}^{N}\left(h_{eq}(x_i,y_i)-\bar{h}_{eq}\right)^2} \tag{III.9}$$

where $\bar{h}_{eq}$ represents the average value of the equilibrium height and N the number of sampling points from the scanning technique. The commensurability heights for the studied wall topologies are reported in Table III-1. The proposed trends for the ordering of the fluid and the influence on the shear stress, as well as the numerical values of h_{comm} for gold [100] surfaces are coherent with results from the literature [81].
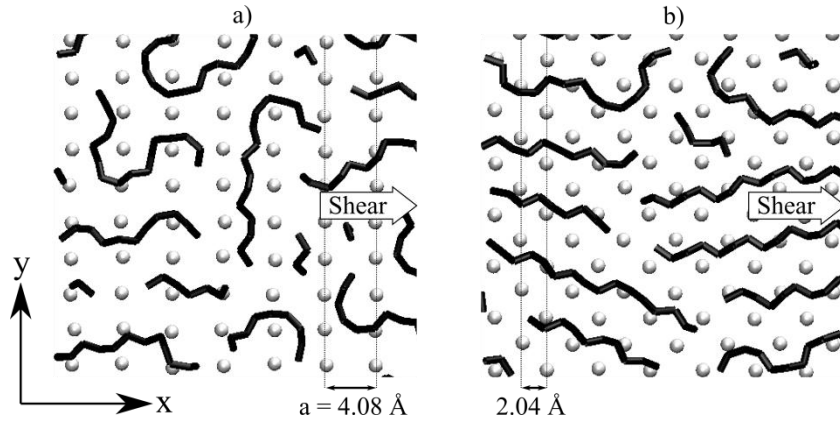
Figure III-8: Example of wall-fluid commensurability for two gold surfaces and hexadecane, from screenshots of the first lubricant layer in proximity of the lower wall. a) [110] cut: fluid molecules fit within the lattice spacing, and some are perpendicular to the shear direction. b) [100] cut: the fluid molecules are mainly oriented in the shear direction.

Finally, a surface interaction parameter ζ_{surf} is proposed to include the corrugation force and commensurability height:

$$\zeta_{surf} = F_{corr} \cdot h_{comm} \tag{III.10}$$

A simple product between these quantities is chosen for three reasons. First, varying independently the wall-fluid interaction energy and the lattice geometry [8, 81] shows that both quantities have a deep effect on interfacial flow. Second, F_{corr} and h_{comm} echo the parameters proposed by Barrat and Bocquet [30, 80] to quantify the occurrence of wall slip for canonical surfaces. In particular, the commensurability height could be related to the structure factor of the fluids, whereas the corrugation force quantifies the potential energy variations near the walls. Third, it will be shown in the following that the characterization parameter ζ_{surf} gives good results for the classification of different wall topologies according to their capability to transfer a shear stress to the confined alkane.

In conclusion, the proposed scanning method can be used to quantify the interfacial momentum transfer for virtually any surface morphology found in a contact interface in the case of alkanes. It is computationally much less expensive than Molecular Dynamics simulations (seconds versus hours or days on the same configuration). Hence, it can be a useful tool for the development of a wall slip prediction model. The next step is to relate the surface characterization parameter ζ_{surf} to the shear stress at the wall-fluid boundary.

III.2.3 Shear stress at the contact interface

Molecular Dynamics simulations are performed for four confined linear alkanes under shearing. A wide range of smooth walls representative of metals and metal oxides (Table III-1) is used. The shear stress are shown in Figure III-9, where each surface is ordered along the abscissa through its characterization parameter ζ_{surf}.
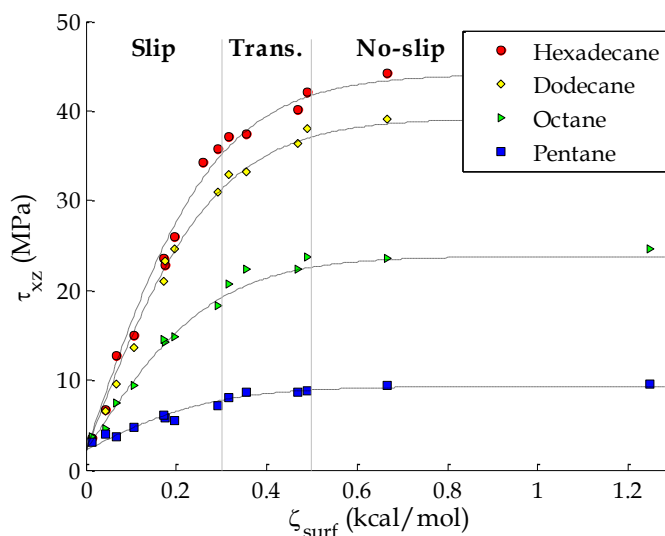
Figure III-9: Shear stress for different linear alkanes as a function of the surface interaction parameter. The points represent results from Molecular Dynamics simulations, the dotted lines the analytical curve fit. P=0.5 GPa, u_2=-u_1=10 m/s, h=4 nm, T_{wall}=300K.

The proposed formulation gives good results for the classification of different wall morphologies according to their capability to transfer a tangential momentum to the fluid. In particular, large values of ζ_{surf} correspond to surfaces featuring strong interaction energies as well as solid-fluid commensurability. Consequently, the transferred shear stress τ_{zx} is high. On the other hand, surfaces with low ζ_{surf} are characterized by small lattice spacing com-

pared to the CH_x radius, and weak wall-fluid interactions. They are seen as geometrically and energetically smooth by the fluid molecules, therefore the transferred momentum is low.

As a consequence, two main regions can be observed in Figure III-9. For ζ_{surf} values smaller than 0.3 kcal/mol, the shear stress increases linearly with the surface interaction parameter. In this case τ_{zx} is limited by the weak wall-fluid interactions and commensurability, and interfacial slip occurs. On the other hand when the surface corrugation parameter is larger than 0.5 kcal/mol, a plateau is reached. Due to the high tangential momentum transfer at the interface, the lubricant is fully sheared. τ_{zx} is then limited by the internal cohesion between layers, which is not dependent on the surface. Hence, the interfacial shear stress remains constant once wall slip disappears. A smooth transition between the two domains is observed for ζ_{surf} values between 0.3 and 0.5 kcal/mol. Here, the boundary flow changes from a slip to a no-slip condition [29], with effects such as locking of lubricant layers occurring in proximity of the walls. These results are coherent with the qualitative explanation proposed in Section III.2.1.

In order to formulate a wall slip prediction model, the evolution of the shear stress with the surface interaction parameter can be quantified through analytical laws. A hyperbolic tangent can adequately represent all the trends observed in Figure III-9: the increase in τ_{zx} for ζ_{surf} small values, the plateau region as well as the transition zone. Hence, the curve fit in Equation (III.11) is proposed: this single expression is valid for all four chosen n-alkanes, with chain lengths from 5 to 16 CH_x groups, under constant operating conditions in pressure P =500 MPa, film thickness h =4 nm, wall speed Δu =20 m/s, and temperature T_w =300 K.

$$\tau_{zx}[MPa] = (\tau_{max}[MPa] - 2.20) \cdot \tanh(3.53 \cdot \zeta_{surf}[kcal/mol]) + 2.20 \qquad \text{(III.11)}$$

An important parameter in Eq. (III.11) is the maximum shear stress τ_{max}, which quantifies the plateau region for each fluid. It can be obtained by running Molecular Dynamics simulations for surfaces with high ζ_{surf} and a no-slip condition such as Fe_2O_3 [001].
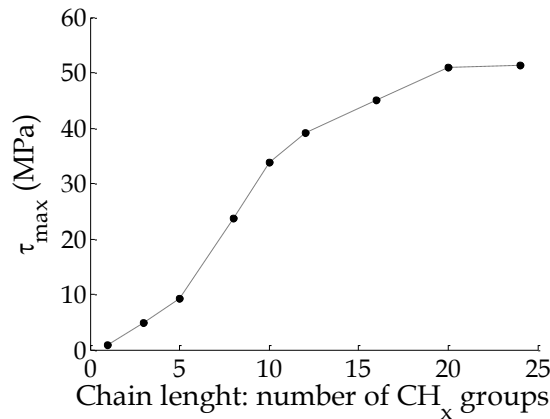
Figure III-10: Maximum shear stress as a function of the n-alkane chain length. The dotted curve is intended as a guideline for the eye. These results were obtained with a Fe₂O₃ [001] surface, which featured no wall slip for all the chosen n-alkanes. P=0.5 GPa, u₂=-u₁=10 m/s, h=4 nm, Twall=300K.

As shown in Figure III-10 for linear alkanes, τ_{max} increases with the chain length up to 20 CH_x groups, then remains roughly constant. Hence, Equation (III.11) could easily be extended to long n-alkanes without the need to perform further computations, by setting τ_{max} to 51.5 MPa.

III.2.4 Bulk and effective fluid viscosity

The formulation of a predictive wall slip model as a function of surface and lubricant nature requires a good understanding of the fluid resistance to shearing under confined conditions, quantified by the effective viscosity η_{eff}. The importance of this term was underlined in Section III.2.1: in particular, Equation (III.4) showed that it can influence the effective lubricant dynamics and shear rate across the film thickness, and consequently interfacial flow. Hence, the lubricant viscosity under confinement must be characterized in order to complete the wall slip prediction model.

The literature provides some guidelines for an analysis. In particular, experimental work by Granick [11] showed that confined alkanes retained a bulk-like behavior down to surface separations of at least ten molecular diameters (4 nm). Furthermore, Gupta [143] showed that the fluid rheology is not affected by confinement at the imposed shear rates typical of Molecular Dynamics simulations for film thicknesses of 5-6 molecular layers. As these conditions are fulfilled in the current study, a possible approach is to predict η_{eff} through a bulk viscosity term.

Following the method proposed by Müller-Plathe [138], reversible non-equilibrium Molecular Dynamics (RNEMD) simulations are used to determine the bulk viscosity η_{bulk} of the four chosen linear alkanes. The system and outputs are shown in Figure III-11. In this case, no solid walls are considered, and periodic boundary conditions are applied along all directions. This effectively simulates a representative elementary volume of the fluid in its bulk like state.
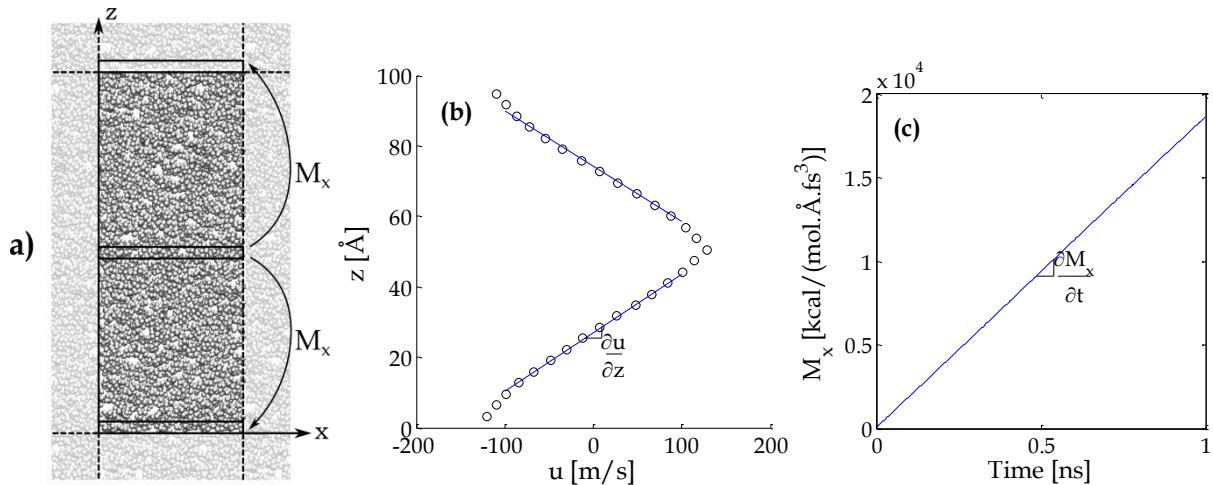
Figure III-11: Müller-Plathe simulation method for the determination of the bulk viscosity. a) Simulation box: the dotted lines represent the periodic boundaries, while the arrows exemplify the momentum transfer from the central to the side layers. b) System response through a linear velocity profile. c) Fixed rate for the momentum transfer.

Momentum M_x is exchanged at a fixed rate along the x-direction between slabs located at the center of the box and its side. A linear velocity profile develops between these slabs: the velocity gradient along the vertical (z-) direction is equal to the shear rate $\dot{\gamma}$. The rate of momentum exchange is used to calculate the shear stress τ_{zx}:

$$\tau_{zx} = \frac{1}{2S}\frac{\partial M_x}{\partial t} \tag{III.12}$$

Finally, the shear viscosity η_{bulk} of the fluid in its bulk state is equal to the ratio between the shear stress and shear rate:

$$\eta_{bulk} = \frac{\tau_{zx}}{\dot{\gamma}} \tag{III.13}$$

The Müller-Plathe method is applied to the four linear alkanes under the chosen pressure (P =500 MPa) and temperature (T_w =300 K). By changing the momentum exchange rate, the response of the fluids can be characterized for different shear stresses and shear rates. The results are shown in Figure III-12 as a function of τ_{zx}.

They are fitted using a modified Carreau model [41], typically used in macroscopic models to describe non-Newtonian shear thinning behavior of fluids at high shear rates and stresses:

$$\eta_{bulk} = \mu(P,T) \cdot \left(1 + \left(\frac{\tau_{xy}}{\mu(P,T)/t_{rel}} \right)^2 \right)^{\frac{N-1}{2N}} \tag{III.14}$$

μ represents the viscosity of the Newtonian plateau, t_{rel} the characteristic relaxation time of the fluid and N the power-law exponent describing the behavior in the shear-thinning region. These parameters, characteristic of each fluid, are reported in Table III-2 for the chosen n-alkanes.
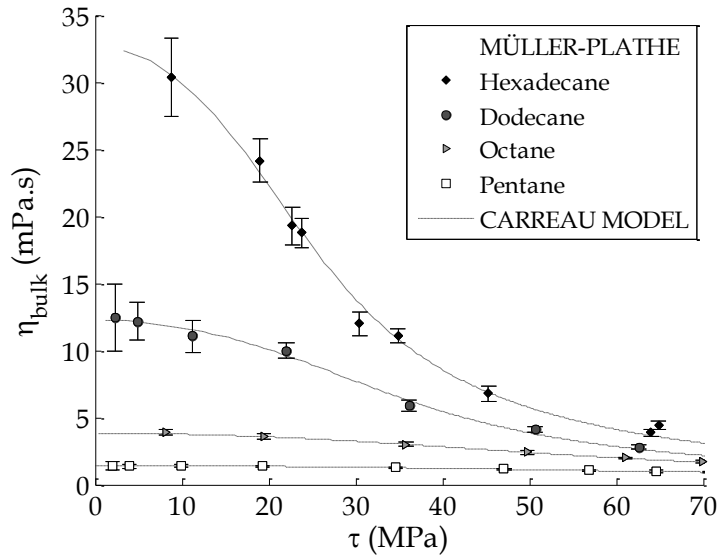
Figure III-12: Bulk viscosity for the four chosen linear alkanes as a function of the shear stress. The points represent the data from NEMD simulations using the Müller-Plathe method [138], the vertical bars the related uncertainty, and the dotted lines the fit using a modified Carreau model [41]. P=500 MPa, T_w=300K.

Fluid	μ (mPa.s)	t_{rel} (10^{-9} s)	N (dimensionless)
n-pentane	1.42	0.0306	0.540
n-octane	3.83	0.0957	0.415
n-dodecane	12.26	0.465	0.362
n-hexadecane	32.69	1.677	0.352

Table III-2: Parameters of the non-newtonian Carreau viscosity model for the chosen n-alkanes. P=500 MPa, T_w=300K.

It is now possible to link the effective viscosity η_{eff} of fluids under confined conditions to the rheological properties of the bulk state. In Figure III-13, results from Molecular Dynamics simulations of nano-thin alkanes are compared to the bulk Carreau model from Equation (III.14) as a function of the shear stress. It can be seen that the confined η_{eff} values are within the uncertainty range (of the order of 10%) of the bulk viscosity curves. Moreover, the shear thinning behavior occurring for long alkane chains at high levels of forcing is also well represented. These results confirm the trends from the literature [13]: bulk viscosity models can adequately describe the nano-rheology in confined fluids with film thicknesses larger than 5-6 molecular diameters, roughly corresponding to 2.5 nanometers in the case of alkanes.
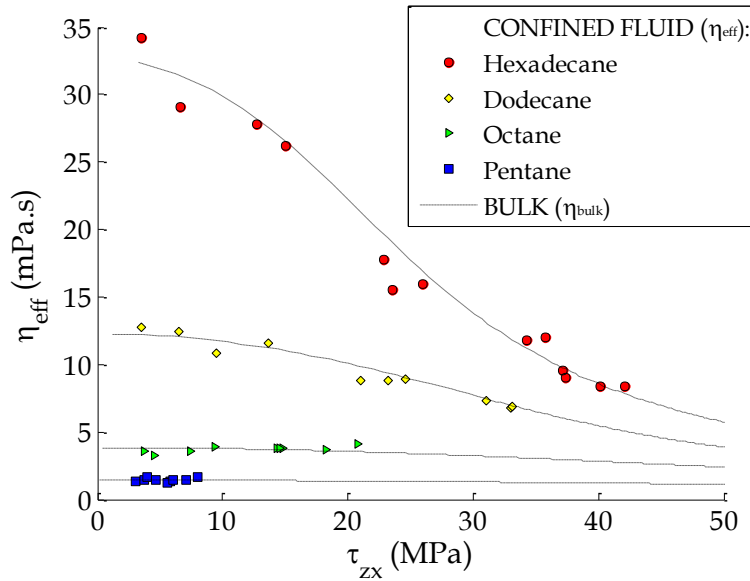
Figure III-13: Effective viscosity as a function of shear stress for the chosen n-alkanes at P = 500 MPa and T = 300K. The points show the results for confined fluids, while the dotted lines represent bulk curves from the Carreau model in Equation (III.14) in absence of confinement.

The simple relationship $\eta_{eff}(\tau_{zx}, P, T) = \eta_{bulk}(\tau_{zx}, P, T)$ opens interesting possibilities. In fact, the fluid behavior in molecularly thin shear flow can be described not only through Molecular Dynamics simulations, but also by models issued from experiments at the macroscopic scale. A straightforward integration of nano-rheology in continuous models for the simulation of a whole contact becomes possible. Finally, as both the fluid viscosity and interfacial shear stress in molecularly thin films are now fully characterized, the wall slip prediction model can be formulated.

III.2.5 A model for wall slip prediction

In Section III.1 the slip parameter s was introduced to describe the effective lubricant dynamics under confinement (Equation (III.2)). It was also shown that the flow at the wall-fluid interface depends on the competition between the interfacial momentum transfer and the fluid resistance to shearing (Equation (III.4)). By combining these expressions, s can be written as:

$$s = 1 - \frac{h}{\Delta u}\frac{\tau_{zx}}{\eta_{eff}} \qquad (III.15)$$

where the film thickness h=4 nm and the wall velocity difference Δu=20 m/s are imposed in the current simulations. Moreover, the interfacial shear stress τ_{zx} and the effective fluid viscosity η_{eff} under confinement were characterized in Sections III.2.3 and III.2.4 respectively.

By combining these results, interfacial slip can be predicted for n-alkanes confined between smooth surfaces representative of metal and metal oxides. The walls can feature both simple and complex lattice structures, any orientation for the cut plane, as well as a wide range of wall-fluid commensurabilities and interaction parameters. The determination of interfacial slip for any new surface follows four main steps.

- First, the new surface is characterized by ζ_{surf}, which accounts for both the energy interaction and the commensurability of the wall-fluid pair. This parameter is obtained through a computationally inexpensive scanning technique; moreover, Table III-1 already gives a variety of results.
- Second, the shear stress τ_{zx} is determined through Equation (III.11) for the chosen alkane-surface pair. In this expression ζ_{surf} is used to characterize the wall, while the maximum shear stress τ_{max} (Figure III-10) quantifies the full shearing of the fluid.
- Third, the effective viscosity is approximated through a bulk model, like for example Equation (III.14), at the chosen operating conditions in pressure and temperature; the previously predicted shear stress τ_{zx} is also included for the quantification of shear thinning effects at high levels of forcing.
- Fourth, the values of τ_{zx} and η_{eff} are injected into Equation (III.15) to predict the wall slip parameter s.

All the aforementioned steps can be combined in the following analytical law for wall slip:

$$s = 1 - \frac{1}{5\cdot 10^9}\frac{\tau_{zx}}{\mu\cdot\left(1+\left(\dfrac{\tau_{zx}}{\mu/t_{rel}}\right)^2\right)^{\frac{N-1}{2N}}} \qquad (III.16)$$

$$\text{with}\quad \tau_{zx}[\text{MPa}] = (\tau_{max}-2.20)\cdot\tanh(3.53\cdot\zeta_{surf})+2.20$$

This Equation is built for the constant shear, pressure and temperature operating conditions: P=500 MPa, Δu=20 m/s, h=4 nm and T_w=300K. The parameters μ, t_{rel} and N for the viscosity model of the confined n-alkanes are given in Table III-2.

The predicted wall slip curves from Equation (III.16) are represented in Figure III-14 for the four chosen n-alkanes as a function of the surface interaction parameter. The results

from Molecular Dynamics simulations of the confined n-alkanes are also reported on the chart: they are adequately approximated by the prediction model. Furthermore, the observed trends are coherent with the proposed explanation for the occurrence of wall slip: an increase in the wall-fluid interaction energy or in commensurability (and therefore ζ_{surf}) leads to a reduction in wall slip. Moreover, for a given surface, longer molecules exhibit larger wall slip values. For example, total slip of confined hexadecane occurs with non-corrugated surfaces (small ζ_{surf}); s is on the other hand limited to roughly 50% in the case of pentane. Hence, the model for wall slip prediction from Equation (III.16) is in accordance with results from Figure III-3 and can be considered accurate for linear alkanes confined between metal and metal oxide surfaces.
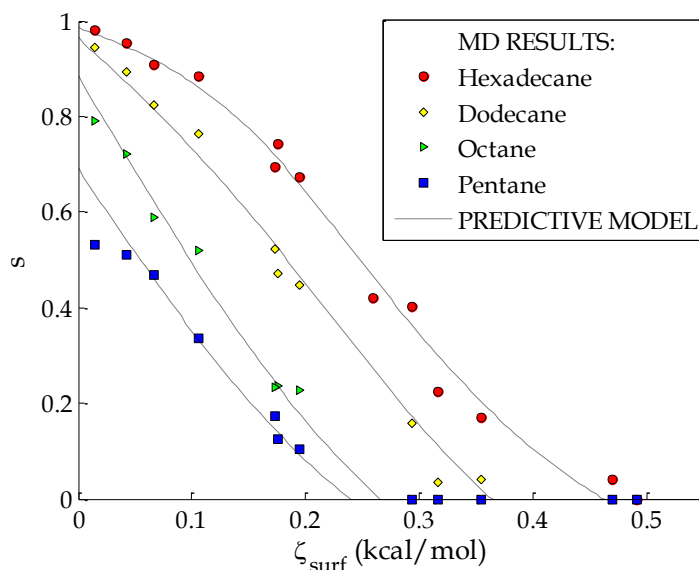
Figure III-14: Wall slip variation for different linear alkanes as a function of the surface interaction parameter. The points represent results from MD simulations, the dotted lines the predicted values. P=0.5 GPa, u₂=-u₁=10 m/s, h=4 nm, T_wall=300K.

In conclusion, the wall slip prediction model is an efficient tool for the quantification of interfacial flow in molecularly confined fluids. In fact, the proposed methodology is valid for a wide range of walls stemming from both canonical and complex crystal lattices. Hence, wall slip can easily be characterized using the analytical law (III.16) for the vast landscape of solid materials and orientations found in contact interfaces in presence of confined n-alkanes. Thus, a significant number of Molecular Dynamics simulations and the related computational costs can be avoided.

It should be reminded that the proposed wall slip model has three major limitations. First, Equation (III.16) was given for linear alkanes, which are representative of standard base oils. However, more complex molecules can be found in lubricants: their structure can influence interfacial flow under confined conditions. For example, the presence of branching results in a higher viscosity compared to linear chains, causing an increase in wall slip [16, 23]. Moreover, antiwear additives deposit on the surfaces and frustrate the slip phenomenon [106]. Polar molecules such as fatty acids and esters form ordered structures with the hydrophilic heads stuck to the surfaces [59]. In this case the wall-fluid interactions are modified by

the presence of electrostatic forces and tribochemical reactions [110]. Hence, these more complex fluid architectures could be further investigated. In particular, branched alkanes will be briefly studied in Appendix B.

Second, the predictive slip model in Eq. (III.16) was obtained for geometrically smooth walls. It was nevertheless reported that the presence of nanometer scale asperities can frustrate the structural effects within the lubricant [9] as well as the occurrence of wall slip [9, 108]. These effects will be explored in Appendix C: another aspect of interfacial flow in molecularly confined fluids, called locking, will be observed and quantified for different wall nano-geometries.

Finally, the wall slip prediction law (III.16) was obtained for a fixed set of operating conditions. It was nevertheless shown in the literature [18, 29, 100, 101, 103, 104] that the level of shearing, confinement and applied load have a significant impact on wall slip. A study on these parameters will be performed in the next Section.

III.3 Slip dependence on the operating conditions

In a contact zone, the local pressure and film thickness can vary greatly from one spot to another. Moreover, a wide range of velocities can be imposed to the walls. Accounting for the variation of interfacial flow with each possible combination of these parameters is necessary to understand contact behavior in presence of molecularly confined fluids.

A direct approach would require a very large number of atomistic simulations, leading to huge computational costs. However, analytical laws can be formulated through a reduced number of Molecular Dynamics studies to quantify wall slip as a function of the wall speed difference Δu, the film thickness h and the external pressure P. The methodology is inspired by the work of Fillot [18], which is extended hereafter by analyzing the coupled effect of the aforementioned parameters.

Molecular dynamics simulations are performed on a system with n-octane (C_8H_{18}) confined between smooth CuO [001] surfaces. According to the characteristic parameter of the previous Section, this wall morphology features a low wall-fluid interaction energy and commensurability, leading to the occurrence of wall slip under molecular confinement. The reference operating conditions of the atomistic simulations are chosen characteristic of an EHD contact featuring an ultra-thin lubricant film in its center [18]: the wall speed difference is Δu_{ref} = 2m/s, the film thickness h_{ref} =3.6 nm and the external pressure P_{ref} =1.5 GPa.

Then, a parametric study is performed on these quantities. Each Molecular Dynamics simulation is regarded as a numerical experiment with the operating conditions as inputs and interfacial flow as the output. These results are finally fitted through analytical laws inspired by the literature.

III.3.1 Slip dependence on wall velocity

One of the most important factors for the occurrence of boundary slip under confinement is the applied shear rate $\dot{\gamma}_{app}$ [29, 103, 104]. In fact, several laws have been proposed

in the literature to describe its impact on the slip length L_s (as a reminder, L_s is related to the slip parameter s used previously by Equation (III.3) in Section III.1).

For example, [30, 80] reported that the slip length is constant and independent on the shear rate: this condition is called the Navier slip boundary condition. Nevertheless, Thompson [146] and Priezjev [104] observed that at high levels of shearing L_s tends towards infinity if a critical shear rate $\dot{\gamma}_{app,crit}$ is reached. Hence, they proposed the law

$$L_s = L_{s,0}\left(1 - \dot{\gamma}_{app} / \dot{\gamma}_{app,crit}\right)^{-0.5} \tag{III.17}$$

where $L_{s,0}$ corresponds to the Navier the slip length at low speeds.

However, Priezjev [17] also observed that the previous formulation is valid for extremely weak wall-fluid interactions, two orders magnitude smaller than for alkanes on metal surfaces. In the case of stronger interaction energies, he reported a linear dependence between the slip length and the shear rate:

$$L_s \propto \dot{\gamma}_{app} \tag{III.18}$$

This trend was later confirmed by Martini in [29] for a linear alkane under high searing; moreover, it was shown that L_s is limited to a maximum value depending on wall stiffness [103].

In order to understand which of these formulations applies to the chosen configuration of n-octane and copper oxide, a parametric study must be performed on the shear rate $\dot{\gamma}_{app}$. In reality, this quantity was defined as the ratio between the wall velocity difference $\Delta u = u_2 - u_1$ and the film thickness h in Equation (III.1). The role played by these two operating conditions will be analyzed separately. The effect of wall speed is considered first: Δu is varied from 0.2 to 20 m/s, whereas the film thickness h_{ref} and external pressure P_{ref} are kept constant. The resulting evolution of the slip length L_s and the dimensionless parameter s are respectively shown in Figure III-15a and Figure III-15b.
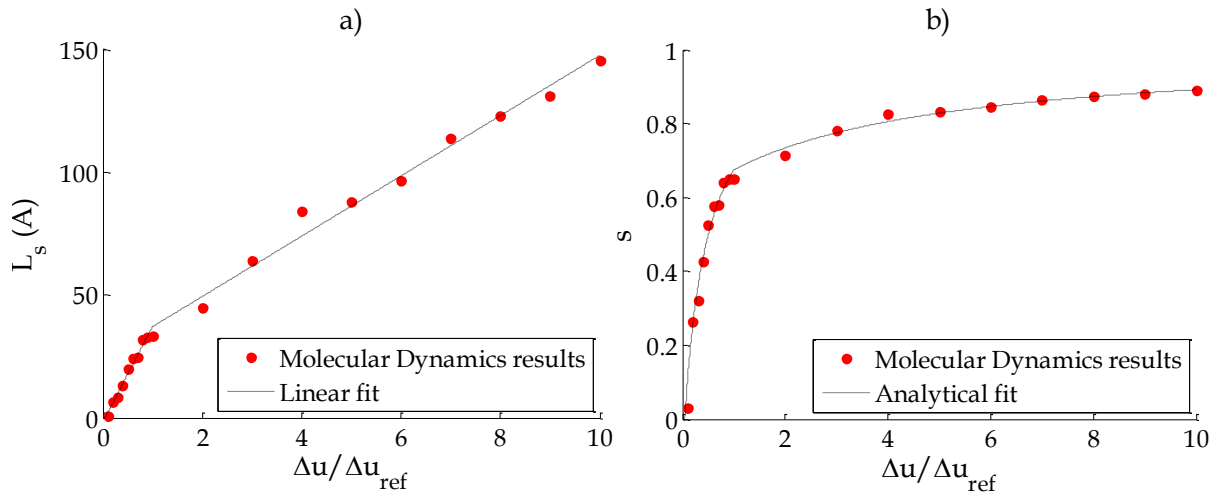
Figure III-15: Dependence of the slip length L_s (a) and the dimensionless parameter s (b) with the wall speed difference Δu. CuO [001] surfaces, n-octane, P=1.5 GPa, Δu$_{ref}$=2 m/s, h=3.6 nm, T$_{wall}$=300K.

The onset of slip occurs at a velocity difference of 0.2 m/s; then, both L_s and s increase with Δu. In particular, the slip lengths evolves depends linearly on the wall speed difference, in coherence with the results by Martini [29] and Priezjev [17] for high levels of shearing and wall-fluid interactions characteristic of alkanes and metal surfaces.

Furthermore, two velocity domains featuring different slopes can be observed in Figure III-15a, which can be interpreted through the existence of several wall slip modes depending on the applied wall speed [29, 103]. At low velocities to moderate shear velocities (Δu <2 m/s) only a few fluid molecules slide locally on the walls independently of the global dynamics of the fluid; this mechanism is called defect slip. On the other hand at higher speeds (Δu >2 m/s) a generalized motion of all the lubricant molecules at the interface is established. In this slip mode, interfacial flow tends towards a global slip condition. This can be observed in Figure III-15b, where the increase in the dimensionless parameter s starts to approach the limit of 1.

In order to model the increase of slip with the imposed wall velocity difference in Figure III-15, as well as the two aforementioned slip regimes, a piecewise linear fit is proposed for L_s as a function of Δu:

$$\frac{L_s(\Delta u, h_{ref}, P_{ref})}{h_{ref}} = 1.09 \frac{\Delta u}{\Delta u_{ref}} - 0.0478 \qquad \text{for} \qquad \Delta u < 2 \,\text{m/s}$$

$$\frac{L_s(\Delta u, h_{ref}, P_{ref})}{h_{ref}} = 0.343 \frac{\Delta u}{\Delta u_{ref}} + 0.692 \qquad \text{for} \qquad \Delta u > 2 \,\text{m/s}$$

(III.19)

By combining Equations (III.3) and (III.19), it is then possible to express a law for the dimensionless slip parameter s:

$$s(\Delta u, h_{ref}, P_{ref}) = 1 - \left(2.18 \frac{\Delta u}{\Delta u_{ref}} + 0.904 \right)^{-1} \qquad \text{for} \qquad \Delta u < 2 \,\text{m/s}$$

$$s(\Delta u, h_{ref}, P_{ref}) = 1 - \left(0.686 \frac{\Delta u}{\Delta u_{ref}} + 2.38 \right)^{-1} \qquad \text{for} \qquad \Delta u > 2 \,\text{m/s}$$

(III.20)

III.3.2 Slip dependence on film thickness

In the majority of the literature studies, the impact of the shear rate on wall slip is often analyzed by changing the imposed wall velocity Δu. Nevertheless, $\dot{\gamma}_{app}$ is also dependent on the inverse of the film thickness h (Equation (III.1)).

In the analysis of molecularly confined films it is important to separate the contribution of these two parameters. In fact they can produce different effects on the lubricant nanorheology [13] and therefore interfacial flow. While viscosity reduction may be observed at larger wall speeds due to shear thinning effects [143], the effective viscosity increases with confinement as h is reduced [11].

Hence, the effect of confinement is investigated hereafter to complement the previous study on wall speed. The film thickness h is varied from 2.5 to 10 nm, corresponding to 6 and 25 molecular diameters respectively, while the wall velocity and pressure are kept equal to the reference values. Figure III-16 shows the evolution of the dimensionless parameter s

with h. The onset of slip occurs for h =7.9 nm, then s increases linearly with the degree of confinement. Hence, a linear fit is proposed:

$$s(\Delta u_{ref}, h, P_{ref}) = -0.52\frac{h}{h_{ref}} + 1.15 \tag{III.21}$$
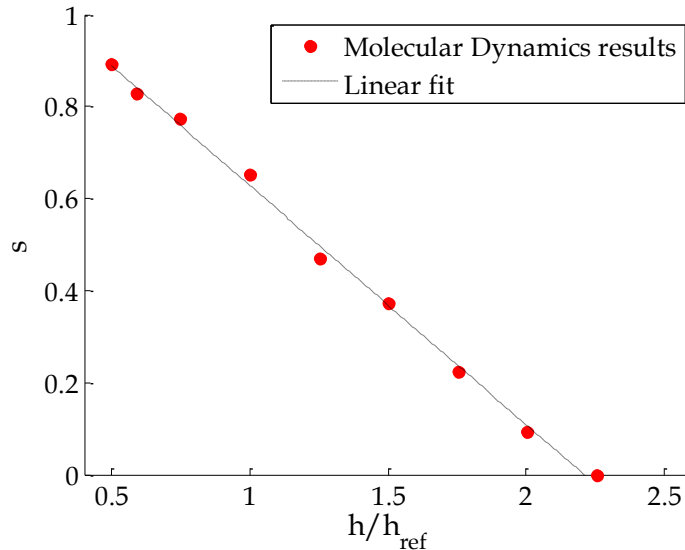
Figure III-16: Dependence of the dimensionless slip parameter s with the film thickness h. CuO [001] surfaces, n-octane, P=1.5 GPa, Δu=2 m/s, h$_{ref}$=3.6 nm, T$_{wall}$=300K.

III.3.3 Viscosity dependence on the film thickness

The limit of validity of Equation (III.21) is obtained for the total slip condition $s(h)$ =1, giving a critical film thickness of h =1.02 nm. This value corresponds to a surface separation of only 2-3 molecular diameters: in this case a solid-like state is expected in the lubricant [12]. The change in nano-rheology with confinement and the transition from a liquid- towards a glass-like state can be observed in Figure III-17.
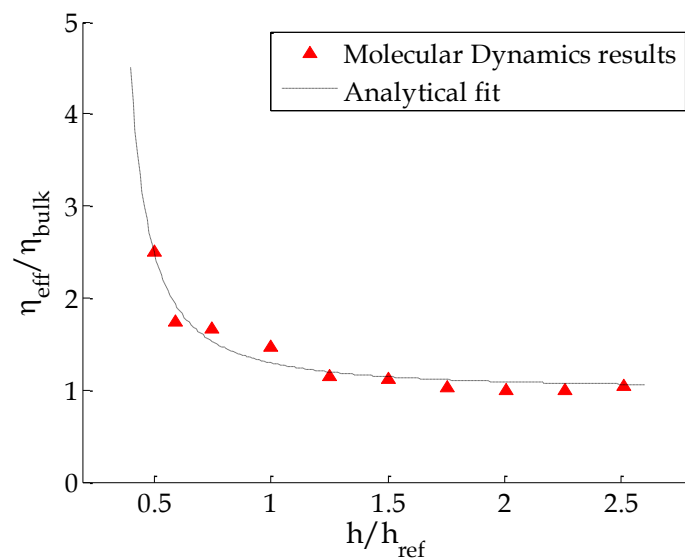
Figure III-17: Dependence of the effective viscosity η$_{eff}$ with the film thickness h. CuO [001] surfaces, n-octane, P=1.5 GPa, Δu=2 m/s, h$_{ref}$=3.6 nm, T$_{wall}$=300K.

In fact, the effective viscosity increases for small film thicknesses (h <5.5 nm), in accordance with the results by Granick [11]. The following Equation is proposed to characterize the dependence of η_{eff} with h from Figure III-17:

$$\eta_{eff} = \eta_{bulk} \cdot \psi(h) = \eta_{bulk}\left[0.187\left(\frac{h}{h_{ref}} - 0.284\right)^{-1.36} + 1 \right] \tag{III.22}$$

with $\eta_{bulk}(\Delta u_{ref}, P_{ref})$ =0.167 Pa.s being the estimated bulk value at large $h \gg h_{ref}$ values, where the effects of confinement disappear. $\psi(h)$ quantifies the viscosity enhancement with the reduction in film thickness. Finally, $0.284 \cdot h_{ref}$ =1.02 nm is the critical surface separation at which the viscosity of the confined lubricant tends towards infinity according to Equation (III.22). In reality, at this film thickness the viscosity increases by several orders of magnitude and the transition towards a solid-like state occurs [12].

III.3.4 Coupled slip dependence on wall velocity and film thickness

In order to formulate of a generalized law for interfacial flow, it is now necessary to analyze the coupled influence of the different operating conditions. Hence, the combined effect of the sliding velocity and degree of confinement on slip is analyzed hereafter.

Figure III-18 shows the evolution of the dimensionless parameter s as a function of the film thickness for three different Δu values.
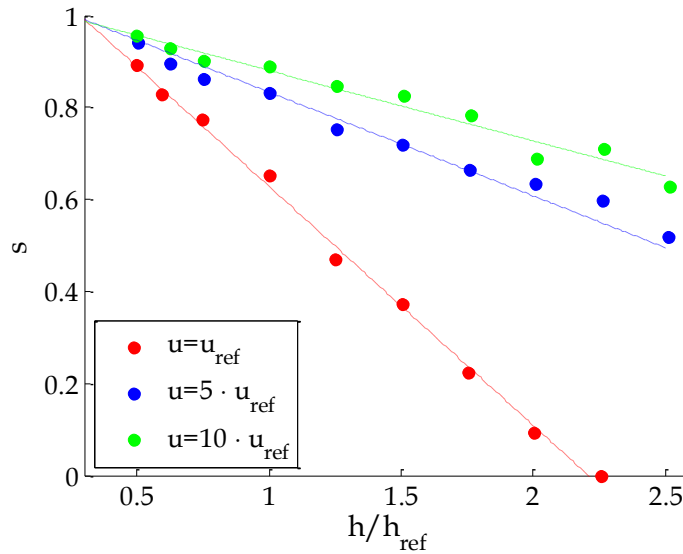
Figure III-18: Dependence of the dimensionless slip parameter s with the film thickness h, for three different wall velocities. CuO [001] surfaces, n-octane, P=1.5 GPa, Δu_ref=2 m/s, h_ref=3.6 nm, T_wall=300K.

A linear dependence is conserved in all three cases for the studied h range. Hence, the generalized slip law for the wall velocity and confinement can be expressed as:

$$s(\Delta u, h, P_{ref}) = A(\Delta u)\frac{h}{h_{ref}} + B(\Delta u) \tag{III.23}$$

The coupling terms are represented by the coefficients A and B of Equation (III.23), which vary significantly with wall velocity: in example $A(\Delta u_{ref}) = -0.52$, $A(5 \cdot \Delta u_{ref}) = -0.195$ and $A(10 \cdot \Delta u_{ref}) = -0.153$.

As a consequence, the film thickness for onset of slip depends strongly on the speed of the surfaces. For $\Delta u_{ref} = 2$ m/s the threshold was $h = 7.9$ nm, whereas at $\Delta u = 10 \cdot \Delta u_{ref} = 20$ m/s it can be estimated through linear interpolation at $h = 24.1$ nm. On the other hand, the minimum thickness h≈1 nm at which the lubricant becomes solid-like and total slip occurs remains unchanged. This is coherent with the trends proposed in [56], who reported that this phase transition for linear chains is generally observed for surface separations less than 4 molecular diameters.

The terms $A(\Delta u)$ and $B(\Delta u)$ must be characterized to describe the combined effect of film thickness and wall velocity on slip. First, a simpler expression is obtained by subtracting from Equation (III.23) the term $s(\Delta u, h_{ref}, P_{ref})$, which is already characterized by Equation (III.20):

$$s(\Delta u, h, P_{ref}) - s(\Delta u, h_{ref}, P_{ref}) = \left[A(\Delta u)\frac{h}{h_{ref}} + B(\Delta u) \right] - \left[A(\Delta u)\frac{h_{ref}}{h_{ref}} + B(\Delta u) \right] \qquad \text{(III.24)}$$

Simplifying Equation (III.24) gives:

$$s(\Delta u, h, P_{ref}) = A(\Delta u)\left(\frac{h}{h_{ref}} - 1 \right) + s(\Delta u, h_{ref}, P_{ref}) \qquad \text{(III.25)}$$

Then, a power-law fit for $A(\Delta u)$, which represents the increase in slip with wall speed, is proposed using the previously given values $A(\Delta u_{ref}) = -0.52$, $A(5 \cdot \Delta u_{ref}) = -0.195$ and $A(10 \cdot \Delta u_{ref}) = -0.153$. Finally, the combined dependence of the slip parameter with both the sliding velocity and degree of confinement is described by:

$$s(\Delta u, h, P_{ref}) = -\left(3.48\frac{\Delta u}{\Delta u_{ref}} \right)^{-0.54} \left(\frac{h}{h_{ref}} - 1 \right) + s(\Delta u, h_{ref}, P_{ref}) \qquad \text{(III.26)}$$

III.3.5 Slip dependence on pressure

Another operating condition which deeply influences interfacial flow under molecular confinement is the external pressure acting on the contact nano-patch [18]. For example, Ehret [152] proposed a preliminary link between slip, the shear stress limitation at the wall-fluid boundary (explained in Section III.2.3) and pressure: he deduced a linear variation of the dimensionless parameter s with P.

In the current configuration, this trend is confirmed by the results in Figure III-19, showing the evolution of s with pressures ranging from 0.25 to 2 GPa for three different wall velocities. A linear dependence is observed in all cases, with some slight deviations as the dimensionless slip parameter approaches the maximum value of one and total slip conditions. Hence, a linear fit is proposed, in coherence with [18, 152]:

$$s(\Delta u, h, P) = 1.03\frac{P - P_{crit}(\Delta u, h)}{P_{ref}} \qquad \text{(III.27)}$$

In Equation (III.27), $P_{crit}(\Delta u, h)$ is the critical pressure at which the onset of slip occurs. Its value depends on wall velocity and the film thickness. For example, Figure III-19 shows that an increase in Δu shifts the onset of slip towards lower pressures: $P_{crit}(\Delta u_{ref}) = 0.59$ GPa, $P_{crit}(5 \cdot \Delta u_{ref}) = 0.39$ GPa and $P_{crit}(10 \cdot \Delta u_{ref}) = 0.192$ GPa.
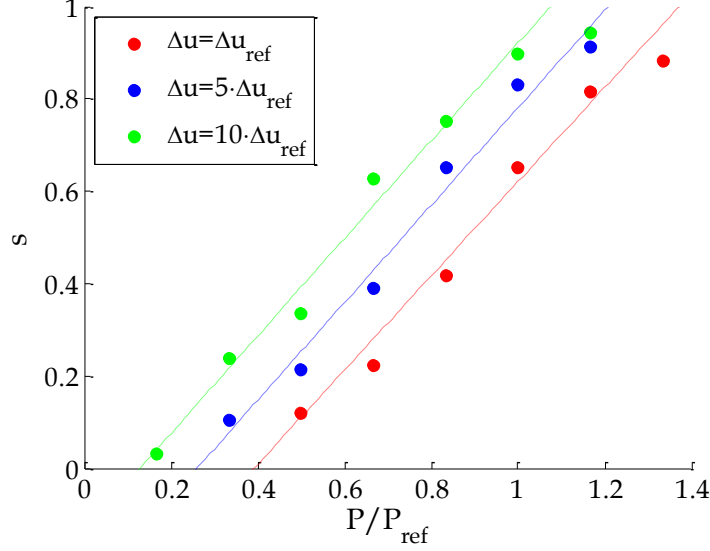
Figure III-19: Dependence of the dimensionless slip parameter s as a function of the pressure P for three different wall velocities. CuO [001] surfaces, n-octane, P_{ref}=1.5 GPa, Δu_{ref}=2 m/s, h=3.6 nm, T_{wall}=300K.

The dependence of P_{crit} with the level of shearing can be estimated by subtracting $s(\Delta u_{ref}, h_{ref}, P_{ref})$ from Equation (III.27) and setting P to its reference value:

$$s(\Delta u, h, P_{ref}) - s(\Delta u_{ref}, h_{ref}, P_{ref}) = 1.03 \left[\frac{P_{ref} - P_{crit}(\Delta u, h)}{P_{ref}} - \frac{P_{ref} - P_{crit}(\Delta u_{ref}, h_{ref})}{P_{ref}} \right] \quad \text{(III.28)}$$

Here $s(\Delta u_{ref}, h_{ref}, P_{ref}) = 0.65$ is the wall slip at the reference operating conditions, whereas $s(\Delta u, h, P_{ref})$ represents its dependence with the imposed surface velocity and the film thickness from Equation (III.26). Finally, simplifying Equation (III.28) gives:

$$\frac{P_{crit}(\Delta u, h)}{P_{ref}} = 1.02 - \frac{s(\Delta u, h, P_{ref})}{1.03} \quad \text{(III.29)}$$

This expression describes how the increase in sliding speed and confinement shifts the onset of slip towards lower pressures. It can finally be coupled with Equation (III.27) to fully characterize the dependence of interfacial flow with the external pressure:

$$s(\Delta u, h, P) = 1.03 \frac{P}{P_{ref}} + s(\Delta u, h, P_{ref}) - 0.99 \quad \text{(III.30)}$$

III.3.6 An analytical slip law for the operating conditions

In conclusion, Molecular Dynamics simulations were used to understand and quantify the occurrence of wall slip in a molecularly confined fluid as a function of operating conditions typical of an elasto-hydrodynamic lubrication case. Parametric studies on the wall ve-

locity (Equation (III.20)), film thickness (Equation (III.26)), and pressure (Equation (III.30)) in a nano-patch of the contact area allow the formulation of a "slip law" based on the fitting of the atomistic results:

$$s(\Delta u, h, P) = 1.03 \frac{P}{P_{ref}} - \left(3.48 \frac{\Delta u}{\Delta u_{ref}} \right)^{-0.54} \left(\frac{h}{h_{ref}} - 1 \right) - \left(2.18 \frac{\Delta u}{\Delta u_{ref}} + 0.904 \right)^{-1}$$
$$\text{for} \qquad \Delta u < 2\,\text{m/s}$$

$$s(\Delta u, h, P) = 1.03 \frac{P}{P_{ref}} - \left(3.48 \frac{\Delta u}{\Delta u_{ref}} \right)^{-0.54} \left(\frac{h}{h_{ref}} - 1 \right) - \left(0.686 \frac{\Delta u}{\Delta u_{ref}} + 2.38 \right)^{-1}$$
$$\text{for} \qquad \Delta u > 2\,\text{m/s}$$

$$(III.31)$$

with the reference operating conditions being Δu_{ref} = 2m/s, h_{ref} =3.6 nm and P_{ref} =1.5 GPa. Equations (III.31) show that slip increases with pressure, confinement and wall speed: the dimensionless parameter s evolves from zero, equivalent to the classical no-slip boundary condition, up to a limiting value of one when total slip occurs. This law can then be directly integrated into macroscale simulations, akin to the methodology presented in [18].

An alternative formulation can be provided to quantify the slip length as a function of the operating conditions by coupling Equation (III.31) with (III.3):

$$L_s(\Delta u, h, P) = \frac{h}{\left(1 - 1.03 \frac{P}{P_{ref}} + \left(3.48 \frac{\Delta u}{\Delta u_{ref}} \right)^{-0.54} \left(\frac{h}{h_{ref}} - 1 \right) + \left(2.18 \frac{\Delta u}{\Delta u_{ref}} + 0.904 \right)^{-1} \right)} - \frac{h}{2}$$
$$\text{for} \qquad \Delta u < 2\,\text{m/s}$$

$$L_s(\Delta u, h, P) = \frac{h}{\left(1 - 1.03 \frac{P}{P_{ref}} + \left(3.48 \frac{\Delta u}{\Delta u_{ref}} \right)^{-0.54} \left(\frac{h}{h_{ref}} - 1 \right) + \left(0.686 \frac{\Delta u}{\Delta u_{ref}} + 2.38 \right)^{-1} \right)} - \frac{h}{2}$$
$$\text{for} \qquad \Delta u > 2\,\text{m/s}$$

$$(III.32)$$

These analytical slip laws can then be directly integrated into a continuous model to analyze the impact of molecular effects on macroscopic contact behavior, in accordance to the methodology proposed in [18].

It should be remembered that this formulation has a major limitation. In fact, it is valid only for a particular surface-fluid pair: n-octane and smooth, oxygen terminated copper oxide walls were used in all simulations. Hence, Equations (III.31) and (III.32) provide a complementary view to the wall slip prediction model in Section III.2, which captures the effect of surface and lubricant nature on interfacial flow for a fixed set of operating conditions.

A coupling of these results could be interesting to investigate the impact of different surfaces topologies in macroscopic contacts with molecularly confined films. A preliminary relationship is proposed to extend the analytical slip laws (III.31) and (III.32) to other wall materials:

$$s_{mat}(\Delta u,h,P) = \frac{s_{mat,ref}}{s_{CuO,ref}} s_{CuO}(\Delta u,h,P)$$

$$\text{and} \quad L_{s,mat}(\Delta u,h,P) = \frac{h}{2} \cdot \left(\frac{1}{1 - s_{mat}(\Delta u,h,P)} - 1 \right)$$

(III.33)

where $s_{mat}(\Delta u,h,P)$ and $L_{s,mat}(\Delta u,h,P)$ respectively describe the evolution of the dimensionless slip parameter and the slip length with the operating conditions, for a new surface composition and orientation.

In Equation (III.33), $s_{CuO}(\Delta u,h,P)$ represents the previously determined dependence of interfacial flow on wall speed, film thickness and pressure for n-octane confined between CuO [001] surfaces. $s_{mat,ref}$ and $s_{CuO,ref}$ respectively represent the slip of a given material and copper oxide at the reference operating conditions Δu_{ref} = 2m/s, h_{ref} =3.6 nm, P_{ref} =1.5 GPa. Some values are given in Table III-3 for surface topologies typical of a bearing steel.

Surface	ζ_{surf} (kcal/mol)	$s_{mat,ref}$ (Δu_{ref}, h_{ref}, P_{ref})
Copper Oxide: CuO [001]	0.173	0.65
Iron oxide: Fe$_2$O$_3$ [001]	2.457	0
Cementite: Fe$_3$C [001]	2.594	0
Ferrite: α-Fe [100]; α-Fe [200]	0.259	0.03
Ferrite: α-Fe [110]	0.0517	0.89

Table III-3: Slip parameter values for n-octane confined between different surface morphologies typical of bearing steel, at the reference conditions P$_{ref}$=1.5 GPa, Δu$_{ref}$=2 m/s, h$_{ref}$=3.6 nm, T$_{wall}$=300K.

Equation (III.33) is qualitatively coherent with the Molecular Dynamics results from this Chapter. Slip increases with the wall velocity difference, pressure and confinement. Moreover, higher velocity jump at the wall-fluid boundary are observed for weakly interacting surfaces such as α-Fe [110], compared to sticky ones like iron oxide [001]. Hence, it will be used in the following Chapter to understand the impact of surface morphology and interfacial flow in macroscopic contacts.

In reality, the coupling of the results from Sections II.2 and II.3 is not as straightforward. In fact the proposed analytical slip laws (III.31) and (III.32) for the operating conditions may vary for each wall-fluid pair. Moreover, they may not be applicable hybrid interfaces, featuring two surfaces with unequal composition and different interfacial flows.

In future work, it would be interesting to further investigate this aspect and obtain a generalized equation for interfacial flow as a function all the parameters in the contact interface. As a guideline, the results from this Section could be explained as the result of the competition between the interfacial momentum transfer and the fluid resistance to shearing, akin to Equation (III.15) in Section III.2. Hence, Equation (III.16) characterizing the shear stress and wall slip as a function of surface and fluid natures could be extended to include the dependence on the operating conditions. Finally, the generalized equation for interfacial flow would take the following form:

$$s\left(\underbrace{\zeta_{surf},\eta}_{wall-fluid\ pair},\underbrace{\Delta u,h,P}_{\substack{operating \\ conditions}}\right)=1-\frac{h}{\Delta u}\frac{\tau_{zx}\left(\zeta_{surf},\Delta u,h,P\right)}{\eta(\tau_{xz},h,P)} \tag{III.34}$$

III.4 Conclusion

The first objective of this work was to explore the local behavior of severely confined fluids in lubricated contact interfaces under operating conditions typical of an elasto-hydrodynamic regime. Emphasis was put on interfacial flow, which can significantly deviate from the no-slip condition classically used in continuous models. Atomistic simulations were used to quantify the occurrence of wall slip as a function of the operating conditions, surface nature and the molecular structure of the lubricant through analytical laws. These can directly be integrated into continuous models, thus allowing a better understanding of the potential role played by molecular effects in macroscopic applications.

The wall slip phenomenon was introduced in Section III.1: the velocity jump at the solid-fluid boundary between the moving surfaces and the neighboring lubricant molecules was quantified through a dimensionless parameter.

Section III.2 focused on interfacial flow for several surface typologies and lubricants which can be found in confined interfaces. The occurrence of wall slip was interpreted as the consequence of the competition between surface and lubricant nature.

Thus, two main parameters were characterized. The first is the shear stress that a given wall can transfer to a lubricant molecule. It was linked to a surface characterization parameter, representative of the wall-fluid interaction energy and commensurability. This quantity is obtained through a numerically inexpensive scanning technique for both canonical and complex crystal lattices. For large values of the surface parameter, the lubricant is fully sheared and the tangential shear stress is limited by the internal cohesion of the fluid. Surfaces with weaker interaction are characterized by lower friction, because they cannot transfer enough momentum to shear the fluid: hence, wall slip occurs. The second quantity which must be determined to predict wall slip is the internal cohesion of the lubricant under confinement. This effective viscosity term was approximated through bulk laws issued from atomistic simulations.

Using these results, an analytical wall-slip prediction model was proposed, which adequately approximated results from Molecular Dynamics. The model is valid for linear alkanes confined between a wide range of geometrically smooth walls stemming from both canonical and complex crystal lattices. Hence, it can be used to quantify interfacial flow for a vast array of configurations in real interfaces without the need to perform further Molecular Dynamics simulations.

The aforementioned predictive model was formulated for reference operating conditions, i.e. at a fixed pressure, wall speed and film thickness. The impact of these quantities on interfacial flow was therefore investigated in Section III.3. A single wall-fluid pair featuring weak interactions and commensurability was considered. A parametric study was performed through Molecular Dynamics on operating conditions typical of an elasto-

hydrodynamic regime: slip was shown to increase with pressure, wall velocity and level of confinement. These variations were then integrated in an analytical slip law.

Finally, Appendix C gives an insight into the opposite phenomenon of wall slip, called locking, which occurs in presence of nano-rough surfaces.

In conclusion, the major parameters influencing interfacial flow in molecularly confined fluids have been identified and studied for a vast variety of configurations. Moreover, the formulation of analytical expressions quantifying the occurrence of wall slip allows a straightforward approach towards the second objective of this research. In fact, the next challenge is the integration of the atomistic results into macroscopic models. A multi-scale approach will be proposed in the following Chapter to investigate the influence of molecular phenomena on lubricated contacts at larger scales.

IV Bridging the gap between nano- and macroscale simulations for lubricated contacts

The analysis of elasto-hydrodynamic lubrication is critical to reach the optimum performance and the maximum longevity of many tribological applications. For instance, rolling element bearings are traditionally designed to operate under this regime. In general, EHD lubrication is characterized by oil films featuring thicknesses down to 0.1 µm, which nevertheless ensure the full separation of the surfaces. Moreover, high contact pressures in the GPa range cause the elastic deformation in the contacting bodies.

In order to characterize this behavior, the classical elasto-hydrodynamic lubrication theory has been developed, based on the following hypotheses for the lubricant flow in the contact:

- The fluid is a continuous medium
- Body forces are negligible
- Inertia and surface tension forces are small compared to viscous ones
- The flow is laminar (low Reynolds number)
- The film thickness is small compared to the other contact dimensions
- The fluid is Newtonian
- The lubricant viscosity and density are constant across the film thickness: no local variations are taken into account
- A no-slip boundary condition applies on the walls
- Stationary conditions: no time related phenomena occur
- Isothermal conditions

These hypotheses allow the derivation of the notorious Reynolds equation, which links the lubricant entrainment in a convergent contact geometry to the ensuing pressure generation which balances the external load. For a line contact, the following expression is obtained [32]:

$$\frac{\partial}{\partial x}\left(\frac{\rho h^3}{12\eta}\frac{\partial P}{\partial x}\right) = \frac{\partial}{\partial x}\left(\rho h \frac{u_1 + u_2}{2}\right) \tag{IV.1}$$

In Equation (IV.1) the contact kinematics are given by the velocities u_1, u_2 of the surfaces, whereas h represent the film thickness, P the pressure, and η, ρ the lubricant viscosity and density. The Reynolds equation is then coupled with the elasticity theory for the solids [35-37], as well as laws quantifying the changes in lubricant properties [37, 39] occurring under the high contact pressures observed in the elasto-hydrodynamic regime.

The resolution of EHD problems has progressed significantly in the last years. Fully coupled multi-physical approaches [44, 45], and fast and accurate computational techniques [47-49] have been developed. Additionally, the classical formulation based of the aforementioned assumptions has been extended to other phenomena, like for instance non-Newtonian lubricant behavior [41, 61], thermal effects [44-46] or transient conditions [153].

Despite these advances, the current trends in film thickness reduction and the resulting presence of molecularly confined fluids undermine several fundamental hypotheses of the standard EHD theory. Since the surface separation is comparable to the molecular size, the fluid may no longer be considered as a continuous medium. In fact, the lubricant is no longer homogeneous: the surface-fluid interactions play a significant role, leading to structural effects in proximity of the walls and significant density variations across the film thick-

ness. The nano-rheology can also be modified by confinement. Finally, the extensive analysis of interfacial flow in the previous Chapter shows that a no-slip boundary condition is not universally valid.

As more and more mechanisms rely on the presence of nano-thin films, it is necessary to integrate these molecular effects into the numerical models for macroscopic contacts. The main difficulty arises from the necessity to describe phenomena occurring over significantly different scales. The classical lubrication theory can describe contacts of a few square millimeters. However, it cannot capture the complex nano-scale behavior typical of severely confined conditions. On the other hand, Molecular Dynamics is a powerful tool for characterizing local molecular effects. Atomistic simulations are nevertheless limited to very small system dimensions (nanometers) and times (nanoseconds). To overcome these issues a multi-scale approach, called nano-EHL, will be developed hereafter.

IV.1 The nano-EHL approach

The integration of molecular effects into continuous models follows the flowchart shown in Figure IV-1. Since this work focuses mainly on the modification of interfacial flow occurring in severely confined lubricants, the standard Reynolds equation is modified to integrate slip effects.
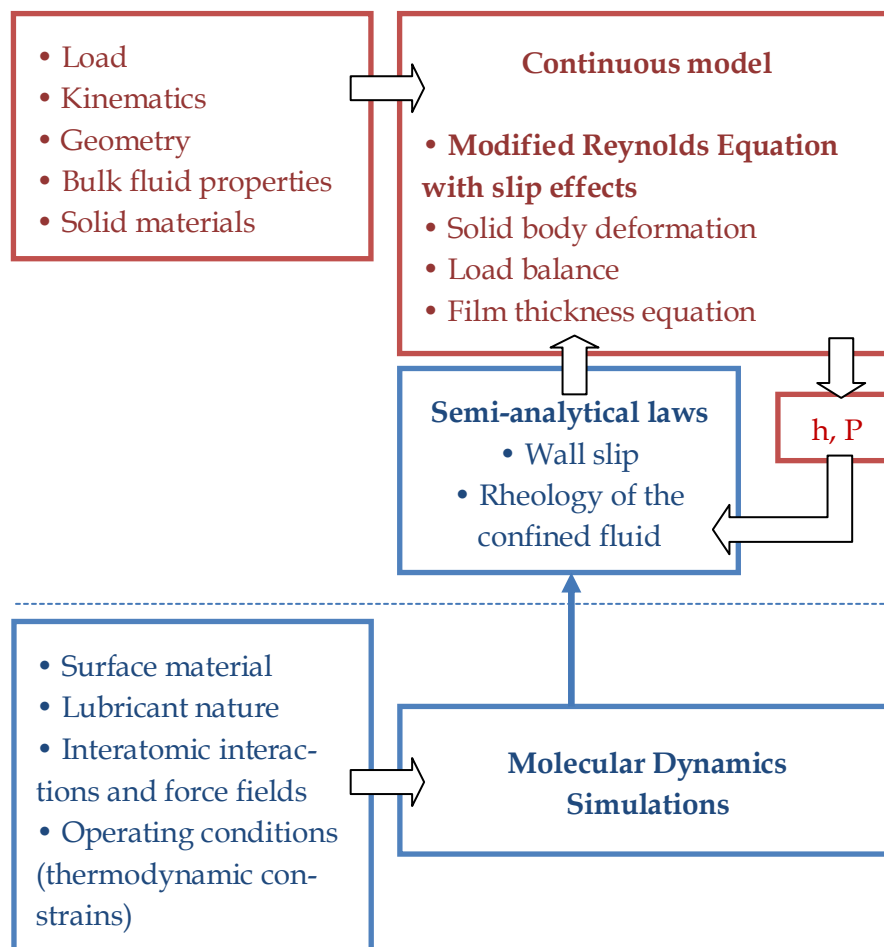
Figure IV-1: Flow chart of the nano-EHL multi-scale approach.

Its resolution alongside with the other continuum equations enables the usual calculation of the pressure distribution P and the film thickness h in the contact. These outputs are then used as boundary conditions in the Molecular Dynamics model, along with other important nano-scale parameters discussed in Chapters II and III. The atomistic simulations allow quantifying molecular effects, such as interfacial slip and the rheological properties of the confined fluid on one spot of the contact interface. Finally, these local nano-scale results are reintroduced into the modified Reynolds equation.

Since Molecular Dynamics simulations require a long computational time to characterize a nano-patch of the contact, a direct coupling with the macroscopic model is not possible. Hence, atomistic results were previously quantified in the form of semi-analytical laws, which account for their dependence on the operating conditions and the nature of the surfaces and lubricant. This procedure was thoroughly detailed in Chapter III for a vast set of configurations.

The macroscopic part of the nano-EHL model will be the main topic of the next Sections. First, the Reynolds equation will be modified to include a slip boundary condition. Then, the other laws of the elasto-hydrodynamic theory will be presented, followed by a brief explanation of the numerical resolution method.

Finally the nano-EHL approach will be applied on a lubrication case featuring interfacial slip. The influence of atomistic effects on important tribological quantifies such as the thickness, lubricant dynamics and friction will be analyzed; modifications in boundary flow due to different surface topologies will also be considered.

IV.2 Derivation of Reynolds equation with slip boundary condition

The first step for the establishment of the modified Reynolds equation involves looking back at of the main hypotheses of the elasto-hydrodynamic theory on the fluid flow, to see which ones can be undermined by the presence of molecularly thin films.

In the following work, configurations featuring film thicknesses larger than 5-6 molecular diameters, corresponding to 2-3 nanometers will be considered. In the state of the art and Chapter III it was shown that under this level of confinement alkane fluids retain a liquid-like state. Moreover, their compressibility and viscosity can be adequately be quantified by bulk laws [23, 143]. Hence, the continuum hypothesis can still be used for nano-scale lubricant flow under load and shear conditions. On the other hand, the slip phenomenon reported and quantified in Chapter III for several wall-fluid pairs contradicts the classical hypothesis of a no-slip boundary, and must therefore be integrated into the Reynolds Equation.

IV.2.1 Reynolds equation with shear-driven slip on two surfaces

The no-slip boundary, where the lubricant moves at the same speed as the neighboring solids, is written as:

$$u(0) = u_1 \quad \text{for the lower wall}$$
$$u(\text{h}) = u_2 \quad \text{for the upper wall}$$

$$(\text{IV.2})$$

Fillot [18], and Ehret [152] proposed to integrate slip effects by modifying this kinematic condition through the dimensionless slip parameter s from Chapter III:

$$
\begin{aligned}
u(0) &= (1-s) \cdot u_1 \quad \text{for the lower wall} \\
u(\text{h}) &= (1-s) \cdot u_2 \quad \text{for the upper wall}
\end{aligned}
\tag{IV.3}
$$

When $s=0$, there is no velocity difference at the boundary, corresponding to the standard no-slip condition. On the other hand, when s reaches the maximum value of one, the fluid is not entrained by the surfaces and total slip occurs.

The new boundary condition is then used to obtain a modified Reynolds equation with shear driven slip on two surfaces:

$$
\frac{\partial}{\partial x}\left(\frac{\rho h^3}{12\eta} \frac{\partial P}{\partial x} \right) = \frac{\partial}{\partial x}\left(\rho h \frac{u_1 + u_2}{2} (1-s) \right)
\tag{IV.4}
$$

In it can be noted that slip influences only the right hand side of Equation (IV.4). This term is often referred as "Couette", linked to a shear driven flow induced by the surfaces entraining the fluid. On the contrary the left hand side, usually called the "Poiseuille term" and related to a pressure driven flow, is unaffected. In fact, boundary condition (IV.3) implies that slip is identical on both surfaces, and is solely due to a wall velocity difference. This is in accordance with the system used in Chapter III to analyze interfacial flow in molecularly confined films. Hence, the analytical laws (III.31) and (III.33) describing the evolution of s with the operating conditions or wall material can be directly coupled to the modified Reynolds equation (IV.4).

IV.2.2 Derivation of Reynolds equation with pressure- and shear-driven slip on one surface

In order to provide a complementary view to the previous formulation, the modified Reynolds equation is re-derived hereafter with two new assumptions.

First, a hybrid interface will be considered, where the two walls feature different materials and interfacial flows. In particular, it will be assumed that slip can occur on the lower surface only, whereas the standard no-slip condition applies to the upper one. This hypothesis can be justified by considering the complex landscape which can be found in real contact interfaces. The roller and raceway of a bearing can be manufactured with different materials and finishing processes, resulting in a wide variety of surface compositions and orientations. Therefore, choosing different boundary flows for the upper and lower surfaces can provide an interesting insight on the role played by surface nature on contacts with molecularly thin films.

Second, it will be assumed that slip on the lower surface will be both shear- and pressure driven, in order analyze the possible modifications of the Poiseuille term in the Reynolds equation and the consequent impact on a macroscopic contact. To model the chosen flow conditions, a standard no-slip boundary is applied on the upper surface, whereas a Navier-type condition [30] describes slip on the lower wall:

$$u(h) = u_2 \quad \text{for the upper wall}$$

$$u(0) = u_1 + L_s \frac{\partial u}{\partial z}(0) \quad \text{for the lower wall} \tag{IV.5}$$

Here, u_1 and $u(0)$ are the respective speeds of the surface and the fluid at the lower boundary. As shown in Figure IV-2, the velocity difference is geometrically related to the slip length L_s and the velocity gradient of the fluid $\partial u / \partial z$ at the interface $z = 0$.
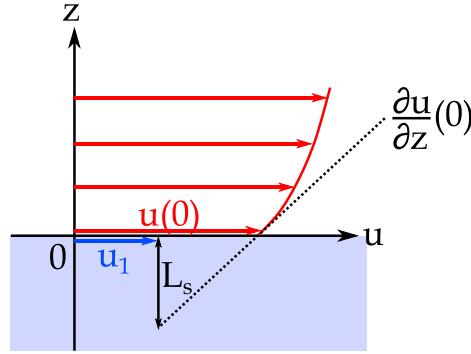
Figure IV-2: Geometrical representation of the Navier-type slip boundary condition

Equations (III.32) and (III.33) from Chapter III will be used to describe the dependence of the slip length L_s with the operating conditions and the nature of the wall-fluid pair. It should be noted that these analytical laws were obtained under simple shear conditions and for two walls featuring identical interfacial flows. Hence, they may not quantify exactly the behavior of a hybrid contact interface and pressure-driven slip.

Nevertheless, several literature studies [17, 80, 91, 102, 104] etc.] show that the same trends from Equations (III.32) and (III.33) are applicable even when a single wall-fluid interface (e.g. the lower surface only) is considered, or in presence of pressure-driven flows: slip increases with the local shear rate at the boundary and for weaker surface-lubricant interactions or commensurabilities. Hence, despite their limitations, these laws can be integrated in the new formulation of the Reynolds equation (with pressure- and shear-driven slip on one surface) to perform a qualitative investigation of molecular effects in macroscopic models.

IV.2.2.a Fluid velocity

Once the boundary conditions are defined, it is possible to obtain the Reynolds equation with wall slip on the lower surface. The starting point is the Navier-Stokes theory for the conservation of momentum in the fluid, simplified for a thin, laminar flow, with negligible inertia effects and body forces [32]:

$$\frac{\partial P}{\partial x} = \frac{\partial \tau_{zx}}{\partial z}$$
$$\frac{\partial P}{\partial z} = 0 \tag{IV.6}$$

where the shear stress τ_{zx} can be expressed as a function of the lubricant viscosity η and the velocity field component u along the x-direction:

$$\tau_{zx} = \eta \frac{\partial u}{\partial z} \tag{IV.7}$$

Equation (IV.6) is integrated twice along the z-axis by assuming a constant viscosity across the film thickness in accordance with the hypotheses of the model. The integration constants are determined through the boundary conditions (IV.5) (see Appendix D for details). This yields the velocity field across the lubricant film:

$$u(z) = \frac{1}{2\eta} \frac{\partial P}{\partial x} \left(z^2 - \frac{L_s + z}{L_s + h} h^2 \right) + u_1 \left(\frac{h - z}{L_s + h} \right) + u_2 \left(\frac{L_s + z}{L_s + h} \right) \tag{IV.8}$$

IV.2.2.b Reynolds equation

The Reynolds equation is obtained by combining the lubricant velocity field with the mass equilibrium equation. In the case of a compressible flow, the latter is given by [32]:

$$\frac{\partial \rho u}{\partial x} + \frac{\partial \rho w}{\partial z} = 0 \tag{IV.9}$$

where ρ is the lubricant density and u the velocity components along the x-direction, given by Equation (IV.8). Finally, the continuity equation (IV.9) is integrated across the film thickness (see Appendix D). The following law is obtained:

$$\frac{\partial}{\partial x} \left(\frac{\rho}{12\eta} \left(h^3 \frac{h + 4L_s}{h + L_s} \right) \frac{\partial P}{\partial x} \right) = \frac{\partial}{\partial x} \left(\frac{\rho h^2}{2(h + L_s)} u_1 + \frac{\rho h(h + 2L_s)}{2(h + L_s)} u_2 \right) \tag{IV.10}$$

This expression constitutes the Reynolds equation for line contacts with pressure- and shear-driven slip on the lower surface. The modification of interfacial flow is quantified by the slip length L_s, issued from Equations (III.32) and (III.33) in Chapter III.

While Equation (IV.10), or alternatively (IV.4), constitute the core of the nano-EHL approach to integrate the modification of interfacial flow in macroscopic contacts, additional laws are required to complete the macroscopic model: the elasticity and load balance equations, along with the expressions for the film thickness, compressibility and piezoviscosity effects. These will be presented in the following, after a simplification of the system geometry.

IV.3 Other continuum equations

IV.3.1 Reduced contact geometry

A line contact is simulated in this study, like the one between the rolling element and raceway in a roller bearing. The two cylinders feature curvature radii R_1 and R_2, and are disposed in a non-conforming geometry (Figure IV-3a). In the usual approximation, the contacting elements are considered infinitely long along one of the principal directions (y-axis). Hence, a plane strain formulation is chosen and only the (x, z) plane is represented. Furthermore, an equivalent cylinder-plane problem can be formulated (Figure IV-3b). In this case, the cylinder is characterized by a reduced radius R defined as [32]:

$$R = \left(\frac{1}{R_1} + \frac{1}{R_2} \right)^{-1} \tag{IV.11}$$

Finally, the origin of the axes is placed on the lower plane in the contact center.
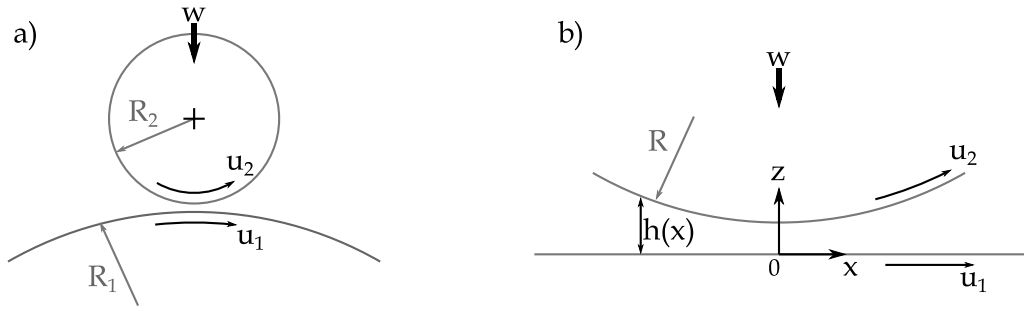
Figure IV-3: Schematic representation of the contact geometry. a) Line contact between two cylinders; b) Equivalent cylinder-plane problem.

IV.3.2 Film thickness equation

The film thickness geometry h inside the contact zone is defined through the following equation [61]:

$$h(x) = \frac{x^2}{R} + h_0 + \delta(x) \tag{IV.12}$$

It results from the superposition of 3 terms. The first refers to the geometry of the surfaces. In particular, the cylinder in the equivalent contact problem of Section IV.3.1 is approximated by a parabolic shape with curvature radius R. $\delta(x)$ describes the elastic deformation of the surfaces due to the high contact pressures; this term will be further analyzed in Section IV.3.5. Finally, h_0 is related to the rigid body displacement, and is determined through the load balance equation.

IV.3.3 Load balance equation

Under steady-state and full-film conditions, the lubricant pressure P generated in the contact domain Ω_C fully supports the external load w. This equilibrium condition is expressed through the load balance equation [61]:

$$w = \int_{\Omega_C} P(x) d\Omega_C = \int_{\Omega_C} P(x) dx \tag{IV.13}$$

which can be satisfied by adjusting the rigid body displacement from the film thickness equation (IV.12).

IV.3.4 Boundary and film separation conditions

The pressure of the lubricant outside of the contact zone is equal to the ambient one: its value is generally taken as a zero reference (relative pressure). Hence, at the boundary $\partial\Omega_C$ of the pressurized contact domain Ω_c the following condition is applied [61]:

$$P = 0 \quad \text{on} \quad \partial\Omega_C \tag{IV.14}$$

Furthermore, it is supposed that the lubricant cannot withstand pressures smaller than the vapor pressure P_{vap}. Should this case arise, the Reynolds cavitation boundary condition can be used to model the ensuing breakup of the fluid film at the contact exit [61]:

$$P > P_{vap} \approx 0 \quad \text{on} \quad \Omega_C; \qquad P = \nabla P \cdot \vec{n}_C = 0 \quad \text{on the cavitation boundary} \qquad \text{(IV.15)}$$

where $\vec{n}_C$ is the outward normal vector at the cavitation boundary in the outlet zone. The first term in Equation (IV.15) prevents the occurrence of negative pressures in the contact, while the second ensures the mass conservation of the lubricant flow when the lubricant film breaks up.

IV.3.5 *Solid body deformation*

In an elasto-hydrodynamic contact the load w is generally distributed over a very small area, leading to high pressures and solid body deformation. The Hertzian theory for dry contacts can give a good approximation of the order of magnitude of these quantities. In a line contact, the maximum Hertzian pressure P_h is given by [34]:

$$P_h = \frac{2w}{\pi b_h} \qquad \text{(IV.16)}$$

where b_h is the half contact width:

$$b = \sqrt{\frac{8wR}{\pi E'}} \qquad \text{(IV.17)}$$

In general P_h can reach some Gigapascals, whereas b_h is typically equal to the tenth of a millimeter. The ensuing elastic deformation of the contacting bodies is related to their reduced Young's modulus E':

$$E' = \frac{2}{\dfrac{1-\nu_p}{E_p} + \dfrac{1-\nu_c}{E_c}} \qquad \text{(IV.18)}$$

where (E_p, ν_p) and (E_c, ν_c) are the elastic material properties (Young's modulus and Poisson's coefficient) of the plane and the cylinder respectively.

The linear elasticity equations are used to determine the solid body deformation due to the pressure field in the elasto-hydrodynamic contact. A simplification of the computational problem is performed first. Instead of considering both the cylinder and the plane, the former will be set as rigid, whereas the latter will accommodate the total elastic deformation. In this case, the equivalent material properties of the deformable plane are given by [61]:

$$E_{eq} = \frac{E_p^2 E_c (1+\nu_c)^2 + E_c^2 E_p (1+\nu_p)^2}{\left[E_c(1+\nu_p) + E_p(1+\nu_c)\right]^2} \quad \text{and} \quad \nu_{eq} = \frac{E_p \nu_c (1+\nu_c) + E_c \nu_p (1+\nu_p)}{E_c(1+\nu_p) + E_p(1+\nu_c)} \qquad \text{(IV.19)}$$

with E_{eq} being the equivalent Young's modulus and ν_{eq} the equivalent Poisson coefficient. Thus, the elasticity equations are applied to the a 2-dimensional square structure schematically shown in Figure IV-4, which approximates the semi-infinite plane.
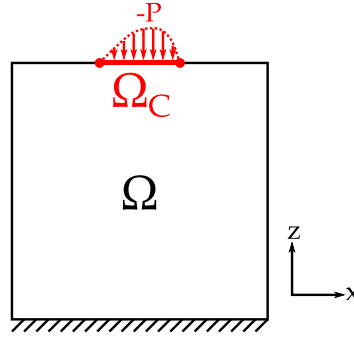
Figure IV-4: Schematic representation of the deformable solid body domain Ω and its boundary conditions.

Inside the interior domain Ω, the force equilibrium on an elemental volume is written as [61]:

$$\nabla \overline{\overline{\sigma}} = 0 \tag{IV.20}$$

where $\overline{\overline{\sigma}} = [\sigma_{xx}, \sigma_{zz}, \tau_{xz}]^{\mathrm{T}} = C\overline{\overline{\varepsilon}}$ is the stress tensor, $\overline{\overline{\varepsilon}} = [\frac{\partial d_x}{\partial x}, \frac{\partial d_z}{\partial z}, \frac{1}{2}\left(\frac{\partial d_x}{\partial z} + \frac{\partial d_z}{\partial x}\right)]^{\mathrm{T}}$ the stain tensor, and (d_x, d_z) the displacement field along the main system axes. The constitutive matrix C is related to material properties of the domain Ω:

$$C = \frac{E_{eq}}{(1+v_{eq})(1-2v_{eq})} \begin{bmatrix} 1-v_{eq} & v_{eq} & 0 \\ v_{eq} & 1-v_{eq} & 0 \\ 0 & 0 & 0.5-v_{eq} \end{bmatrix} \tag{IV.21}$$

Finally, the following boundary conditions are applied to the deformable domain Ω in Figure IV-4:

$$\begin{cases} \overline{\overline{\sigma}}n = -P & \text{on the contact domain } \Omega_C \\ d_x, d_z = 0 & \text{on the lower boundary of } \Omega \\ \overline{\overline{\sigma}}n = 0 & \text{on the other boundaries} \end{cases} \tag{IV.22}$$

In particular, the first equation implies that the lubricant pressure generated in the contact domain Ω_C is transferred to the solid body, thus causing its deformation. Through this boundary condition, the elasticity theory for the solid materials is strongly coupled to the Reynolds equation for fluid flow. Finally, the surface deformation $\delta(x)$ in the film thickness equation (IV.12) is equal to the absolute value of the vertical displacement field along the z-direction:

$$\delta(x) = |d_z(x)| \tag{IV.23}$$

IV.3.6 Lubricant properties

Another consequence of the high contact pressures in the elasto-hydrodynamic regime is the significant change in the lubricant properties. Two terms of the Reynolds equation are influenced: the density ρ and the viscosity η.

The evolution of the former with the external load is expressed by the compressibility law formulated experimentally by Dowson and Higginson [37]:

$$\rho(P) = \rho_0 \left[\frac{5.9 \cdot 10^8 + 1.34 \cdot P[\text{Pa}]}{5.9 \cdot 10^8 + P[\text{Pa}]} \right] \tag{IV.24}$$

where ρ_0 is the density at ambient pressure. This equation translates an increase in lubricant density of roughly 30% under high loads. The Dowson-Higginson is not always accurate and is purely empirical. However, it is often used due to its simple mathematical form and its independence on lubricant nature. Furthermore, it was valid for simple fluids like linear alkanes also under severely confined conditions (see Section II.3.2 and [18, 23]): therefore, it will be chosen for the rest of this study.

Under contact pressures in the GPa range, the lubricant viscosity η increases of several order of magnitude compared to ambient conditions. To model its dependence with P and h, a modified Roelands equation is used [39]:

$$\eta(P,h) = \eta_0 \cdot \psi(h) \cdot \exp \left[(\ln(\eta_0[\text{Pa.s}]) + 9.67) \left(-1 + \left(1 + \frac{P}{P_R} \right)^{z_R} \right) \right] \tag{IV.25}$$

where η_0 is the lubricant viscosity at ambient pressure, z_R the Roelands exponent given by:

$$z_R = \frac{\alpha_R P_R}{\ln(\eta_0[\text{Pa.s}]) + 9.67} \tag{IV.26}$$

and α_R, P_R are empirically determined coefficients characteristic of each fluid. Compared to the standard bulk law, the additional term $\psi(h)$ translates the viscosity enhancement occurring under confinement at film thicknesses smaller than 2-3 nanometers. In example, for n-octane this term was given by Equation (III.22). However, when the gap thickness becomes larger than 4-5 nanometers, $\psi(h) \approx 1$ and standard bulk viscosity values describe the lubricant rheology, in accordance with the findings of Section III.3.3.

The description of the lubricant properties concludes the set of equations of the continuous lubrication theory. The fluid flow in the contact, the ensuing pressure generation as well as the solid body response are now fully characterized. Additionally, the modification of the boundary flow under confinement was integrated in the Reynolds equation, and quantified through semi-analytical laws from atomistic simulation results. Hence, the nano-EHL model is now complete. Its numerical resolution will be the topic of the next Section.

IV.4 Numerical resolution of the nano-EHL model

The analysis of a line EHD contact problem including wall slip effects is based on a fully coupled resolution of several laws: the Reynolds, elasticity and load balance equations, along with the expressions for the film thickness, compressibility and piezoviscosity effects, and interfacial flow.

A Finite Element formulation is employed, which was extensively described in [61]. The numerical procedure is summarized hereafter. The constitutive equations are written in

their dimensionless form, followed by a brief description of the method, the numerical system and its parameters.

IV.4.1 Dimensionless equations

The EHL equations in Sections IV.2 and IV.3 are usually written in a dimensionless form to increase the stability of the numerical resolution. This procedure enables handling variables close to unity, thus achieving a better conditioning of the system. Several dimensionless variables are introduced:

$$X = \frac{x}{b_h}; \quad H = \frac{hR}{b_h^2}; \quad \overline{L}_s = \frac{L_s}{h}; \quad \overline{P} = \frac{P}{P_h}; \quad \overline{\eta} = \frac{\eta}{\eta_0}; \quad \overline{\rho} = \frac{\rho}{\rho_0};$$

$$\beta = \frac{12\eta_0 R^2 u_m}{b_h^3 P_h}; \quad \xi = \frac{\overline{\rho}H^3}{\overline{\eta}\beta} \tag{IV.27}$$

u_m represents the mean entrainment speed, equal to the average of the surface velocities:

$$u_m = \frac{u_1 + u_2}{2} \tag{IV.28}$$

An additional term is introduced to characterize the kinematics of the solid bodies. The Slide to Roll Ratio SRR is defined as the ratio between the wall speed difference and mean entrainment speed:

$$SRR = \frac{u_2 - u_1}{u_m} = \frac{\Delta u}{u_m} \tag{IV.29}$$

By using the terms (IV.27)-(IV.29), the Reynolds equation with slip effects on the lower surface (IV.10) can be written in its dimensionless form:

$$\frac{\partial}{\partial X}\left(\xi\left(\frac{1+4\overline{L}_s}{1+\overline{L}_s}\right)\frac{\partial\overline{P}}{\partial X} - \frac{\overline{\rho}H}{1+\overline{L}_s}\left[1+\overline{L}_s(1+\frac{SRR}{2})\right]\right) = 0 \tag{IV.30}$$

with the associated boundary condition:

$$\overline{P} > 0 \text{ on } \Omega_C; \quad \overline{P} = 0 \text{ on } \partial\Omega_C; \quad \overline{P} = \nabla\overline{P}\cdot\vec{n}_C = 0 \text{ on the cavitation boundary} \tag{IV.31}$$

The film thickness equation becomes:

$$H(X) = \frac{X^2}{2} + H_0 + \overline{\delta}(X) \tag{IV.32}$$

where $\overline{\delta}(X) = \delta(X)\cdot b_h / R$ is the dimensionless deformation caused by the dimensionless pressure $\overline{P}(X)$ on the contact domain. Finally the load balance equation is written as:

$$\int_{\Omega_C} \overline{P}(X)d\Omega_C = \frac{w}{P_h \cdot b_h} = \frac{\pi}{2} \tag{IV.33}$$

IV.4.2 Numerical method and parameters

The dimensionless equations of the contact model are solved through a fully coupled Finite Element method implemented in the software COMSOL-Multiphysics. A brief sum-

mary of the approach and the numerical parameters are given hereafter; for more details the reader can refer to [61].
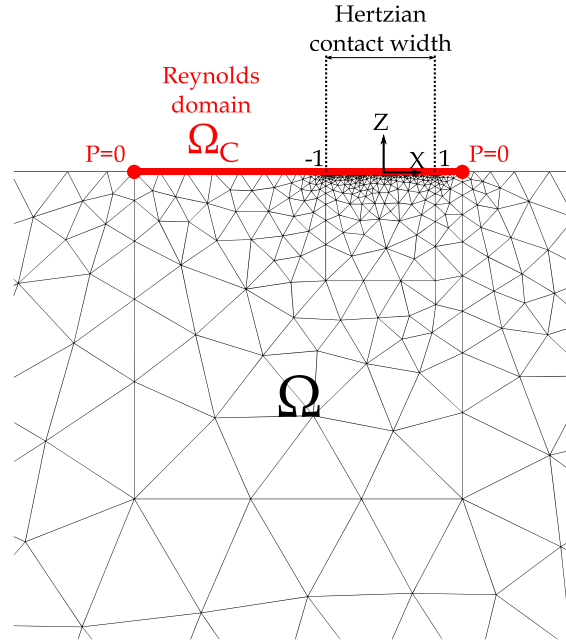
Figure IV-5: System representation with the Finite Element mesh

The equations are discretized using the Galerkin method over the triangular Finite Element grid shown in Figure IV-5. A fine meshing is employed in the contact zone and on the Reynolds boundary for accuracy, whereas a coarser grid is chosen in the rest of the solid body for improving the computational speed. Typically, 10000 quadratic 2-D elments (50000 degrees of freedom) discretize the deformable plane, while 1000 2-D quintic ones (5000 d.o.f.) are used for Reynolds domain.

The discretized EHD equations are linearized through a Newton-Raphson technique. They are fully coupled in a single matrix formulation: the information loss and slow convergence rate of a semi-system approach, where the elasticity and fluid flow problems are treated separately is thus avoided. The system resolution employs an iterative Newton method, which is repeated until the norm of the residual error falls below a certain threshold (10^{-6}).

Three main calculation steps are performed. First, the Hertzian pressure and corresponding solid-body deformation are evaluated to provide initial values for these quantities. Then, the standard EHL problem is solved with a no-slip boundary condition. This step is performed to provide reference results. It usually takes 15-20 Newton iterations to converge. Starting from the result of the standard EHD calculation, the modified Reynolds equation with slip boundary condition is solved together with the semi-analytical laws issued from atomistic simulations. Convergence for the full nano-EHD model is reached after 2-3 iterations; furthermore, consecutive calculations involving slight variations of the operating conditions are very fast, allowing easy parametric studies. In general, the whole resolution process lasts roughly one minute on a 2.27GHz dual core processor.

IV.5 Results of the nano-EHL approach

The nano-EHD model is applied on a standard lubrication case to investigate the impact of slip on macroscopic behavior under the elasto-hydrodynamic regime. The main parameters (Table IV-1) are chosen according to [18] to reach a nanometric film thickness in the center of the contact. The solid bodies are composed of copper and feature smooth surfaces. N-octane is used to lubricate the contact. This alkane is typically present in fuels and consequently in engine contacts. Its viscosity is much lower compared to traditional base oils, making it a good example for an ultra-low-viscosity operating fluid. η is described through a Roelands piezoviscosity law (Equation (IV.25)) stemming from experimental data [154, 155]. The dependence is plotted in Figure IV-6, with the corresponding Roelands parameters summarized in Table IV-1. Furthermore, this fluid does not feature shear thinning effects until very high shear rates, as shown by the bulk viscosity results in Section III.2.4. Under the chosen operating conditions, its behavior remains Newtonian.

Parameter	Symbol	Value
Equivalent contact radius	R	$5 \cdot 10^{-3}$ m
Line load	W	$5 \cdot 10^{5}$ N/m
Mean entrainment speed	u_m	1 m/s
Young's modulus of copper	E_{Cu}	124 GPa
Poisson's coefficient of copper	ν_{Cu}	0.33
Maximum Hertzian's pressure	P_h	1.49 GPa
Half contact width	B	$0.214 \cdot 10^{-3}$ m
n-octane density at ambient pressure	ρ_0	695 kg/m^3
n-octane viscosity at ambient pressure	η_0	0.483 mPa.s
Roelands parameter	A	9.75 GPa^{-1}
Roelands pressure	P_R	0.112 GPa

Table IV-1: Macroscopic parameters of the nano-EHL model.
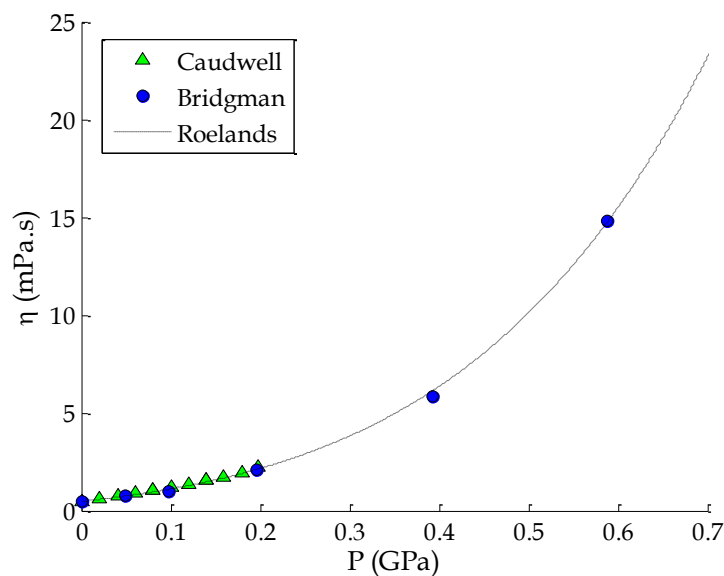
Figure IV-6: Roelands viscosity-pressure dependence for n-octane, from results by [154, 155].

Reference results for this configuration are calculated using the Reynolds equation with the standard no-slip condition. The pressure build-up and film thickness along the contact abscissa x are shown in Figure IV-7a. The trends of an elasto-hydrodynamic regime are obtained. P is close to the elliptical Hertzian distribution in the central zone; h features the typical striction effect and film thickness minimum located between the high pressure domain and outlet region. However, the gap width in the contact center is of the order of magnitude of some nanometers. According to the semi-analytical law (III.31) a change in boundary flow and the occurrence of slip can be expected.
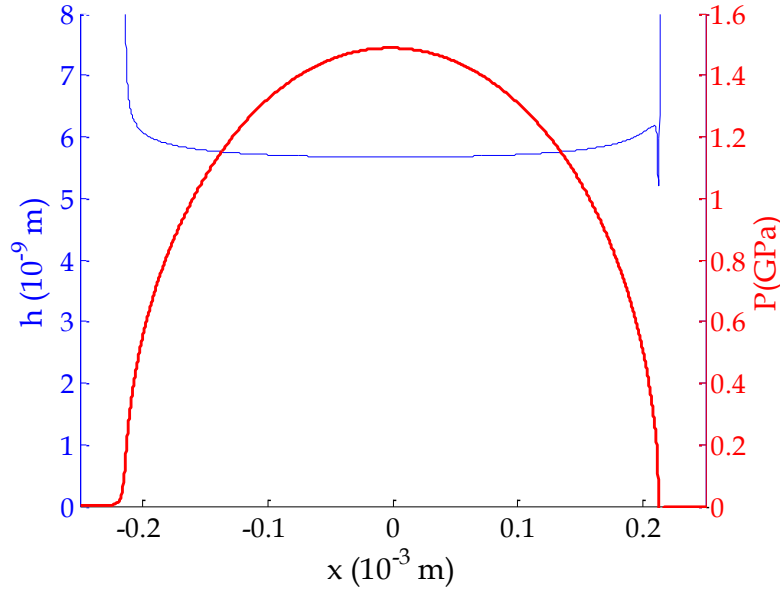
Figure IV-7: Pressure distribution and film thickness in the contact for the standard no-slip boundary. The reader is invited to notice the sensibly different scale lengths for the abscissa and film thickness.

IV.5.1 *Film thickness results with shear driven slip on two surfaces*

The full nano-EHL model is then solved for the previous configuration. The modified Reynolds equation with shear driven slip from Section IV.2.1 is applied first as a reminder of the main trends from the literature [18, 152].

A parametric study is performed on the Slide-to-Roll ratio parameter (Equation (IV.29)). While the mean entrainment speed of the lubricant is kept constant, the wall velocity difference Δu is varied from zero to both positive and negative values. In the no-slip case with a Newtonian fluid and isothermal conditions, the solution is independent on this parameter. On the other hand, in a slip configuration, changing SRR and Δu can alter interfacial flow, as well as the behavior in the whole contact.

In fact, a remarkable result of the nano-EHL model is the significant modification of the film thickness in the contact center, shown in Figure IV-8. When $SRR{\neq}0$: the gap height increases, and the curvature of the surface changes sign. In the literature this phenomenon is referred to as a dimple [156, 157].
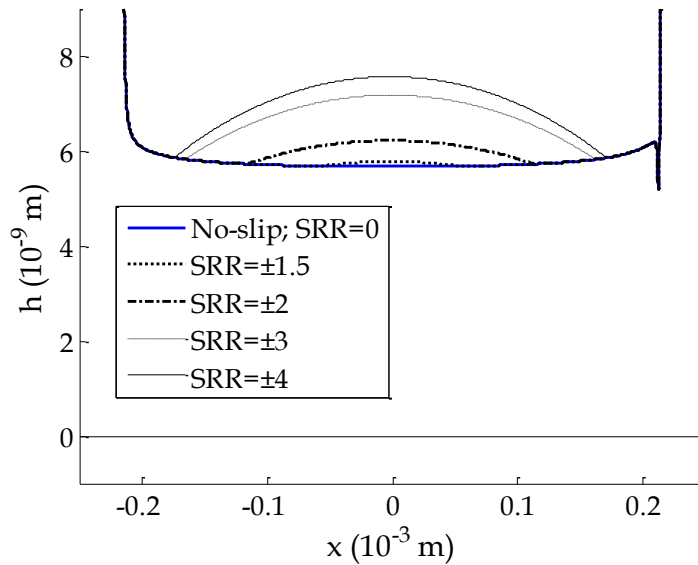
Figure IV-8: Film thickness modification with SRR for the nano-EHL model featuring slip on two surfaces.

In [18] its formation was related to the occurrence of slip in the central domain of the contact (Figure IV-9). In this zone, all the conditions for the modification of interfacial flow in the chosen CuO-octane configuration are fulfilled: a nanometric film thickness, a pressure in the Gigapascal range, and a wall velocity difference of some meters per second for $SRR \neq 0$. On the other hand, slip does not occur at the inlet and outlet zones, where the pressure and confinement are lower. Hence, the lubricant is entrained normally inside the contact, while in the central domain it is slowed down by the occurrence of slip, causing its stagnation and the formation of a fluid reservoir with larger film thickness.
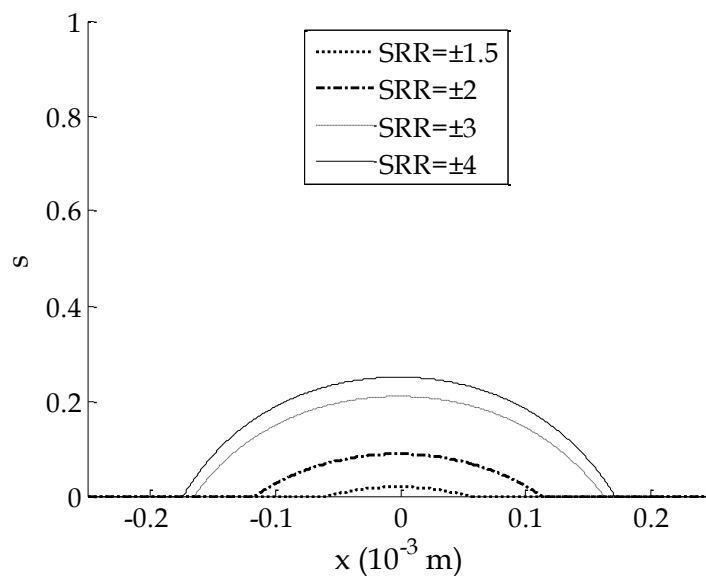
Figure IV-9: Dimensionless slip parameter s along the contact abscissa for the nano-EHL model featuring slip on two surfaces.

It can be noticed that the increase in h tends to saturate for high Slide-to-Roll-Ratios. On one hand, this phenomenon is enhanced by the increase in slip with larger SRR values. On the other hand, this effect is limited by the slip reduction as for lower levels of confinement. Hence, the maximum value for s stagnates around 0.3.

IV.5.2 *Film thickness results with pressure and shear driven slip on the lower surface*

The modified Reynolds equation used previously involves symmetrical slip conditions on the two walls. Hence, the results do not depend on the sign of SRR, i.e. which of the surfaces moves faster. This may not be the case for the new formulation of the modified Reynolds equation proposed in Section IV.2.2, where slip is present only on the lower wall. In fact, for $SRR > 0$ the upper "sticking" surface is animated with a larger speed along the x-direction compared to the lower one, and entrains the lubricant in and out of the contact. On the other hand, for negative SRR values the lower "slipping" wall moves faster and is primarily responsible for the fluid entrainment.

This case will be analyzed first: the corresponding film thickness modification is shown in Figure IV-10a. Similarly to the results in the previous Section, a dimple is observed, which can be explained through the reduction of the lubricant velocity and the formation of a fluid reservoir in the center of the contact because of slip effects. Moreover, the maximum of s is also limited to a value of 0.3 (Figure IV-10b). Again, this is the due to the competition between the enhancement in film thickness, and the consequent reduction in slip as confinement decreases.
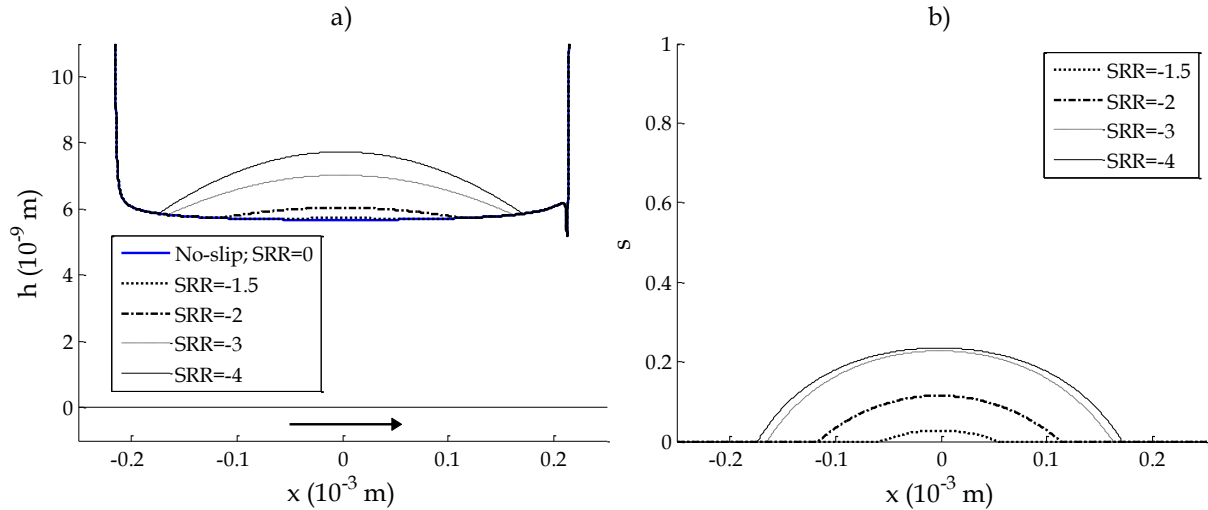
Figure IV-10: Film thickness modification (a) and slip domain dependence (b) for negative SRR values, obtained from the nano-EHL model with slip on the lower surface. The arrow represents the surface entraining the fluid in the contact.

While the results for SRR<0 and slip on a single surface are similar to the case with two slipping surfaces, the behavior in the contact is completely changed as the Slide-to-Roll-Ratio becomes positive. In Figure IV-11a a severe film thickness reduction is observed, and the minimum of h is shifted from the outlet to the central zone of the contact. Moreover, as the level of confinement increases, so does slip, which in turn causes an additional film

thickness decrease. This mutual enhancement between the change in interfacial flow and the reduction in *h* leads to slip values close to unity (total slip) at high *SRR* (Figure IV-11b).

This remarkable result cannot be explained through the qualitative analysis proposed in Section IV.5.1, which assumed that a lower lubricant speed in the contact center led to the formation of a dimple. In fact, since the film thickness is reduced, an acceleration of the lubricant could instead occur in presence of slip. To confirm this hypothesis, a quantitative explanation, based on the lubricant dynamics in the contact center, is proposed hereafter. In particular, it will encompass all the results of this Section, to create a link between the occurrence of slip and the modifications in film thickness observed in the nano-EHL approach.
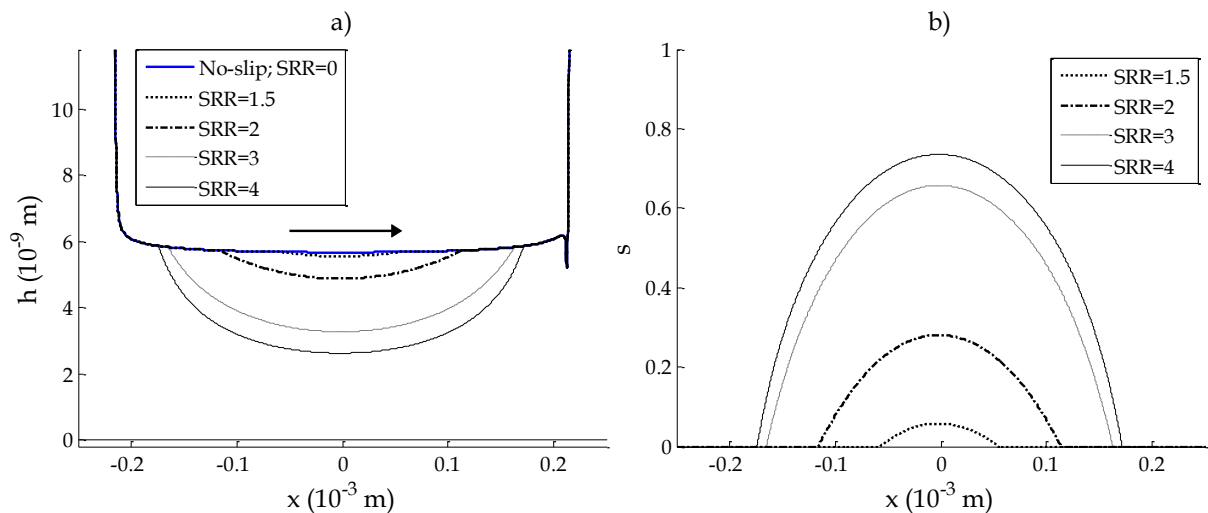
Figure IV-11: Film thickness modification (a) and slip domain dependence (b) for positive SRR values, obtained from the nano-EHL model with slip on the lower surface. The arrow represents the surface entraining the fluid in the contact.

IV.5.3 *Relationship between slip, film thickness and lubricant flow*

To analyze the interdependence between interfacial flow and the gap height, it is necessary to consider lubricant flow in the contact zone. In fact, a change occurring at the boundary can influence the dynamic behavior in the lubricant across the whole film thickness. To exemplify this phenomenon, two main configurations will be compared to the Reynolds no-slip solution:

- *SRR*=-2, where the lower "slipping" surface moves at a speed $u_1 = 2u_m$ =2 m/s and the upper "sticking" one is stationary;
- *SRR*=+2, where the upper wall entrains the fluid and the lower one is fixed.

Figure IV-12 shows the velocity profiles across the film thickness for the *SRR*=-2 case. The no-slip boundary is valid in the inlet and outlet zones, where the lubricant moves with the imposed wall speed on both solids. However, the occurrence of wall slip in the contact center decelerates the lubricant near the lower 'non sticking' wall. The corresponding mass flow can be calculated as the integral of the velocity profile, visualized by the shaded areas in Figure IV-12:

$$\phi_m(x) = \rho(x)\left[\frac{1}{2\eta}\frac{\partial P}{\partial x}\cdot h^3\left(\frac{1}{3} - \frac{L_s + 0.5h}{L_s + h}\right) + u_2\left(\frac{L_s + 0.5h}{L_s + h}\right) + \frac{u_1}{2}\left(\frac{h}{L_s + h}\right)\right] \quad \text{(IV.34)}$$

where $u_2 = 0$ for *SRR*=-2. It should be noted that in the contact center the flow is mainly shear-driven and $u(z)$ is sensibly linear. In fact the Poiseuille term is negligible, as the pressure gradient $\approx 10^{12}$ Pa/m is several orders of magnitude smaller than $h^3 \approx 10^{-25}$ m^3. Hence, the contribution of pressure-driven slip on contact behavior can also be neglected. Thus, Equation (IV.34) simplifies to:

$$\phi_m(x) \approx \frac{\rho(x)u_1}{2}\left(\frac{h}{L_s + h}\right) \quad \text{(IV.35)}$$

When slip occurs, $L_s > 0$ and ϕ_m becomes smaller. However, this quantity must be conserved along the whole contact length, according to the fundamental hypotheses of the Reynolds equation. Thus, the formation of a dimple balances the flow decrease. This effect is shown graphically in Figure IV-12: the increased film thickness in the contact center compensates the deceleration of the lubricant, and the shaded area (representative of ϕ_m) stays constant.
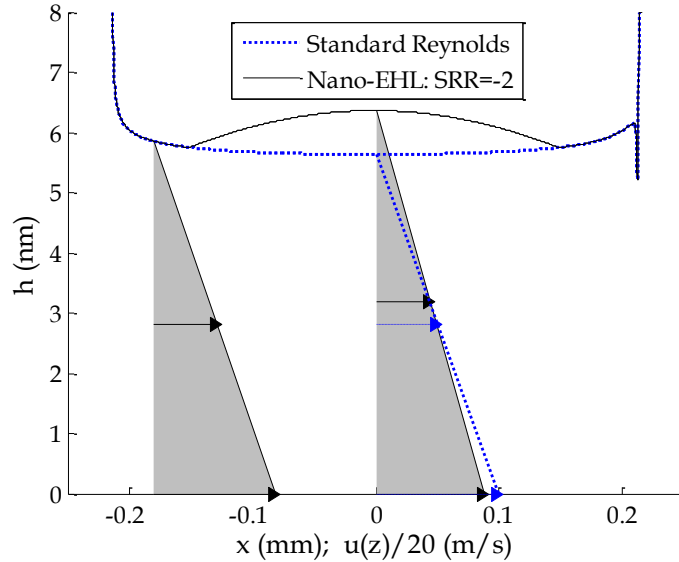
Figure IV-12: Lubricant dynamics in the contact for SRR=-2, where the lower "slipping" surface entrains the fluid. The arrows represent the velocity field in the lubricant (scaled by a factor of 20) and the shaded areas the fluid flow.

The opposite phenomenon occurs for *SRR*=2. In this case the upper, "sticking" surface entrains the fluid in and out of the contact. The occurrence of slip accelerates the lubricant near the lower wall (Figure IV-13), thereby increasing fluid flow in the center of the contact. This trend is confirmed by the following equation:

$$\phi_m(x) \approx \rho(x)u_2\left[1 - \frac{h}{2(L_s + h)}\right] \quad \text{(IV.36)}$$

When slip occurs, $L_s > 0$ and ϕ_m becomes larger. A decrease in film thickness occurs to compensate this phenomenon and ensure the continuity of the lubricant flow in the whole domain. As shown graphically in Figure IV-13, the minimum of h is shifted from the outlet to

the slip zone to compensate the acceleration of the lubricant, and the shaded area stays constant.
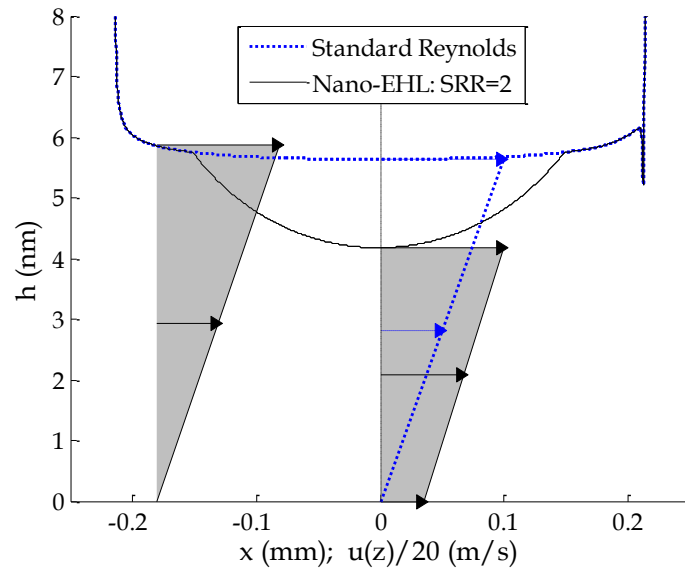
Figure IV-13: Lubricant dynamics in the contact for SRR=2. Lubricant dynamics in the contact for SRR=-2, where the upper "sticking" surface entrains the fluid. The arrows represent the velocity field in the lubricant (scaled by a factor of 20) and the shaded areas the fluid flow.

IV.5.4 *Pressure results in presence of slip on the lower surface*

An important quantity in a lubricated contact is the pressure distribution *P* in the contact domain, which balances the external load. This result of the Reynolds equation depends on the geometry of the gap separating the surfaces. As the occurrence of slip affects the film thickness, causing sudden changes in wall curvature, this phenomenon may also impact the Poiseuille term and the resulting pressure field.
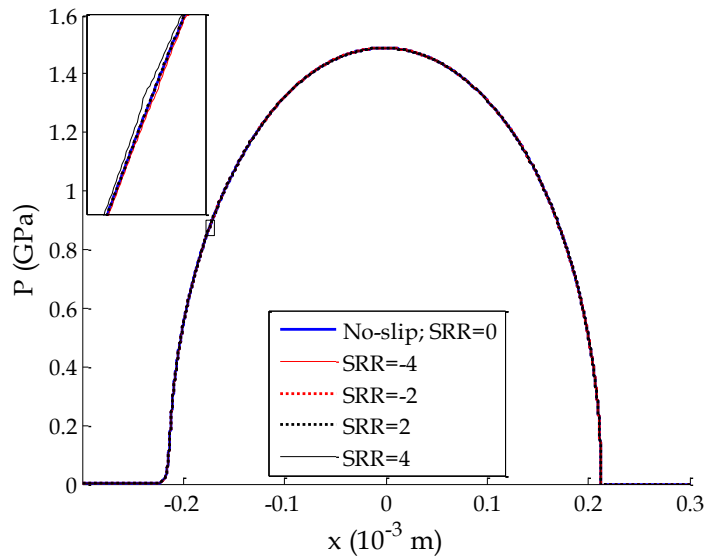
Figure IV-14: Pressure distribution along the contact abscissa for different SRR values. A zoom reveals the presence of low amplitude spikes and dips in the profile (here for SRR=4).

Nevertheless, Figure IV-14 shows that P is not significantly modified with respect to the no-slip case. Some spikes and dips are observed on the curves in correspondence with the dimple formation or the reduction in the gap height. Their amplitude is extremely small. In fact, the aforementioned film thickness gradients occur in the central zone, where h is of the order of magnitude of some nanometers and the Poiseuille term of the Reynolds equation is negligible.

IV.5.5 Influence of slip on friction

Another fundamental parameter for the performance of a lubricated contact is the global friction coefficient c_f, related to the tangential force opposing the movement of the solid bodies and the ensuing energy losses. In an elasto-hydrodynamic regime where no surface contact occurs, it is governed by shearing of the fluid.

However, in Chapter III it was shown that the wall-fluid momentum transfer, represented by the local shear stress τ_{zx} at the interface, plays a significant role under confined conditions. This quantity is limited for weakly corrugated surfaces like the chosen CuO[001]. As a consequence, the lubricant is not fully sheared and the wall velocity difference is accommodated through interfacial slip: the local shear stress is smaller than in the standard no-slip case.

The friction coefficient is obtained by integrating τ_{zx} along the shearing direction over the whole pressurized zone, and dividing the result by the external load w. In the case of two slipping surfaces, c_f is given by:

$$c_f = \frac{1}{w}\int_{\Omega_C}\tau_{zx}(x)dx = \int_{\Omega_C}\left[\eta\frac{(1-s)(u_2-u_1)}{h} - \frac{h}{2}\frac{\partial P}{\partial x}\right]dx \approx \int_{\Omega_C}\left[\eta\frac{(1-s)(u_2-u_1)}{h}\right]dx \qquad \text{(IV.37)}$$

In the configuration with slip solely on the lower surface, the following expression is used:

$$c_f = \frac{1}{w}\int_{\Omega_C}\tau_{zx}(x)dx = \int_{\Omega_C}\left[\eta\frac{u_2-u_1}{L_s+h} - \frac{\partial P}{\partial x}\frac{h^2}{2(L_s+h)}\right]dx \approx \int_{\Omega_C}\left[\eta\frac{u_2-u_1}{L_s+h}\right]dx \qquad \text{(IV.38)}$$

In both cases c_f is mainly governed by the shearing of the fluid in the contact center. As shown by the previous nano-EHL results, this domain is heavily affected by the presence of slip. Hence, a friction modification can also be expected at a macroscopic level.

A traction curve can be obtained by tracing the friction coefficient as a function of the Slide-to-Roll Ratio. This is first done in Figure IV-15 for the modified Reynolds equation with two slipping surfaces (Section IV.2.1).

The no-slip Reynolds theory for a Newtonian fluid and isothermal conditions predicts a linear (c_f, SRR) dependence. This trend is followed by the nano-EHL model for SRR values ranging from -1.5 to 1.5: under these conditions, slip is limited by the low wall velocity difference and the effect on friction is negligible.

On the other hand, a significant slip enhancement in the contact center occurs for $|SRR| \geq 2$, and c_f is smaller in comparison to the no-slip case. In fact, the larger film thickness (dimple) in the contact center leads to reduced shear rates and lower friction, in accordance with Equation (IV.37). Since no shear-thinning or thermal effects are considered, the

phenomenon is solely due to the modification of interfacial flow in the contact. Finally, the friction reduction is limited due to the saturation of slip: the friction coefficient still increases linearly with SRR, but with a lower rate than for the no-slip case.
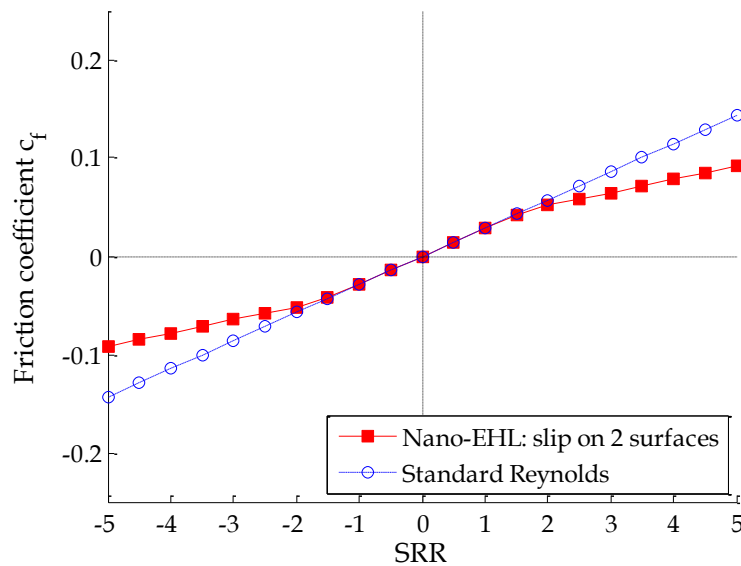
Figure IV-15: Traction curves for the no-slip case and nano-EHL model featuring identical slip conditions on both surfaces.

While the previous configuration with two slipping surfaces showed a symmetrical evolution of c_f with positive or negative Slide-to-Roll-Ratios, the behavior for the nano-EHL model with slip on a single surface must now be analyzed. The corresponding traction curve is shown in Figure IV-16: as was the case for the film thickness, opposite behaviors characterize positive and negative wall velocity differences.
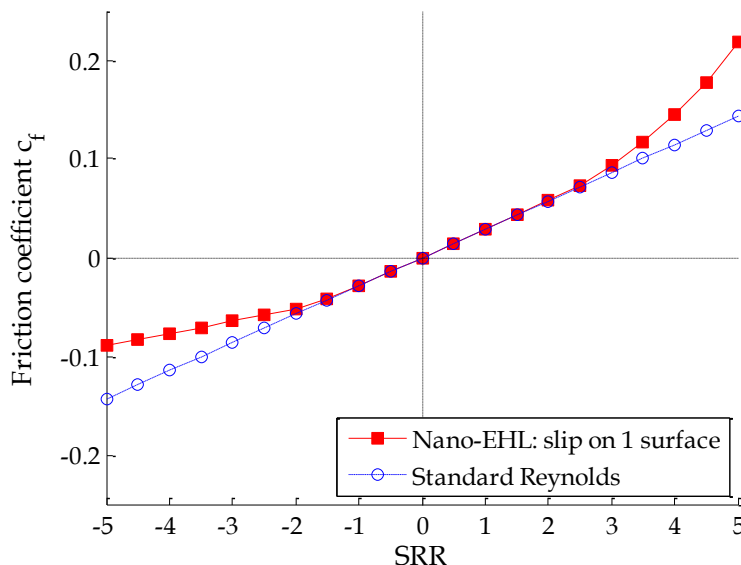
Figure IV-16: Traction curves for the no-slip case and nano-EHL model featuring slip on the lower surface only.

The results for $SRR<0$, where the slipping surface entrains the fluid, are very similar to the previous ones from Figure IV-15. The friction coefficient is reduced as a significant

modification of interfacial flows occurs for SRR<-2 in the contact center. Again, the dimple formation leads to lower shear rates and stresses, in accordance with Equation (IV.38). Moreover, these results are in accordance with the trends from Molecular Dynamics simulations from Chapter III.2, which reported that the modification of interfacial flow entrains a local shear stress reduction compared to the no-slip case.

On the other hand, Figure IV-15 shows a significant friction increase for positive Slide-to-Roll-Ratios, starting from SRR>2. This evolution is more difficult to interpret, because it seems to contradict nano-scale results. Nevertheless, in the local friction analysis of Section III.2 the shear stress reduction was observed on a single nano-patch of the contact featuring a constant gap width.

In reality, the film thickness is severely reduced in the macroscopic model. As a result, the shear rate is increased leading to higher tangential stresses in Equation (IV.38). Additionally, the lubricant viscosity η rises due to the higher degree of confinement, as shown in Figure IV-17 by the enhancement term $\psi(x)$ from Equation (IV.25).
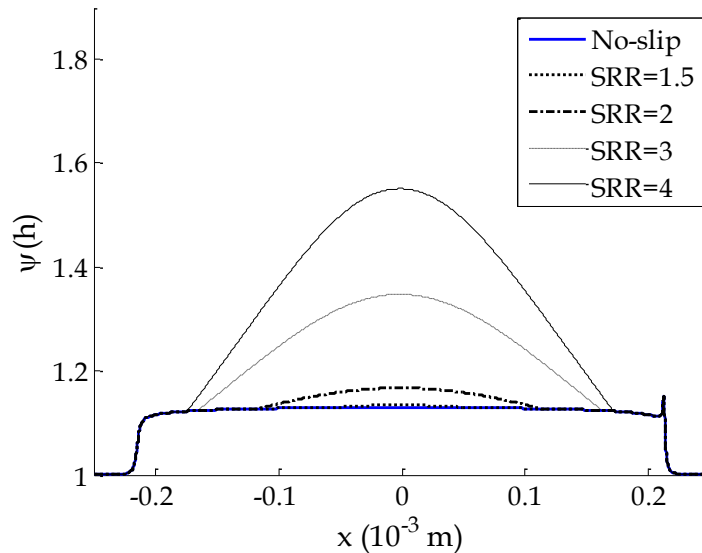
Figure IV-17: Viscosity enhancement term ψ along the contact abscissa for positive SRR, obtained from the nano-EHL model with slip on the lower surface.

In the no-slip case the central film thickness is around 6 nanometers, and the viscosity increase is roughly 10 %. As interfacial flow is modified, h drops to 3 nm at high Slide-to-Roll Ratios: the fluid enters the transition zone towards a glass-like state (see Section III.3.3) and the enhancement term is around 60 %. According to Equation (IV.38), both the film thickness decrease and higher lubricant viscosity contribute to the larger friction values.

In conclusion, the nano-EHL model shows that the occurrence of slip in molecularly confined films can severely affect the frictional behavior of a macroscopic contact with molecularly thin films. In fact, the modification of interfacial flow may entrain a dimple formation and lower shear stresses, or a film thickness reduction causing a friction enhancement. Hence, understanding the causes of slip is capital to fully characterize the behavior of modern tribological applications. The role played by the operating conditions was already identified in the previous Sections; the effect of wall topology will be investigated hereafter.

IV.5.6 Influence of surface nature

Contact interfaces feature a complex landscape of materials and orientations. Micrometer structures such as grains can be observed: each of them is characterized by a particular composition and disposition of nanometer-scale lattices. Molecular Dynamics simulations of Chapter III.2 showed that under confinement, a wide range of slip values can be obtained depending on the wall-fluid pair. As the surface topology varies significantly along a contact, similar trends can be expected for boundary flow.

In order to analyze its impact, different wall topologies characteristic of 100Cr6 bearing steel [147] are introduced in the nano-EHL model with slip on the lower surface. Though a semi-analytical slip law combining both surface nature and the operating conditions was not provided, qualitative results can be obtained by using the preliminary Equation (III.33) given at the end of the previous Chapter. The results are shown in Figure IV-18 for different materials. In accordance with atomistic simulations of Table III-3, weakly corrugated surfaces such as α–Fe[110] show larger modifications in boundary flow and film thickness. On the other hand, sticky surfaces like iron oxide maintain the no-slip condition even for high wall velocity differences, and the classical EHD solution is obtained.
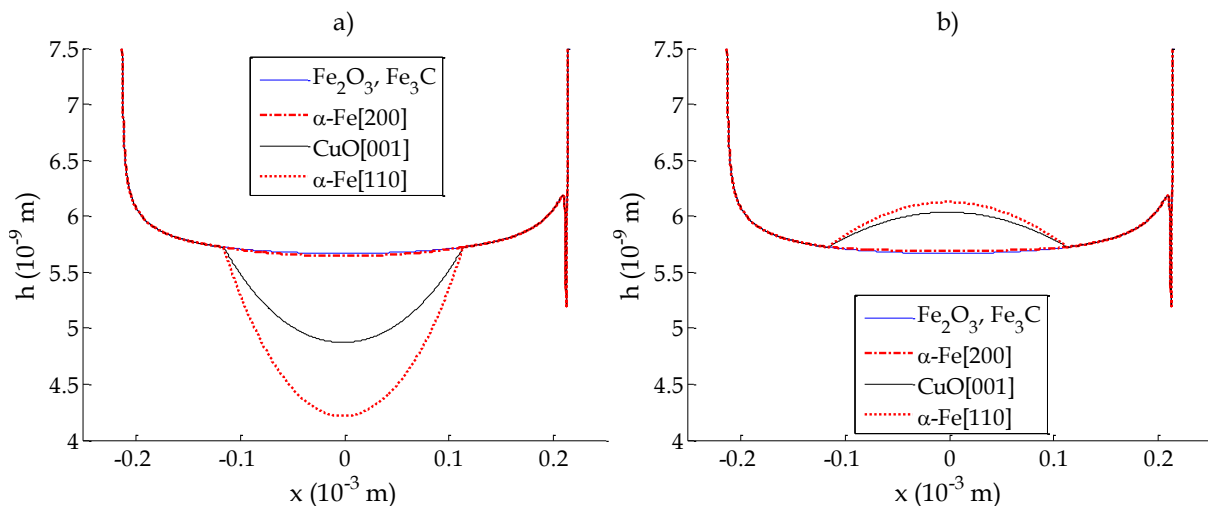
Figure IV-18: Film thickness along the contact abscissa for different surface materials, from the nano-EHL model with slip on the lower surface. a) SRR=2; b) SRR=-2.

To conclude the multi-scale study on surface nature, the impact of variations in surface composition along the contact is then analyzed. Some grains are introduced on the lower wall on the x-direction: their size is 30 μm [148], roughly corresponding to one fifteenth of the Hertzian contact width. In absence of characterization data on their nanometric structure, it will be assumed that the material and atomic orientation are constant on each grain. Furthermore, only the SRR=2 case is considered to avoid transient effects related to the movement of the lower, slipping surface and the associated grain structure. The evolution of the film thickness and pressure distribution along the contact length are shown in Figure IV-19 and Figure IV-20 respectively.
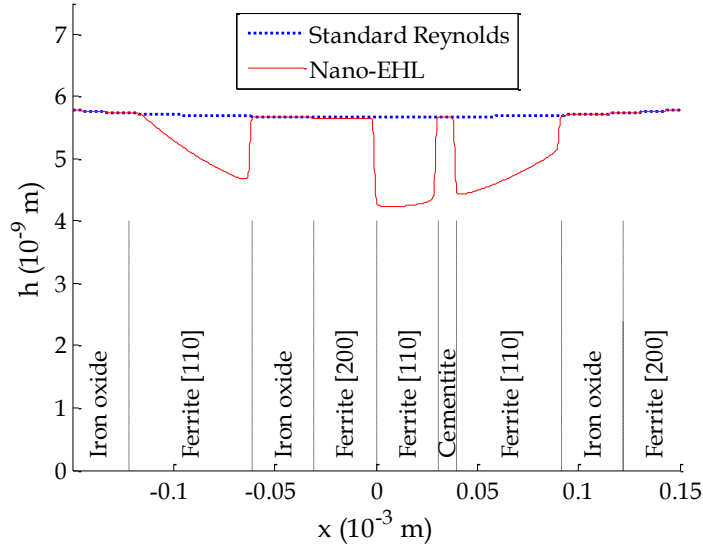
Figure IV-19: Zoom on the central film thickness in presence of grains from the nano-EHL model with slip on the lower surface, for SRR=2. The reader is invited to notice the sensibly different scale lengths for the abscissa and film thickness.
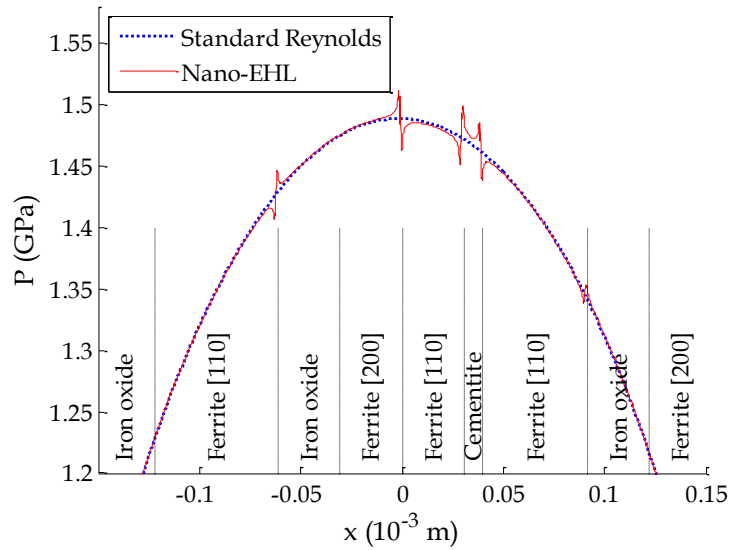
Figure IV-20: Zoom on the central pressure distribution in presence of grains from the nano-EHL model with slip on the lower surface, for SRR=2.

Two striking results can be observed. First, the gap width varies locally following the surface composition. At the grain boundaries the slip condition can change significantly, causing sudden variations in lubricant flow in the film thickness. Second, these jumps entrain a modification of the pressure distribution along the contact, with the formation of pressure spikes and dips. Their amplitude is larger than the slight kinks observed in Section IV.5.4 due to the higher gradients in h.

The effect of lubricant nature will not be considered in this study. Throughout this Chapter, the presence of a nanometric film for the chosen configuration with smooth surfaces was due to the use of an Ultra-Low-Viscosity Fluid (n-octane). Traditional base oils feature

longer alkane chains or branched architectures, and their viscosity is 1-2 orders of magnitude larger. As a consequence, the film thickness under the elasto-hydrodynamic regime is around 0.1 μm, and the effects of molecular confinement disappear [65].

Nevertheless, the impact of different lubricant types could be considered in continuous models where real surface roughness profiles are accounted for. In fact, a micrometer-scale waviness is typically present on the solid bodies, with an amplitude comparable to the gap height. Hence, the reduction in lubricant quantity in modern tribological application could lead to direct asperity contacts with nano-thin films trapped in the junctions. These possible extensions of the nano-EHL theory will be presented in the concluding remarks hereafter.

IV.6 Conclusion

The second objective of this research was to investigate the impact of nanometer scale effects on macroscopic contacts. For this purpose a multi-scale strategy, called nano-EHL, was proposed to integrate results of atomistic simulations into continuous models. On one hand semi-analytical laws issued from Molecular Dynamics characterize the behavior of thin lubricant films. On the other hand, the classical equations of the lubrication theory are modified to take into account the effects occurring under severely confined conditions.

The role of wall slip was investigated in this Chapter. The Reynolds equation for the fluid flow was modified to take into account this phenomenon, and the classical no-slip condition was replaced by a Navier-type boundary. The corresponding slip length was characterized as a function of the operating conditions, surface and lubricant nature through the semi-analytical laws provided in the previous Chapter. The coupled resolution of these two equations constituted the core of the nano-EHL approach. The model was completed by the elasticity theory for solid body deformation, the pressure-viscosity and pressure-density relationships for the lubricant and the load balance and film thickness equations. The numerical system was solved through a Finite Element method based on a fully coupled approach.

The nano-EHL model was applied on a stationary, isothermal line contact under operating conditions typical of the elasto-hydrodynamic regime. Furthermore, an ultra-low viscosity lubricant was employed, resulting in a nanometric film thickness. As a consequence slip occurred at the center of the contact zone when the wall velocity difference was not nil. This phenomenon leads to a profound modification in the film thickness, lubricant flow and friction compared to the standard lubrication theory.

In the configuration with identical slip on two surfaces, the literature reported the formation of a dimple, i.e. an increase in the gap height in the center of the contact. This phenomenon was also observed in the newly developed nano-EHL model with both a 'sticking' and a 'slipping' wall, when the latter entrained the fluid in the contact. As wall slip occurs in the central zone, the fluid velocity and mass flow are reduced: an increase in film thickness compensates this phenomenon and ensures the continuity of the lubricant flow in the whole domain. The increase in gap height results in a lower shear rate and friction.

Nevertheless, the opposite effect was also observed through the nano-EHL model with one slipping wall. In configurations where the 'sticking' surface entrains the lubricant, the modification of interfacial flow on the opposite wall accelerates the fluid across the film thickness. This effect is balanced by a severe reduction of the gap width to ensure the continuity of mass flow, and the minimum of h is shifted from the outlet zone to the center of the contact. The increase in confinement leads to larger shear rates, an enhancement of the lubricant viscosity, and consequently higher friction.

Finally, an interface featuring grains with different compositions and orientations was considered; wall slip and boundary flow change significantly for each material. As a consequence, the film thickness and pressure distribution vary locally following the micrometer-scale structure of the surface, with jumps occurring at the grain boundaries.

These results show the importance of using a multi-scale approach to better characterize the performance of modern tribological applications. The reduction of the lubricant quantity or the use of ultra-low-viscosity fluids leads to nanometer-scale confinement in the fluid. In return, the ensuing molecular effects have a deep influence on the macroscopic contact behavior.

While this Chapter was dedicated to the occurrence wall slip, other atomistic phenomena may nevertheless come into play in confined interfaces. During the development of the nano-EHL approach, it was supposed that the lubricant remains in its liquid-like state. While this condition holds true even for gap widths down to 3-4 nanometers, even smaller surface separations can be expected from the current trends in film thickness reduction, in presence of starvation effects and roughness on the surfaces.

Two main phenomena are expected under these conditions. First, the lubricant loses its liquid-like state and undergoes a glass transition, featuring a much higher viscosity and significantly different rheological properties. Second, spots of the surfaces can come into direct contact, leading to a dry friction regime. This process, called local film breakdown, will be explored in the next Chapter.

V Towards local film breakdown

The main hypothesis of the standard full-film lubrication theory is the continuity of the lubricant film and the absence of contact spots between the solid bodies. This condition holds true in presence of smooth surfaces. In the previous Chapter, no direct wall-wall interactions were observed even for molecularly thin film thicknesses and the resulting nanometer-scale effects.

However, a micrometric roughness with amplitudes between 0.01 and 1 μm is typically present on real surfaces [58]. As the film thickness is severely reduced to the nanometer scale, the separation of the solid bodies is not guaranteed in the whole contact zone. This effect is enhanced by the use of ultra-low viscosity fluids or by starvation conditions typical of the current trends in lubricated applications [61]. Hence, film breakdown may occur locally and the peaks of the asperities could come into direct contact. In this scenario, a mixed regime is achieved, where molecularly thin films and dry friction zones coexist.

In the asperity junctions very severe conditions in pressure and shearing are concentrated, leading to significant wear and heat generation. Friction is typical of a dry regime, and is usually very large compared to that of a lubricated part of the contact. The characterization of the contact spots between solid bodies is therefore of capital importance for the performance of the mechanism.

At the macroscopic scale, a global friction coefficient is imposed to model the tangential interactions. However, its value varies enormously with the surface composition, finishing process, environmental and operating conditions etc. [53]. Moreover, molecularly thin lubricant films can stay trapped between the surfaces: their presence determines the interfacial properties of the junctions under shearing, as well as friction in the whole system.

It was previously shown that even at surface separations of 2-3 nanometers the oil retains a liquid-like behavior. However, its properties change significantly as confinement is increased and the last molecular layers are squeezed out from the contact. A viscosity enhancement of several orders of magnitude was observed experimentally in correspondence with the transformation towards a solid-like state [11, 84, 85]. Moreover, a reversible glass transition was reported for surface separations lower than one nanometer [12, 64]. A stick-slip behavior occurred under shearing; continuous sliding was obtained if a critical yield stress was exceeded [12].

Atomistic simulations provided a deeper insight on the structural effects in the fluid. In a series of articles [6, 9, 14, 72], Gao et al. investigated alkane films down to two lubricant layers separating the surfaces under low pressure conditions. They reported a step-like reduction in the film thickness, a strong ordering of the lubricant and oscillating solvation forces, coherent with the crystallization of the lubricant. These effects were frustrated by molecular branching or by the presence of surface roughness. Persson and coworkers [73-77] developed a large-scale model in order to understand the squeeze-out of alkanes with different chain lengths between two asperities. They confirmed the previous trends for the lubricant behavior prior to solid body contact. Moreover, they observed that longer chains allow a better surface separation, as they are able to withstand larger pressures before being squeezed out of the asperity junction.

However, the aforementioned studies did not focus on the behavior under shearing conditions during local film breakdown; hence, the objective of this Chapter is to propose a first insight on the dynamics and friction under shearing of the last lubricant layers prior to the direct contact of the surfaces. Hence, some limits of both the nano-EHL model and the semi-analytical laws for boundary flow in molecularly confined fluids will be explored.

The work is organized as follows. After a brief explanation of the chosen configurations and parameters, reference results will be presented for a system with smooth, wettable surfaces under a severe reduction of the film thickness. A particular focus will be placed on the fluid structure and dynamics, as well as on the connection with friction and heat generation in the system. The influence of the molecular structure of the lubricant will be discussed afterwards. Finally, in the last section the impact of surface geometry and wettability on the behavior at the interface will be investigated under increasingly severe conditions, from molecularly thin films to solid body contact.

V.1 Reducing the lubricant quantity

The frictional behavior under shearing of the last lubricant layers separating the surfaces before the occurrence of solid body contact is studied using Molecular Dynamics simulations. The system is very similar to the one presented in Chapter II, and corresponds to a nano-patch of the contact area. The dimensions along the x- and y-directions are increased to provide good statistical averaging despite the reduction in the number of lubricant molecules during local film breakdown. They are chosen roughly $L_x \approx 10$ nm in length and $L_y \approx 10$ nm in width; the micrometer-scale surface curvature is not considered. Again, periodic boundary conditions are applied along x and y, allowing the determination of the shear response of the confined fluid. Hence, the quantity of lubricant during a simulation stays constant and can be defined through the number of carbon groups per surface unit $\bar{n}_{CHx}$:

$$\bar{n}_{CHx} = \frac{n_{mol} \cdot n_{CHx,mol}}{L_x \cdot L_y} = \frac{n_{mol} \cdot n_{CHx,mol}}{S} \tag{IV.39}$$

with n_{mol} the number of fluid molecules in the system, $n_{CHx,mol}$ the number of carbon groups per alkane (for example 16 for n-hexadecane), and $S = L_x \cdot L_y$ the area of the contact patch. Since no outflow of the lubricant takes place and a constant external load is applied on the walls, the film thickness stays constant for a given $\bar{n}_{CHx}$. In order to achieve the direct contact between the solid bodies and simulate the transition to a mixed lubrication regime, simulation sets are performed where n_{mol}, and consequently $\bar{n}_{CHx}$, are progressively reduced. The resulting approach between solid bodies is quantified by the gap width h, measured as the minimum distance between the atoms of the lower and upper walls. When h decreases to zero, the surfaces come into direct contact and film breakdown occurs.

Reference results are obtained using this method for n-hexadecane, representative of a standard base oil. The surfaces are composed of smooth iron oxide (Fe$_2$O$_3$ [001]), which features a strong interaction with the lubricant (see Chapter III) and is therefore non-slipping. The simulations are performed under the operating conditions from Section III.2: $\Delta u =20$ m/s, $P =500$ MPa and $T_w =300$K. The evolution of the film thickness, the lubricant

structure and dynamics, friction and heat generation as a function of the quantity of fluid in the contact will be discussed hereafter.

V.1.1 Film thickness and density

Figure V-1 shows the surface separation h as a function of the quantity of lubricant in the contact. This evolution does not represent a dynamic squeeze-out process, but a series of snapshots obtained through an artificial reduction of the number of fluid molecules in the system. As expected, the film thickness decreases with $\bar{n}_{CHx}$; furthermore a step-like profile is observed, because only an integer number of lubricant layers can form parallel to the surfaces [9, 91]. For high $\bar{n}_{CHx}$ values, the curve stays relatively smooth, as the layer structure remains compressible under high pressures [75]. However, the steps become more marked as n_C decreases: in fact, the ordering action of the surface potential on the fluid becomes stronger due to the lower film thickness, causing a significant deviation from bulk properties. Finally, the height of the steps and the layers is roughly 4 Å, which is consistent with the molecular width of an alkane chain [7]. This value also corresponds to the minimum surface separation: hence, geometrically smooth surfaces remain separated by at least one lubricant layer for the chosen $\bar{n}_{CHx}$ range and operating conditions.
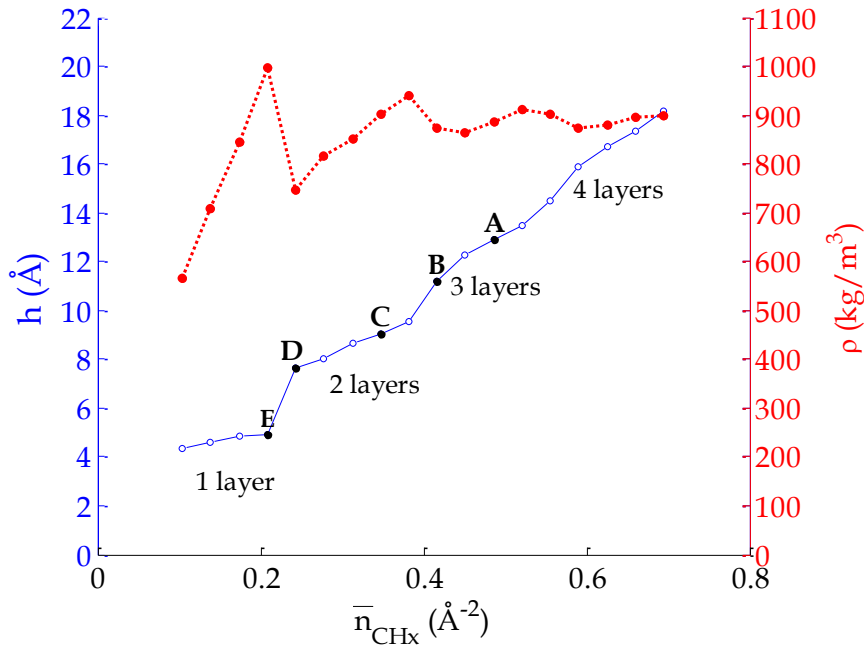
Figure V-1: Film thickness and average lubricant density as a function of the n-hexadecane quantity in the nano-patch. Fe$_2$O$_3$ walls, P=0.5 GPa, u$_2$=-u$_1$=10 m/s, T$_{wall}$=300K.

The average lubricant density ρ is also shown in Figure V-1. For high $\bar{n}_{CHx}$, its value is roughly equal to 890 kg/m^3, which corresponds to the bulk density for n-hexadecane under an external pressure of P =500 MPa [37]. However, oscillations appear as the number of fluid molecules in the contact is reduced. All the layers are fully saturated at local ρ maxima, whereas they are only partially filled just before the transition to a lower layer number, corresponding to the local ρ minima [6, 91]. These oscillations become more marked for low $\bar{n}_{CHx}$ values, which is due to the increasing influence of the surface potential on the fluid and to the resulting deviation from bulk properties.

Further insight into the lubricant structure is provided by the density profiles across the film thickness and the corresponding snapshots of the system in Figure V-2. In all cases, well-ordered layers form near the surfaces with a constant maximum density of 2550 kg/m³.

a) Configuration A: $\bar{n}_{CHx}$ =0.486 Å^{-2}

shearing (x-) direction →

b) Configuration B: $\bar{n}_{CHx}$ =0.417 Å^{-2}

shearing (x-) direction →

c) Configuration C: $\bar{n}_{CHx}$ =0.347 Å^{-2}

shearing (x-) direction →

d) Configuration D: $\bar{n}_{CHx}$ =0.243 Å^{-2}

shearing (x-) direction →

e) Configuration E: $\bar{n}_{CHx}$ =0.208 Å^{-2}

shearing (x-) direction →
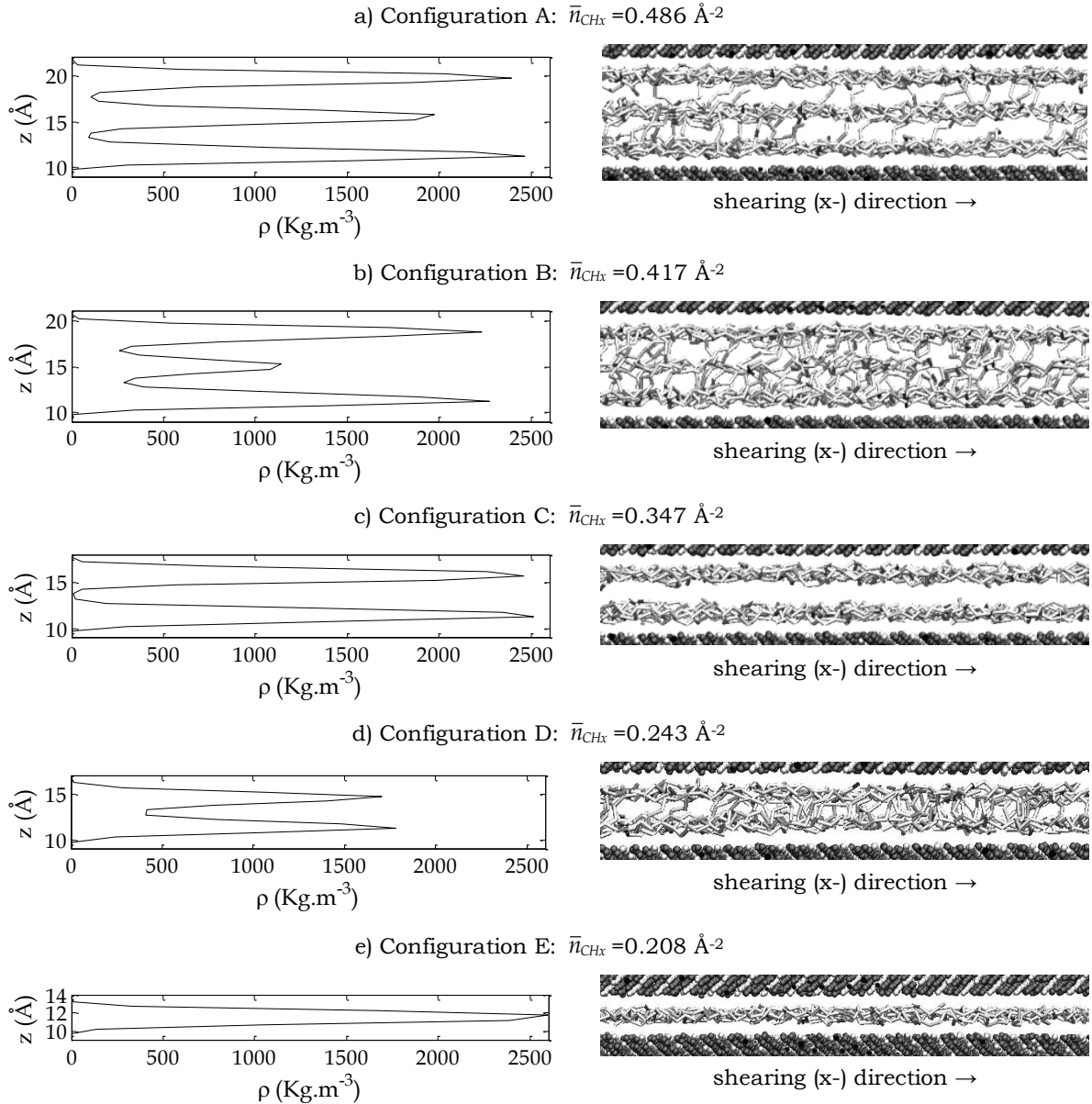
Figure V-2: Density profiles and snapshots of the system for the configurations A to E (see Figure V-1), showing the succession of well-layered and disordered states at the transitions from 3 to 1 layers.

On the other hand, the structure at the center of the film can feature significantly different states. For example a well-ordered, three-layered structure with few bridges is shown in Figure V-2a. When the quantity of lubricant in the contact is reduced, the density of the central layer decreases and a disordered configuration is observed (Figure V-2b). In particular, the snapshot of the system shows zones along the shearing direction where the central layer is formed, whereas in others no clear ordering of the lubricant can be seen and the fluid molecules are severely entangled. This configuration will probably not be stable during a squeeze-out process [73, 74]; however, it can provide an insight on the frictional behavior

during the transition between integer numbers of layers and will be further considered. Finally, the central layer disappears as $\bar{n}_{CHx}$ is decreased and a two-layered ordered state is achieved, featuring no bridges (Figure V-2c). A similar process characterizes the transition between four to three and two to one layers. The density profiles from Figure V-2 are coherent with results from [6, 14] for a system with smooth surfaces.

In conclusion, even if the squeeze-out of the fluid from the system is not directly simulated, the simulation sets with decreasing $\bar{n}_{CHx}$ capture the main phenomena reported in experimental [11, 12, 64, 84, 85] and numerical studies [6, 9, 14, 72] about the transition from ultra-thin full-film lubrication towards solid body contact. The ordering effect of the surface potential extends across the whole film thickness. As the lubricant is disposed into a slab-like structure with superimposed layers, it cannot be considered anymore in a liquid state. Hence, its dynamics and frictional behavior under shearing may deviate significantly from the typical fluid bulk properties: these quantities are analyzed hereafter under local film breakdown conditions.

V.1.2 *Lubricant dynamics and friction*

The velocity profiles within the film thickness for different quantities of fluid in the contact are shown in Figure V-3.
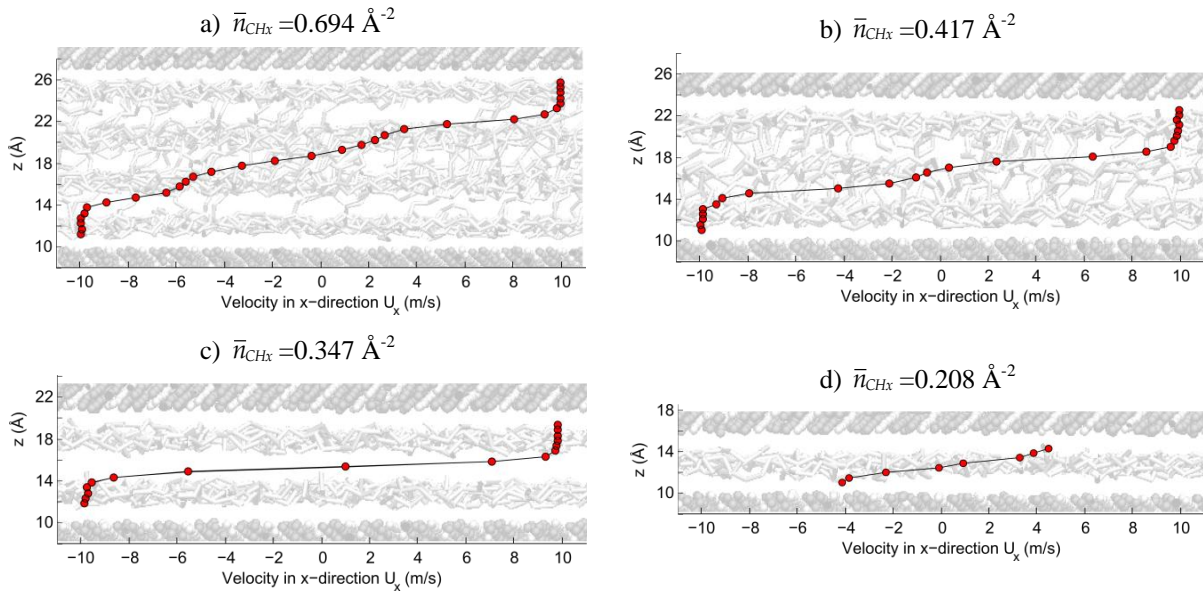
Figure V-3: Velocity profiles across the film thickness for different quantities of n-hexadecane in the nano-patch. Smooth Fe_2O_3 walls, P=0.5 GPa, $u_2=-u_1=10$ m/s, $T_{wall}=300K$.

A step-like profile can be observed for two or more layers. The outmost ones are locked to the surfaces and move with the imposed wall velocities, due to the strong tangential solid-fluid interaction for the chosen iron oxide lattice. Shearing occurs between layers, in correspondence with the jumps in the velocity profiles. Hence, the lubricant behaves like a superposition of solid slabs (the layers) sliding on top of each other. Finally, when a single lubricant layer separates the solids, shearing occurs mainly at the surface-fluid interface: large wall slip is observed in Figure V-3d, with some velocity accommodation occurring within the layer.

Such remarkable behavior confirms the glass transition towards a solid-like state reported in the literature [12]. The standard notion of viscosity is therefore no longer applicable under extreme confinement, in contrast with systems featuring a film thickness of six or more molecular widths in Chapter III.2. This result also underlines the limits of the proposed semi-analytical slip laws and the nano-EHL model during local film breakdown. Though the nano-rheology of the lubricant cannot be described by bulk properties, its resistance to shearing can nevertheless be quantified by the friction force opposing the movement of the surfaces. A representative value is the shear stress τ_{zx}; its evolution as a function of the quantity of lubricant in the contact is shown in Figure V-4.
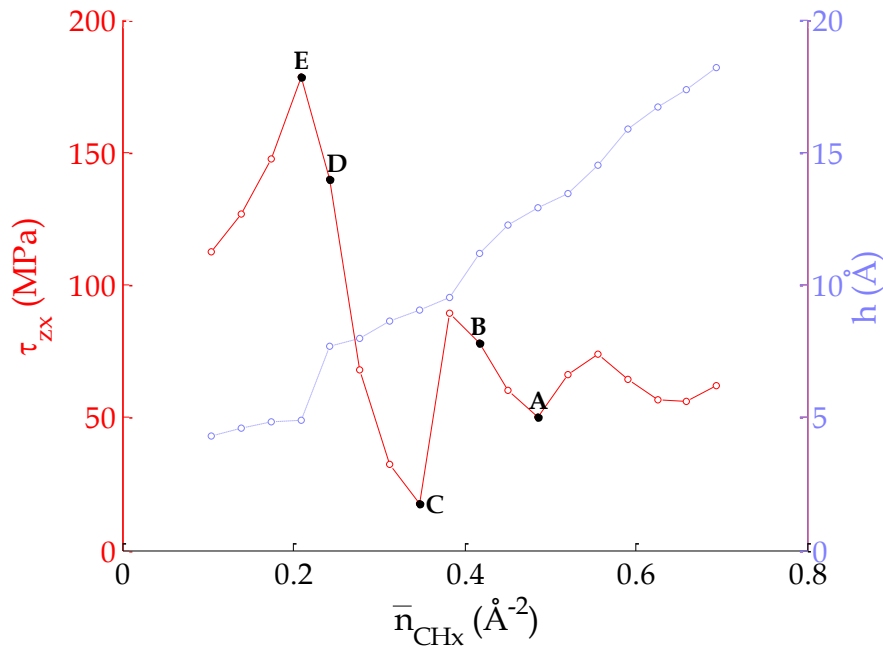
Figure V-4: Shear stress and as a function of the quantity of n-hexadecane in the contact. Smooth Fe$_2$O$_3$ walls, P=0.5 GPa, u$_2$=-u$_1$=10 m/s, T$_{wall}$=300K.

Large oscillations in the friction values are observed, which become increasingly larger when $\bar{n}_{CHx}$ is reduced. A comparison with the fluid structure and density profiles from Figure V-2 clearly shows the dependence between shear stress values and the organization state of the lubricant molecules. When two or more layers separate the surfaces, no wall slip takes place and friction is solely determined by the internal cohesion of the lubricant. In particular, the number of inter-layer bridges is responsible for the resistance to shearing of the slab-like structure described in Section V.1.1.

In well-ordered configurations A and C, only a very small number of bridges prevents the layers from sliding on top of each other, resulting in low friction. On the other hand, significantly larger shear stresses are required to disentangle the disordered states (in example configuration B). Such dependence of the fluid internal cohesion and resistance to shearing with bridging is coherent with results from the literature for highly confined lubricants [23, 149]. Furthermore, the existence of a low friction state for n-alkanes under severe confinement and shearing, where the fluid molecules were disposed in a slab-like structure without bridges was reported in [158].

The maximum in friction is reached as one single lubricant layer separates the surfaces (configuration E). In this case, a new phenomenon governs the friction process: interfacial slip occurs and a significant velocity accommodation takes place at the wall-fluid boundary instead of between the fluid layers. As shown in Section III.2, the shear stress is determined by the maximum tangential momentum transfer from the surface to the lubricant. Since the chosen iron oxide surfaces feature very strong wall-fluid interactions, a high shear stress ensues. Moreover, the onset of strong adhesion effects is observed. As the gap width is smaller than the cutoff distance of the van-der-Waals forces, the surfaces interact along the z-direction through the Lennard-Jones potential. The resulting adhesion pressure, shown in Figure V-5, is of the same order of magnitude as the external one, further increasing friction [56]; this effect may be amplified by long-range Coulombic interactions between walls, which are not considered in this study.
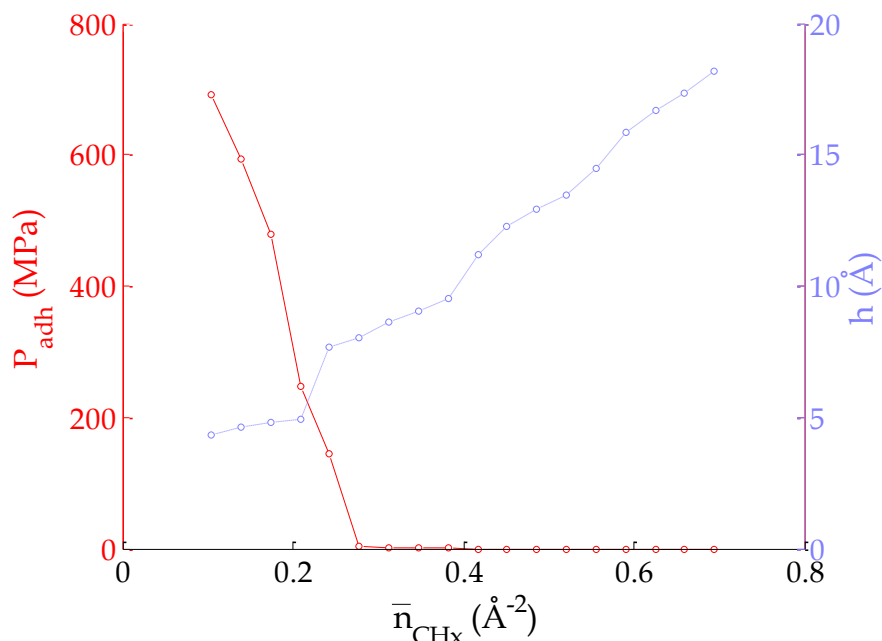
**Figure V-5: Normal adhesion pressure and film thickness as a function of the quantity of n-hexadecane in the contact. Smooth Fe₂O₃ walls, P=0.5 GPa, u₂=-u₁=10 m/s, Twall=300K.**

Finally, a shear stress decrease is observed when the lubricant quantity is further reduced. The last layer features a reduction in density and becomes rarified, but it still fully supports the external load and adhesion forces between the walls. Fewer molecules must slide on the surfaces, resulting in a lower tangential force opposing the movement of the walls. As a consequence, friction is reduced compared to the full-layer configuration.

V.1.3   Heat generation in the contact

The significant changes in nano-rheology and the transition to a solid-like behavior occurring during local film breakdown may significantly impact thermal effects in the contact zone. In fact, studies on heat generation for highly confined lubricants [23, 28, 159] showed that the thermal energy generated by the shearing of the lubricant is related to friction in the system.

Under the chosen operating conditions and for film thicknesses down to 5-6 molecular diameters, no significant temperature increase was observed in the contact: all the simulations were therefore performed at a constant wall temperature. However, the aforementioned literature reveals also the existence of critical shear rate from which the lubricant starts to heat up severely. This threshold is exceeded for the small film thicknesses reached under local film breakdown. As outlined in the previous section, friction is profoundly modified under a severe film thickness reduction, and depends on the organization state of the lubricant molecules. Hence, a preliminary study on heat generation and the temperature evolution in the system is performed.

Instead of imposing a constant surface temperature, a Variable Boundary Temperature algorithm [28, 159] is used hereafter. The heat flux dissipated by the wall thermostat is imposed as a boundary condition on semi-infinite steel bodies with thermal conductivity $\Lambda = 50$ W/mK and diffusivity $\alpha = 13.6 \cdot 10^{-6}$ m²/s [44]. The surface temperature is then calculated dynamically from the dissipated heat flux, the bulk properties of steel and the temperature far away from the contact interface.

Moreover, three configurations typical of local film breakdown are chosen in order to understand the relation between heat generation, friction and lubricant ordering. One is characteristic of a disordered state (configuration B), the second of a highly ordered structure without inter-layer bridges (configuration C), and the third corresponds to the maximum in friction with one full layer separating the surfaces (configuration E). Figure V-6a and Figure V-6b show the evolution of the fluid temperature and shear stress with time.
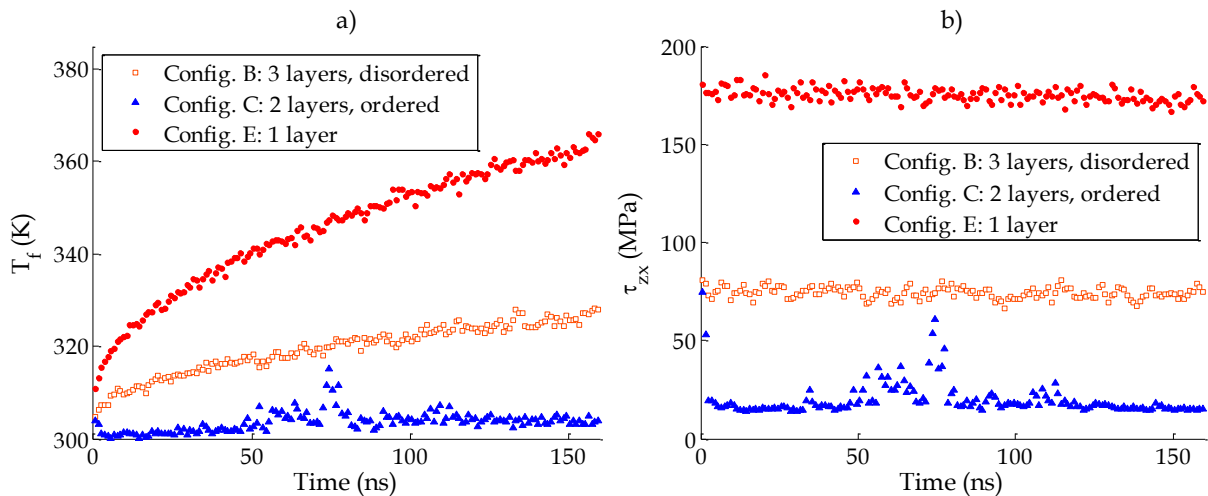
Figure V-6: Thermal effects in the confined n-hexadecane as a function of time, obtained using the VBT algorithm [28, 159] for smooth Fe2O3 walls. a) Fluid temperature b) Shear stress.

The low friction configuration shows no significant temperature increase due to the small heat source term. Some heating effects appear in correspondence with a rise in friction, caused by the momentary formation of interlayer bridges; however, they soon disappear as the lubricant resumes a bridgeless configuration, and a stable temperature value is reached.

On the other hand, both high friction configurations feature a significant temperature increase, and no thermal steady state is achieved in a simulation time of 160 ns. In these cases, the heat generated by the shearing of the lubricant is not dissipated fast enough through

the walls. Moreover, Figure V-6b shows no significant decrease of the friction during time: thermal thinning does not occur, since the lubricant has a slab-like structure and the shear stress is only influenced by inter-layer bridging. As a consequence, a significant heating of the system could ensue, causing the dissociation and oxidation of the molecules [160, 161]. A detailed study of these phenomena would require the implementation of tribochemical reactions in the simulations, which lies beyond the scope of this preliminary study.

Nevertheless, the current model can be used to understand which parameters cause high friction in the system and therefore predict the occurrence of significant thermal effects. In the following, the impact of the lubricant molecular shape and the surface topology will be investigated.

V.2 Impact of surface and lubricant nature during local film breakdown

V.2.1 Influence of the lubricant type

It has been thoroughly reported in the literature that the molecular structure of the confined fluid has a significant impact on the ordering of the lubricant in ultra-thin films [10, 14, 16, 162]. Experiments showed that spherical molecules are more sensible to the wall potential than linear chains: layered structures and the transition towards a glass-like state are observed at larger film thicknesses. On the other hand, the presence of branching reduced the ordering effects, and the lubricant remained liquid-like even under extreme confinement.

Sections V.1.1 and V.1.2 showed that the formation or absence of well- layered structures is a key parameter for the local frictional behavior during local film breakdown. Hence, two additional alkanes, representative of a Lennard-Jones fluid (methane) and a branched molecule (phytane), are studied under severe film thickness reduction and compared to linear hexadecane. The evolution of the surface separation and average density as a function of the quantity of lubricant in the contact for the chosen molecular structures are represented in Figure V-7.

For a given $\bar{n}_{CHx}$, methane features a larger film thickness compared to the other lubricants (Figure V-7a). In fact, the non-bonded CH_4 groups have a larger diameter than the CH_x-CH_x bond length in alkane chains, and therefore occupy a larger volume. The resulting density is lower, as shown in Figure V-7b. Moreover, marked steps in the film thickness evolution and density oscillations can be seen up to surface separations of five layers.

These effects show that spherical molecules are very sensible to the ordering effects of the wall potential, and the transition towards a solid like state occurs at large surface separations. In the case of linear chains, the deviation from bulk properties becomes apparent only for a film thickness of 2-3 molecular widths: hexadecane and phytane feature a smoother evolution for h and ρ. These results are coherent with the trends from the literature. In fact, while Lennard-Jones fluids confined between smooth, commensurate surfaces tend to form highly ordered structures, such layering effect is reduced when the chain length of the alkanes is increased [10].
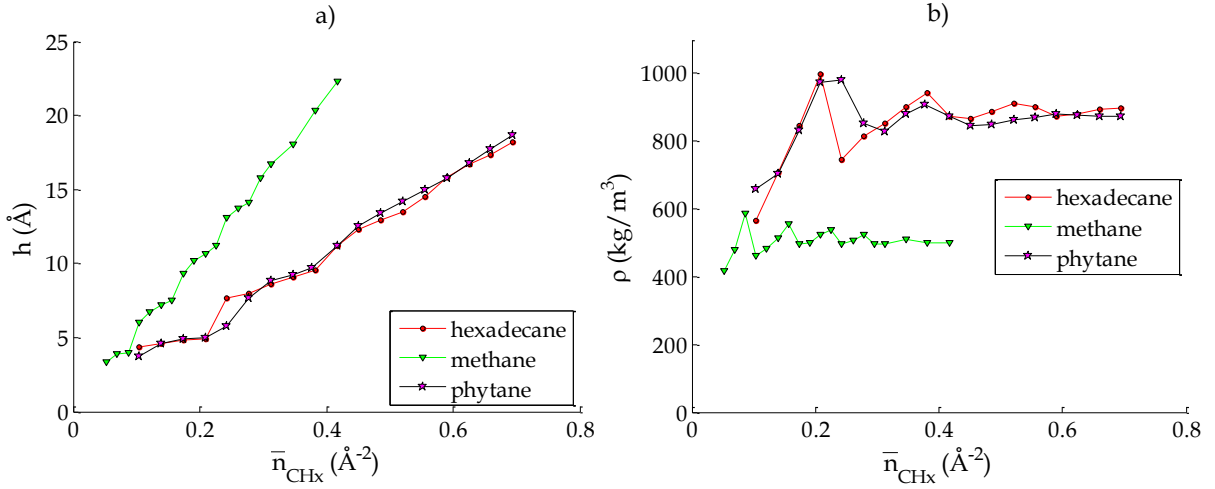
Figure V-7: Film thickness (a) and average lubricant density (b) as a function of the lubricant quantity in the nano-patch, for three different molecular architectures. Fe$_2$O$_3$ walls, P=0.5 GPa, u$_2$=-u$_1$=10 m/s, T$_{wall}$=300K.

Finally, the ordering effect of the surfaces is frustrated for branched molecules, and the formation of interlayer bridges is encouraged, resulting in a bulk-like behavior and less pronounced density oscillations compared to linear alkanes [14]. Hence, in the case of phytane the surface separation decreases quite smoothly down to two layers.

Figure V-8 represents the shear stress evolution for the chosen fluids. Methane is characterized by significantly lower τ_{zx} values compared to hexadecane. In fact, no inter-layer bridges can form, due to the spherical nature of the molecules, which reduces the internal cohesion of the fluid [23]. Furthermore, the disordered, entangled states and high friction maxima characteristic of linear alkanes cannot exist. Hence, the oscillations in shear stress observed for linear molecules are severely reduced. The small local maxima and minima are due to changes in diffusivity of confined Lennard-Jones fluids for full or partially filled layers respectively [91]. The significant increase in friction for low $\bar{n}_{CHx}$ is due to the occurrence of wall slip and the high adhesion forces between the surfaces.

Contrary to linear and spherical molecules, phytane shows high shear stress values for all the studied $\bar{n}_{CHx}$ range. Because of the molecular branching, strong interlayer bridging is observed in all configurations, resulting in a high internal cohesion of the fluid and high friction. However, when one single layer separates the surfaces, shear stress values are similar for phytane and n-hexadecane, as the friction process is governed by wall slip (see Section V.1.2). Hence, the same decrease in τ_{zx} is observed when the density of the last layer is reduced.
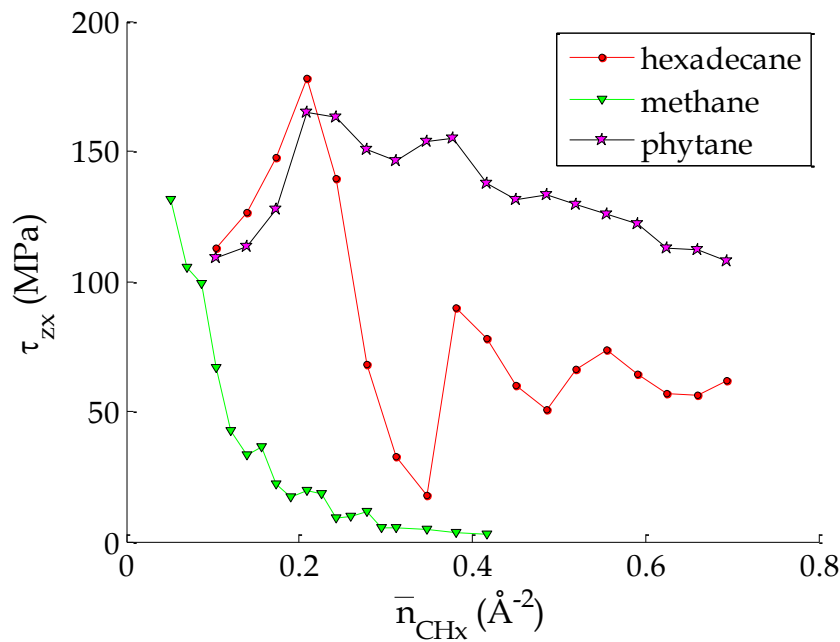
Figure V-8: Shear stress as a function of the lubricant quantity in the nano-patch, for three different molecular architectures. Fe₂O₃ walls, P=0.5 GPa, u₂=-u₁=10 m/s, T_wall=300K.

In conclusion, the ordering effects previously reported are therefore severely dependent on lubricant nature. However, the morphology and nano-geometry of the surfaces can also affect significantly the lubricant behavior during local film breakdown: their impact will be analyzed in the following Sections.

V.2.2 *Influence of surface nano-roughness: towards solid body contact*

According to the literature for nanometer-thick lubricant films [9, 104, 108] and the results from Appendix C, the presence of nanometer scale roughness can frustrate the formation of well-ordered layer structures. A similar behavior could be expected under local film breakdown, leading to a modification in the lubricant response to shearing. Moreover, the asperity peaks can interact directly and a mixed lubrication regime can be reached at the nanometer scale. To study these phenomena, nano-roughness is introduced on the upper wall by carving in the lattice a sinusoidal profile with a wavelength λ =24 Å and a peak-to-peak amplitude A =6 Å: the asperities are along the shearing (x-) direction only. The lower surface is kept geometrically smooth, and as previously both walls are composed of iron oxide.

The resulting evolution of the surface separation as a function of quantity of fluid in the system for smooth-rough case is shown in Figure V-9. In this case h is calculated as the distance between the asperity peaks and the lower wall. For a given $\bar{n}_{CHx}$, the film thickness is lower compared to a smooth-smooth configuration, as the lubricant molecules fill the asperity valleys. Moreover, the nano-rough wall frustrates the ordering in the lubricant, and the density peak characteristic of a well-defined fluid layer near the upper surface disappears (Figure V-10).
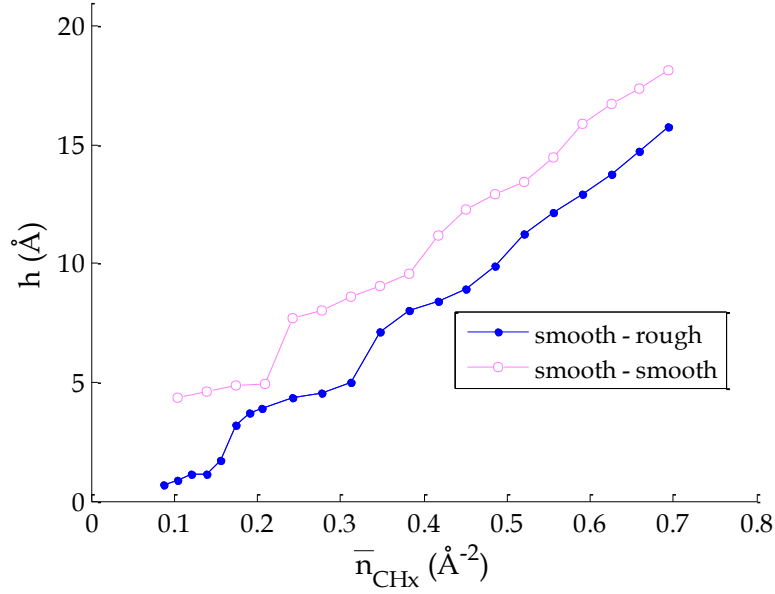
Figure V-9: Film thickness as a function of the n-hexadecane quantity in the nano-patch, for smooth-rough and smooth-smooth Fe$_2$O$_3$ walls. P=0.5 GPa, u$_2$=-u$_1$=10 m/s, T$_{wall}$=300K.
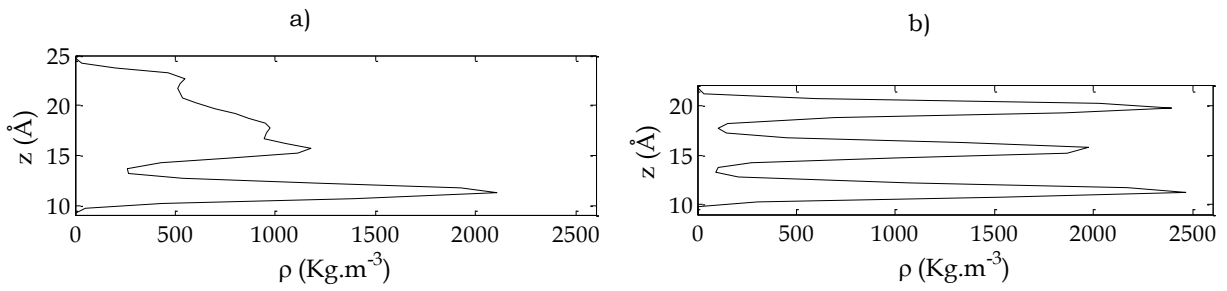
Figure V-10: Density profiles across the lubricant for smooth-rough (a) and smooth-smooth (b) Fe$_2$O$_3$ walls. $\bar{n}_{CHx}$ =0.486 Å^{-2}, P=0.5 GPa, u$_2$=-u$_1$=10 m/s, T$_{wall}$=300K.

Hence, low friction configurations with few interlayer bridges cannot be formed. As shown in Figure V-11, the shear stress rises in a monotonic fashion as the lubricant quantity is reduced, up to a local maximum for a film thickness of one molecular layer (configuration F). No large friction oscillations, characteristic of the system with two smooth walls, are observed.

As the lubricant quantity is further reduced, it is possible to observe local film breakdown. The surface separation between the asperities and the lower surface (Figure V-9) decreases to less than 0.1 nm, and is of the order of magnitude of the interatomic distance in the iron oxide lattice. Hence, direct surface contact is observed while lubricant molecules are still present in the contact: a mixed lubrication regime is reached at the nanometer scale.

This process is detailed in Figure V-12, while the corresponding friction behavior is shown in Figure V-11. In Configuration F (Figure V-12a) the two surfaces are separated by a full layer of hexadecane molecules. Friction is governed by the occurrence of wall slip, akin to the results for Configuration E in Section V.1.2. When $\bar{n}_{CHx}$ is further reduced, the density of the last layer separating the surfaces decreases (Configuration G, Figure V-12b). The shear stress is also lower, as fewer molecules must slide on the walls. The last layer then splits into

pockets located in the valleys of the roughness profile (Configuration H, Figure V-12c), which fully support the external pressure. Due to the small surface separation, extremely strong adhesion forces act between the top of the asperities and the lower surface: the resulting local increase in pressure is of 1.75 GPa, corresponding to 3.5 times the applied one on the Molecular Dynamics system. A significant rise in shear ensues, and a friction behavior typical of solid-body contact starts to appear [163].
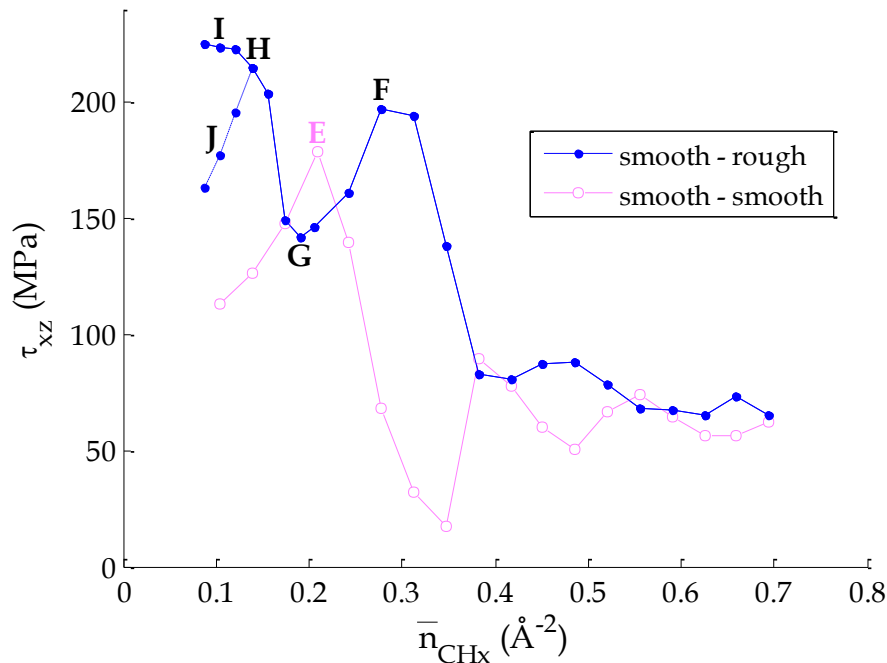
Figure V-11: Shear stress as a function of the n-hexadcane quantity in the nano-patch, for smooth-rough Fe_2O_3 walls. P=0.5 GPa, u_2=-u_1=10 m/s, T_{wall}=300K.

A further reduction of the lubricant quantity may lead to different scenarios depending on the disposition of the fluid molecules in the contact patch. At the beginning of each simulation the alkane chains can be evenly or unevenly distributed in the asperity valleys. Such configuration is kept during the whole simulation, as the chosen nano-roughness profile prevents the flow of the fluid from one asperity valley to the other once the last layer splits into pockets.

The first case occurs when the fluid is initially uniformly spread in the contact patch, which is representative of the squeeze-out of a full lubricant film [76]: Configuration I (Figure 9.d) is then reached. In this state, the fluid pockets do not provide enough lift to separate the surfaces, leading to the maximum in friction due to the strong wall-wall interactions. It is also possible to observe the flattening of the asperity peaks in the contact spots, which was reported in the literature for a dry friction regime between surfaces [164]. It should be noted that, as the crystal lattices of the solid bodies come into direct contact plastic deformation and wear may occur, which cannot be simulated by the current modeling. Hence, improved potentials between metal atoms, such as EAM [128], should be used to characterize such effects, though this lies beyond the scope of this work.

a) Configuration F: $\bar{n}_{CHx}$ =0.278 Å^{-2}

shearing (x-) direction →

b) Configuration G: $\bar{n}_{CHx}$ =0.191 Å^{-2}

shearing (x-) direction →

c) Configuration H: $\bar{n}_{CHx}$ =0.139 Å^{-2}

shearing (x-) direction →

d) Configuration I: $\bar{n}_{CHx}$ =0.104 Å^{-2}

shearing (x-) direction →

e) Configuration J: $\bar{n}_{CHx}$ =0.104 Å^{-2}

shearing (x-) direction →
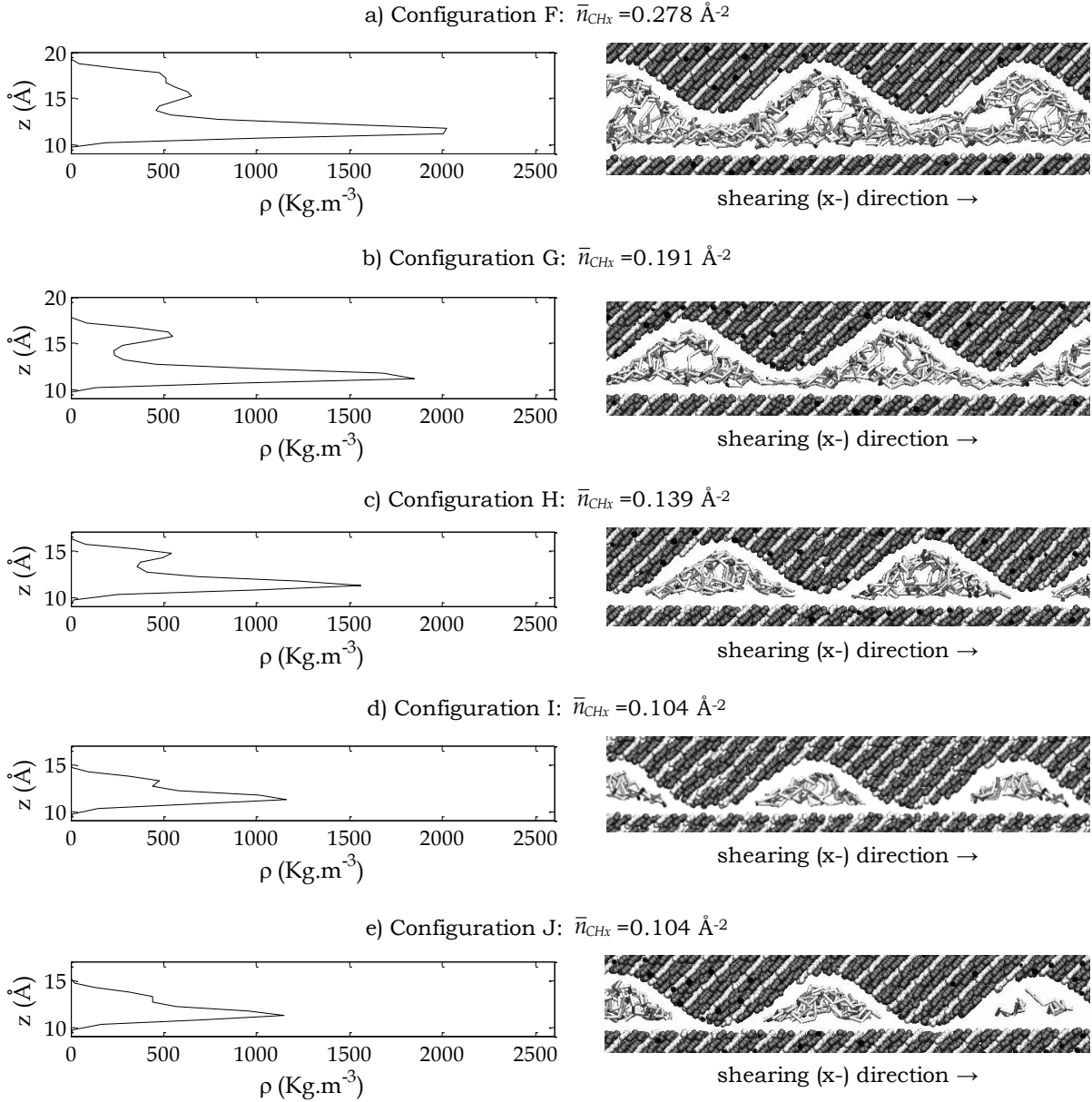
Figure V-12: Density profiles and snapshots of the system for configurations F to J (Figure 8) for local film breakdown. a and b) one layer between the surfaces; c) formation of lubricant pockets in the roughness valleys; d) flattening of the asperity peaks; e) alternative configuration to I with partially and fully filled pockets.

A second scenario is observed if the alkane chains are not evenly distributed in the asperity valleys at the beginning of the simulation. This may occur during the squeeze-out of liquid bridges and under severely starved conditions where the contact area is not completely filled with lubricant [75]. As a consequence, in Configuration J (Figure V-12.e) some pockets are almost empty of fluid molecules, whereas others are almost completely filled and fully support the external load. Hence, the fluid retains its lubricating function, which results in a reduction in friction compared to Configuration I. In order to understand which of these two possible states would be most likely in a real contact, the shear simulations should be coupled with a squeeze-out model of the lubricant under an increasing external load [73, 76].

Different roughness profiles should also be considered, in particular to study the flow of the confined molecules around the asperities.

An additional parameter which can influence the lubricant behavior and friction during local film breakdown is the surface material. Its impact will be analyzed in the following.

V.2.3   *Influence of surface material and nano-geometry*

According to the results in Chapter III, each surface material and orientation features a characteristic tangential momentum transfer and flow boundary condition at the wall-fluid interface. This property influences interfacial flow in nano-confined films. For example, wall slip was observed for some morphologies, along with a reduction in friction. In order to determine whether a similar behavior can be expected under local film breakdown conditions, different combinations of surface composition and nanometer-scale roughness are analyzed.

Two surface materials with significantly different wall-fluid interaction properties are chosen. Iron oxide (Fe_2O_3 [001]) was used previously as an example of a non-slipping surface, as it features a strong corrugation potential and high commensurability with the lubricant. On the other hand, oxygen-terminated copper oxide (CuO [001]) is characterized by a weak tangential interaction with the fluid molecules, which favors the occurrence of wall slip under high pressure and shear rates (see Chapter III). Concerning the surface nano-geometry, the lower wall is kept smooth, whereas the upper one can be either flat or feature a sinusoidal roughness with a wavelength of 24 Å and a peak-to-peak amplitude of 6 Å.

Friction results for different configurations in wall materials and nano-geometry are reported in Figure V-13, while the corresponding lubricant dynamics across the film thickness, set at a constant $\bar{n}_{CHx}$ =0.550 Å^{-2}, are shown in Figure V-14.
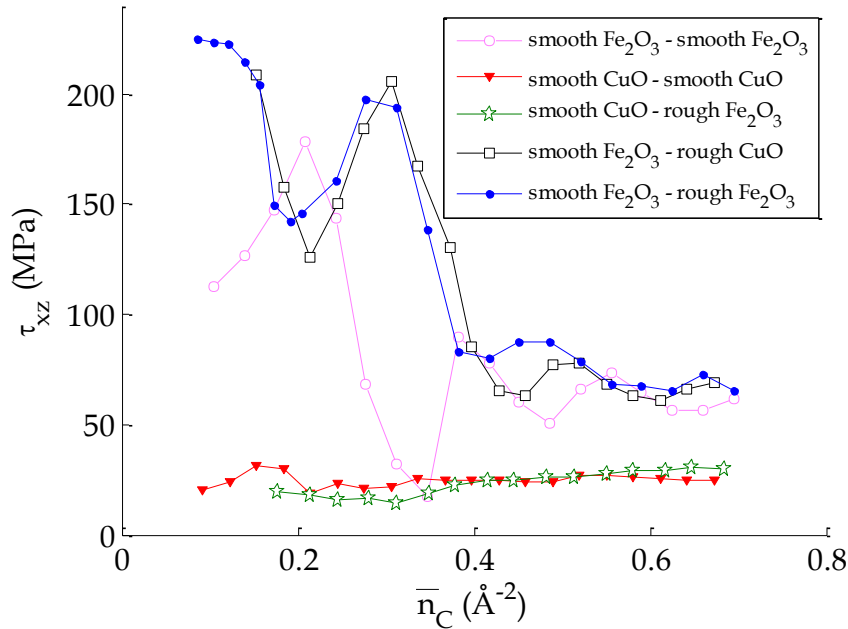
Figure V-13: Shear stress as a function of the n-hexadcane quantity in the nano-patch, for some combinations of wall materials and nano-roughness. P=0.5 GPa, u₂=-u₁=10 m/s, T_wall=300K.
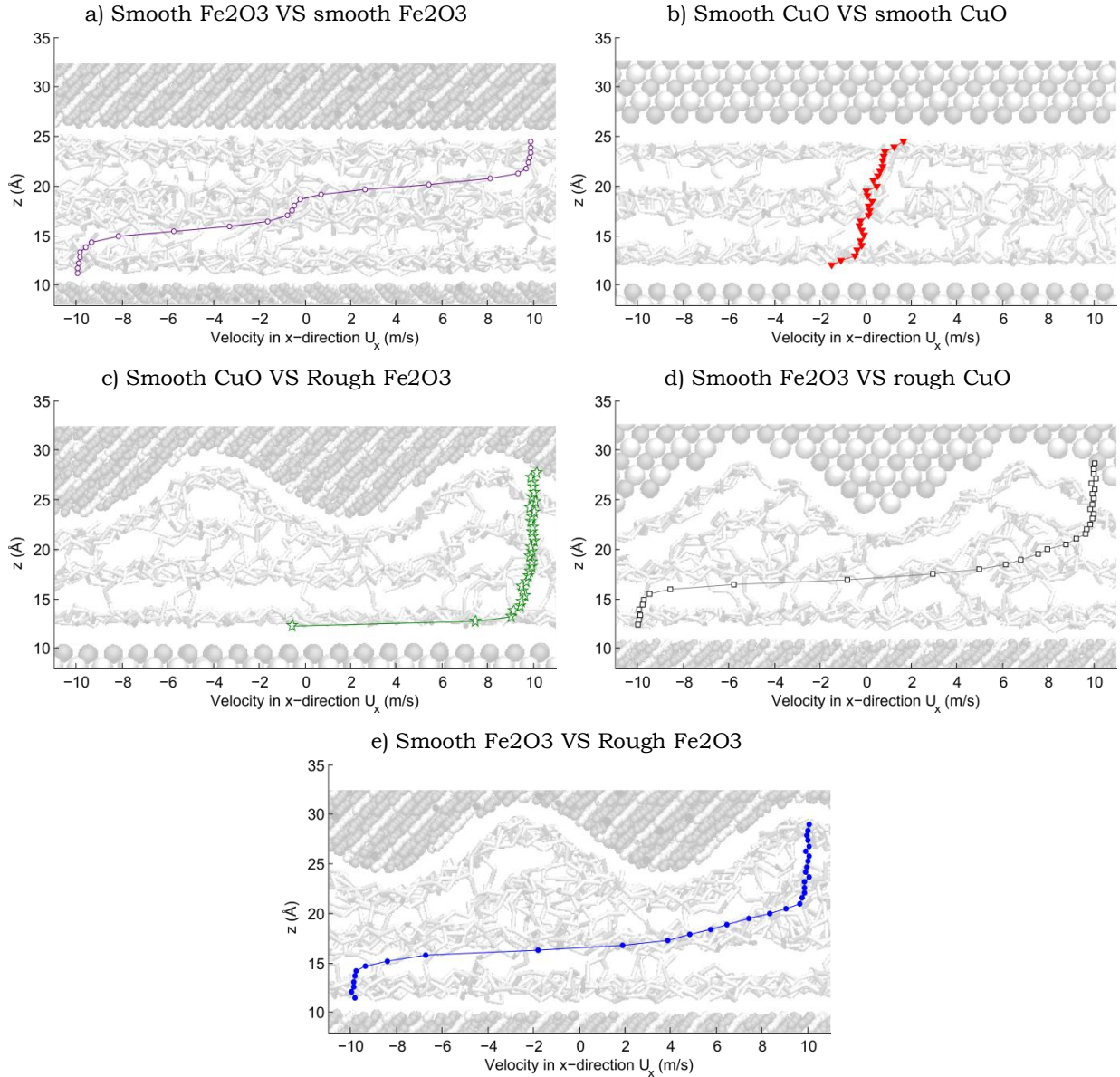
Figure V-14: Velocity profiles across the film thickness for different combinations of wall materials and nano-roughness ($\bar{n}_{CHx}$ =0.550 Å^{-2}).

In the case of two smooth iron oxide walls and surface separations larger than two molecular widths, no wall slip was observed (Section V.1.2). Shearing occurred between layers, in correspondence with the jumps in the velocity profiles. However, when two smooth CuO surfaces are present in the system, the tangential momentum transfer at the wall-fluid interface is limited by the weak interactions and commensurability. As a consequence wall slip occurs: the fluid is not entrained and the velocity accommodation across the gap height occurs only at the wall-fluid interfaces (Figure V-14b). This phenomenon limits friction to a small, almost constant value, independent of the surface separation. Figure V-13 shows that a single smooth, non-wettable CuO surface is sufficient to limit friction in the system whatever the nature or morphology of the other wall: total slip occurs on the lower copper oxide wall and the fluid is fully entrained by the upper one (Figure V-14c).

The presence of surface roughness completely suppresses the wall slip phenomenon on non-wettable surfaces [108]. This is well shown in Figure V-14d by the velocity profiles of the lubricant confined between a rough CuO wall and a smooth Fe_2O_3 one. The outmost fluid layers are entrained by the surfaces with the imposed wall velocities, akin to the case represented in Figure V-14e for two wettable iron oxide surfaces. Finally, as both the lubricant ordering and wall slip are frustrated by nano-roughness on the CuO surface, no low friction state is present and high shear stress ensues (Figure V-13).

V.3 Conclusion

The objective of this Chapter was to explore the limits of the previous studies in this work. In particular, the slip laws and the nano-EHL model were formulated by assuming a liquid-like state for the confined fluid. While this hypothesis was verified for film thicknesses down to 10 molecular widths, it may not be valid anymore as the last lubricant molecules are squeezed out of the contact. In fact the fluid may undergo a transition towards a solid-like state, and direct surface contact could occur, leading to a mixed lubrication regime at the nanometer scale.

To simulate this process, called local film breakdown, the current Molecular Dynamics simulations were pushed to their limit. By reducing the quantity of lubricant molecules in the system it was possible to characterize the behavior under shearing of the last lubricant layers separating the walls.

The film thickness evolves in a step-like manner, corresponding to the formation of an integer number of layers in the lubricant. The fluid can reach two possible configurations. Ordered structures are characterized by well-defined layers with little to no bridging. On the other hand, transition zones where the central layers merge together feature a disordered, entangled state. A stepped velocity profile is observed under shearing, with velocity jumps occurring between layers. The standard notion of viscosity is therefore no longer applicable during local film breakdown, and the fluid undergoes a solid-like transition. In the absence of wall slip for smooth wettable surfaces, inter-layer bridging and the degree of organization within the lubricant determines the fluid resistance to shearing. Hence, shear stress values oscillate when the thickness is reduced featuring local minima for well-ordered configurations and maxima for entangled states. A friction maximum is reached for a surface separation of one single lubricant layer, where large wall slip takes place. High shear rates and friction in the system lead to significant heat generation, as well as a rapid temperature increase in the lubricant and the surfaces. On the other hand, friction and heat generation are reduced in well-ordered states, and no significant heating of the lubricant is observed.

It was also shown that lubricant nature affects the tribological behavior of the system. Compared to linear molecules, methane (representative of a Lennard-Jones fluid) cannot form inter-layer bridges, resulting in lower friction and no oscillations in shear stress when the lubricant quantity is reduced. On the other hand, the present results suggest that branching favors the presence of bridges and the shear stress minima characteristic of linear molecules disappear.

Nanometer-scale roughness on the walls frustrates the ordering in the lubricant, leading to high shear stress values; in this case significant thermal effects may also be expected. Furthermore, spots of the surfaces can come in direct contact: the tribological behavior is typical of a dry friction regime, characterized by high adhesion, shear stresses and asperity deformation. Finally, friction can be limited by the occurrence of wall slip for smooth surfaces; however, this phenomenon clearly disappears when nanometer-scale roughness is present on the walls.

The results obtained in this Chapter open new possibilities for the characterization of direct surface interactions occurring as the lubricant quantity in an EHD contact is reduced significantly. Analytical laws can for instance be formulated to quantify the shear stress or the friction coefficient evolution with the local film thickness, operating conditions or the natures of the surface and the lubricant. These expressions would enable a straightforward integration into macroscopic models, thus allowing a deeper insight on the underlying physical phenomena in modern lubricated devices running under extreme conditions.

The study on local film breakdown concludes this manuscript. In the following, a general conclusion will summarize the main results obtained throughout this work. Finally, recommendations for future work will be given.

General conclusion

Nowadays, the demand is increasing for smaller, lighter, more efficient and environmentally friendly tribological systems. The consequent reduction in the quantity of oil and additives, as well as the use of low viscosity operating fluids as lubricants, is leading to a great reduction in the film thickness, which can reach the order of magnitude of a few nanometers. Under this state of molecular confinement, the fluid exhibits a behavior which contradicts many laws of continuum fluid mechanics. For example, oscillating solvation forces, density layering, a viscosity increase by several orders of magnitude and a transition to solid like state were reported in the literature. Finally, wall slip may occur at the surface-lubricant interface, in clear contradiction with the classical hypothesis of a no-slip boundary condition.

The aim of this work was to further investigate these molecular phenomena, in order to determine their dependence on the typical parameters characterizing a lubricated interface, as well as to understand their impact on the macroscopic behavior.

In **Chapter II**, atomistic simulations using the Molecular Dynamics method were developed to simulate the local behavior of severely confined fluids under shearing. A nano-patch of the contact domain was considered: all its elements were parametrized to account for realistic properties for the surface material, the fluid and the interface. Moreover, the disposition and dynamics of the fluid molecules under confined conditions were linked to the classical quantities of lubrication models, like the film thickness, density, velocity, viscosity, and friction.

In **Chapter III**, the Molecular Dynamics model was used to quantify interfacial flow through analytical laws as a function of different parameters characteristic of a contact interface. In particular the wall slip phenomenon, consisting of a velocity jump at the solid-fluid boundary between the moving surfaces and the neighboring lubricant molecules, was investigated.

A predictive model, based on the competition between surface and fluid natures, was developed to quantify this effect in presence of base oils confined between geometrically smooth walls. A surface parameter, obtained through a computationally inexpensive scanning technique, accounted for the wall-fluid interaction and commensurability with respect to alkanes. Contrary to slip models from the literature for canonical crystal lattices, this quantification method is also valid in the case of complex wall structures found in real contacts.

The surface parameter was then linked to the shear stress transferred to the fluid molecules at the interface. Low surface parameter values characterized weakly interacting surfaces, which featured limited friction and the occurrence of wall slip. On the other hand sticky walls with high surface parameters cause high interfacial shear stresses and the full shearing of the fluid.

The internal cohesion of the lubricant under confined conditions was described by a bulk viscosity term. Finally, an analytical law for wall slip prediction including both the fluid

viscosity and the surface characterization parameter was proposed. This approach allows quantifying slip for different wall-fluid pairs without the need to run expensive atomistic simulations.

The impact of the local operating conditions on interfacial slip was also studied through Molecular Dynamics simulations for a particular wall-fluid pair. Parametric studies were performed on pressures, surface velocities and film thicknesses characteristic of an elasto-hydrodynamic contact with a nano-confined film. The increase in wall slip with the level of shearing, confinement and pressure was fitted through an analytical law.

The expressions obtained in this Chapter can be used to quantify the flow at the wall-fluid boundary in each nano-patch of a contact zone for a wide variety of configurations typical of lubricated interfaces in EHD contacts. Thus, they allow a straightforward integration of nanometer slip effects into continuous models for the characterization of EHD applications with nano-thin films.

Chapter IV aimed at understanding the impact of interfacial slip on macroscopic contact behavior. For this purpose a multi-scale approach, called nano-EHL, was developed to bridge the gap between atomistic simulations and continuous models. The starting point was the classical elasto-hydrodynamic lubrication theory, based on the Reynolds equation for the lubricant flow and the elastic deformation of the solid bodies. The Reynolds equation was modified to include the occurrence of slip on a single surface. This molecular phenomenon was integrated into the macroscopic model through the analytical laws issued from Molecular Dynamics simulations of Chapter III.

The nano-EHL approach was then applied to a line contact with an ultra-low-viscosity lubricant and consequently a film thickness of a few nanometers. Wall slip on the lower surface, which featured weak wall-fluid interactions, is observed in the central zone of the contact. Its occurrence leads to a significant change in the lubricant flow, film thickness and friction.

A dimple was formed when the slipping wall entrained the fluid in the contact. In this case, the modification of interfacial flow causes a reduction of the fluid velocity and the mass flow across the gap height. A local increase in film thickness occurs to compensate this phenomenon and to ensure the continuity of the lubricant flow in the whole contact domain. Moreover, friction is reduced under high shearing conditions compared to the classical case with no slip.

The opposite behavior was observed when the sticking surface entrains the lubricant. The occurrence of slip at the opposite wall leads to an acceleration of the fluid, and consequently a larger mass flow across the gap height. This effect is balanced by a severe reduction of the film thickness. The ensuing increase in confinement generates viscosity enhancement effects and higher friction compared to the no-slip case.

Finally, the influence of surface composition characteristic of a more realistic contact interface was studied by considering a slipping wall with a grain-like structure. Local variations in slip for each grain material are reflected by jumps in the film thickness and oscillations in the pressure distribution at the grain boundaries.

Hence, this Chapter showed that the characterization of modern EHD applications, such as bearings lubricated through Ultra-Low-Viscosity fluids, required a comprehensive understanding of both their macro- and nanoscopic behavior. In this framework, the nano-EHL approach proved a promising tool for such multi-scale analysis, and may be extended from slip effects explored here to other physical phenomena characteristic of nano-confined fluids.

In **Chapter V** local film breakdown was studied through Molecular Dynamics to explore the limits of the previous approaches, which are valid for full-film conditions. By reducing the number of molecules in the contact, the transition from ultra-thin lubrication to solid body contact was simulated.

The formation of quantized layer structures and a step-like evolution of the film thickness were observed for linear alkanes confined between smooth walls. Shearing occurred between the layers, which behave like solid slabs sliding on top of each other. This shows that the lubricant is no longer in a liquid-like state during local film breakdown. Moreover, inter-layer bridging and the degree of organization within the lubricant determine the fluid resistance to shearing. An alternation of well-layered, low friction states and entangled configurations, characterized by high friction and heat generation, is observed.

The molecular structure influences the ordering of the fluid and the resulting shear stress. Spherical molecules were characterized by low friction due to the absence of inter-layer bridges, opposed to the always entangled states and high shear stresses for branched chains.

Surface geometry also affects the behavior of the confined interface: nanometer scale roughness frustrates the ordering of the fluid molecules, leading to high friction states whatever the surface composition. Furthermore, local film breakdown is observed when the asperities come into contact, with strong wall-wall interactions causing the shear stress maximum. Finally, the occurrence of slip for smooth, weakly interacting surfaces limited friction to a low, constant value; this phenomenon is nevertheless frustrated by the presence of a nanometric roughness on the surfaces.

In conclusion, this work opens new ways to characterize contact behavior in presence of nanometric films, by proposing an extensive characterization of molecular phenomena through atomistic simulations, and their integration into traditional continuous models through a multi-scale approach. The scope of application of this methodology encompasses elasto-hydrodynamic applications developed in the modern industrial context, which rely more and more on highly confined fluids. In addition to the slip effects analyzed throughout this work, the proposed approach could be extended to new physical phenomena and configurations, which would constitute a significant advance towards the formulation of numerical predictive tools for the development of modern tribological applications.

Recommendations

There are numerous opportunities to use the nano-EHL approach for a deeper understanding of the underlying phenomena occurring in a contact interface, as well as their influence on a whole contact domain. In particular, this study revolves around three different scales: the nanometer one for molecularly confined fluids, the micrometer one for the roughness asperity junctions, and the macroscopic one for the whole contact domain.

At the **nanometer scale**, the current Molecular Dynamics model could be expanded to characterize the behavior of complex lubricant architectures, like for instance polar fluids. As an example, fatty acids can be considered to understand how molecular adsorption on the surfaces can influence interfacial flow and friction in a contact interface. A similar study should be performed on adsorbed additive tribolayers. Moreover, ionic liquids can be analyzed to determine the role played by structural effects due to electrostatic forces on the fluid nano-rheology under confinement.

Concerning surface nature, different nanometer-scale geometries characteristic of real asperities should be investigated, as well as their impact on the structure and dynamics of the lubricant. Moreover, solid body contact during local film breakdown could be characterized, with a particular focus on the formation of dislocations in the crystalline structures and the detachment of atoms from the walls. Hence, an insight on plastic deformation and wear of the nanometer scale would be obtained. This study requires improved Molecular Dynamics simulations with potentials capable of simulating the rearrangement of the surface atoms (EAM, MEAM etc.).

The analysis of local film breakdown can be extended to the dynamic squeeze out of the last lubricant layers separating the surfaces under increasing pressure. This would allow to understand the stability of the layer structure under load and predict the occurrence of direct surface contact. Moreover, the role played by additive could be investigated, since their presence can influence the local friction and protect the walls from wear. Such analysis could facilitate the design of special lubricants capable of separating the surfaces even under extreme contact conditions.

Finally, local thermal effects may appear under extreme conditions, and should be accounted for. In particular, the proposed slip laws can be extended to describe the dependence of interfacial flow and fluid nano-rheology on the temperature. Moreover, severe heating effects occurring under local film breakdown should lead to tribochemical reactions, which could be studied through a coupling with quantum mechanics.

At the **macroscopic scale**, the current nano-EHL model can be applied to new configurations, in order to find a possible link between the occurrence of slip effects and the dimple formation observed experimentally in the literature [156, 157].

Then, future studies should aim at extending the approach to new physical phenomena. Macroscopic effects like a non-Newtonian rheology for the fluid or thermal effects in the whole contact can for instance be implemented. Additional molecular phenomena, such

as locking, solvation forces or a local temperature increase can be integrated in the model through extended laws issued from atomistic simulations.

Another fundamental point of interest is the presence of roughness on the surfaces, whose amplitude is of the order of magnitude of the micrometer. Its influence on the classical tribological quantities of film thickness or pressure generation could be investigated in a full-film configuration. Moreover, a direct contact between the roughness asperities may be reached in some configurations due to the film thickness reduction trends.

A **micrometer scale** analysis can then be performed for each asperity junction, with a particular focus on the frictional behavior and the elasto-plastic deformation of the roughness profile. In this case data from Molecular Dynamics simulations would characterize the influence of the last lubricant or additive layers trapped between the surfaces on the asperity contact.

Finally, a **nano-micro-EHL model** could be developed to bridge the gap between the three aforementioned scales. Molecular effects (nanometer scale) would then be coupled with the phenomena occurring on each asperity junction (micrometer scale) and in the whole contact (macroscopic scale). Once this overall description of the contact is completed, it would be possible to validate it through experimental approaches and use it as a design tool for tribological applications running under extreme conditions.

Appendixes

Appendix A.   Wall-Fluid interaction energy

In this Appendix the determination of a crucial parameter for Molecular Dynamics simulations is discussed: the interaction energy ε_{w-f} between the wall and the fluid molecules. Variations of this quantity have a significant impact on structural effects and interfacial flow in nano-confined fluids. For example, stronger epitaxial ordering of the molecules near the surfaces, as well as a transition from wall slip to a no slip condition were observed by increasing ε_{w-f} [8, 106, 145]. Hence, a realistic parameterization should be made to obtain accurate results in friction, velocity, density etc.

In the following, two methods for the determination on the wall-fluid interaction energy are presented. The first one, issued from the work of Berro [23], is based on the desorption energy of alkanes on the surfaces. A more general formulation, based on the notion of surface energy, is then introduced: this approach has the advantage of being linked to both the molecular and macroscopic scales. Finally, the two methodologies are compared and an interaction parameter valid for metal surfaces is suggested.

A.1. Adsorption/Desorption of carbon groups

The energy well-depth ε_{w-f} of the Lennard-Jones potential between wall and fluid atoms is defined as:

$$\varepsilon_{w-f} = \kappa \cdot \varepsilon_f \tag{A.1}$$

ε_f represents the average interaction strength between the lubricant molecules. As the lubricant molecules typically include atoms of different nature, this quantity is calculated as follows:

$$\varepsilon_f = \frac{1}{m_{mol}} \sum_{i=1}^{N} m_i \varepsilon_i \tag{A.2}$$

where m_{mol} is the mass of the molecule, N the number of atoms/groups and m_i, ε_i the mass and Lennard-Jones well depth of atom/group i. These parameters can be found in force fields describing the non-bonded interactions in the fluid (see Table II-2). In the case of alkanes, ε_f is typically of the order of magnitude of 0.1 kcal/mol [23]: in example ε_{w-f} = 0.1344 kcal/mol for pentane and 0.105 kcal/mol for hexadecane.

The factor κ in Equation (A.1) represents the ratio between the interaction strengths at the wall-fluid interface and inside the fluid. It ranges from 0.4 to 4 according to the literature, covering weakly to highly adsorbing surfaces. However, a more accurate choice for this parameter should be made to obtain accurate results for the behaviour of molecularly confined fluids. The literature [23, 25, 81] suggest tuning κ to fit the experimental measurement of adsorption/desorption energies of molecules on different wall topologies. In particular, Temperature Programmed Desorption experiments rated the adsorption energy for alkanes

at 1-1.4 kcal/mol for each CH_x segment on different metal surfaces [165-167]. This criterion will be used in the following to determine the wall-fluid interaction parameter.

The procedure is performed using the Molecular Dynamics system shown in Figure A-1 [23]. A metal surface is covered by an adsorbed layer of alkane molecules with a thickness of 10 Å, equal to the cutoff limit for the van-der-Waals interactions between the wall and the fluid. The surface is thermostatted at 90K to avoid spontaneous desorption. An average potential energy per molecule, corresponding to the adsorption/desorption energy of the alkane, can then be measured inside the fluid layer.
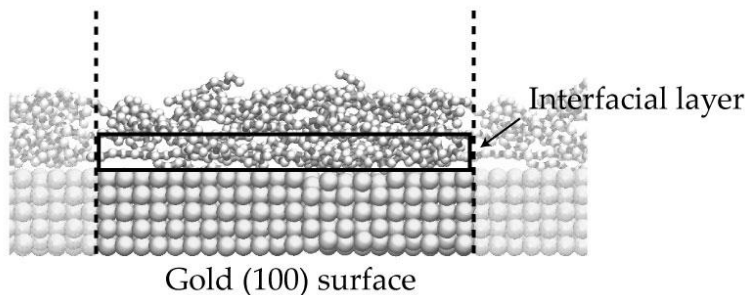
Figure A-1: Molecular Dynamics system for the measurement of the desorption energy for alkanes molecules on various surfaces; an Au-100 wall and n-hexadecane are represented here. From [23].

The factor κ must then be tuned to obtain the correct wall-fluid interaction energy. In the Molecular Dynamics simulations, this is ultimately done by changing the Lennard-Jones energy parameter ε_w of the wall atoms according to the Lorentz-Berthelot mixing rules. By combining Equations (A.1) and (II.11) one obtains:

$$\varepsilon_{w-f} = \kappa \cdot \varepsilon_f = \sqrt{\varepsilon_w \cdot \varepsilon_f} \qquad (A.3)$$

Therefore, the energy well-depth for the wall atoms in the Molecular Dynamics system becomes:

$$\varepsilon_w = \kappa^2 \cdot \varepsilon_f \qquad (A.4)$$

Increasing κ (and ε_w) for a given wall causes a rise of the adsorption energy E_{ads} per fluid molecule, shown in Figure A-2 for pentane and hexadecane with gold surfaces.
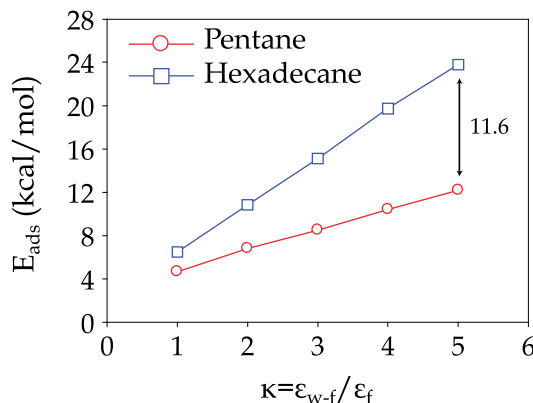
Figure A-2: Variation of the adsorption energy on Au[100] surfaces for pentane and hexadecane as a function of the ratio κ between the wall-fluid and fluid-fluid interaction energies. From [23].

These two alkanes feature difference in length equal to 11 CH_x groups. Hence, the corresponding variation in adsorption energy given experimentally is equal to 11-15.4 kcal/mol. From all the considered κ range in Figure A-2, this condition is satisfied for a value κ =5. The corresponding Lennard Jones interaction parameters for the gold atoms in the surfaces (Equation (A.4)) is equal to ε_w =2.625 kcal/mol, and will be used in the Molecular Dynamics model from Chapter II.

This method for the parameterization of the wall-fluid interactions was applied in [23] for different metal surfaces. Values were shown to vary from κ =4 for ferrite Fe[100] surfaces, to as high as κ =8 in the case of iron oxide (Fe_2O_3[001]), and were of the same order of magnitude as the ones proposed in the literature [25, 133, 168, 169].

Despite being the only proposed guideline for the determination of realistic wall-fluid interaction energies, this method presents some limitations. First of all, it is only valid for the case of alkanes on metal surfaces. Furthermore, it is affected by the large uncertainty (40%) on the experimental values for the desorption energy of CH_x segments. A new methodology based on surface energy is then proposed to overcome these issues.

A.2. Surface energy

Surface energy is a macroscopic quantity defined as "*the work required to increase the surface area of a material by one unit*" [170]. A schematical representation is proposed in Figure A-3 to illustrate this concept. A block of a homogeneous, isotropic material is cut in two parts, thus creating two new surfaces which are brought at an infinite distance from one another. To perform this operation, a work per unit area W/S must be supplied to the system to overcome the cohesion forces inside the material. The corresponding surface energy γ is then defined as:

$$\gamma = \frac{W}{2 \cdot S} \tag{A.5}$$

The factor 2 is due to the fact that two surfaces are created when dividing the initial block.
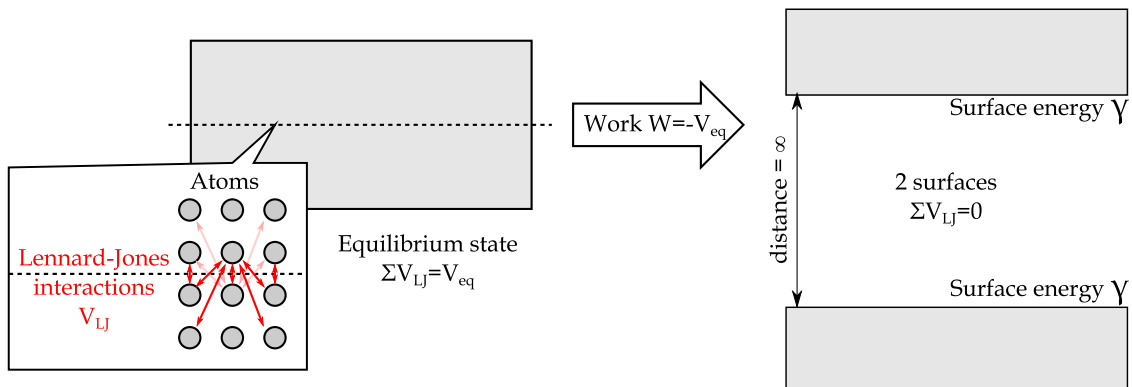
Figure A-3: Example for the definition of surface energy: a block of material is cut in two parts, thus creating two new surfaces. The work per unit area which must be given to the system corresponds to twice the surface energy (since two surfaces are created).

In the illustrative system from Figure A-3, it will be supposed that the internal forces assuring the cohesion of the material are of van-der-Waals nature. Hence, they can be described through a Lennard-Jones potential between the atoms in the block, thus creating a clear link with the molecular scale.

Hence, the equilibrium state in the uncut material is represented by energy minimum V_{eq}. This quantity can be expressed as the sum of Lennard-Jones forces acting between atoms the lower (index i) and higher (index j) parts of the block:

$$V_{eq} = \sum V_{LJ,ij} < 0 \tag{A.6}$$

Its norm corresponds to the work W that must be supplied to the system to overcome the Lennard-Jones attraction forces and dividing the initial block in two. The surface energy is then related to V_{eq} by:

$$\gamma = \frac{W}{2 \cdot S} = -\frac{V_{eq}}{2 \cdot S} = -\frac{\sum V_{LJ,ij}}{2 \cdot S} \tag{A.7}$$

Hence, the strength of the Lennard-Jones interactions at the nanometer scale determines the macroscopic surface energy of the material. For example, an increase in the well depth parameter for the wall atoms ε leads to an augmentation of γ [26].

While the previous definition of surface energy was obtained for a single material, a more general formulation is necessary to characterize the behavior of a solid-liquid interface. In this case, The Young-Dupré equations allow mixing the surfaces energies for different substances [4, 170]:

$$\gamma_{12} = \gamma_1 + \gamma_2 - \frac{W_{12}}{S}$$
$$\text{with} \quad \frac{W_{12}}{S} = 2\sqrt{\gamma_1 \cdot \gamma_2} \tag{A.8}$$

Indexes $_1$ and $_2$ correspond to the two materials, which can both be solid or liquid. Hence, a solid-solid, liquid-liquid or solid-liquid interface can be represented, characterized by a combined surface energy γ_{12}. Finally, W_{12} is the work required to separate the two materials, and is related to van-der-Vaals forces acting at the interface:

$$\frac{W_{12}}{S} = -\frac{\sum V_{LJ,12}}{S} \tag{A.9}$$

The Young-Dupré equations are the equivalent for a macroscopic model of the Lorentz-Berthelot mixing rules for the Lennard-Jones potential. In fact, $\sqrt{\gamma_1 \gamma_2}$ echoes the term $\varepsilon_{12} = \sqrt{\varepsilon_1 \cdot \varepsilon_2}$ in Equation (II.11), used to mix the energy interactions for atoms of different nature. Such strong link between scales is further exploited to obtain a new guideline for the parameterization of the wall-fluid interactions in the Molecular Dynamics system.

The procedure is illustrated hereafter for an alkane on a metal surface. The model from the adsorption/desorption method (Figure A-1) is still used. The Lennard-Jones interactions $V_{LJ,alkane-surface}$ at the wall-fluid interface are directly measured within the numerical simulation. As previously, they can be adjusted by tuning the energy parameter for the wall atoms through the factor κ in Equation (A.4).

This procedure also changes the surface energy at the interface $\gamma_{alkane-surface}$ according to Equation (A.9). The objective is therefore to fine-tune κ to match $\gamma_{alkane-surface}$ with values issued from the Young-Dupré equations.

In the case of alkanes, the surface energy is equal to γ_{alkane} = 25 mJ/m² [171]. On the other hand, $\gamma_{surface}$ is given in the literature for the corresponding wall material: for example $\gamma_{surface}$ = 1 J/m² for gold surfaces [172]. The combined surface energy of the interface is given by Equation (A.8): in the case of alkanes on gold, $\gamma_{alkane-surface}$ =0.316 J/m². To match this value, the factor κ must be set to 5.2. This result is in coherence with the method for the adsorption/desorption of carbon groups presented in Section A.1.

A.3. Comparison of the methods

Further comparison between the proposed guidelines for the parametrization of the wall-fluid interactions is performed hereafter through the analysis of different metal and metal oxide surfaces. The results are presented in Table A-1.

Surface		Au [100]	Cu [111]	Fe [100]	Fe [111]	Fe$_2$O$_3$ [001]	Fe$_2$C [100]
Method							
Adsorption of carbon groups	Min(κ)	4.8	3.1	4.0	4.1	5.5	4.6
	Max(κ)	6.2	4.3	5.4	5.6	8.0	6.6
Surface energy	$\gamma_{surface}$ (J/m²)	1.0	1.6 - 2.0	2.25	2.54	1.52	2.0 - 2.5
	κ	5.2	3.8 - 4.3	5.0	5.5	7.0	5.2 - 6.2

Table A-1: Comparison between the two methodologies for the determination of the wall-fluid interactions in the case of alkanes on various metal surfaces. For the adsorption/desorption method, the minimum and maximum values of κ correspond to a CH$_x$ desorption energy of 1 and 1.4 kcal/mol respectively. The surface energy values are taken from [171-176].

The minimum and maximum limits for the adsorption method correspond to desorption energies for CH$_x$ groups of 1 kcal/mol and 1.4 kcal/mol respectively [165-167]. This 40% uncertainty entrains a significant dispersion on the values of κ. More consistent results are obtained through the surface energy method. A further advantage is its validity for a wider range of interfaces, like for instance with non-metallic surfaces or fluid architectures different than alkanes. In fact, more data is available in the literature to characterize these wall-fluid combinations.

However, both guidelines deliver results of the same order of magnitude, comforting their validity for the determination of realistic wall-fluid interaction properties. Finally, results from Table A-1 show that κ =5 adequately characterizes most configurations. This value can therefore be chosen as a starting point to parametrize the interaction of metal surfaces in contact with alkanes without performing trial and error calculations for each wall morphology.

Appendix B.   Branched alkanes

The aim of this Appendix is to investigate the behavior of branched alkanes under confined conditions. It was shown in the literature that the presence of branching plays a major role on the structure and dynamics in molecularly thin shear flow: a frustration of the ordering effects across the film thickness was reported in [10, 14, 78]. Moreover, branched architectures features larger slip values compared to linear molecules [16, 23].

To investigate these phenomena, the Molecular Dynamics model from Chapter II is used. The operating conditions in pressure, wall speed, film thickness, and temperature are chosen according to Section III.2: P=500 MPa, Δu=20 m/s, h=4 nm and T_w=300K. The surfaces are representative of metal and metal oxides (see Table II-1). Finally, three branched alkanes are considered: phytane (2,6,10,14-tetramethylhexadecane), 5-ethyl-2-methyldecane, and a paraffin (branched tetracosane). Their molecular structures are shown in Figure B-1.

Figure B-1: Molecular structure of the chosen branched alkanes in comparison with linear n-hexadecane.

B.1.   Structural effects

The first interesting result is the density profile across the film thickness, shown in Figure B-2 for phytane in comparison with n-hexadecane. It should be noted that both molecules feature a chain length of 16 hydrocarbons and the observed differences are only due to branching.
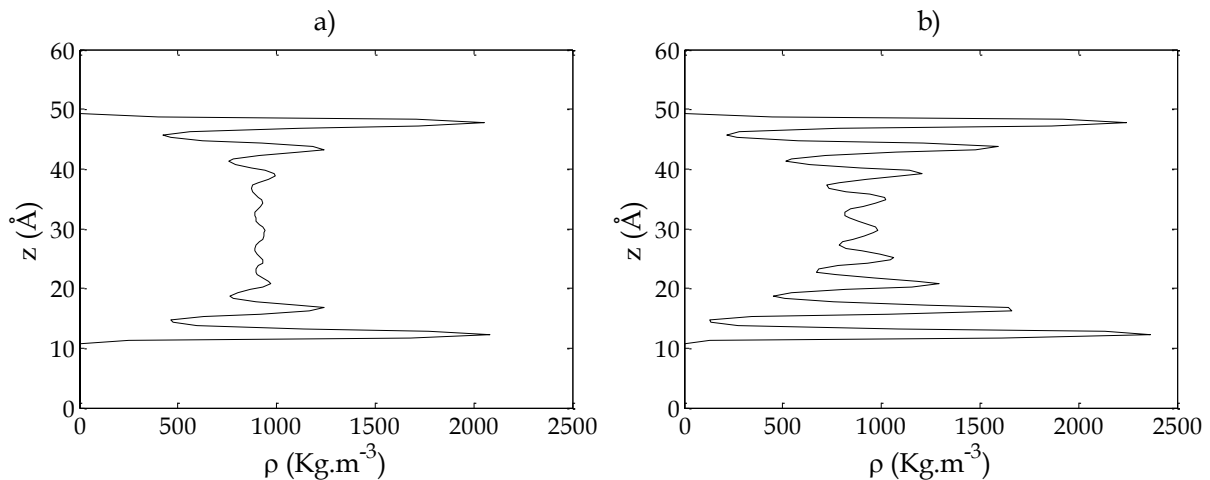

Figure B-2: Density profile across the film thickness for phytane (a) and n-hexadecane (b) confined between Au[110] surfaces. P=0.5 GPa, u$_2$=-u$_1$=10 m/s, h=4 nm, T$_{wall}$=300K.

In the case of phytane the density oscillations characteristic of the formation of ordered structures are significantly damped at 3 molecular diameters from the surfaces; the density is homogeneous in the center of the film. On the other hand, the density oscillations feature a larger amplitude in the case of linear hexadecane, and the layering effect remains clearly distinguishable across the whole gap height. Such differences in the fluid ordering can be explained by the stronger internal cohesion for branched molecules, which reduces the influence of the surfaces on the confined fluid. This result is coherent with the trends from the literature [10, 14, 16]: in example, a similar behavior was observed for 5-ethyl-2-methyldecane compared to linear n-decane in [23].

B.2. Wall slip

The stronger cohesion for branched architectures also leads to a larger shear viscosity compared to linear molecules of the same chain length. Consequently, higher wall slip is observed, as shown in Figure B-3 for phytane and n-hexadecane confined between Face-Centered-Cubic surfaces with a lattice spacing of 3 Å.
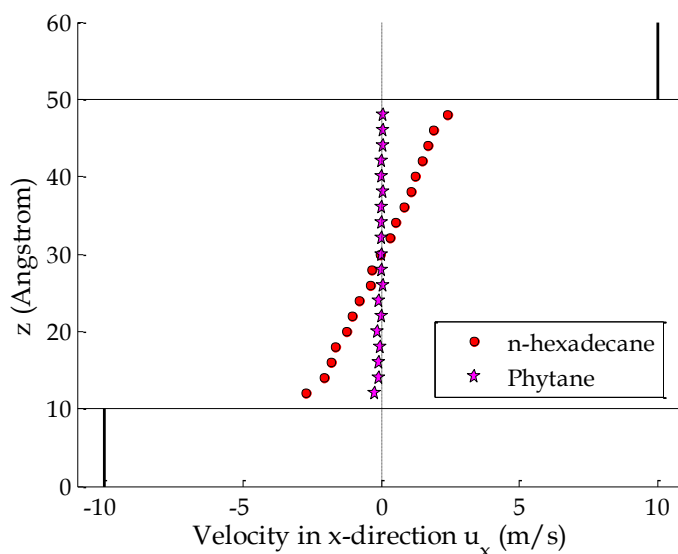
Figure B-3: Wall slip dependence on branching for a canonical surface with cubic structure and lattice constant a=3Å. P=0.5 GPa, $u_2=-u_1=10$ m/s, h=4 nm, T_{wall}=300K.

The combined effect of branching and chain length on the velocity profiles across the film thickness is shown in Figure B-4 for two Face-Centered-Cubic surfaces with different lattice spacing. The comparison between n-hexadecane and paraffin is straightforward. The latter molecule features both branching and a longer chain length: both these factors contribute to a higher internal cohesion and shear viscosity. Hence, the velocity jump between the fluid molecules and the walls is larger, and total slip is reached for the given surface morphology.

On the other hand, no clear conclusion can be drawn from the comparison of linear hexadecane and the chosen branched decane. In Figure B-4a, the velocity jump at the wall-

fluid boundary is larger for 5-ethyl-2-methyldecane, whereas in Figure B-4b slip is higher for n-hexadecane.
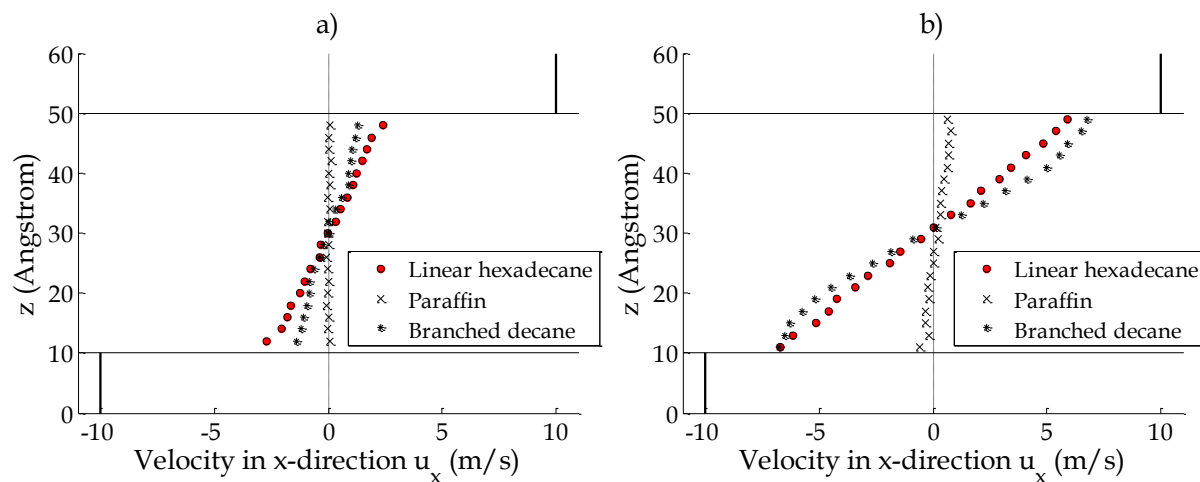
Figure B-4: Velocity profiles for hexadecane, paraffin and 5-Ethyl-2-methyldecane confined between canonical surfaces. a) Cubic structure with lattice constant a=3 Å; b) Face-Centered-Cubic structure with lattice constant a=4.5 Å. P=0.5 GPa, u_2=-u_1=10 m/s, h=4 nm, T_{wall}=300K.

These results can be interpreted as the result of the competition between the reduction in chain length and the presence of branching, which influences the internal cohesion of branched decane. Consequently, interfacial flow under shearing in confined conditions is also affected, in accordance with Section III.2.

In order to fully understand the specific role played by the chain length and the shape of the branches on wall slip, several combinations of these two parameters would have to be investigated. This study lies out of the scope of this Appendix; instead, some elements for a wall slip prediction model will be discussed hereafter, with a particular focus on the momentum transfer at the wall-fluid interface.

B.3. Towards wall slip prediction for branched alkanes

There is a large number of architectures for branched molecules, each one characterized by a particular chain length and shape of the ramifications. Hence, a wall slip prediction model should be developed to characterize all the possible configurations which can be found in base oils, confined between surfaces typical of a contact interface. The analysis hereafter will follow the methodology proposed in Section III.2 for linear alkanes. In particular, interfacial flow is interpreted as the consequence of the competition between fluid and surface natures.

The characterization of wall slip as a function of molecular architecture requires the characterization of the fluid shear viscosity under confined conditions. According to the literature, this quantity can be expressed through a bulk viscosity term for film thicknesses down to 5-6 molecular diameters [143]. In fact, the presence of branching frustrates the formation of ordered structures across the film thickness [10, 14, 16, 23]. The effect of confinement is thus reduced and the fluid retains its bulk-like state.

Appendix B – Branched alkanes

The second parameter which must be determined for the slip prediction model is momentum transfer at the wall-fluid interface. In Section III.2.2 a surface characterization parameter ζ_{surf}, obtained from a scanning technique, was proposed in the case of linear alkanes. Moreover, this quantity was linked to the interfacial shear stress τ_{xy} in III.2.3.

It will be supposed that this methodology can still be applied for branched alkanes. In fact, the scanning technique was based on the size of the hydrocarbon groups (CH_x), which does not vary compared to linear alkanes. Hence, ζ_{surf} values from Table III-1 can be used to investigate the tangential momentum transfer at the walls. The (ζ_{surf}, τ_{xy}) curves for the three chosen branched alkanes are represented in Figure B-5 in comparison to n-hexadecane.
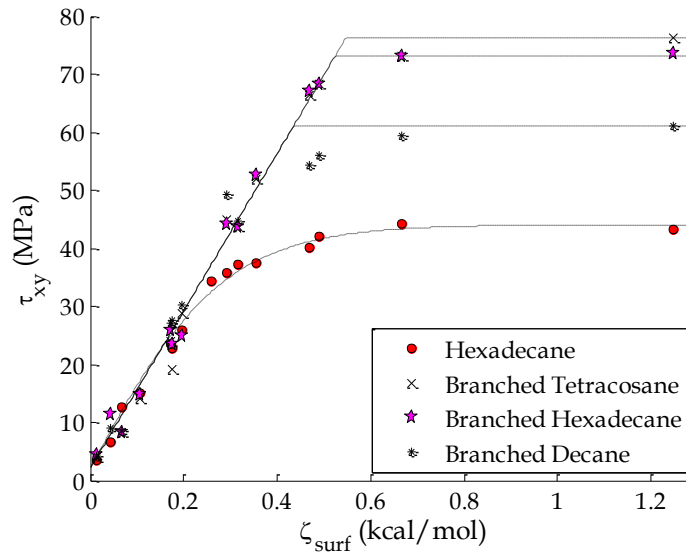
Figure B-5: Shear stress for different branched alkanes as a function of the surface interaction parameter. The points represent the results from Molecular Dynamics simulations, the dotted lines the analytical curve fit. P=0.5 GPa, u₂=-u₁=10 m/s, h=4 nm, Twall=300K.

Even in case of branched architectures, ζ_{surf} gives good results for ordering different wall topologies according to their capability to transfer a shear stress to the confined alkane. Moreover, the same trends can be observed for both linear and branched molecules. The shear stress increases linearly with ζ_{surf} for weakly interacting surfaces, for which wall slip occurs. After a transition zone, a plateau is reached for walls featuring strong interactions and commensurability with the alkane molecules: the fluids are fully sheared and τ_{xy} is limited by their internal cohesion.

Hence, the (ζ_{surf}, τ_{xy}) curves of Figure B-5 can be fitted through analytical laws. It can be seen that the slope of the linear region at low ζ_{surf} seems to be independent on both the chain length and branching for the chosen alkanes. However, the transition zone from no-slip to slip and the shear stress of the plateau varies for each fluid. Hence, an Equation based on fitting the asymptotes with straight lines is proposed:

$$\tau_{zx}\left[MPa\right] = \min\left(135.3 \cdot \zeta_{surf}\left[kcal/mol\right] + 2.20,\ \tau_{max}\left[MPa\right]\right) \tag{B.1}$$

τ_{max} quantifies the plateau region for each fluid, and can be determined by running Molecular Dynamics simulations for surfaces with high ζ_{surf}, such as Fe_2O_3[001] (see Table

III-1). Here, $\tau_{\max}$ =76.3 MPa for paraffin, 73.1 MPa for phytane, and 61.2 MPa for branched decane.

Alternatively, the maximum shear stress for each fluid can be determined by considering that wall slip does not occur in the plateau region ($\dot{\gamma}_{eff} = \dot{\gamma}_{app}$), and $\tau_{\max}$ is only related to the resistance to shearing of the lubricant under confinement. As explained previously, this term can be quantified by a bulk viscosity η_{bulk} as a function of the operating conditions in apparent shear rate, pressure, temperature and confinement. Hence the following expression is obtained:

$$\tau_{\max} = \eta_{bulk}(\dot{\gamma}_{app}, P, T, h) \cdot \dot{\gamma}_{app} \tag{II.2}$$

where η_{bulk} is a viscosity model issued from experiments or Non-Equilibrium Molecular Dynamics simulations [138].

In conclusion, the surface characterization method proposed in Section III.2.2 for the prediction of the tangential momentum transfer at the wall-fluid interface is still valid in the case of branched alkanes. In future studies, the validity of Equation (B.1) could be further investigated for different combinations of chain lengths and branching. Finally, this analytical law should be coupled with bulk viscosity models, as detailed in Section III.2.5, in order to obtain a wall slip prediction model for branched alkanes.

Appendix C.   Nanometer-scale roughness and locking

Smooth walls are often used in macroscopic models for the characterization of lubricated mechanisms. In reality, a roughness with amplitude between 1 nm and 1 μm and wavelength of some micrometers is present on engineered surfaces [58]. This micro-geometry was characterized through numerous studies as a function of the materials, the finishing process and wear during running-in [177].

On the other hand, the measurement of nanometer scale asperities is not straightforward. Most of the time the experimental techniques are employed on areas of some square micrometers, and do not have a sufficient lateral resolution to capture in detail the atomic structure of the walls [177]. Furthermore, Atomic Force Microscopy is rarely used to analyze the nanometer-scale geometry of real machined surfaces. The rare experimental data shows roughness wavelengths ranging from 0.2 nm to 50 nm [109]. Hence, different characteristic scale lengths are involved, ranging from the lattice spacing to wall waviness [108].

As an example, geometrically smooth walls in Chapter III were obtained by cutting a crystal lattice with a plane. Due to their discrete nature, the surfaces feature nevertheless a wavy interaction potential and height with the fluid molecules, revealed by the scanning technique in Section III.2. These variations correspond to the atomic spacing of the lattice structure [108] and have a characteristic wavelength of some Ångstroms: they can be interpreted as an atomic roughness.

However, the asperity dimensions in tribological interfaces can be of the order of magnitude of some nanometers [109]. For example, lattice dislocations due to mechanical [53], thermal [9] or chemical stress [178] can lead to a deformation of the crystal structure and result in wall waviness. Furthermore, both machining processes and wear lead to the detachment of surface atoms creating random imperfections [179]. A contact interface also features a heterogeneous composition with grains constituted of various materials [147]. Due to the different crystalline structures, lattice jumps are found at the grain boundaries.

There are few Molecular Dynamics studies on the influence of nanometer scale roughness on boundary flow [9, 19, 104, 108]. Furthermore, they often use simplified representations for the asperities which do not take into account the complex landscape at a contact interface. Nevertheless, a general trend emerges from all the literature references. Gao [9] reported that random imperfections on the walls frustrated the layering phenomenon typical of geometrically smooth surfaces; wall slip also disappeared, resulting in the full shearing of the lubricant and higher friction. Jabbarzadeh [108] showed that large asperity amplitudes reduced the velocity jump at the surface-fluid boundary for confined n-alkanes under very high shear rates; similar results were obtained by Priezjev [104]. Finally, Ding [19] observed both through Molecular Dynamics simulations and experiments a no-slip condition near nano-rough walls, as well as the formation of locked fluid layers pinned to the surfaces.

The aim of this Appendix is to further analyze molecularly confined films in presence of nanometer scale asperities, thus completing the Molecular Dynamics characterization of

boundary flow as a function of surface nature. This study is organized as follows. First, the impact of roughness on the average film thickness and ordering effects within the lubricant will be discussed through a comparison with smooth surfaces. The locking phenomenon will then be defined by analyzing the dynamics within the confined fluid. A parametric study will be performed to quantify the influence of surface roughness and the operating conditions on boundary flow. Finally, the relationship between locking and friction will be discussed.

C.1. Film thickness, density and structural effects

The Molecular Dynamics system is similar to the one used in Section III.2. Linear hexadecane is confined between Fe_2O_3 and CuO surfaces, which were shown to have very different boundary flow with flat surfaces. The operating conditions are chosen the same as previously (P =500 MPa, Δu =20 m/s and T_w =300K). Furthermore, all the simulations are initialized with the same initial density ρ =890 kg/m³, corresponding to the value obtained for smooth surfaces under confinement This allows a meaningful comparison between different roughness geometries and the results for flat walls from Section III.2.

Sinusoidal asperities are then carved on the walls along the shearing direction, akin to Jabbarzadeh [108]. Their wavelength λ varies between 0.8 nm and 10 nm, corresponding to 0.5 and 6 times the length of an n-hexadecane molecule [108]. The amplitude A ranges from an atomic scale roughness (0.05 nm) and roughly three lattice spacings (0.5 nm). A snapshot of a Molecular Dynamics simulation during the shear phase is shown in Figure C-1.
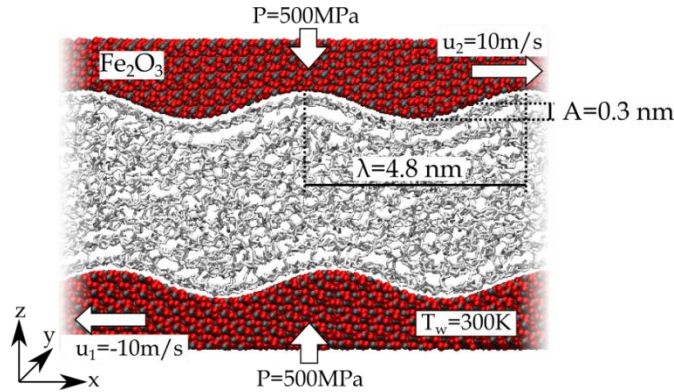
Figure C-1: Snapshots of a Molecular Dynamics simulation with rough walls during shearing.

The impact of nanometer-scale roughness on the film thickness h is considered first. It is therefore necessary to define this term in presence of sinusoidal asperities: the procedure is shown schematically in Figure C-2. The roughness profiles of the lower and upper walls are characterized by their average planes $z_{avg,1}$ and $z_{avg,2}$ respectively. The average film thickness h_{avg} is defined by:

$$h_{avg} = z_{avg,1} - z_{avg,2} \tag{C.1}$$
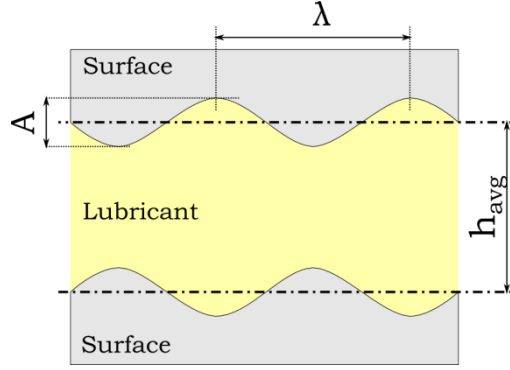
Figure C-2: Schematic representation of the film thickness calculation for rough surfaces.

Figure C-3a shows the evolution of h_{avg} as a function of the wavelength λ of the asperities. The average film thickness is almost constant and features values similar to smooth surfaces. A slight increase can be observed when λ is smaller than the chain length of n-hexadecane. In this case the wall potential prevents the lubricant molecules from reaching the bottom of the roughness valleys. As a result the empty volume between the surfaces and the first fluid layer is larger [9]. However, this film thickness increase remains under 5% for the considered wavelengths.
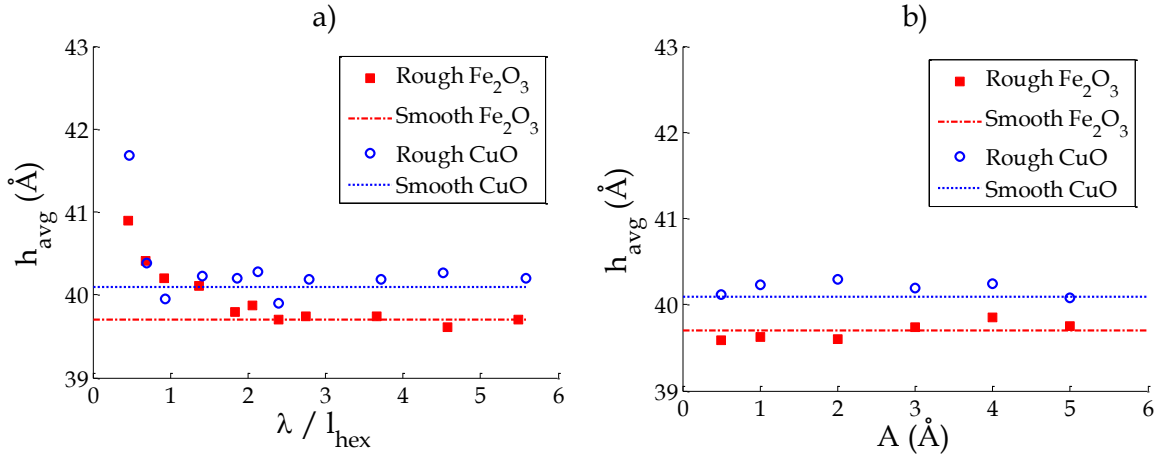
Figure C-3: Dependence of the average film thickness with the asperity wavelength (a) and amplitude (b). L_{hex}=1.75nm is the chain length of hexadecane [108]. P=0.5 GPa, u_2=-u_1=10 m/s, T_{wall}=300K.

Furthermore, h_{avg} stays constant for asperity amplitudes ranging from an atomic diameter to a few lattice spacings, as shown in Figure C-3b. Hence, the average film thickness does not depend on the geometrical parameters of the roughness profile, and corresponds to the surface separation between flat walls.

Moreover, the average fluid density ρ_{avg} can be defined through the average film thickness [15, 108]:

$$\rho_{avg} = \frac{\sum_{i=1}^{n_{mol}} m_{mol,i}}{S \cdot h_{avg}} \tag{C.2}$$

with n_{mol} the number of fluid molecules in the system, $m_{mol,i}$ the mass of each molecule, and S the area of the nano-patch. It should be reminded that all the chosen configurations were initialized with the same number of molcules per surface unit. As the average film thickness does not vary significantly with roughness geometry, ρ_{avg} also stays constant for a given external pressure. In this case, a value of 890 kg/m³ is obtained, akin to smooth walls and the Dowson-Higginson bulk law for n-hexadecane under P=500 MPa [23, 37].

While nano-roughness has a limited impact on h_{avg} and ρ_{avg}, structural effects in the confined fluid and the corresponding density profile across the film thickness can be severely affected [9, 93]. In fact, the ordering effect of the wall potential is limited to the formation of a single lubricant layer near each surface, following the geometry of the asperities. On the other hand, the rest of the fluid remains in a disordered state. The density profile across the film thickness (Figure C-4a) shows that the presence of nanometer-scale roughness frustrates structural effects characteristic of smooth walls (Figure C-4b). In fact, sharp density peaks representative of well-defined layers decrease in amplitude, in coherence with results from the literature [9, 108].
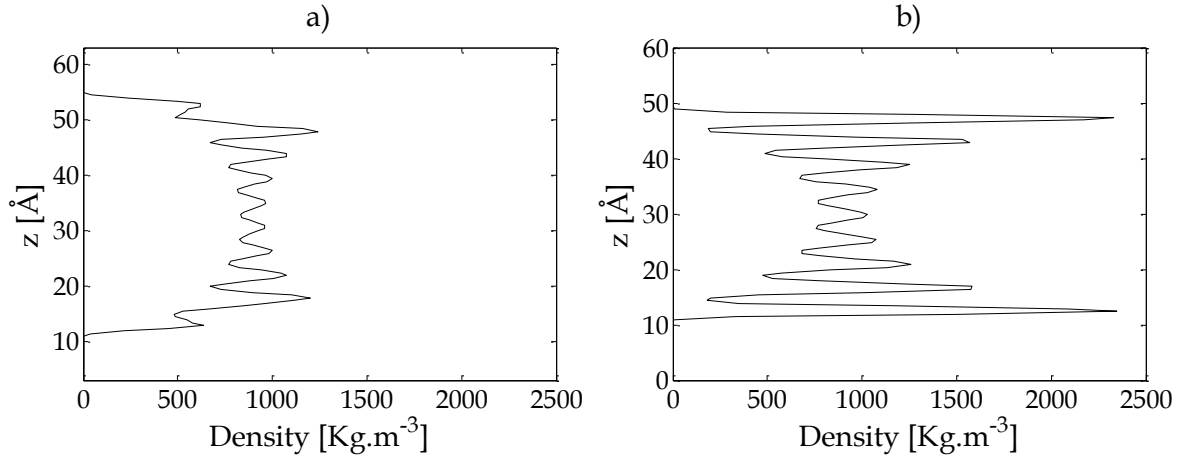
Figure C-4: Density profiles across the film thickness. a) Rough surfaces (λ=4.8 nm, A=0.3 nm). b) Smooth walls. P=0.5 GPa, u_2=-u_1=10 m/s, T_{wall}=300K.

C.2. The locking phenomenon

The presence of nano-roughness has a profound impact also on the shear flow under confinement [9, 93]. Locking at the wall-fluid interface was observed in numerical studies [19, 104], as well as Surface Force Apparatus experiments [109]. This new boundary condition is quantified hereafter through an analysis of the velocity profile across the film thickness. Results for a reference case are represented in Figure C-5.

It can be seen that the fluid is not sheared within the whole gap height. In fact locking occurs: the outmost molecule layers stick to the nearby surfaces and move with the imposed wall velocity. On the other hand the fluid is fully sheared in the center of the film, which features a linear velocity profile [18, 101] representative of a bulk-like response [108]. A transition zone is observed between the pinned and the central regions: the fluid molecules located between the asperity peaks are not fully stuck to the walls and may be slightly sheared.
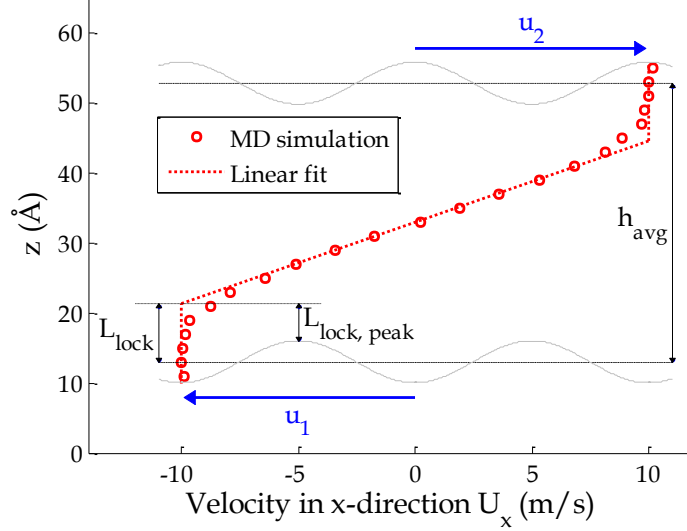
Figure C-5: Velocity profile across the film thickness and corresponding piecewise linear approximation. λ=4.8 nm, A=0.3 nm, P=0.5 GPa, u₂=-u₁=10 m/s, T_wall=300K.

According to the literature, locking can be considered as the opposite of wall slip phenomenon. Hence, "a negative slip length" is often used to represent the height of the pinned layers on top of the surfaces [23, 104]. In order to determine its value, the velocity profile within the fluid is approximated by a piecewise linear interpolation (Figure C-5). The velocity of the locked molecules in proximity of the surfaces is set equal to the imposed wall speed. On the other hand, the effective shear rate $\dot{\gamma}_{eff}$ accounts for the dynamics in the center of the film: this term is equal to the velocity gradient along the z-direction, similarly to flat walls. Hence, the height of the central, fully sheared region, also called effective film thickness h_{eff}, is defined by:

$$h_{eff} = \frac{u_2 - u_1}{\dot{\gamma}_{eff}} = \frac{\Delta u}{\dot{\gamma}_{eff}} \tag{C.3}$$

For each wall i, the height of the pinned lubricant layers above the roughness average plane is quantified by the locking length $L_{lock,i}$:

$$L_{lock,1} + L_{lock,2} = h_{avg} - h_{eff} \tag{C.4}$$

In this work both surfaces feature the same roughness profile and the system is symmetric. Hence, $L_{lock,1} = L_{lock,2} = L_{lock}$ and Equation (C.4) becomes:

$$L_{lock} = \frac{h_{avg} - h_{eff}}{2} \tag{C.5}$$

Locking occurs when $h_{avg} - h_{eff}$ and L_{lock} are larger than zero. On the other hand, a wall slip boundary corresponds to $h_{avg} - h_{eff} < 0$: in this case the slip length parameter used in Section III.1 is then equal to $L_s = -L_{lock}$.

The definition of L_{lock} in Equation (C.5) provides a direct link with the film thickness. In order to allow the comparison between different asperity amplitudes, the locking length above the asperity peaks $L_{lock,peak}$ is introduced:

$$L_{lock,peak} = L_{lock} - A \tag{C.6}$$

Through these terms it is finally possible to characterize molecularly thin shear flows in presence of nanometer scale roughness. The velocity profile in Figure C-5 is considered as an example. The effective film thickness h_{eff} =2.33 nm is significantly smaller than the average one (h_{avg} =3.97 nm). As a consequence, the effective shear rate $\dot{\gamma}_{eff}$ =8.6·10^9 s^{-1} in the center of the film is almost doubled compared to the classical no-slip boundary condition ($\dot{\gamma}_{app}$ =5·10^9 s^{-1}). Finally, $L_{lock,peak}$ is equal to 0.52 nm, which roughly corresponds to the width of one hexadecane layer [7] pinned above the asperity peaks, in accordance with [19].

Such significant changes of lubricant flow under confined conditions must be further analyzed to fully understand the impact of surface roughness in contact interfaces. A parametric study is performed to determine the role played by wall geometry, material, and the operating conditions on the locking phenomenon.

C.3. Influence of the roughness geometry and surface material

It was shown in [108] that changing the wavelength and amplitude of the asperities influences the occurrence of wall slip in confined alkanes at very high shear rates ($\dot{\gamma}_{app} \approx 10^{11}$ s^{-1}). A similar analysis is performed hereafter on the geometrical parameters of the roughness profile. However, lower levels of forcing ($\dot{\gamma}_{app}$ =5·10^9 s^{-1}) are used to be more representative of a real contact under elasto-hydrodynamic conditions.

The asperity wavelength is considered first: Figure C-6 represents the corresponding evolution of the locking length above the asperities for both Fe$_2$O$_3$ and CuO walls. For all the considered λ range, varying between 0.5 and 6 times the size of a hexadecane molecule, locking occurs and some lubricant molecules are pinned on top of the asperity peaks. This phenomenon is independent from the wall-fluid interaction energy and commensurability of the chosen materials. In fact, it occurs for both iron and copper oxide, which featured significantly different interfacial flows when smooth surfaces were considered (Section III.2).
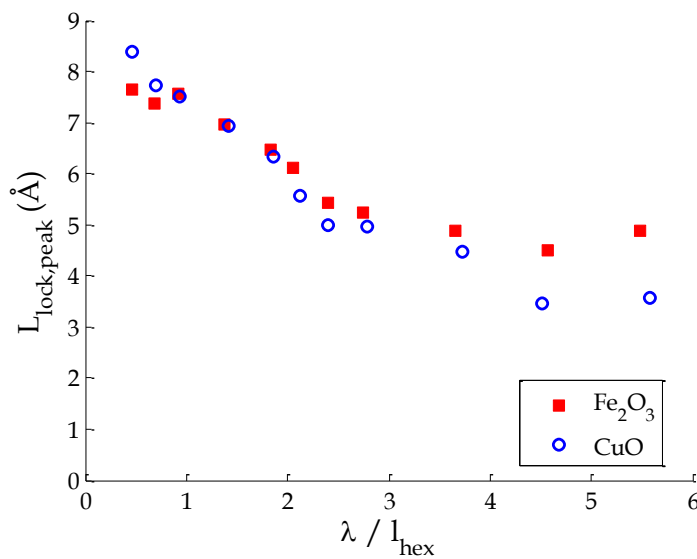

Figure C-6: Dependence of the locking length above the asperities with the roughness wavelength. A=0.3 nm, P=0.5 GPa, u$_2$=-u$_1$=10 m/s, T$_{wall}$=300K.

Further analysis of $L_{lock,peak}$ reveals interesting trends. When the asperity wavelength is shorter than the molecule chain, the height of the pinned layers corresponds to two molecular widths of n-hexadecane. As λ increases, a reduction in locking is observed, whose intensity depends on surface material. In the case of Fe_2O_3 a constant $L_{lock,peak}$ value is reached for $\lambda \cong 3l_{hex}$, corresponding to a single immobile layer on the surfaces. This result is due to the strong wall-fluid interaction potential of iron oxide.

On the other hand, CuO is characterized by weaker interactions with n-hexadecane. Hence, the reduction of $L_{lock,peak}$ with increasing asperity wavelength is more marked. The behavior for larger λ values is difficult to analyze with the current Molecular Dynamics simulations, where the system size and consequently the periodicity of the roughness profile are limited to a few nanometers only. The literature proposes contradicting trends on this issue. According to [108] locking would eventually disappear for larger λ values, leading to the occurrence of wall slip akin to a smooth wall case. However, the same study showed that a no-slip boundary condition could still be valid for large asperity amplitudes typical of engineered surfaces. For now, it will be concluded that $L_{lock,peak}$ is roughly equal to the thickness of one or two lubricant layers for roughness wavelengths up to six times the size of the alkane chain, in coherence with Figure C-6b.

The amplitude A of the asperities also plays a significant role on locking, as shown in Figure C-7a. Since the average film thickness remains constant in all cases, the distance separating the roughness peaks of both surfaces becomes smaller as A increases. As a consequence, the effective film thickness h_{eff} is reduced and larger shear rates are observed in the center of the fluid.
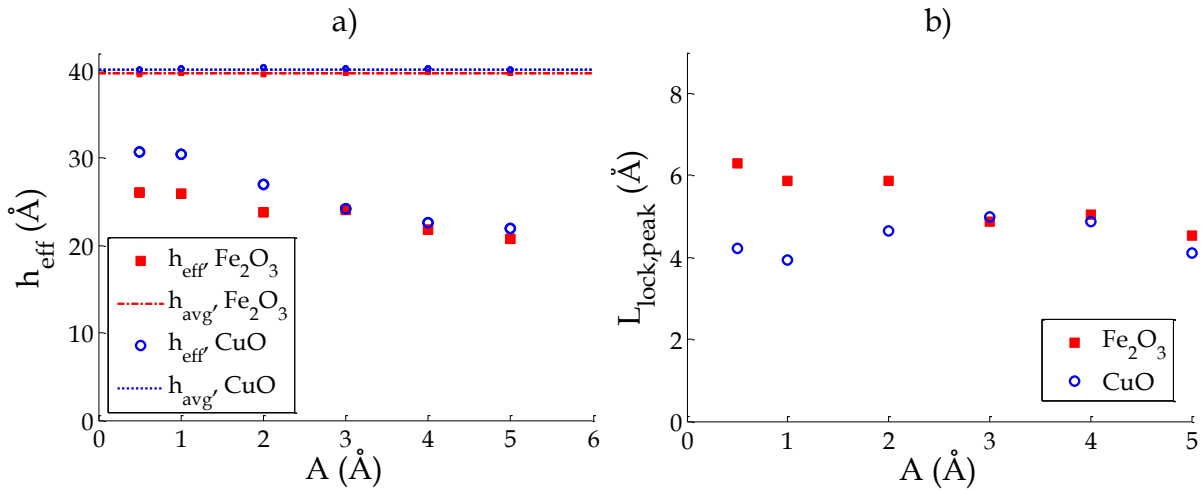
Figure C-7: Dependence of the effective film thickness (a) and locking length above the asperities (b) with the roughness amplitude. λ=4.8 nm, P=0.5 GPa, u_2=-u_1=10 m/s, T_{wall}=300K.

Further insight is provided in Figure C-7b by the locked length above the asperities. In the case of iron oxide, $L_{lock,peak}$ is larger for smaller roughness amplitudes. This phenomenon can be explained as the result of two coexisting effects related to surface nature. On one side, locking is caused by the presence of roughness, as reported previously. On the other side, the strong wall-fluid interaction generates structural effects in proximity of smooth walls. Such phenomenon is still present for asperities lower than a molecular width of hexadecane, but it is progressively frustrated as A increases [9]. In the case of copper oxide the

wall-fluid potential is weaker, and only the presence of roughness causes locking. As a consequence, $L_{lock,peak}$ is roughly equal to the thickness of a single lubricant layer for all the considered amplitude range.

In conclusion, it was shown that the locking phenomenon appears in presence of nano-rough surfaces for asperity wavelengths up to a few molecular lengths, and amplitudes ranging from atomic roughness to a few lattice constants. In particular, 1-2 layers of molecules were pinned on top of the asperity peaks in all the studied configurations. This preliminary result was also shown to be in accordance with trends in simulations and experiments from the literature. However, the understanding of real engineered surfaces requires further analysis. Larger systems should be simulated to bridge the gap between nanometer and micrometer scale waviness. Moreover complex geometries representative of the topography in a contact interface should be analyzed. Due to computational limits of the Molecular Dynamics model, these aspects will not be considered in the present work. Instead, the role played by the operating conditions on locking will be discussed.

C.4. Influence of the operating conditions

According to the methodology used in Section III.3, interfacial flow in molecularly thin films was characterized as a function of the pressure and wall speed. This allowed the formulation of laws which can directly be integrated into macroscopic simulations. The same procedure is used in the following to quantify the locking phenomenon in the case of rough surfaces.

The influence of the wall velocity difference is considered first. Figure C-8 shows the evolution of the locking length above the asperities for Δu values from 2 to 20 m/s.
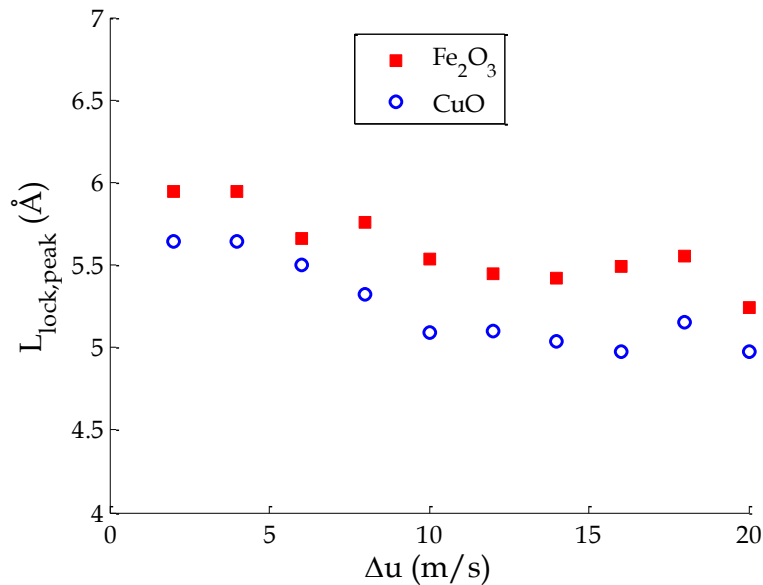
Figure C-8: Dependence of the locking length above the asperities with the wall velocity difference. λ=4.8 nm, A=0.3 nm, P=0.5 GPa, T$_{wall}$=300K.

An almost constant value for $L_{lock,peak}$ is obtained, roughly equal to the diameter of a hexadecane molecule [7]. Locking decreases slightly (10%) for high wall speeds. In this case,

the surface roughness and wall-fluid interactions are not sufficient to keep the molecules in the asperity valleys from moving. However, such trend is limited by the occurrence of shear thinning effects at high shear rates, and $L_{lock,peak}$ achieves a stable value for a wall velocity difference of Δu =10 m/s.

The effect of the external pressure on the contact nano-patch is shown in Figure C-9a for P ranging between 0.1 and 2 GPa. Both the average and effective film thickness decrease as the external load rises, due to compressibility effects in the lubricant [37] well approximated by the Dowson-Higginson bulk law. The dimensionless variable $\bar{L}_{lock,peak}$ is introduced to quantify locking film independently of variation in the gap width with pressure:

$$\bar{L}_{lock,peak} = \frac{L_{lock,peak}}{h_{avg}} \tag{C.7}$$

Figure C-9b shows that $\bar{L}_{lock,peak}$ is almost constant for the considered pressure range. This shows that the boundary layers are compressed at high loads, similarly to the rest of the fluid. The locking dependence on pressure can then be estimated by:

$$L_{lock,peak}(P) = L_{lock,peak}(P_{ref}) \frac{\rho(P_{ref})}{\rho(P)} \tag{C.8}$$

In Equation (C.8), $L_{lock,peak}(P_{ref})$ represents the locking length at a given reference pressure. This value can be obtained through Molecular Dynamics: in example, $L_{lock,peak}$ =0.52 nm at P_{ref} =500 MPa from Figure C-5. Alternatively, the height of one molecular layer of hexadecane under confined conditions can be used. The density-pressure dependence can be expressed through bulk compressibility laws like the Dowson-Higginson relationship [37].
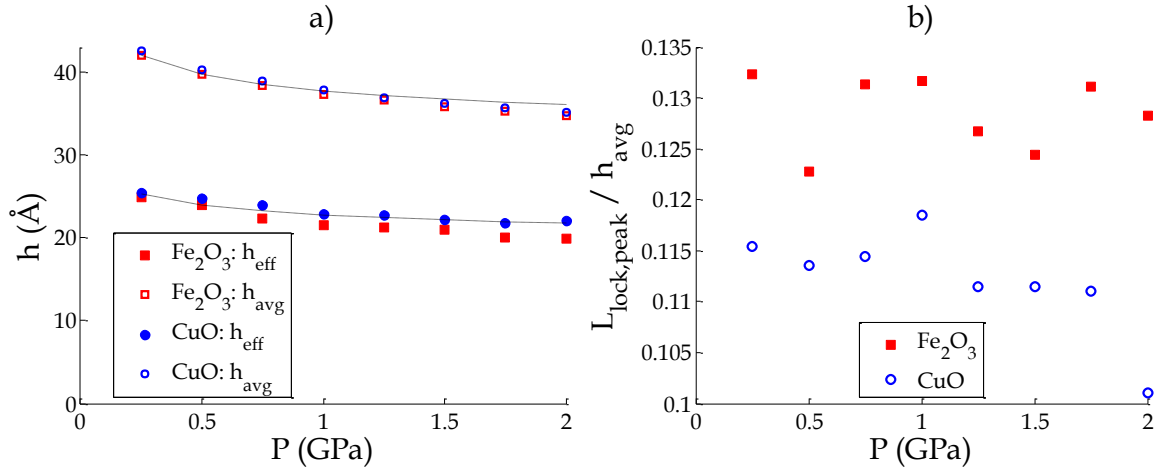
Figure C-9: Dependence of the film thickness (a) and dimensionless locking length above the asperities (b) with pressure. The dashed lines in (a) represent the thickness evolution according to the Dowson-Higginson compressibility law. λ=4.8 nm, A=0.3 nm, u2=-u1=10 m/s, Twall=300K.

In conclusion, the pinned layers on top of the roughness peaks feature a height roughly equal to the diameter of an n-hexadecane molecule. Furthermore, their compressibility under high loads is comparable with the rest of the fluid. This condition holds true for the operating conditions in pressure and speed typical of an elasto-hydrodynamic contact. Hence, the formulation of a semi-analytical law for locking is straightforward:

$$L_{lock}[\text{nm}] = A[\text{nm}] + 0.52 \frac{\rho(500\,\text{MPa})}{\rho(P)} \tag{C.9}$$

where A is the asperity amplitude and the second term corresponding to $L_{lock,peak}(P)$ from Equation (C.8). This formulation is valid for asperity wavelengths between 1 and 10 nm, and amplitudes ranging from atomic roughness to a few lattice constants.

C.5. Influence of locking on friction and nano-rheology

In molecularly confined films the wall waviness can be of the order of magnitude of the surface separation [109]. According to the predictive law in Equation (C.9), the pinned layers extend deeply within the gap width for large asperity amplitudes. Consequently, the thickness h_{eff} of the sheared region in the film center is severely reduced, and the effective shear rate increases significantly (see Section C.2). Both the rheology of the confined fluid and friction can be affected by this change in the lubricant dynamics: their dependence with locking will be studied hereafter. The shear rate increase in the center of the film is obtained by combining Equations (C.3) and (C.5):

$$\dot{\gamma}_{eff} = \frac{\Delta u}{h_{eff}} = \frac{\Delta u}{h_{avg} - 2L_{Lock}} \tag{C.10}$$

The corresponding shear stress τ_{zx} in the system can be expressed as:

$$\tau_{zx} = \eta(\dot{\gamma}_{eff}) \cdot \dot{\gamma}_{eff} \tag{C.11}$$

where $\eta(\dot{\gamma}_{eff})$ is the viscosity of the lubricant in the fully sheared region of the film. A rise in friction with locking is expected, compared to the no-slip boundary condition where $L_{lock} = 0$ and the shear rate is equal to $\dot{\gamma}_{app} = \Delta u / h_{avg}$. The change in shear stress can be obtained by combining Equations (C.10) and (C.11):

$$\frac{\tau_{zx}(L_{lock})}{\tau_{zx}(L_{lock}=0)} = \frac{\eta(\dot{\gamma}_{eff})}{\eta(\dot{\gamma}_{avg})} \cdot \frac{h_{avg}}{h_{eff}} = \frac{\eta(\dot{\gamma}_{eff})}{\eta(\dot{\gamma}_{avg})} \cdot \left(1 - \frac{2L_{lock}}{h_{avg}}\right)^{-1} \tag{C.12}$$

For Newtonian fluids, whose viscosity does not depend on the shear rate, Equation (C.12) can be simplified to:

$$\frac{\tau_{zx}(L_{lock})}{\tau_{zx}(L_{lock}=0)} = \left(1 - \frac{2L_{lock}}{h_{avg}}\right)^{-1} \tag{C.13}$$

thus giving a direct relationship between the increase in friction and locking. On the other hand, shear thinning effects may occur in the lubricant under high levels of forcing. In this case, the shear rate dependence of the viscosity in Equation (C.12) must be accounted for.

The dependence of friction on the height of the pinned layers is shown in Figure C-10 for a Newtonian fluid, as well as for the current study of n-hexadecane confined between rough surfaces. According to Section III.2.4, shear thinning effects occur in $C_{16}H_{34}$ under the chosen operating conditions. As a consequence, the shear stress increase is less marked. This is well exemplified by Figure C-10. At a locking length of $L_{lock}/h_{avg} = 0.25$, corresponding to a doubling of the effective shear rate compared to the no-slip condition, friction is also

doubled for a Newtonian case. On the other hand, an increase of only 30% is observed for confined hexadecane.
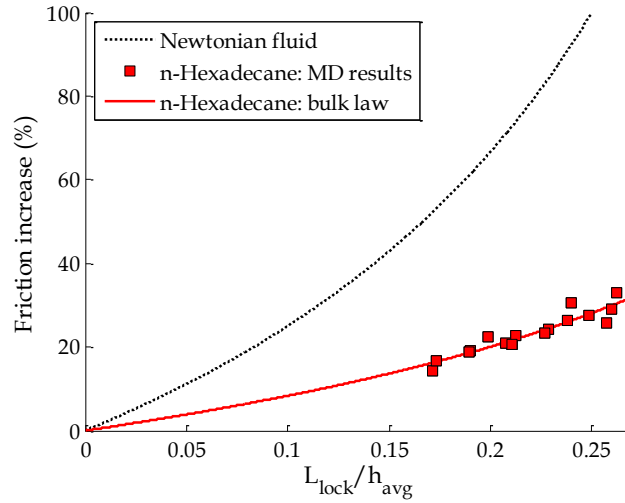
Figure C-10: Friction increase with the locking length, compared to a standard no-slip case. Both the evolution for a Newtonian fluid and P=0.5 GPa, u_2=-u_1=10 m/s, T_{wall}=300K.

Molecular Dynamics friction results can be predicted by coupling Equation (C.12) with bulk rheological models. The procedure supposes that the fluid under confinement is characterized by a disordered structure with a bulk like behavior in its center: this hypothesis is in accordance with results from the literature [13, 95], and was validated in Section III.2.4. In the present case, the modified Carreau model from Equation (III.14) is used for n-hexadecane. The predicted increase in friction using bulk properties matches well the results issued from Molecular Dynamics.

C.6. Conclusion

In conclusion, this Appendix proposes a first insight on the influence of nanometer scale roughness on the behavior of nano-confined films. The results show a deep change in the lubricant density and dynamics compared to flat walls. Interfacial flow under shear changes to a locking condition independently of the wall-fluid interaction energy and commensurability. This occurs for roughness wavelengths up to a few molecular lengths, and amplitudes ranging from the atomic size to a few lattice constants. Furthermore, the height of the locked layers is independent on the level of forcing, but is subject to compressibility effects under high loads. Finally, an increase in both the shear rate and friction is observed compared to a smooth wall case, though the latter can be limited by non-Newtonian effects at high levels of forcing.

Appendix D. Derivation of the 1-D Reynolds equation with slip on the lower wall

In this Appendix, the derivation of the 1-dimensional Reynolds equation including slip effects on the lower wall is detailed. Its formulation is based on the hypotheses of an isothermal, steady state line contact and a Newtonian, compressible fluid (see Chapter IV). The procedure requires two main steps: the calculation of the velocity profiles using the simplified Navier-Stokes equations, and the coupling with the mass conservation law to obtain the Reynolds equation.

D.1. Fluid velocity

The classical Navier-Stokes equations for fluid flow are simplified according to the standard assumptions of the lubrication theory (thin film, laminar flow, no inertia effects) [32]. Equation (D.1) represents the starting point for the calculation of the velocity profiles in the film:

$$\frac{\partial u}{\partial z}\left(\eta \frac{\partial u}{\partial z}\right) = \frac{\partial P}{\partial x} \tag{D.1}$$

Integrating twice along z yields:

$$u(z) = \frac{1}{\eta}\frac{\partial P}{\partial x}\frac{z^2}{2} + Az + B \tag{D.2}$$

The integration constants A and B can be obtained from the boundary conditions for the fluid flow. For a reminder, no-slip was imposed on the upper wall, whereas a Navier-type boundary condition is chosen for the lower wall, with the slip length L_s quantifying the modification of interfacial flow (see Chapter IV):

$$u(h) = u_2 \tag{D.3}$$

$$u(0) = u_1 + L_s \frac{\partial u}{\partial z}(0) \tag{D.4}$$

By using Equation (D.4), one obtains the following integration constants:

$$A = \frac{\partial u}{\partial z}(0) = \frac{1}{L_s}(u(0) - u_1) \tag{D.5}$$
$$B = u(0)$$

which can then be combined in Equation (D.2):

$$u(z) = \frac{1}{\eta}\frac{\partial P}{\partial x}\frac{z^2}{2} - \frac{u_1 z}{L_s} + u(0)\left(1 + \frac{z}{L_s}\right) \tag{D.6}$$

The no-slip boundary condition from Equation (D.3) is applied:

Appendix D – Derivation of the 1-D Reynolds equation with slip on the lower wall

$$u(h) = u_2 = \frac{1}{\eta}\frac{\partial P}{\partial x}\frac{h^2}{2} - \frac{u_1 h}{L_s} + u(0)\left(1 + \frac{h}{L_s}\right) \tag{D.7}$$

This allows the determination of the fluid velocity $u(0)$ at the lower wall as a function of the imposed wall speeds and the slip length:

$$u(0) = \left(u_2 - \frac{1}{\eta}\frac{\partial P}{\partial x}\frac{h^2}{2} + \frac{u_1 h}{L_s}\right)\left(\frac{L_s}{L_s + h}\right) \tag{D.8}$$

Finally, combining Equations (D.6) and (D.7) finally gives the velocity profile within the lubricant film:

$$u(z) = \frac{1}{2\eta}\frac{\partial P}{\partial x}\left(z^2 - \frac{L_s + z}{L_s + h}h^2\right) + u_1\left(\frac{h - z}{L_s + h}\right) + u_2\left(\frac{L_s + z}{L_s + h}\right) \tag{D.9}$$

D.2. Reynolds Equation

The velocity profile from Equation (D.9) can then be coupled with the mass conservation law, which can be written as follows for a line contact and a compressible flow:

$$\frac{\partial \rho u}{\partial x} + \frac{\partial \rho w}{\partial z} = 0 \tag{D.10}$$

By integrating Eq. (D.10) across the film thickness and using Leibnitz's integration rule to interchange derivation and integration one obtains:

$$\rho w\big|_0^h = -\int_0^h \frac{\partial \rho u(z)}{\partial x}dz = -\frac{d}{dx}\left(\rho \int_0^h u(z)dz\right) + \rho u(h)\frac{\partial h}{\partial x} - \rho u(0)\frac{\partial 0}{\partial x} \tag{D.11}$$

Equations (D.9) and (D.11) are then combined:

$$\rho w\big|_0^h = -\frac{d}{dx}\left(\int_0^h \rho\left[\frac{1}{2\eta}\frac{\partial P}{\partial x}\left(z^2 - \frac{L_s + z}{L_s + h}h^2\right) + u_1\left(\frac{h - z}{L_s + h}\right) + u_2\left(\frac{L_s + z}{L_s + h}\right)\right]dz\right) + \rho u_2\frac{\partial h}{\partial x}$$
$$= -\frac{\partial}{\partial x}\left(\frac{\rho}{2\eta}\frac{\partial P}{\partial x}\left(\frac{h^3}{3} - h^3\frac{L_s + h/2}{L_s + h}\right) + \rho u_1\left(h\frac{h - h/2}{L_s + h}\right) + \rho u_2\left(h\frac{L_s + h/2}{L_s + h}\right)\right) + \rho u_2\frac{\partial h}{\partial x} \tag{D.12}$$

Further simplification gives:

$$\rho w\big|_0^h = \frac{\partial}{\partial x}\left(\frac{\rho}{12\eta}\left(h^3\frac{h + 4L_s}{h + L_s}\right)\frac{\partial P}{\partial x} - \frac{\rho h^2}{2(h + L_s)}u_1 - \frac{\rho h(h + 2L_s)}{2(h + L_s)}u_2\right) + \rho u_2\frac{\partial h}{\partial x} \tag{D.13}$$

By considering that the surface curvature is very small across the film thickness, the left hand side term, equal to the approach velocity of the surfaces, can be approximated by [32]:

$$\rho w\big|_0^h \approx \rho\frac{\partial h}{\partial t} + \rho u_2\frac{\partial h}{\partial x} \tag{D.14}$$

Moreover, $\partial h / \partial t = 0$ under steady state conditions. Hence, the 1-dimensional, isothermal Reynolds equation with slip boundary condition on the lower wall for a Newtonian, compressible fluid is finally obtained:

Appendix D – Derivation of the 1-D Reynolds equation with slip on the lower wall

$$\frac{\partial}{\partial x}\left(\frac{\rho}{12\eta}\left(h^3\frac{h+4L_s}{h+L_s}\right)\frac{\partial P}{\partial x} - \frac{\rho h^2}{2(h+L_s)}u_1 - \frac{\rho h(h+2L_s)}{2(h+L_s)}u_2\right) = 0 \qquad (\text{D.15})$$

Bibliography

[1] D. Dowson. *History of Tribology*. Longman, London, 1979.

[2] O. Reynolds. On the theory of lubrication and its application to Mr. Beauchamp Tower's experiments, including an experimental determination of the viscosity of olive oil. *Philos. Trans. Roy. Soc. London*, 177:157–234, 1886.

[3] R.G. Horn and J.N. Israelachvili. Direct measurement of structural forces between two surfaces in a nonpolar liquid. *J. Chem. Phys.*, 75(3):1400–1411, 1981.

[4] J.N. Israelachvili. *Intermolecular and Surface Forces*. Colloid Science. Academic Press Inc, 2nd revised edition, 1991.

[5] M.P. Allen and D.J. Tildesley. *Computer Simulations of Liquids*. Clarendon Press, Oxford, 1987.

[6] J. Gao, W.D. Luedtke, and U. Landman. Layering transitions and dynamics of confined liquid films. *Phys. Rev. Lett.*, 79(4):705–708, 1997.

[7] H.K. Christenson, D.W.R. Gruen, R.G. Horn, and J.N. Israelachvili. Structuring in liquid alkanes between solid surfaces: Force measurements and mean-field theory. *J. Chem. Phys.*, 87(3):1834–1841, 1987.

[8] P.A. Thompson and M.O. Robbins. Shear flow near solids: Epitaxial order and flow boundary conditions. *Physical Review A*, 41(12):6830–6837, 1990.

[9] J. Gao, W.D. Luedtke, and U. Landman. Structures, solvation forces and shear of molecular films in a rough nano-confinement. *Tribol. Lett.*, 9:3–13, 2000.

[10] P. Padilla and S. Toxvaerd. Fluid alkanes in confined geometries. *J. Chem. Phys.*, 101(2):1490–1502, 1994.

[11] S. Granick. Motions and relaxations of confined liquids. *Science*, 253(5026):1374–1379, 1991.

[12] M.L. Gee, P.M. McGuiggan, J.N. Israelachvili, and A.M. Homola. Liquid to solidlike transitions of molecularly thin films under shear. *J. Chem. Phys.*, 93(3):1895–1906, 1990.

[13] G. Luengo, J. Israelachvili, and S. Granick. Generalized effects in confined fluids: New friction map for boundary lubrication. *Wear*, 200(1-2):328 – 335, 1996.

[14] J. Gao, W.D. Luedtke, and U. Landman. Structure and solvation forces in confined films: Linear and branched alkanes. *J. Chem. Phys.*, 106(10):4309–4318, 1997.

[15] A. Jabbarzadeh, J.D. Atkinson, and R.I. Tanner. Rheological properties of thin liquid films by molecular dynamics simulations. *Journal of Non-Newtonian Fluid Mechanics*, 69(2-3):169 – 193, 1997.

[16]   A. Jabbarzadeh, J.D. Atkinson, and R.I. Tanner. The effect of branching on slip and rheological properties of lubricants in molecular dynamics simulation of couette shear flow. *Tribol. Int.*, 35:35–46, 2002.

[17]   N.V. Priezjev. Rate-dependent slip boundary conditions for simple fluids. *Phys. Rev. E*, 75:051605, 2007.

[18]   N. Fillot, H. Berro, and P. Vergne. From continuous to molecular scale in modelling elastohydrodynamic lubrication: Nanoscale surface slip effects on film thickness and friction. *Tribol. Lett.*, 43:257–266, 2011.

[19]   J.N. Ding, J. Chen, and J.C. Yang. The effects of surface roughness on nanotribology of confined two-dimensional films. *Wear*, 260:205–208, 2006.

[20]   T. Kato and H. Matsuoka. Molecular layering in thin-film elastohydrodynamics. *Proc. IMechE Part J: J. Eng. Tribol.*, 213:363–369, 1999.

[21]   M. Teodorescu, S. Balakrishnan, and H. Rahnejat. Physics of ultra-thin surface films on molecularly smooth surfaces. *Proc. IMechE Part N: J. Nanoengineering and Nanosystems*, 220:7–18, 2006.

[22]   L.M. Chu, J.R. Lin, W.L. Li, and J.M. Lu. A model for line-contact EHL problems — consideration of effects of Navier-slip and lubricant rheology. *J. Tribol.*, 134(3):031502, 2012.

[23]   H. Berro. *A Molecular Dynamics Approach to Nano-scale Lubrication*. PhD thesis, MEGA, INSA de Lyon, October 11th, 2010. 2010ISAL0084.

[24]   W.L. Jorgensen and J. Tirado-Rives. The OPLS forcefield for proteins. energy minimizations for crystals of cyclic peptides and crambin. *J. Am. Chem. Soc.*, 110:1657–1723, 1988.

[25]   T.K. Xia, J. Ouyang, M.W. Ribarsky, and U. Landman. Interfacial alkane films. *Phys. Rev. Lett.*, 69(13):1967–1970, 1992.

[26]   R. Shuttleworth. The surface tension of solids. *Proceedings of the Physical Society A*, 63(5):444–457, 1950.

[27]   T. Schneider and E. Stoll. Molecular-dynamics study of a three-dimensional one-component model for distortive phase transitions. *Phys. Rev. B*, 17(3):1302–1322, 1978.

[28]   H. Berro, N. Fillot, P. Vergne, T. Tokumasu, T. Ohara, and G. Kikugawa. Energy dissipation in non-isothermal molecular dynamics simulations of confined liquids under shear. *J. Chem. Phys.*, 135:134708, 2011.

[29]   A. Martini, A. Roxin, R.Q. Snurr, Q. Wang, and S. Lichter. Molecular mechanisms of liquid slip. *J. Fluid Mech.*, 600:257–269, 2008.

[30]   L. Bocquet and J.-L. Barrat. Flow boundary conditions from nano- to micro-scales. *Soft Matter*, 3:685–693, 2007.

[31]   B. Tower. First report on friction experiments (friction of lubricated bearings). *Proc. Instn. Mech. Engrs.*, page 632–659, 1883.

[32] A.S. Szeri. *Fluid Film Lubrication: Theory and Design*. Cambridge University Press, 2005.

[33] R. Stribeck. Die wesentlichen Eigenschaften der Gleit- und Rollenlager. *Z. Verein. Deut. Ing.*, 46:1341–1348, 1902.

[34] H. Hertz. Über die Berührung fester elastischer Körper. *Journal für die reine und angewandte Mathematik*, 92:156–171, 1881.

[35] A. Ertel. Hydrodynamic lubrication based on new principles. *Akad. SSR Prikadnaya Mathematica i Mekhanika*, 2:41–52, 1939.

[36] A.N. Grubin and I.E. Vinogradova. *Investigation of the contact of machine components*. Central Scientific Research Institute for Technology and Mechanical Engineering Moscow, 1949.

[37] D. Dowson and G.R. Higginson. *Elastohydrodynamic Lubrication, The Fundamentals of Roller and Gear Lubrication*. Pergamon Press, 1966.

[38] C. Barus. Isothermal, isopiestics and isometrics relative to viscosity. *Am. J. Sci.*, 45:87–96, 1893.

[39] C.J.A. Roelands. *Correlational aspects of the viscosity-temperature-pressure relationship of lubricating oil*. PhD thesis, Techische Hogeschool Delft, 1966.

[40] M.L. Williams, R.F. Landel, and J.D. Ferry. The temperature dependence of relaxation mechanisms in amorphous polymers and other glass-forming liquids. *J. Am. Chem. Soc.*, 77(14):3701–3707, 1955.

[41] S. Bair. A rough shear-thinning correction for ehd film thickness. *STLE Trib. Trans.*, 47:361–365, 2004.

[42] H.S. Cheng and B. Sternlicht. A numerical solution for the pressure, temperature, and film thickness between two infinitely long, lubricated rolling and sliding cylinders, under heavy loads, journal of basic engineering,. *J. Basic Eng.*, 87(3):695–704, 1965.

[43] H.S. Cheng. A refined solution to the thermal-elastohydrodynamic lubrication of rolling and sliding cylinders. *ASLE Trans.*, 8:397–410, 1965.

[44] W. Habchi, P. Vergne, S. Bair, O. Andersson, D. Eyheramendy, and G.E. Morales-Espejel. Influence of pressure and temperature dependence of thermal properties of a lubricant on the behaviour of circular TEHD contacts. *Tribol. Int.*, 43:1842–1850, 2010.

[45] V. Bruyere, N. Fillot, G.E. Morales-Espejel, and P. Vergne. Computational fluid dynamics and full elasticity model for sliding line thermal elastohydrodynamic contacts. *Tribol. Int.*, 46(1):3–13, 2012.

[46] T. Doki-Thonon, N. Fillot, G.E. Morales-Espejel, M. Querry, D. Philippon, N. Devaux, and P. Vergne. A dual experimental / numerical approach for film thickness analysis in TEHL spinning skewing circular contacts. *Tribol. Lett.*, 50(1):115–126, 2013.

[47] W. Habchi and J. Issa. Fast and reduced full-system finite element solution of ehl problems: Line contacts. *Advances in Engineering Software*, 56:51–62, 2013.

[48] H.P. Evans and G. Hughes. Evaluation of deflection in semi-infinite bodies by a differential method. *Proc. IMechE Part C: Journal of Mechanical Engineering Science*, 214(4):563–584, 2000.

[49] C.H. Venner and A.A. Lubrecht. *Multi-Level Methods in Lubrication*. Elsevier, 2000.

[50] F. Robbe-Valloire. Statistical analysis of asperities on a rough surface. *Wear*, 249:401–408, 2001.

[51] B. Lorentz and A. Albers. A numerical model for mixed lubrication taking into account surface topography, tangential adhesion effects and plastic deformations. *Tribol. Int.*, 59:259 – 266, 2013.

[52] R. Holm. The friction force over the real area of contact. *Wiss. Veröff. Siemens-Werk*, 17(4):38–42, 1938.

[53] F.P. Bowden and D. Tabor. *The friction and lubrication of solids*. Oxford University Press, 1950.

[54] Y. Hori. *Hydrodynamic Lubrication*. Springer-Verlag, Tokyo, 2006.

[55] P. Wriggers and P.D. Panagiotopoulos. *New developments in contact problems*. Springer Verlag, 1999.

[56] A.D. Berman and J.N. Israelachvili. *Modern Tribology Handbook*, volume 1, chapter 16: Microtribology and Microrheology or Molecularly Thin Liquid Films, pages 567–616. CRC Press LLC, 2001.

[57] P.M. Lugt and G.E. Morales-Espejel. A review of elasto-hydrodynamic lubrication theory. *Tribol. Trans.*, 54:470–496, 2011.

[58] P.M. Lugt, R.W.M. Severt, J. Fogelström, and J.H. Tripp. Influence of surface topography on friction, film breakdown and running-in in the mixed lubrication regime. *Proceedings of the Institution of Mechanical Engineers, Part J: Journal of Engineering Tribology*, 215:519–533, 2001.

[59] S.M. Lundgren, K. Persson, and G. Mueller. Unsaturated fatty acids in alkane solution: adsorption to steel surfaces. *Langmuir*, 23:10598–10602, 2007.

[60] W. Habchi, P. Vergne, D. Eyheramendy, and G.E. Morales-Espejel. Numerical investigation of the use of machinery low-viscosity working fluids as lubricants in elasto-hydrodynamic lubricated point contacts. *Proc. IMechE Part J: J. Engineering Tribology*, 225:465–477, 2011.

[61] W. Habchi. *A full-system finite element approach to elastohydrodynamic lubrication problems: application to ultra-low-viscosity fluids*. PhD thesis, MEGA, INSA de Lyon, July 1st, 2008. 2008ISAL0038.

[62] P. Frantz, N. Agrait, and M. Salmeron. Use of capacitance to measure surface forces. 1. Measuring distance of separation with enhanced spatial and time resolution. *Langmuir*, 12(13):3289–3294, 1996.

[63] R.W. Carpick and M. Salmeron. Scratching the surface: Fundamental investigations of tribology with atomic force microscopy. *Chem. Rev.*, 97(4):1163–1194, 1997.

[64] J. Van Alsten and S. Granick. Molecular tribometry of ultrathin liquid films. *Phys. Rev. Lett.*, 61(22):2570–2573, 1988.

[65] D.Y.C. Chan and R.G. Horn. The drainage of thin liquid films between solid surfaces. *J. Chem. Phys.*, 83(10):5311–5324, 1985.

[66] N. Metropolis and S.Ulam. The Monte Carlo method. *J. Am. Stat. Assoc.*, 44(247):335–341, 1949.

[67] N. Metropolis, A.W. Rosenbluth, M.N. Rosenbluth, A.H. Teller, and E. Teller. Equation of state calculations by fast computing machines. *J. Chem. Phys.*, 21(6):1087, 1953.

[68] R.G. Horn and J.N. Israelachvili. Molecular organization and viscosity of a thin film of molten polymer between two surfaces as probed by force measurements. *Macromolecules*, 21(3):2836–2841, 1988.

[69] H.K. Christenson, R.G. Horn, and J.N. Israelachvili. Measurement of forces due to structure in hydrocarbon liquids. *J. Colloid Interface Sci.*, 88(1):79 – 88, 1982.

[70] F.F. Abraham. The interfacial density profile of a Lennard-Jones fluid in contact with a (100) Lennard-Jones wall and its relationship to idealized fluid/wall systems: A Monte Carlo simulation. *J. Chem. Phys.*, 68(8):3713–3716, 1978.

[71] I.K. Snook and W. van Megan. Solvation forces in simple dense fluids. *J. Chem. Phys.*, 72(5):2907–2913, 1980.

[72] J. Gao, W.D. Luedtke, and U. Landman. Origins of solvation forces in confined films. *J. Phys. Chem. B*, 101:4013–4023, 1997.

[73] B.N.J. Persson and P. Ballone. Boundary lubrication: layering transition for curved solid surfaces with long-range elasticity. *Solid State Commun.*, 115:599–604, 2000.

[74] I.M. Sivebaek, V.N. Samoilov, and B.N.J. Persson. Squeezing molecular thin alkane films between curved solid surfaces with long-range elasticity: Layering transitions and wear. *J. Chem. Phys.*, 119:2314–2321, 2003.

[75] B.N.J. Persson and F. Mugele. Squeeze-out and wear: fundamental principles and applications. *J. Phys.: Condens. Matter*, 16:295–355, 2004.

[76] V.N. Samoilov, I.M. Sivebaek, and B.N.J. Persson. The effect of surface roughness on the adhesion of solid surfaces for systems with and without liquid lubricant. *J. Chem. Phys.*, 121(19):1997, 2004.

[77] U. Tartaglino, I.M. Sivebaek, B.N.J. Persson, and E. Tosatti. Impact of molecular structure on the lubricant squeeze-out between curved surfaces with long range elasticity. *J. Chem. Phys.*, 125(1):014704, 2006.

[78] J.N. Israelachvili and S. Kott. Liquid structuring at solid interfaces as probed by direct force measurements: The transition from simple to complex liquids and polymer fluids. *J. Chem. Phys.*, 88:7162–7166, 1988.

[79] A.D. Berman and J.N. Israelachvili. *Handbook of Micro/Nanotribology*, chapter Surface forces and microrheology of molecularly thin liquid films. CRC Press, 1999.

[80] J.-L. Barrat and L. Bocquet. Influence of wetting properties on the hydrodynamic boundary condition at a fluid-solid interface. *Faraday Discuss.*, 112(9812218):119–128, 1999.

[81] A. Jabbarzadeh and R.I. Tanner. Thin lubricant films confined between crystalline surfaces: Gold versus mica. *Tribol. Int.*, 44:711–719, 2011.

[82] J. Van Alsten and S. Granick. The origin of static friction in ultrathin liquid films. *Langmuir*, 6:876–880, 1990.

[83] J. Van Alsten and S. Granick. Shear rheology in a confined geometry - polysiloxane melts. *Macromolecules*, 23:4856–4862, 1990.

[84] J. Klein and E. Kumacheva. Confinement-induced phase transitions in simple liquids. *Science*, 269:816–819, 1995.

[85] H.-W. Hu, G.A. Carson, and S. Granick. Relaxation time of confined liquids under shear. *Phys. Rev. Lett.*, 66(21):2758–2761, 1991.

[86] J.N. Israelachvili. Measurement of the viscosity of liquids in very thin films. *Journal of Colloid and Interface Science*, 110(1):263 – 271, 1986.

[87] J. Klein and E. Kumacheva. Simple liquids confined to molecularly thin layers. I. Confinement induced liquid-to-solid phase transitions. *J. Chem. Phys.*, 108:6996–7009, 1998.

[88] J.N. Israelachvili and P.M. McGuiggan. Forces between surfaces in liquids. *Science*, 241(4867):795–800, 1988.

[89] J. Gao, W.D. Luedtke, and U. Landman. Friction control in thin-film lubrication. *J. Phys. Chem. B*, 102:5033–5037, 1998.

[90] P.A. Thompson, G.S. Grest, and M.O. Robbins. Phase transitions and universal dynamics in confined films. *Phys. Rev. Lett.*, 68(23):3448–3451, 1992.

[91] S.A. Somers and H.T. Davis. Microscopic dynamics of fluids confined between smooth and atomically structured solid surfaces. *J. Chem. Phys.*, 96(7):5389–5407, 1992.

[92] A. Jabbarzadeh, P. Harrowel, and R.I. Tanner. Crystal bridge formation marks the transition to rigidity in a thin lubrication film. *Phys. Rev. Lett.*, 96(206102):1–4, 2006.

[93] A. Jabbarzadeh, P. Harrowel, and R.I. Tanner. Low friction lubrication between amorphous walls: Unraveling the contributions of surface roughness and in-plane disorder. *J. Chem. Phys.*, 125(3):034703, 2006.

[94] A. Jabbarzadeh, J.D. Atkinson, and R.I. Tanner. Nanorheology of molecularly thin films of n-hexadecane in couette shear flow by molecular dynamics simulation. *Journal of Non-Newtonian Fluid Mechanics*, 77(1-2):53 – 78, 1998.

[95] S.A. Gupta, H.D. Cochran, and P.T. Cummings. Shear behavior of squalane and tetracosane under extreme confinement. III. Effect of confinement on viscosity. *J. Chem. Phys.*, 107(23):10335–10343, 1997.

[96] G. Luengo, F.J. Schmitt, R. Hill, and J.N. Israelachvili. Thin film rheology and tribology of confined polymer melts: Contrasts with bulk properties. *Macromolecules*, 30(8):2482–2494, 1997.

[97] A. V. Ramamurthy. Wall slip in viscous fluids and influence of materials of construction. *Journal of Rheology*, 30(2):337–357, 1986.

[98] S. G. Hatzikiriakos and J. M. Dealy. Wall slip of molten high density polyethylene. I. sliding plate rheometer studies. *Journal of Rheology*, 35(4):497–523, 1991.

[99] K.B. Migler, H. Hervet, and L. Leger. Slip transition of a polymer melt under shear stress. *Phys. Rev. Lett.*, 70(3):287–290, 1993.

[100] U. Heinbuch and J. Fischer. Liquid flow in pores: Slip, no-slip, or multilayer sticking. *Phys. Rev. A*, 40(2):1144–1146, 1989.

[101] A. Jabbarzadeh, J.D. Atkinson, and R.I. Tanner. Wall slip in the molecular dynamics simulation of thin films of hexadecane. *J. Chem. Phys.*, 110(5):2612–2620, 1999.

[102] K. Falk, F. Sedlmeier, L. Joly, R.R. Netz, and L. Bocquet. Molecular origin of fast water transport in carbon nanotube membranes: Superlubricity versus curvature dependent friction. *Nano Letters*, 10:4067, 2010.

[103] A. Martini, H.Y. Hsu, N.A. Patankar, and S. Lichter. Slip at high shear rates. *Phys. Rev. Lett.*, 100(206001):1–4, 2008.

[104] N.V. Priezjev. Shear rate threshold for the boundary slip in dense polymer films. *Physical Review*, E 80:031608, 2009.

[105] N.V. Priezjev and S.M. Troian. Molecular origin and dynamic behavior of slip in sheared polymer films. *Phys. Rev. Lett.*, 92(1):018302, 2004.

[106] H. Berro, N. Fillot, and P. Vergne. Molecular dynamics simulation of surface energy and ZDDP effects on friction in nano-scale lubricated contacts. *Tribol. Int.*, 43(10):1811–1822, 2010.

[107] C. Trozzi and G. Ciccotti. Stationary nonequilibrium states by molecular dynamics. II. newton's law. *Phys. Rev. A*, 29:916–925, 1984.

[108] A. Jabbarzadeh, J.D. Atkinson, and R.I. Tanner. Effect of the wall roughness on slip and rheological properties of hexadecane in molecular dynamics simulation of couette shear flow between two sinusoidal walls. *Phys. Rev. E*, 61(1):690–699, 2000.

[109] M. Georges, S. Millot, J.L. Loubet, A. Tonck, and D. Mazuyer. Surface roughness and squeezed films at molecular level. In D. Dowson, editor, *Thin Films in Tribology: Proceedings of the 19th Leeds-Lyon Symposium*, number 25 in Tribology Series, page 443–452. Elsevier, 1993.

[110] A. Suzuki, K. Nakamura, R. Sato, K. Okushi, H. Tsuboi, N. Hatakeyama, A. Endou, H. Takaba, M. Kubo, M.C. Williams, and A. Miyamoto. Multi-scale theoretical study of support effect on sintering dynamics of Pt. *Surface Science*, 603:3049–3056, 2009.

[111] P.Z. Zhu, Y.Z. Hu, and H Wang. A hybrid model for multiscale simulations of nanoindentation. *Proc. IMechE Part J: J. Engineering Tribology*, 225:845–853, 2011.

[112] E. Lidorikis, M.E. Bachlechner, R.K. Kalia, A. Nakano, P. Vashishta, and G.Z. Voyiadjis. Coupling length scales for multiscale atomistics continuum simulations: atomistically induced stress distributions in Si/Si3N4 nanopixels. *Phys. Rev. Lett.*, 87:086104, 2001.

[113] C. Yang, U. Tartaglino, and B.N.J. Persson. A multiscale molecular dynamics approach to contact mechanics. *Eur. Phys. J. E*, 19:47–58, 2006.

[114] K.A. Blencoe and J.A. Williams. Friction of sliding surfaces carrying boundary films. *Wear*, 203(4):722–729, 1997.

[115] K.A. Blencoe, G.W. Roper, and J.A. Williams. The influence of lubricant rheology and surface topography in modelling friction at concentrated contacts. *Proc. IMechE Part J: J. Eng. Tribol.*, 212:391–400, 1998.

[116] K.A. Amuzu, B.J. Briscoe, and D. Tabor. The shear properties of thin inorganic films. *Rev. Deformation Behavior Mater.*, 3:151–191, 1980.

[117] A.I. Vakis, M. Eriten, and A.A. Polycarpou. Modeling bearing and shear forces in molecularly thin lubricants. *Tribol. Lett.*, 41(3):573–586, 2011.

[118] H. Matsuoka and T. Kato. An ultra-thin liquid film lubrication theory - calculation method of solvation pressure and its application to EHL problem. *J. Tribol.*, 119:217–226, 1997.

[119] S. Jang and J.A. Tichy. Modelling of mixed hydrodynamic and boundary lubrication: Layered structures and shear thinning. *Proc. IMechE Part J: J. Eng. Tribol.*, 212:171–177, 1998.

[120] M.F. Al-Samieh and H. Rahnejat. Nano-lubricant film formation due to combined elastohydrodynamic and surface force action under isothermal conditions. *Proc. IMechE Part C: Journal of Mechanical Engineering Science*, 34:1019–1029, 2001.

[121] A. Martini, Y. Liu, R.Q. Snurr, and Q.J. Wang. Molecular dynamics characterization of thin film viscosity for EHL simulation. *Tribol. Lett.*, 21(3):217–225, 2006.

[122] T.L. Sham and J.A. Tichy. A scheme for hybrid Molecular-Dynamics Finite-Element analysis of thin-film lubrication. *Wear*, 207(1-2):100–106, 1997.

[123] J.A. Tichy. A surface layer model for thin film lubrication. *ASLE Trans.*, 38(3):577–582, 1995.

[124] G.S. Beavers and D.D. Joseph. Boundary condition at a naturally permeable wall. *J. Fluid Mech.*, 30(1):197–207, 1967.

[125] H.A. Spikes. The half-wetted bearing. Part 1: extended Reynolds equation. *Proc. IMechE Part J: J. Eng. Tribol.*, 217:1–14, 2003.

[126] M.H. Meurisse and G.E. Morales Espejel. Reynolds equation,apparent slip,and viscous friction in a three-layered fluid film. *Proc. IMechE Part J: J. Engineering Tribology*, 222:369–380, 2008.

[127] D. Lide. *Handbook of Chemistry and Physics, 85th edn.* CRC Press, 2004-2005.

[128] S.M. Foiles, M.I. Baskes, and M.S. Daw. Embedded-Atom-Method functions for the FCC metals Cu, Ag, Au, Ni, Pd, Pt, and their alloys. *Phys. Rev. B*, 33(12):7983–7991, 1986.

[129] U.D. Lanke and M. Vedawyas. Ion beam processing of oriented CuO films deposited on (1 0 0) YSZ by laser ablation. *Nucl. Inst. Meth. Phys. Res. B*, 155:97, 1999.

[130] G. Rollmann, A. Rohrbach, P. Entel, and J. Hafner. First-principles calculation of the structure and magnetic phases of hematite. *Phys. Rev. B*, 69(16):165107, 2004.

[131] O. Borgen and H. M. Seip. The crystal structure of beta-si3n4. *Acta Chem. Scand.*, 15:1789, 1961.

[132] W.-Y. Ching, Y.-N. Xu, J.D. Gale, and M. Rühle. Ab-initio total energy calculation of alpha- and beta-silicon nitride and the derivation of effective pair potentials with application to lattice dynamics. *J. Am. Ceram. Soc.*, 81(12):3189–3196, 1998.

[133] L. Zhang, R. Balasundaram, S.H. Gehrke, and S. Jiang. Nonequilibrium molecular dynamics simulations of confined fluids in contact with the bulk. *J. Chem. Phys.*, 114(15):6869–6877, 2001.

[134] L. Zhao, L. Liu, and H. Sun. Semi-ionic model for metal oxides and their interfaces with organic molecules. *J. Phys. Chem. C*, 111(28):10610–10617, 2007.

[135] J. Kierfeld and V. Vinokur. Lindemann criterion and vortex lattice phase transitions in type-II superconductors. *Phys. Rev. B*, 69(024501):1–21, 2004.

[136] C. Kittel. *Introduction to Solid State Physics, 7th edition*. Wiley, 1995.

[137] J. Fraxedas, S. Garcia-Manyes, P. Gorostiza, and F. Sanz. Nanoindentation: Toward the sensing of atomic interactions. *PNAS*, 99(8):5228 –5232, 2002.

[138] F. Müller-Plathe and D. Reith. Cause and effect reversed in non-equilibrium molecular dynamics: an easy route to transport coefficients. *Computational and Theoretical Polymer Science*, 9:203–209, 1999.

[139] W.D. Cornell, P. Cieplak, C.I. Bayly, I.R. Gould, K.M. Merz, D.M. Ferguson, D.C. Spellmeyer, T. Fox, J.W. Caldwell, and P.A. Kollman. A second generation force field for the simulation of proteins, nucleic acids and organic molecules. *J. Am. Chem. Soc.*, (117):5179–5197, 1995.

[140] C. Minfray, T. Le Mogne, J.-M. Martin, T. Onodera, S. Nara, S. Takahashi, H. Tsuboi, M. Koyama, A. Endou, H. Takaba, M. Kubo, C.A. Del Carpio, and A. Miyamoto. Experimental and molecular dynamics simulations of tribochemical reactions with ZDDP: Zinc phosphate-iron oxide reaction. *Tribol. Trans.*, 51:589–601, 2008.

[141] R. Khare, J. de Pablo, and A. Yethiraj. Molecular simulation and continuum mechanics study of simple fluids in non-isothermal planar Couette flows. *J. Chem. Phys.*, 107(7):2589–2596, 1997.

[142] S.Y. Liem, D. Brown, and J.H.R. Clarke. Investigation of the homogeneous-shear non-equilibrium-molecular-dynamics method. *Phys. Rev. A*, 45(6):3706–3713, 1992.

[143] S.A. Gupta, H.D. Cochran, and P.T. Cummings. Nanorheology of liquid alkanes. *Fluid Phase Equilibr.*, 150-151:125–131, 1998.

[144] H. Hoang and G. Galliero. Local viscosity of a fluid confined in a narrow pore. *Phys. Rev. E*, 86:021202, 2012.

[145] M.J. Stevens, M. Mondello, G.S. Grest, S.T. Cui, H.D. Cochran, and P.T. Cummings. Comparison of shear flow of hexadecane in a confined geometry and in bulk. *J. Chem. Phys.*, 106(17):7303–7314, 1997.

[146] P.A. Thompson and S.M. Troian. A general boundary condition for liquid flowat solid surfaces. *Nature*, 389:360–362, 1997.

[147] L. Rogal, J. Dutkiewicz, T. Czeppe, J. Bonarski, and B. Olszowska-Sobieraj. Characteristics of 100Cr6 bearing steel after thixoforming process performed with prototype device. *Transactions of Nonferrous Metals Society of China*, 20:1033–1036, 2010.

[148] M. Perez, C. Sidoroff, A. Vincent, and C. Esnouf. Microstructural evolution of martensitic 100cr6 bearing steel during tempering: From thermoelectric power measurements to the prediction of dimensional changes. *Acta Mater.*, 57:3170–3181, 2009.

[149] D. Kamei, H. Zhou, K. Suzuki, K. Konno, S. Takami, M. Kubo, and A. Miyamoto. Computational chemistry study on the dynamics of lubricant molecules under shear conditions. *Tribol. Int.*, 36:297–202, 2003.

[150] A. Vadakkepatt, Y. Dong, S. Lichter, and A. Martini. Effect of molecular structure on liquid slip. *Phys. Rev. E*, 84:066311, 2011.

[151] M.O. Robbins and M.H. Müser. *Modern Tribology Handbook*, volume 1, chapter 20: Computer Simulations of Friction, Lubrication, and Wear, pages 717–765. CRC Press LLC, 2001.

[152] P. Ehret, D. Dowson, and C.M. Taylor. On lubricant transport conditions in elastohydrodynamic conjuctions. *Proc. Roy. Soc. Lond. A*, 454(1971):763–787, 1998.

[153] C.H. Venner and A.A. Lubrecht. Transient analysis of surface features in an ehl line contact in the case of sliding. *J. Tribol.*, 116(2):186–193, 1994.

[154] P.W. Bridgman. The effect of pressure on the viscosity of forty-three pure liquids. *Proceedings of the American Academy of Art and Sciences*, 61(3):57–99, 1926.

[155] D.R. Cauldwell, J.P.M. Trusler, V. Vesovic, and W.A. Wakeham. Viscosity and density of five hydrocarbon liquids at pressures up to 200 MPa and temperatures up to 473 K. *J. Chem. Eng. Data*, 54:359–366, 2009.

[156] M. Kaneta, H. Nishikawa, T. Kanada, and K. Matsuda. Abnormal phenomena appearing in EHL contacts. *J. Tribol.*, 118:886–892, 1996.

[157] K. Yagi, P. Vergne, and T. Nakahara. In situ pressure measurements in dimpled elastohydrodynamic sliding contacts by Raman microscopy. *Tribol. Int.*, 42:724–730, 2009.

[158] A. Jabbarzadeh, P. Harrowel, and R.I. Tanner. Very low friction state of a dodecane film confined between mica surfaces. *Phys. Rev. Lett.*, 94(126103):1–4, 2005.

[159] H. Berro, N. Fillot, and P. Vergne. Hybrid diffusion: an efficient method for kinetic temperature calculation in molecular dynamics simulations of confined lubricant films. *Tribol. Lett.*, 37(1):1–13, 2010.

[160] S. Naidu, E. Klaus, and J. Duda. Evaluation of liquid phase oxidation products of ester and mineral oil lubricants. *Ind. Eng. Chem. Prod. RD*, 23(4):613–619, 1984.

[161] S. Naidu, E. Klaus, and J. Duda. Kinetic model for high-temperature oxidation of lubricants. *Ind. Eng. Chem. Prod. RD*, 25(4):596–603, 1986.

[162] P. Padilla. Chemical structure effects on the equilibrium and under shear properties of thin films in confined geometries: A molecular dynamics simulation study. *J. Chem. Phys.*, 103(6):2157–2168, 1995.

[163] C.L. Kelchner, S.J. Plimpton, and J.C. Hamilton. Dislocation nucleation and defect structure during surface indentation. *Phys. Rev. B*, 58:11085–11088, 1998.

[164] P. Spijker, G. Anciaux, and J.-F. Molinari. Dry sliding contact between rough surfaces at the atomistic scale. *Tribol. Lett.*, 44:279–285, 2011.

[165] A.V. Hamza and R.J. Madix. The activation of alkanes on Ni(100). *Surface Science*, 179(1):25–46, 1987.

[166] Q. Dai and A.J. Gellman. A HREELS study of C1-C5 straight chain alcohols on clean and pre-oxidized ag(110) surfaces. *Surface Science*, 257(1-3):103 – 112, 1991.

[167] S. M. Wetterer, D. J. Lavrich, T. Cummings, S. L. Bernasek, and G. Scoles. Energetics and kinetics of the physisorption of hydrocarbons on au(111). *J. Phys. Chem. B*, 102(46):9266–9275, 1998.

[168] A. Baranyai, D.J. Evans, and P.J. Daivis. Isothermal shear-induced heat flow. *Phys. Rev. A*, 46(12):7593–7600, 1992.

[169] J.H. Lienhard-IV and J.H. Lienhard-V. *A Heat Transfer Textbook*. Phlogiston Press, Cambridge Massachusetts, 3 edition, January 2008.

[170] H.N.V. Temperley and D.H. Trevena. *Liquids and their properties: a molecular and macroscopic treatise with applications*. Halsted Press, 1978.

[171] X.-G. Wang, W. Weiss, Sh. K. Shaikhutdinov, M. Ritter, M. Petersen, F. Wagner, R. Schlögl, and M. Scheffler. The hematite (a-Fe2O3) (0001) surface: Evidence for domains of distinct chemistry. *Phisical Review Letters*, 81(5):1038–1041, 1998.

[172] E. Ricci and R. Novakovic. Wetting and surface tension measurements on gold alloys. *Gold Bulletin*, 34(2):41–49, 2001.

[173] M. Jia, Y. Lai, Z. Tian, and Y. Liu. Calculation of the surface free energy of fcc copper nanoparticles. *Modelling and Simulation in Materials Science and Engineering*, 17:015006, 2009.

[174] Y.-N. Wen and J.-M. Zhang. Surface energy calculation of the BCC metals by using the MEAM. *Computational Materials Science*, 2008:281–285, 42.

[175] L. Bao, C. Huo, C. Deng, and Y. Li. Structure and stability of the crystal Fe2C and low index surfaces. *Journal of Fuel Chemistry and Technology*, 37(1):104–108, 2009.

[176] P. Blonski and A. Kiejna. Calculation of surface properties of BCC iron. *Vacuum*, 74:179–183, 2004.

[177] B. Bhushan. *Modern Tribology Handbook*, volume 1, chapter 2: Surface Roughness Analysis and Measurement Techniques, pages 49–120. CRC Press LLC, 2001.

[178] K.-S. Kim, J.A. Hurtado, , and H. Tan. Evolution of a surface-roughness spectrum caused by stress in nanometer-scale chemical etching. *Phys. Rev. Lett.*, 83(19):3872–3875, 1999.

[179] U. Landman, W.D. Luedtke, and J. Gao. Atomic-scale issues in tribology: Interfacial junctions and nano-elastohydrodynamics. *Langmuir*, 12:4514–4528, 1996.

Publications and conferences

Publications:

[1] D. Savio, N. Fillot, P. Vergne, and M. Zaccheddu. A model for wall slip prediction of confined n-alkanes: effect of wall-fluid interaction versus fluid resistance, **Tribol. Lett.**, 46:11-22, 2012

[2] D. Savio, N. Fillot, and P. Vergne. A molecular dynamics study of the transition from ultra-thin film lubrication towards local film breakdown, **Tribol. Lett.**, 50:207-220, 2013

Conferences:

[1] D. Savio, H. Berro, N. Fillot, and P. Vergne. Lubrification à l'échelle nanométrique: influence de la structure des surfaces et du lubrifiant, Journées Internationales Francophones de Tribologie 2011, "Le nano et le micro dans la tribologie", **Obernai, France, May 11-13 2011**

[2] D. Savio, N. Fillot, and P. Vergne. A wall slip model at the nanometer scale: fluid resistance to shearing versus surface topology, 38th Leeds-Lyon Symposium on Tribology: "Energy and Health", **Lyon, France, Sep. 6-9 2011**

[3] D. Savio, N. Fillot, and P. Vergne. A model for predicting wall slip of alkanes confined between smooth surfaces, Engineering Conferences International: "Advances in Lubrication: Linking Molecular, Meso, and Machine Scales", **Puntarenas, Costa Rica, Jan. 8-13 2012**

[4] D. Savio, N. Fillot, P. Vergne, and M. Zaccheddu. From full film lubrication to local film breakdown: a molecular dynamics approach, International Joint Tribology Congress, **Denver, Colorado (USA), Oct. 8-10 2012**

[5] D. Savio, N. Fillot, and P. Vergne. From full film lubrication to local film breakdown: a molecular dynamics approach, ELyTLab, **Zao To-o-gatta, Japan, Feb. 18-20 2013 -** *Best poster award*

[6] D. Savio, N. Fillot, P. Vergne, H. Hetzler, W. Seemann, R. Pasaribu, and G. Morales-Espejel. Multi-scale modeling of lubricated contacts: a study on the velocity boundary condition at the wall-fluid interface, World Tribology Congress, **Torino, Italy, Sept. 9-13 2013**

FOLIO ADMINISTRATIF

THESE SOUTENUE DEVANT L'INSTITUT NATIONAL DES SCIENCES APPLIQUEES DE LYON

NOM : SAVIO   DATE de SOUTENANCE : 31/10/2013

Prénoms : Daniele

TITRE :

Nanoscale phenomena in lubrication:
from atomistic simulations to their integration into continuous models

NATURE : Doctorat   Numéro d'ordre : 2013-ISAL-0112

Ecole doctorale : Mécanique, Energétique, Génie civil, Acoustique (MEGA)

Spécialité : Mécanique

RESUME :
The modern trends in lubrication aim at reducing the oil quantity in tribological applications. As a consequence, the film thickness in the contact zone decreases significantly and can reach the order of magnitude of a few nanometres. Hence, the surface separation is ensured by very few lubricant molecules.
Atomistic simulations based on the Molecular Dynamics method are used to analyze the local behavior of these severely confined films. A particular attention is paid to the occurrence of wall slip: predictive models and analytical laws are formulated to quantify and predict this phenomenon as a function of the surface-lubricant pair or the local operating conditions in a contact interface.
Then, the coupling between Molecular Dynamics simulations and macroscopic models is explored. The classical lubrication theory is modified to include slip effects characterized previously. This approach is employed to study an entire contact featuring a nano-confined lubricant in its center, showing a severe modification of the film thickness and friction.
Finally, the lubricant quantity reduction is pushed to the limits up to the occurrence of local film breakdown and direct surface contact. In this scenario, atomistic simulations allow to understand the relationship between the configuration of the last fluid molecules in the contact and the local tribological behavior.

MOTS-CLES : tribology, lubrication, Molecular Dynamics, wall slip, multi-scale simulations, local film breakdown

Laboratoire (s) de recherche : LaMCoS (INSA-Lyon), ITM (Karlsruher Institut für Technologie)

Directeurs de thèse: Dr. Philippe VERGNE, Prof. Wolfgang SEEMANN, Dr. Nicolas FILLOT, Dr.-Ing. Hartmut HETZLER

Président de jury : Prof. Jean-Louis BARRAT

Composition du jury :

      Prof. Jean-Louis BARRAT (Examinateur)
      Prof. Guillaume GALLIERO (Rapporteur)
      Prof. Peter GUMBSCH (Rapporteur)
      Dr. Nicolas FILLOT (Co-directeur)
      Dr.-Ing. Hartmut HETZLER (Co-Directeur)
      Dr. Guillermo MORALES-ESPEJEL (Examinateur)
      Prof. Wolfgang SEEMANN (Directeur)
      Dr. Philippe VERGNE (Directeur)

Nanoscale phenomena in lubrication:
from atomistic simulations to their integration into continuous models

Keywords: tribology, lubrication, Molecular Dynamics, wall slip, multi-scale simulations, local film breakdown

The modern trends in lubrication aim at reducing the oil quantity in tribological applications. As a consequence, the film thickness in the contact zone decreases significantly and can reach the order of magnitude of a few nanometres. Hence, the surface separation is ensured by very few lubricant molecules.

Atomistic simulations based on the Molecular Dynamics method are used to analyze the local behavior of these severely confined films. A particular attention is paid to the occurrence of wall slip: predictive models and analytical laws are formulated to quantify and predict this phenomenon as a function of the surface-lubricant pair or the local operating conditions in a contact interface.

Then, the coupling between Molecular Dynamics simulations and macroscopic models is explored. The classical lubrication theory is modified to include slip effects characterized previously. This approach is employed to study an entire contact featuring a nano-confined lubricant in its center, showing a severe modification of the film thickness and friction.

Finally, the lubricant quantity reduction is pushed to the limits up to the occurrence of local film breakdown and direct surface contact. In this scenario, atomistic simulations allow to understand the relationship between the configuration of the last fluid molecules in the contact and the local tribological behavior.

Schlüsselwörter: Tribologie, Schmierungstechnik, Molekulardynamik, Wandschlupf, Multi-Skala-Simulationen, Zusammenbrechen des Schmierfilmes

Die heutigen Trends in der tribologischen Entwicklung führen zu einer Reduzierung der Ölmenge in geschmierten Mechanismen. Folglich nimmt die Schmierfilmdicke zwischen Festkörpern stark ab und erreicht oftmals Größenordnungen weniger Nanometer. In diesem Fall werden die Oberflächen nur von wenigen Ölmolekülen getrennt.

Atomistische Simulationen mit der Molekulardynamik-Methode wurden zur Charakterisierung des lokalen Verhaltens in nanometer-dünnen Schmierfilmen verwendet. Insbesondere wurde Wandschlupf an der Wand-Fluid-Grenzfläche untersucht. Ein Vorhersagemodell und analytische Gesetzte wurden entwickelt, um dieses Phänomen in Abhängigkeit von der Oberflächen-Schmiermittel-Paarung und den lokalen Betriebsbedingungen zu quantifizieren.

Durch diese modellhaften Beschreibungen wurden atomistische Simulationen mit makroskopischen Modellen für elasto-hydrodynamische (EHD) Kontakte gekoppelt. Insbesondere wurde die klassische EHD-Theorie verändert, um auch das durch Molekulardynamik charakterisierte Wandgleiten zu berücksichtigen. Anhand dieses Nano-EHD-Modells konnte ein Kontakt mit einer Schmierfilmdicke im Nanometerbereich untersucht werden. Hierbei zeigte sich, dass das Auftreten des Wandschlupfes in der Mitte des Kontaktes eine Veränderung der Spalthöhe und Reibung verursachen kann.

Schließlich wurde eine extreme Verminderung der Ölmenge bis hin zum lokalen Zusammenbrechen des Schmierfilms und dem direkten Festkörperkontakt untersucht. Durch Molekulardynamik-Simulationen konnte der Zusammenhang zwischen der Anordnung der letzten Molekülschichten im Kontaktbereich, das lokale Scherverhalten des Schmiermittels und Reibung festgestellt werden.